Dedicated to my parents

CERTIFICATE

This is to certify that the thesis entitled Studies on Long Term Average Optical Efficiency for Principal Solar Collectors and Shading Factors for Windows, submitted by **A. N. M. Mizanur Rahman** for the award of the degree of Doctor of Philosophy in Engineering to the Indian Institute of Technology, Kharagpur, is a record of bonafide work carried out by him under my supervision and guidance. The thesis has fulfilled the requirements according to the regulations of this Institute and in my opinion, has reached the necessary standard for submission. The results, embodied in this thesis, have not been submitted to any other University or Institute for award of any degree or diploma.

(V. V. Satyamurty)
Professor
Department of Mechanical Engineering
Indian Institute of Technology
Kharagpur – 721 302, India

STUDIES ON LONG TERM AVERAGE OPTICAL EFFICIENCY FOR PRINCIPAL SOLAR COLLECTORS AND SHADING FACTORS FOR WINDOWS

Thesis submitted in partial fulfilment of the requirements for the award of the degree of

Doctor of Philosophy in Engineering

by

A. N. M. Mizanur Rahman

under the supervision of

Professor V. V. Satyamurty

Department of Mechanical Engineering
Indian Institute of Technology, Kharagpur, India.

September, 1997

BIO-DATA

A. N. M. Mizanur Rahman was born on September 30, 1961. He received Bachelor of Science in Mechanical Engineering degree from Rajshahi University, Bangladesh in 1984. He received Master of Engineering degree with specialization in Energy Technology from Asian Institute of Technology, Bangkok, Thailand in 1989. He had served as a Lecturer in the Department of Mechanical Engineering of Bangladesh Institute of Technology, Khulna, Bangladesh from 1984 to 1987 and till date he has been serving as an Assistant Professor in the same Department of the same Institute. His fields of interest include design and performance evaluation of solar thermal systems, simulations, energy conservation, energy conversion and renewable energy sources in general. Following is the list of his publications:

1. Ranu Pentananunt, A. N. M. Mizanur Rahman, and S. C. Bhattacharya, *Upgrading of Biomass by means of Torrefaction*, Energy, vol. 15, No. 12, pp.1175-1179, 1990, (Published by Pergamon Press plc).

2. V. V. Satyamurty and A. N. M. Mizanur Rahman, *Algorithms for Designing of Overhangs*, Proceedings of **NAFEN's Xth International Congress & Exhibition on Non Conventional Energy Sources – 2000**, held at New Delhi on 15-17th December, 1996, pp.257-265.

3. A. N. M. Mizanur Rahman and V. V. Satyamurty, *Shading Factor Values Evaluated under Extra-terrestrial and Terrestrial Conditions*, Communicated to International Journal of Energy Research.

ACKNOWLEDGEMENTS

My utmost gratitude and praise goes to Almighty, who has created me and sent me to this universe with the light of knowledge and guided me to learn from His creation.

I sincerely express my indebtedness to Prefessor V. V. Satyamurty for his complete guidance during the entire course of this work. The systematic and logical approach of Prof. V. V. Satyamurty in analyzing the problems, his untiring enthusiasm and overall human presence shall be recalled by me in all of my future activities.

I am grateful to Prof. M. A. Faruqi for allowing me to use all computational facilities in the CAD-CAM Lab of Mechanical Engineering Department extensively. I am also grateful to the Head of the Deaprtment of Mechanical Engineering for providing facilities liberally in the department .

I am thankful to the Board of Governors, Bangladesh Institute of Technology, Khulna, Bangladesh, for deputing me to I. I. T., Kharagpur, India to pursue Ph. D. programme. I am also thankful to ICCR, Government of India for giving me the scholarship and financial assistance during my entire Ph. D. programme.

I express thanks to the staff members of Energy System Lab, CAD-CAM Lab and other Labs of the Department of Mechanical Engineering, I. I. T., Kharagpur, India who have encouraged and helped me at different stages.

I record my appreciation of my wife and my children who have made considerable sacrifice throughout my study period. I express my gratitude to my elder brother Dr. A. M. Muzaffor Uddin Ahmed, who inspired me and encouraged me to pursue hogher studies. I am also grateful to my friends, colleagues and well wishers for their warm company, moral support and help during my stay at I. I. T. , Kharagpur.

(A. N. M. Mizanur Rahman)

ABSTRACT

Assessment of techno-economic viabiity of solar energy systems is based on long term performance. The popular design methods for active as well as passive solar energy systems require certain proprocessed parameters in addition to meteorological information on appropriate time scale.

The present thesis deals with defining monthly average transmittance-absorptance product for flat plate collectors and optical efficiency for concentrating collectors consistent with the definition of monthly average daily utilizability. The procedure involved comparing the monthly average daily useful energy gain for flat plate collectors obtained by hour by hour summation procedure with the monthly average daily useful energy gain obtained as a product of heat removal factor, monthly average daily solar radiation on the collector aperture, monthly average daily utilizability and monthly average transmittance-absorptance product. In the second calculation, transmittance-absorptance product is an all day average value on the mean day of the month. The differences and an examination of the definition of monthly average daily utilizability established that the transmittance-absorptance product needs to be defined as a weighted average of the instantaneous transmittance-absorptance product and solar radiation on the collector aperture above the critical radiation level.

An equivalent mean day (EMD) calculation has been proposed and validated to obtain the monthly average transmittance-absorptance product for flat plate collectors and the optical efficiency for concentrating collectors tracked in the five principal modes according to the above definition.

A method to estimate the monthly average shading factors for receivers shaded by finite overhangs taking atmospheric transmittance into account has been developed and validated. The procedure involved developing simple equations relating finite shading factor values to the infinite values which are easily calculable in terms of the tilt factors for different planes. The present approach is valid for south facing as well as non-south facing receivers.

Finally, expressions for the monthly average shading factors for infinite wingwalls, analogous to the expressions for infinite overhangs, have been developed and validated. A feature of these algorithms is that they take into account the monthly average daily diffuse fraction and are valid for south facaing as well as for non-south facing receivers.

Key Words: Transmittance-absorptance product, Optical efficiency, shading factors, Overhangs, Wingwalls.

Contents

List of Figures

List of Tables

NOMENCLATURE

English letter symbols

A	$\sin\delta(\sin\phi\cos\beta - \cos\phi\sin\beta\cos\gamma)$, Eq. (2.5)
A^*	A with $\beta = \beta^*$, Eq. (5.24)
A_a, A_r	aperture area and receiver area for concentrating collectors
A_c	$1 - \sin^2\delta\cos^2\phi$, Eq. (4.71)
A_b, A_d, A_g	asymmetry parameters for direct, diffuse and global radiation defined as the ratio of forenoon direct, diffuse and global radiation to afternoon direct, diffuse and global radiation on a horizontal surface
A_i	beam irradiated area of the window
A_s	shaded area of the window caused by overhang or wingwalls
A_{shp}	area of the shading plane for overhang
A_{shp1}, A_{shp2}	areas of the shading planes (1 and 2) for overhang when a gap exists and also shading plane areas for wingwalls (1 and 2)
A_w	area of the window
A'	$\sin\phi\sin\delta$, Eq. (2,9)
a	denotes one of the five principal tracking modes for concentrating collectors, a plane rotated about a horizontal east-west axis with a single daily adjustment so that its surface-normal coincides with solar beam at noon each day
a	a constant in the correlation for r_t due to Collares-Pereira and Rabl [12], Eq. (2.20)
a_1	$(a - D_f)$ or $(a - \bar{D_f})$, Eq. (2.28)
a'	a constant in the correlation for r_d due to Satyamurty and Lahiri [15], Eq. (2.23)
B	$\cos\delta(\cos\phi\cos\beta + \sin\phi\sin\beta\cos\gamma)$, Eq. (2.6)
B^*	B with $\beta = \beta^*$, Eq. (5.25)
B_c	$2\sin\phi\sin\delta\cos\phi\cos\delta$, Eq. (4.72)
B'	$\cos\phi\cos\delta$, Eq. (2.9)
b	denotes one of the five principal tracking modes for concentrating

	collectors, a plane rotated about a horizontal east-west axis with continuous adjustment to minimize the angle of incidence
b	a constant in the correlation for r_t due to Collares-Pereira and Rabl [12], Eq. (2.21)
b_o	incidence angle modifier coefficient
b'	a constant in the correlation for r_d due to Satyamurty and Lahiri [15], Eq. (2.24)
C	$\cos\delta \sin\beta \sin\gamma$, Eq. (2.7)
C^*	C with $\beta = \beta^*$, Eq. (5.26)
C_c	$-\cos^2\delta \sin^2\phi$, Eq. (4.73)
C_r	area concentration ratio, $(= A_a/A_r)$
C_1	$1/[2B'(\sin\omega_s - \omega_s\cos\omega_s)]$, Eq. (5.38)
C_2	$(\omega_s/2 - \sin 2\omega_s/4)/(\sin\omega_s - \omega_s\cos\omega_s)$, Eq. (5.39)
c	denotes one of the five principal tracking modes for concentrating collectors, a plane rotated about a horizontal north-south axis with continuous adjustment to minimize the angle of incidence
D_f	daily diffuse fraction, H_d/H
$\bar{D}_f$	monthly average daily diffuse fraction, $\bar{H}_d/\bar{H}$
d	denotes one of the five principal tracking modes for concentrating collectors, a plane rotated about a horizontal north-south axis parallel to the earth's axis with continuous adjustment
EMD	equivalent mean day
e	denotes one of the five principal tracking modes for concentrating collectors, a two-axis tracking surface continuously oriented to face the sun
E, e	extension and non-dimensional extension of the overhang for the window
F_R	collector heat removal factor
f	monthly solar load fraction
f_i	instantaneous shading factor
f_{i1}, f_{i2}	instantaneous shading factor due to wingwall 1 and due to wingwall 2
$\bar{f}_i$	monthly average shading factor for finite overhang

$\bar{f}_{ip1}, \bar{f}_{ip2}$	monthly average shading factor values for finite overhangs corresponding to two projections $p1$ and $p2$
$\bar{f}_{i1}, \bar{f}_{i2}$	monthly average shading factor part values during ω_{sr} to ω_o and ω_o to ω_{ss} for non-south facing receivers shaded by finite overhang
$\bar{f}_{i\infty}$	monthly average shading factor for infinite overhang or wingwalls
$\bar{f}_{io\infty}$	monthly average shading factor for infinite overhang or wingwalls under extra-terrestrial conditions
$\bar{f}_{i\infty 1}, \bar{f}_{i\infty 2}$	monthly average shading factor (part values) corresponding to $\bar{f}_{i1}$ and $\bar{f}_{i2}$ when the overhang is infinite
$\bar{f}_{i\infty p1}, \bar{f}_{i\infty p2}$	monthly average shading factor values for infinite overhangs corresponding to two projections $p1$ and $p2$
$\bar{f}_i^o$	monthly average shading factor for finite overhang when $\bar{f}_{i\infty} = 0.0$
$\bar{f}_{i1}^o, \bar{f}_{i2}^o$	monthly average part shading factors for non-south facing finite overhang when $\bar{f}_{i1\infty}, \bar{f}_{i2\infty} = 0.0$
G, g	gap and non-dimensional gap between the overhang and the window top or between the wingwall and side of the window
H_w, H'	height of the vertical receiver and height measured along the non-vertical receiver
$H, \bar{H}$	daily and monthly average daily global radiation on a horizontal surface
$H_b, \bar{H}_b$	daily and monthly average daily direct radiation on a horizontal surface
$\bar{H}_{coll}$	monthly average daily radiation on the collector according to Collares-Pereira and Rabl's [12] definition
$H_d, \bar{H}_d$	daily and monthly average daily diffuse radiation on a horizontal surface
$\bar{H}_{ds}$	monthly average daily diffuse radiation on a shaded receiver
$H_o, \bar{H}_o$	daily and monthly average daily extraterrestrial radiation on a horizontal surface
$\bar{H}_s$	monthly average daily radiation on the shaded receiver
$H_T, \bar{H}_T$	daily and monthly average daily radiation on the collector aperture or tilted surface
$\bar{H}_{Ty}$	yearly average daily radiation on the collector aperture or tilted surface
$\bar{H}_y$	yearly average daily global radiation on a horizontal surface

h	altitude of any location
I, I_b, I_d	hourly global, direct and diffuse components of solar radiation on a horizontal surface
$\bar{I}, \bar{I}_b, \bar{I}_d$	monthly average hourly global, direct and diffuse components of solar radiation on a horizontal surface
I_{bs}	hourly direct radiation on a shaded receiver (window)
I_c	critical radiation level for a solar collector
I_{ds}	hourly total diffuse (sky diffuse and ground reflected) radiation on a shaded receiver
$I_o, \bar{I}_o$	hourly, monthly average hourly extra-terrestrial radiation on horizontal surface
I_s	hourly solar radiation on a shaded receiver
I_T	hourly solar radiation on the aperture of the collector
$I_{T,m}$	maximum hourly solar radiation on the aperture of the collector during the day which occurs around $\omega = \omega_m$
$\bar{I}^*_{T,m}$	maximum hourly solar radiation on the aperture of the collector during the day which occurs around $\omega = \omega_m$ on the equivalent mean day
$\bar{I}_{T,m}$	maximum hourly solar radiation on the aperture of the collector during the day which occurs around $\omega = \omega_m$ on the mean day of the month
I_{Tc}	critical radiation level for a passive structure
$I_{T,n}$	hourly solar radiation on the collector aperture at solar noon, $\omega = 0$
$\bar{I}_{T,n}$	hourly solar radiation on the collector aperture at solar noon, $\omega = 0$, on the mean day of the month
$\bar{I}^*_{T,n}$	hourly solar radiation on the collector aperture at solar noon, $\omega = 0$, on the equivalent mean day
$I_{P1}(\omega)$	$\int \cos\theta \, d\omega$, Eq. (3.44)
$I_{P2}(\omega)$	$\int \cos\theta \cos\omega \, d\omega$, Eq. (3.45)
$I_{P3}(\omega)$	$\int \cos^2\theta \, d\omega$, Eq. (3.46)
$I_{P4}(\omega)$	$\int \cos^2\theta \cos\omega \, d\omega$, Eq. (3.47)
$I_{P5}(\omega)$	$\int \cos\omega \, d\omega$, Eq. (3.48)
$I_{P6}(\omega)$	$\int \cos^2\omega \, d\omega$, Eq. (3.49)

$I_{P7}(\omega)$	$\int 1/(P+\cos\omega)\,d\omega$, Eq. (3.92)
$I_{P8}(\omega)$	$\int 1/(Q+\cos\omega)\,d\omega$, Eq. (3.93)
K	Extinction coefficient
K_T	daily clearness index, $(= H/H_o)$
$\bar{K}_T$	monthly average daily clearness index, $(\bar{H}/\bar{H}_o)$
$\bar{K}_T^*$	average daily clearness index for the contributing days in a month, Eq. (1.8)
$K_{T,min}$	minimum daily clearness index in a month below which there is no contribution to the useful energy
$K_{T,max}$	maximum daily clearness index in a month of average clearness index $\bar{K}_T$
K_1	$\pi/[24(\sin\omega_s - \omega_s\cos\omega_s)]$, Eq. (2.19)
K_2	$= (1+\cos\beta)/2$ for fixed surfaces and $= 1/C_r$ for concentrating collectors, Eq. (1.4)
K_3	$= (1-\cos\beta)/2$ for fixed surfaces and $= 0$ for concentrating collectors, Eq. (1.5)
K_4	$K_1 K_T H_o/B'$, Eq. (3.42)
K_5	$(a - b\cos\omega_s)$ Eq. (3.43)
K_6	$(B'D_f/C_r)$, Eq. (4.53)
k_T	hourly clearness index, $(= I/I_o)$
$\bar{k}_T$	monthly average hourly clearness index, $(= \bar{I}/\bar{I}_o)$
L	monthly heating load
L_A	auxiliary energy requirement for a month
L_{Ai}	auxiliary energy requirement for infinite capacity structure
L_{Az}	auxiliary energy requirement for zero capacity structure
n	day of the year (1 to 365) with January 1st as 1
N	number of days in a month
N_c	number of days in a month that contribute to the useful energy
P, p	projection and non-dimensional projection for overhang or wingwall
Q_D	dumped energy or energy in excess of the load in passive system
$\dot{Q}$	rate of dumped energy
$Q_r, \bar{Q}_r$	daily, monthly average daily net energy transfer from a receiver

Q_u	useful energy gain for a short time interval
$Q_{u,day}$	single day useful energy gain from a collector
$Q'_{u,day}$	single day useful energy gain from a collector when all day average transmittance-absorptance product is used
$\bar{Q}_{u,m}$	monthly average useful energy gain from a collector
$\bar{Q}'_{u,m}$	monthly average useful energy gain from a collector when all day monthly average transmittance-absorptance product is used
$\bar{R}$	daily or monthly average daily tilt factor for solar radiation
$\bar{R}^*$	monthly average daily tilt factor for solar radiation for the contributing days, i.e., $\bar{R}$ at $K_T = \bar{K}_T^*$
R_b	instantaneous tilt factor for direct radiation at an hour angle ω
$R_{b,m}$	R_b at the hour angle ω_m
R_b^*	instantaneous tilt factor for direct radiation for the shading plane
R_{b1}^*, R_{b2}^*	instantaneous tilt factors for direct radiation for shading planes corresponding to wingwall 1 and wingwall 2
$\bar{R}_b$	daily or monthly average daily tilt factor for direct radiation for a tilted surface
$\bar{R}_b^*$	daily or monthly average daily tilt factor for direct radiation for the shading plane
$\bar{R}_{bo}$	$\bar{R}_b$ evaluated under extra-terrestrial conditions
$\bar{R}_{bo}^*$	$\bar{R}_b^*$ evaluated under extra-terrestrial condition
$\bar{R}_{b1}^*, \bar{R}_{b2}^*$	average tilt factors for the durations ω_{sr} to ω_o and ω_o to ω_{ss} for the shading plane of an overhang. Also, average tilt factor for shading planes 1 and 2 corresponding to wingwalls 1 and 2
$\bar{R}_{bo1}^*, \bar{R}_{bo2}^*$	$\bar{R}_{b1}^*, \bar{R}_{b2}^*$ evaluated under extra-terrestrial conditions
R_m	instantaneous tilt factor for solar radiation at the hour angle ω_m
$\bar{R}_m, \bar{R}_m^*$	instantaneous tilt factors for solar radiation at $\omega = \omega_m$ on the mean day and equivalent mean day of the month
R_f	daily rainfall of any location
R_{fy}	yearly average rainfall of any location
RH	relative humidity

r_d, r_t	ratios of hourly diffuse and global radiation to daily diffuse and global radiation on a horizontal surface
$r_{t,m}, \bar{r}_{t,m}$	r_t at the hour angle ω_m on any day and on the monthly mean day
$r_{d,m}, \bar{r}_{d,m}$	r_d at the hour angle ω_m on any day and on the monthly mean day
S	number of hours of bright sunshine
$\bar{S}$	monthly average daily absorbed radiation by a solar collector, also, long term average number of hours of bright sunshine
$S/S_o, \bar{S}/\bar{S}_o$	daily, monthly average daily sunshine fraction
$T_a, \bar{T}_a$	daily, monthly average daily ambient temperatures
T_b	building temperature
$\bar{T}_{ay}$	yearly average ambient temperature
T_i	collector inlet fluid temperature
T_{min}	minimum temperature above which energy is supplied from the collector
$T_r, \bar{T}_r$	daily, monthly average daily room temperature
t	solar time, hour of the day
$U_L, \bar{U}_L$	overall collector heat loss coefficients
$(UA)_h$	building load coefficient
X_c	non-dimensional critical level for a day
$\bar{X}_c$	monthly average non-dimensional critical level
X_c^*	non-dimensional critical level for the equivalent mean day
W, w	width and non-dimensional width of the window

Greek letter symbols

α	absorptance of the receiver
α_1	$B^2 + C^2 - A^2$, Eq. (B.3)
α'	$B^2 + C^2 - (A - 0.5)^2$, Eq. (B.13)
α_s	solar altitude angle (complement of zenith angle)
α_e	effective absorptance of the window-room combination
β	slope, the angle between the tilted plane and the horizontal
β^*	slope of the shading plane Eq. (5.27)

β_e	beam extinction coefficient (Appears in Table 1.1)
β_1^*	slope of the shading plale 1 for overhang when gap exists
β_2^*	slope of the shading plane 2 for overhang when gap exists
δ, δ_m	solar declination for any day and mean day of the month
Δ_d	percentage difference in useful energy gain for a single day
$\bar{\Delta}_d$	percentage difference in the monthly average useful energy gain
$\Delta_{d,max}$	maximum percentage difference in useful energy gain for a single day
η_o	instantaneous optical efficiency for concentrating collectors
$\eta_{o,day}$	single day optical efficiency according to Collares-Pereira and Rabl [12]
$\eta^*_{o,day}$	single day optical efficiency as defined in the present studies
$\bar{\eta}_o$	monthly average optical efficiency for concentrating collectors
$\bar{\eta}^*_o$	monthly average optical efficiency for concentrating collectors as defined in the present studies
$\bar{\eta}^*_{o,emd}$	monthly average optical efficiency for concentrating collectors as defined in the present studies obtained by EMD approach
η_1, η_2, η_3	optical factors for direct, diffuse and ground reflected components of solar radiation
$\bar{\eta}_1, \bar{\eta}_2, \bar{\eta}_3$	monthly average optical factors for direct, diffuse and ground reflected components of solar radiation
γ	surface azimuth angle, negative towards east and positive towards west, zero due south
γ_s	solar azimuth angle, negative towards east and positive towards west, zero due to south
γ_d	$= (\gamma_s - \gamma)$
γ_1^*, γ_2^*	azimuthal angles of the shading planes corresponding to wingwalls 1 and 2
ω	solar hour angle, forenoon negative, afternoon positive, zero at solar noon
ω_o	hour angle corresponding to $(\gamma_s - \gamma) = 0$
ω_c	critical hour angle, the hour angle when the solar radiation incident on the collector is equal to the critical radiation for flat plate collectors facing south ($\gamma = 0$) or tracking solar collectors
ω_{c1}, ω_{c2}	critical hour angles in general, the hour angles when the solar radiation

	incident on the collector is equal to the critical radiation level
ω'_{c1}	$[max(\omega_{c1}, \omega_{sr})]$
ω'_{c2}	$[min(\omega_{c2}, \omega_{ss})]$
ω_m	the hour angle corresponding to maximum solar radiation incident on the collector aperture during the day
ω_s	sunset hour angle for a horizontal surface
ω'_s	apparent sunset hour angle for a south facing tilted surface or for a tracking collector
ω'_{so}	$(\omega_o - \omega_{sr})$ for $\gamma > 0$; $(\omega_{ss} - \omega_o)$ for $\gamma < 0$
ω_{sr}	apparent sunrise hour angle for a tilted surface
ω_{ss}	apparent sunset hour angle for a tilted surface
ω^*_{sr}	apparent sunrise hour angle for the shading plane
ω^*_{ss}	apparent sunset hour angle for the shading planes
ω^*_{sr1}	apparent sunrise hour angle for shading plane corresponding to wingwall 1
ω^*_{ss2}	apparent sunset hour angle for shading plane corresponding to wingwall 2
ω_1, ω_2	hour angles corresponding to angle of incidence $\theta = 60^o$
ϕ	latitude of a location, north positive
ϕ_{CPR}	utilizability for a single day or monthly average daily utilizability (according to Collares-Pereira and Rabl [68]
ϕ_{day}	utilizability for a single day
ϕ_E	utilizability for the equivalent mean day
$\bar{\phi}$	monthly average daily utilizability
$\bar{\phi}_y$	yearly average daily utilizability
ρ	ground reflectance
ρ_2	reflectivity of the underside of the overhang
ψ	angle between the shading plane for the overhang and the vertical
ψ_1, ψ_2	angles between the shading planes and the receiver
τ	transmittance of collector cover
τ_b, τ_d, τ_g	transmittance for direct, diffuse and ground reflected components of solar radiation

$(\tau\alpha)$	transmittance-absorptance product for the collector-cover system at any hour angle ω
$(\tau\alpha)_b$	transmittance-absorptance product at any hour angle ω for direct radiation
$(\tau\alpha)_d$	transmittance-absorptance product at any hour angle ω for diffuse radiation
$(\tau\alpha)_g$	transmittance-absorptance product at any hour angle ω for ground reflected radiation
$(\tau\alpha)_n$	transmittance-absorptance product at normal incidence
$(\tau\alpha)_{day}$	single day average transmittance-absorptance product for flat plate collectors
$(\tau\alpha)^*_{day}$	single day average transmittance-absorptance product for flat plate collectors as defined in the present studies
$(\overline{\tau\alpha})$	monthly average daily transmittance-absorptance product
$(\overline{\tau\alpha})^*$	monthly average daily transmittance-absorptance product as defined in the present studies
$(\overline{\tau\alpha})^*_{emd}$	monthly average daily transmittance-absorptance product as defined in the present studies obtained by EMD approach
$(\overline{\tau\alpha})_b$	monthly average daily transmittance-absorptance product for direct component of solar radiation
$(\overline{\tau\alpha})_d$	monthly average daily transmittance-absorptance product for diffuse component of solar radiation
$(\overline{\tau\alpha})_g$	monthly average daily transmittance-absorptance product for ground reflected component of solar radiation
$(\overline{\tau\alpha})_y$	yearly average daily transmittance-absorptance product
θ	angle of incidence for direct radiation for a tilted surface
θ_d	effective angle of incidence for diffuse solar radiation for calculating $(\tau\alpha)_d$
θ_g	effective angle of incidence for ground reflected radiation for calculating $(\tau\alpha)_g$
θ_m, θ_n	angle of incidence at the hour angle $\omega = \omega_m$ and $\omega = 0$
θ_z	angle of incidence for direct radiation for a horizontal surface, zenith angle
θ_1, θ_2	angles of incidence at hour angles ω_{c1} and ω_{c2}

Chapter 1

Introduction

Renewed interest by scientists and engineers worldwide to harness alternate energy sources is a consequence of realizing that fossil fuel reserves are fast depleting. Price hike of fuel oil in 1973 influenced the economic viability of the systems based on alternate energy sources. The role of solar energy is expected to be not insignificant among the alternate energy sources that are currently under active consideration. Solar energy is an attractive alternate energy source because it is non-polluting and abundantly available almost all over the world.

Conversion of solar energy to useful energy may be carried out through two major technological routes. In the first route, the photovoltaic conversion, solar energy is directly converted to electrical energy. In the second route, solar energy is converted to useful thermal energy which may be directly used or converted into shaft work. The output from the devices in both the routes is strongly dependent upon the solar radiation received. The useful energy from a solar thermal energy system can be delivered at temperatures ranging from 40°C to 1000°C or more. Generally, focussing or concentrating collectors are employed for higher temperatures say, above 100°C. For applications requiring energy at temperatures below 100°C, systems based on flat plate collectors are commercially available. Some of the applications are, space heating or cooling, agricultural and industrial product drying and power generation. In addition to the thermal systems that employ a collection device externally, solar energy may be utilized by passive means. Though, active and passive systems can not be strictly demarkated, the following examples are generally considered to be passive devices. Examples of passive devices are: solar stills, green houses, cabinet type driers, direct gain windows, overhangs and wingwalls etc. Passive systems like direct gain windows, Trombe walls, overhangs and wingwalls are potential candidates for wider exploration as a means to conserve energy and provide better indoor comfort condition.

Active solar energy thermal systems usually consist of components like, the solar collector to collect solar energy, a thermal storage device, non-solar auxiliary system, distribution system to transfer energy from the collector array to the storage and from storage to the load points and the control system. Transport of the working fluid to transfer energy is accomplished by means of a pump or a fan or at times by natural circulation. The non-solar auxiliary system is activated when the solar storage is depleted. The control determines the operation of the pumps, tracking of the collectors etc.

Passive solar energy systems are characterized by the following features. Generally, the collection device and the storage unit are integrated with the structure of the building. Storage is provided by the building structure as sensible heat. Also, many passive systems require no mechanical energy for moving the working fluid. In hybrid systems, mechanical energy may be used to distribute absorbed energy from one part of the building to another. In general, components of passive systems thus, are analogous to the components present in active systems. For example, in a passive system of the thermal-storage-wall type the solar collector consists of the glazing and the wall surface. Storage is integrated with the absorber surface and can be either a concrete slab or a water wall immediately behind and in contact with the collecting surface. The non-solar auxiliary is used to meet the load when passive storage is insufficient. The control elements are integral part of the passive system. Backdraft dampers are a control mechanism for storage wall systems which eliminate the possibility of reverse thermocirculation through the wall air slots which are used to supply warm air during the day.

Although, the solar collection device is the heart of the system, the performance of the system depends critically upon the other components in the system, like storage, heat exchangers, controls, and the load and its distribution. In general, environmentally driven systems and solar energy systems in particular, do not operate at either pre-determinable or uniform conditions. This necessitates predicting a working indication of the performance usually based on the statistical averages of the meteorological variables which influence the performance of the systems.

Design of active or passive solar energy systems needs to be based on long term performance. For solar energy systems, the time period over which long term performance assessed, is usually one year. Also, the economic viability of the systems is assessed based on the long term performance. For assessing long term performance, different input information and derived or processed information are needed. The time scale over which this information is called for, depends upon the method of long term performance prediction. Long term performance estimates, depending upon the accuracy needed, are based

on simulation of all the components in a system throughout the year, smallest time scale being an hour or less. At the other extreme, the yearly performance is assessed through a single equation or correlation developed by different techniques. In order to bring out the input and derived information needed for long term performance prediction of active and passive solar energy systems, the methods available are reviewed in the following sections. This review is aimed to identify the limitations of the existing methods in calculating the long term processed parameters and the scope for further studies.

1.1 Active Solar Energy Systems

1.1.1 Experiments

When possible, actual experiments are the best tools to determine long term performance of solar energy systems. However, conducting system scale long term experiments is prohibitively expensive and time consuming. Also, the results obtained from experiments conducted at a particular location may not be valid for another location. Further, the effects of changes in the design and operational parameters can not be easily studied. Though, there have been several experimental studies on components in the system, system scale experiments have been limited. One such study has been reported by Mitchell, Beckman and Pawelsky [1].

1.1.2 Simulations

Next to actual experiments, assessment of long term performance of solar energy systems is based on detailed simulations. Simulations are relatively quick and inexpensive. Also, information on the effects of changes in the design and operational variables can be obtained with ease. The system performance obtained from simulations along with cost data can determine an economically optimum configuration. Reliability of the results of simulations, however, depends on the validity of the models employed for the components in the system and accuracy and details of the meteorological information available. For successful implementation of simulation techniques, extensive meteorological data base are necessary. For developing component models, component scale experiments are needed. Nevertheless, system scale experiments are warranted to gain insight into the practical problems which the simulations may not reveal. SIMSHAC [2], *Simulation program for Solar Heating and Cooling of Buildings*, is one comprehensive modular program. Winn [3] presented a comparative assessment of several programs for the design of solar energy systems. TRNSYS [4, 5], *Transient System Simulations Program*, is another popular modular solar process simulation program. TRNSYS contains several component models required

in typical solar energy systems. A list of components in the TRNSYS library can be found in [4, 5] and in Duffie and Beckman [6].

Meteorological Input for Simulations

a) *Data*

In addition to the component models, the simulation programs in general require the following key input information.

a) Hourly global and diffuse solar radiation values.
b) Ambient temperature.
c) Wind velocity and it's direction.
d) Relative humidity.
e) Rainfall data.

The input information mentioned above are available from different meteorological data bases. SOLMET data [7] is one such widely used data base developed by National Oceanic and Atmospheric Administration (NOAA). SOLMET gives information about 23 climatic parameters of 240 US locations (of which, 26 are primary locations and the rest are secondary locations) over a period from 1952-1975. *National Solar Radiation Data Base* (NSRDB), developed by National Renewable Energy Laboratory, Boulevard, Colorado, is available as TMY2 data set [8]. This data base gives, along with solar radiation values, 23 climatic parameters for 239 locations of US and its territory (of which 56 are primary locations and 183 are secondary locations) over a period of 30 years from 1961-1990. Hourly radiation values for 18 Indian locations over a period of 8 years (1971-1978) are available from Aerological Data of India [9]. For Indian locations, both global and diffuse radiation are available for 14 locations and only global radiation is available for the other 4 locations.

b) *Synthetic Data*

In order to carry out simulations for locations for which data are not available and at times, for convenience in computations, use of synthetic data also has been reported (see Knight, Klein and Duffie [10]) in the literature. Recently, Gansler, Klein and Beckman [11] investigated the accuracy of using reduced and synthesized sets of meteolorogical models for solar applications. In the broadest sense, several correlations available in the literature to predict global and diffuse components of solar radiation, ambient temperature, etc. can be considered as a part of synthetic data generation. Obtaining daily diffuse radiation from daily global radiation from Collares-Pereira and Rabl [12] or Erbs, Klein and Duffie [13] is an example. Similarly, hourly global and diffuse solar radiation can be estimated

from the corresponding daily values using the correlations for r_t (see Collares-Pereira and Rabl [12], Jain, Jain and Ratto [14] and Satyamurty and Lahiri [15]) and r_d (see Liu and Jordan [16], Jain, Jain and Ratto [14] and Satyamurty and Lahiri [15]) respectively. Also, distribution of clearness indices, due to Liu and Jordan [16], analytically represented by Bendt, Collares-Pereira and Rabl [17], can be used to obtain hourly or daily global radiation values from monthly average hourly or daily values. Different correlations in this category are given in Table 1.1.

Attempts at predicting ambient temperature in terms of more readily available information are lesser compared to the body of literature available to predict the solar radiation. Erbs, Klein and Beckman [40] and Morrison and Sudjito [25] presented correlations to predict the monthly average hourly ambient temperature. Erbs, Klein and Beckman also presented distribution of daily average ambient temperatures as a function of monthly average daily ambient temperature and long term standard deviations. Recently, Choudhury [39] examined the correlations, presented by Erbs et al. [40] and Morrison [25], to predict the monthly average hourly ambient temperature and found that the swing in the daily ambient temperature correlated to the monthly average daily clearness index in Erbs et al. [40] is highly location dependent. Choudhury developed correlations to predict monthly average hourly ambient temperature in terms of the maximum and minimum temperatures of the day. Choudhury also developed correlations for the monthly average ($\bar{T}_a$) and yearly average ($\bar{T}_{ay}$) daily ambient temperature using multiple regression analysis using a data base for 220 locations with latitude range of $8^o < \phi < 62^o$. The correlations developed by Choudhury [39] employ differing number of predictors, among - latitude (ϕ), declination (δ), altitude (h), rainfall (R_f) or (R_{fy}) and global solar radiation ($\bar{H}$) or (H_y).

Derived Information in Simulation Programs

The following are the derived information/parameters.

a) Solar radiation on the surface of interest.
b) Absorbed radiation which calls for optical properties of the collector-cover system.
c) Overall heat loss factors.
d) Degree-days.

Solar radiation on any surface of interest (other than horizontal) is estimated from the solar radiation on a horizontal surface multiplied by a tilt factor, R. Methods to estimate the tilt factor, R, applicable for a small interval of time are available in Duffie and Beckman [6] based on the developments due to Liu and Jordan [41]. According to

Table 1.1: Literature on correlations to get more details on solar radiation information

Quantities	Methods available in	Predictors	Used for
I_d/I	Orgill and Hollands [18]	k_T	Calculating I_d
	Erbs, Klein and Duffie [13]	k_T	
	Spencer [19]	k_T, ϕ	
	Hollands and Huget [20]	k_T, τ at upper and lower atm.	
	Soler [21]	k_T	
	Suehrcke amd McCormick [22]	$\bar{K}_T, \theta_z, \beta_e$	
	Reindl, Beckman and Duffie [23]	k_T, m_r, T_a, RH	
	Camps and Soler [24]	$k_T, \theta_z, S/S_o$	
	Morrison and Sudjito [25]	Evaluated the correlation due to Spencer [19]	
r_d	Liu and Jordan [16]	ω_s, ω	Calculating I_d
	Newell [26]		
	Mani and Rangarajan [27]	Graphs	
	Satyamurty and Lahiri [15]	$D_f, \omega_s, \omega, A_d$	
$\bar{I}_d/\bar{I}_o$	Soler [28]	$\bar{k}_T, \bar{S}/\bar{S}_o, \theta_z$	Calculating $\bar{I}_d$
I_d/I_o	Skartveit and Olseth [29]	$\bar{I}_b/\bar{I}o$	I_b
I_b	Suehrcke and McCormick [22]	$\bar{K}_T, \theta_z, \beta_e$	I_b
k_T	Liu and Jordan [16]	$\bar{k}_T$	Distribution of k_Ts and Is
r_t	Mani and Rangarajan [27]	ω, ω_s	I
	Collares-Pereira and Rabl [12]	ω_s, ω	
	Jain, Jain and Ratto [14]	ω_s, ω and some location dependent parameters	
	Satyamurty and Lahiri [15]	$D_f, \omega_s, \omega, A_g$	

Table 1.1 *Continued*

Quantities	Methods available in	Predictors	Used for
H_d/H	Liu and Jordan [16]	K_T	Calculating H_d
	Collares-Pereira and Rabl [12]		
	Erbs, Klein and Duffie [13]		
	Davis and Mckay [30]	Evaluated the performance of the correlations reported in [12] and [13]	
	Elhadidy and Abdel-Nabi [31]	K_T and season	
	Gopinathan [32]	$K_T, S/S_o$	
$\bar{H}_d/\bar{H}$	Collares-Pereira and Rabl [12]	$\bar{K}_T, \omega_s$	$\bar{H}_d$
	Erbs, Klein and Duffie [13]	$\bar{K}_T$	
	Al-Hamdani, Al-Riahi and Tahir [33], Soler [34]	$\bar{K}_T, \bar{S}/\bar{S}_o$	
	Soler [35]	$\bar{K}_T, \phi$	
$\bar{H}_b/H_o$	Wenxian [36]	K_T, h, R_f	H_b, H_d
K_T	Liu and Jordan [16], Bendt Collares-Pereira, Rabl [17]	$\bar{K}_T$	Distribution of k_Ts
	Feuillard, Abillon and Bonhomme [37]	$\bar{K}_T, \bar{S}/\bar{S}_o$	
$\bar{H}_y$	Stanhill [38]	ϕ, h	
	Choudhury [39]	$\phi, \delta, h, R_f, \bar{H}$	

Note: Meteorological quantities (long term average or longer time duration) direct or derived, such as, H, $\bar{H}$, H_d/H, $\bar{H}_d/\bar{H}$, $\bar{H}_y$ are not needed in the simulations. However, they are needed in general, in the design methods. Also, a long term average value may be the starting point for synthetic data generation on smaller time scale.

Liu and Jordan [41], the radiation on the tilted surface comprises of three components: direct, sky-diffuse and solar radiation reflected from the ground. Solar radiation absorbed by the solar collector is the product of solar radiation on the surface of interest multiplied by an effective transmittance-absorptance product $(\tau\alpha)$, or in general, optical efficiency of the collector-cover system. $(\tau\alpha)$ can be estimated from the transmittance of the cover, τ, absorptance of the receiver, α, and the reflectance of the cover system for diffuse radiation, ρ_d which is a fucntion of extinction coefficient K [see, Duffie and Beckman [6], chapter 5, page 216-229]. It may be noted that both τ and α depend on the angle of incidence of solar radiation. ASHRAE [42] suggests that the ratio of transmittance-absorptance product $(\tau\alpha)$ at any incidence angle to that at normal incidence angle, $(\tau\alpha)_n$, can be expressed as,

$$\frac{(\tau\alpha)}{(\tau\alpha)_n} = 1 + b_o \left(\frac{1}{\cos\theta} - 1\right) \qquad \text{for} \quad 0^o < \theta < 60^o \tag{1.1}$$

In Eq. (1.1), b_o is the incidence angle modifier coefficient and θ is the angle of incidence. Eq. (1.1) is valid for gray surfaces and can not be used for selective surfaces. Tabulated values of $(\tau\alpha)/(\tau\alpha)_n$ for single and double glass covers for incidence angle range of $0 < \theta < 90^o$ are available in f-chart manual [43]. Visalakhsi [44] presented an expression for $(\tau\alpha)/(\tau\alpha)_n$ for the range $60^o < \theta < 90^o$ as,

$$\frac{(\tau\alpha)}{(\tau\alpha)_n} = 2\,(1 + b_o)\,\cos\theta \qquad \text{for} \quad 60^o < \theta < 90^o \tag{1.2}$$

which agrees closely with the data values given in [43]. For concentrating collectors, ratio of optical efficiency at any incidence angle to the optical efficiency at normal incidence is available in Gaul and Rabl [45]. Gaul and Rabl correlated optical efficiency for parabolic trough concentrators of five different makes in a polynomial form.

Overall heat loss coefficient for flat plate collectors comprises of a top loss coefficient and a bottom loss coefficient. These can be estimated when the required relations for the free convective and force convective heat transfer coefficients are known. In general, it may be considered that a fair body of heat transfer literature exists on heat transfer coefficient required in estimating the loss coefficient and is not dealt with in this review. Radiative heat transfer coefficient, being dependent upon the temperatures of the surfaces, makes the process of estimating the top loss coefficient iterative. Similar procedure is followed to obtain receiver overall heat loss coefficient for the concentrating collectors. For flat plate collectors, Klein [46], following the procedure of Hottel and Woertz [47], developed a correlation for the top loss coefficient as a function of number of glass covers, collector tilt, emittance of glass and plate, ambient temperature, mean plate temperature and wind heat transfer coefficient. Recently, Samdarshi and Mullick [48] developed a generalized analytical equation for the top loss factor, valid for flat plate collector with N glass covers.

The degree-day method of estimating heating loads is based on the principle that the energy loss from a building is proportional to the difference in temperature between indoors and outdoors. Values of monthly average degree-days for 240 US locations are available in Duffie and Beckman [6]. Also, Tables of degree-days for several base temperatures are available in Balcomb, Jones, McFarland and Wray [49]. A method to estimate the number of degree-days is described in Erbs, Klein and Beckman [40] also.

1.1.3 Short-cut Simulations

To cut down the expense of computations involved in the detailed simulation methods, such as, TRNSYS [4, 5], short-cut simulation techniques have been reported in the literature. SOLCOST [50] is one such short-cut simulation method, whereby system simulation is performed over a clear day and a cloudy day and the results of both days' system performance are weighted by taking the monthly average daily clearness index into account in order to arrive at a monthly estimate of the system performance. Typical Meteorological Day (TMD) method due Feuermann, Gordon, and Zarmi [51], and the MIRA method due to Reddy [52] and Reddy, Gordon and DeSilva [53] employ one repetitive day calculation. These methods [51, 52, 53], valid for systems employing energy storage, attempt to determine the mean diurnal cycle by an iterative procedure to satisfy a quasi-steady state condition. Quasi-steady state condition ensures that the tank temperature at the start and after a day remains the same. Iterations are not necessary for systems without storage. For both the methods, a mean day needs to be chosen which contains all the necessary statistical information concerning the time dependence of solar radiation and fluctuation patterns as experienced by the solar collector.

1.1.4 Design methods developed as correlations to simulation results or on analytical considerations

a) Monthly correlations

The simulation methods described in the preceeding section, in general, are not restricted to any specific system. Models for new components can be added as and when become available. The system configurations for certain applications of solar energy heating systems such as space heating, domestic water heating, industrial process heating etc., have become more or less standard. For standard system configurations, from the results of detailed simulations, correlations to predict the monthly solar load fraction have been developed. The monthly solar load fraction, f, is defined as the ratio of energy delivered by the solar energy system to the load on the system ignoring the energy produced by the system in excess of the load. f-chart method [54, 55, 56] is one such simplified design

method for systems supplying energy at or above $20°C$ and has been successfully employed for designing space heating and domestic hot water (DHW) systems. In the f-chart method [54, 55, 56] the monthly solar load fraction is correlated to two non-dimensional variables, the non-dimensional collector loss and the non-dimensional absorbed energy. Experimental verification of f-chart results have been reported by Duffie and Mitchell [57], Fanney and Klein [58] etc. Similar correlations to predict the monthly solar load fraction have been reported in Buckles and Klein [59] and Lunde [60]. $\bar{\phi}$, f-chart [61, 62] is another popular design method to predict the monthly solar load fraction for systems delivering energy at or above a desired minimum temperature. $\bar{\phi}$, f-chart method combines the utilizability method with the f-chart concept. In the $\bar{\phi}$, f-chart method, in addition to the two non-dimensional variables described in the f-chart method, the monthly average daily utilizability, $\bar{\phi}$, also is required. The two non-dimensional variables, viz. the non-dimensional collector loss and the non-dimensional absorbed energy common to both f-chart and $\bar{\phi}$, f-chart, require the monthly average daily solar radiation falling on the collector surface, $\bar{H}_T$, and the monthly average transmittance-absorptance product ($\overline{\tau\alpha}$), also referred to as monthly average optical efficiency, $\bar{\eta}_o$.

Monthly Average Processed Parameters

Monthly Average Daily Tilt Factor: The monthly average daily solar radiation, $\bar{H}_T$, falling on flat plate or concentrating collectors can be estimated from the monthly average daily global radiation on a horizontal surface, $\bar{H}$, as,

$$H_T = RH = H\left[(1 - D_f)R_b + K_2 D_f + K_3\right] \tag{1.3}$$

where, $\bar{R}_b$ is the monthly average daily tilt factor for direct radiation defined as the ratio of monthly average daily direct radiation on a tilted surface to that on a horizontal surface. $\bar{D}_f$ $(= \bar{H}_d/\bar{H})$ introduced for brevity, is the monthly average daily diffuse fraction and K_2 and K_3 are constants. When solar radiation data are not available, $\bar{D}_f$ can be calculated from [63, 16, 12, 13]. The constants K_2 and K_3 are defined by,

$$K_2 = \begin{cases} (1 + \cos\beta)/2 & \text{for flat plate collectors} \\ 1/C_r & \text{for concentrating collectors} \end{cases} \tag{1.4}$$

$$K_3 = \begin{cases} \rho\,(1 - \cos\beta)/2 & \text{for flat plate collectors} \\ 0 & \text{for concentrating collectors} \end{cases} \tag{1.5}$$

In Eqs. (1.4) and (1.5), β is the slope of the collector. In the second expression of Eq. (1.4), C_r, is the concentration ratio defined as the ratio of the aperture area of the collector to the area of the receiver and in Eq. (1.5), ρ is the ground reflectance. In general, concentrating

collectors do not "see" the ground-reflected solar radiation and hence the second expression in Eq. (1.5) is zero. From Eq. (1.3), $\bar{R}$ can be expressed as,

$$\bar{R} = [(1 - \bar{D}_f)\bar{R}_b + K_2\bar{D}_f + K_3] \tag{1.6}$$

$\bar{R}_b$ in Eq. (1.6) can be estimated from Liu and Jordan [64], Klein [65] or Klein and Theilacker [66]. Lahiri [67] also presented methods to estimate $\bar{R}_b$ considering asymmetry in the solar radiation distribution. Collares-Pereira and Rabl [68, 69] presented methods to calculate $\bar{H}_{coll}$, the monthly average daily solar radiation, received during an average collector operating time period for flat plate as well as concentrating collectors tracked in the five principal modes[1]. Lahiri [67] developed explicit expressions for calculating $\bar{R}_b$ for concentrating collectors tracked in the five principal modes.

All the methods [64, 65, 66, 68, 69, 67] for estimating solar radiation on tilted surfaces discussed above, employ isotropic sky-diffuse radiation model. Descriptions for anisotropic sky-diffuse radiation have been reported in the literature. Some of the models are due to Temps and Coulson [70], Hay [71], Klutcher [72], Hay and Davis [73], Perez, Stewart, Arbogast, Seals and Scott [74], Gueymard [75], Perez, Seals, Ineichen and Stewart [76], Perez, Seals, Ineichen, Stewart and Menicucci [77], Reddy and Attalage [78]. Ma and Iqbal [79] have compared the predicted solar radiation values using the isotropic model and the anisotropic models due to Hay [71] and Klutcher [72] against measured values on tilted surfaces for one Canadian location and found that the anisotropic models agree better with the measured values. Abdelrahman and Elhadidy [80] reported opposite observations for an Arabian location, where the agreement with the measured radiation values is better with the isotropic model rather than with the anisotropic models due to Hay [71] and Klutcher [72]. Recently, Utrillas and Martinez-Lozano [81] evaluated the performance of [74, 76] and concluded that the simplified circumsolar model approximates measured values more closely. However, Kambezidis, Psiloglou and Gueymard [82] reported that Perez model does not perform well for Athens data. In view of the inconclusive results and in the absence of verification against widespread measured information, the models for anisotropic sky-diffuse radiation perhaps need further scrutiny.

[1]The five principal modes of tracking considered by Collares-Pereira and Rabl are -

Mode **a**: A plane rotated about a horizontal east-west axis with a single daily adjustment so that its surface-normal coincides with solar beam at noon each day.

Mode **b**: A plane rotated about a horizontal east-west axis with continuous adjustment to minimize the angle of incidence

Mode **c**: A plane rotated about a horizontal north-south axis with continuous adjustment to minimize the angle of incidence.

Mode **d**: A plane rotated about a north-south axis parallel to earth's axis, with continuous adjustment.

Mode **e**: A two-axis tracking surface continuously oriented to face the sun

Monthly Average Daily Utilizability: Collares-Pereira and Rabl [68] suggested that ϕ,f-chart correlation [61] can be used for systems employing concentrating collectors as well when the monthly average daily utilizability and the optical efficiency correspond to the concentrating collectors employed. Hottel and Whiller [83] introduced the monthly average hourly utilizability which was later generalized by Liu and Jordon [41]. Monthly average daily utilizability, $\bar{\phi}$, as defined by Klein [84] is the ratio of the sum for a month, over all hours and all days, of the radiation received by the collector surface above a critical radiation level to the total radiation falling on the collector surface over the same month. The critical radiation level corresponds to zero useful energy gain from the collector. However, Collares-Pereira and Rabl [68, 69] defined the monthly average daily utilizability (designated in the present thesis as ϕ_{CPR} for clarity) in a slightly different way, as the ratio of solar radiation received by the collector above the critical level over a month to the total radiation during the collector operating time period over the same month. Klein [84] presented a correlation to calculate $\bar{\phi}$ for flat plate collectors facing the equator. Collares-Pereira and Rabl [68, 69] have presented generalized correlations for ϕ_{CPR} which include non-south facing flat plate collectors and concentrating collectors tracked in the five principal modes. Retaining the same form of the correlation due to Klein [84], the constants have been rederived by Theilacker and Klein [85]. Other correlations valid for flat plate collectors facing the equator are due to Evans, Rule and Wood [86] and Lunde [87]. The correlation for the long term hourly utilizability due to Clark, Klein and Beckman [88], valid for flat plate collectors with no restriction on the surface azimuthal angle, can be employed for obtaining the monthly average daily utilizability by numerical integration of the hourly values. The method of Hollands and Huget [89] to predict long term hourly utilizability for solar collectors also calls for numerical integration to obtain the monthly average daily utilizability. Klein and Beckman [90] presented an excellent comparative study of the different correlations [85, 86, 87, 88, 68, 69] available for evaluating the monthly average daily utilizability and suggested that studies be pursued to develop methods for estimating the monthly average daily utilizability with sufficient accuracy when the utilizability is low. Yearly average utilizability for principal types of solar collectors can be obtained from the data based correlations due to Rabl [91]. Gordon and Zarmi [92, 93] have developed a simple method of estimating the yearly average utilizability valid for concentrating collectors. The method of Gordon and Zarmi has been developed for clear climates which fortuitously works for cloudy conditions as well.

In an attempt to develop general enough method to estimate monthly average daily utilizability, Acharya [94] studied the limitations of the correlations of Klein [84] and

Collares-Pereira and Rabl [68, 69]. Acharya [94] introduced an equivalent mean day (EMD) calculation to obtain the monthly average daily utilizability as a single day calculation for south facing flat plate collectors. Employing the correlations for r_t [12] and r_d [16] to express I_T, expressions for the utilizability for a single day have been obtained from,

$$\phi_{day} = \frac{\int_{\omega_{c1}}^{\omega_{c2}} (I_T - I_c)\, d\omega}{\int_{-\omega_s}^{\omega_s} I_T\, d\omega} \tag{1.7}$$

where, ω_{c1} and ω_{c2} are the hour angles corresponding to $I_T = I_c$. Lahiri [67] generalized the method to include non-south facing flat plate collectors and concentrating collectors. Choudhury [39] studied the influence of asymmetry in the solar radiation distribution on the monthly average daily utilizability for principal types of collectors. The equivalent mean day is defined as the average day of the days in a month that contribute to the useful energy. The days that contribute to the useful energy have been identified as the days with clearness indices higher than a certain minimum clearness index, $K_{T,min}$. $K_{T,min}$ can be obtained by equating the critical radiation level to the maximum radiation on the collector surface during a day. Explicit expressions to obtain $K_{T,min}$ are available in Lahiri [67]. The fractional time for which $K_T > K_{T,min}$ or the ratio of the contributing days, N_c, to the total number of days in a month, N, can be obtained from the generalized distribution of clearness indices for a given $\bar{K}_T$ due to Liu and Jordan [16] or from analytical expressions presented by Bendt et al. [17]. Indeed, in this method any distribution of K_T can be employed. The equivalent mean day is characterized by an average clearness index of $\bar{K}_T^*$, which is the average of clearness indices of the contributing days, i. e. days with $K_T > K_{T,min}$. Let, the utilizability for the equivalent mean day be ϕ_E. Monthly average daily utilizability is obtained from the utilizability for the equivalent mean day (Single day), realizing that the solar radiation in a month falling on the collector surface above the critical level is the same, calculated as, $\bar{\phi}\, N\, \bar{H}_T$ or $\phi_E\, N_c\, \bar{H}_T^*$. Thus,

$$\bar{\phi} = \phi_E \frac{N_c \bar{R}^*\, \bar{K}_T^*}{N\, \bar{R}\, \bar{K}_T} \tag{1.8}$$

where $\bar{R}^*$ is the average tilt factor for the contributing days in a month. The aforementioned studies [94, 67, 39] are, general enough, any distribution of clearness indices can be employed, and are valid in the range $0 < \bar{\phi} < 1$ within a rms difference of 4 % compared to the hour by hour computations employing solar radiation data.

Monthly Average Transmittance-Absorptance Product or Optical Efficiency: The other processed parameter needed in calculating the non-dimensional absorbed energy (one of the two variables in the f-chart and $\bar{\phi}$, f-chart correlation) is the monthly average daily optical efficiency. In the present thesis, generally the term transmittance-absorptance

product has been used for flat plate collectors and optical efficiency for concentrating collectors. Also, when literature is reviewed the original notation of the author is preserved. Collares-Pereira and Rabl [68, 69] introduced monthly average optical efficiency, η_o for solar collectors defined during the operational time period of the collectors. However, no method to explicitly calculate either the operating time period or the long term optical efficiency, $\bar{\eta}_o$ has been presented. To date, studies to calculate monthly average transmittance-absorptance product, $(\overline{\tau\alpha})$, pertaining to flat plate collectors are due to Klein [95], Sfeir [96], Satyamurty and Acharya [97] and Choudhury [39]. The methods reported in [95, 96, 97, 39] define the monthly average daily transmittance-absorptance product for flat plate collectors as a weighted average during the entire month, the weighting function being the incident solar radiation. The monthly average daily absorbed energy, S, (see Duffie and Beckman [6]) is expressed as,

$$\bar{S} = \bar{H}_T(\overline{\tau\alpha}) = \bar{H}_b\bar{R}_b(\overline{\tau\alpha})_b + K_2\bar{H}_d(\overline{\tau\alpha})_d + K_3\bar{H}(\overline{\tau\alpha})_g \tag{1.9}$$

where, $(\overline{\tau\alpha})_b$, $(\overline{\tau\alpha})_d$ and $(\overline{\tau\alpha})_g$ are the monthly average transmittance-absorptance product values for direct, diffuse and ground reflected radiation respectively. From Eq. (1.9), $(\overline{\tau\alpha})$ can be expressed as,

$$(\overline{\tau\alpha}) = \frac{\bar{H}_b\bar{R}_b(\overline{\tau\alpha})_b + K_2\bar{H}_d(\overline{\tau\alpha})_d + K_3\bar{H}(\overline{\tau\alpha})_g}{\bar{H}_b\bar{R}_b + K_2\bar{H}_d + K_3\bar{H}} \tag{1.10}$$

$(\overline{\tau\alpha})_d$ and $(\overline{\tau\alpha})_g$ can be estimated easily employing the correlations for the effective angles of incidence θ_d and θ_g, for diffuse and ground reflected radiation respectively according to Brandemuehl and Beckman [98]. $(\overline{\tau\alpha})_b$ is the weighted average of direct radiation on the tilted surface and the corresponding transmittance-absorptance product over all the hours and all the days in the month and is expressed as,

$$(\overline{\tau\alpha})_b = \frac{\sum_{days}\sum_{hours} I_b R_b(\tau\alpha)_b\, d\omega}{\sum_{days}\sum_{hours} I_b R_b\, d\omega} \tag{1.11}$$

Klein obtained effective angles of incidence θ_b to calculate $(\overline{\tau\alpha})_b$. θ_b has been presented graphically, evaluating Eq. (1.11) on the mean day of the month, as a function of the latitude ϕ, the collector slope β, and the surface azimuth angle γ, for all the months of the year. The graphical results of Klein [95] can not be easily computer implemented. Further, the results do not show the dependence of θ_b on the number of glass covers or any climatic feature, say, clearness index or diffuse fraction. Following the approach similar to Klein and Theilacker [66] in evaluating $\bar{R}_b$, Sfeir [96] developed an analytical expression for $\bar{\eta}_{o,b}$. Sfeir employed a relation to describe the angular distribution of $(\eta_{o,b}/\eta_{o,n})$ in terms of the incidence angle modifier coefficient b_o, valid for $0^o < \theta < 60^o$, in the entire

range of $0^o < \theta < 90^o$. Satyamurty and Acharya [97] have eliminated the limitations of Sfeir's expression by employing piece-wise continuous functions of θ that closely follow the distribution of $(\eta_o/\eta_{o,n})$ in the entire range of $0^o < \theta < 90^o$. The functions satisfy $(\eta_o/\eta_{o,n}) = 1$, $(1 + b_o)$ and 0 at $\theta = 0^o$, 60^o and 90^o respectively. Satyamurty and Acharya [97] developed expressions for $(\bar{\eta}_{o,b}/\eta_{o,n})$ under extraterrestrial conditions and related the values to the terrestrial values as a function of the daily diffuse fraction for south facing flat plate collectors. Choudhury [39] has shown that the expression of Sfeir [96] leads to serious error since the apparent sunrise and sunset hour angles for a tilted surface have been implicitly set equal to the sunrise and sunset hour angles for the horizontal surface. Choudhury has shown that, indeed this is responsible for large errors according to Sfeir's expressions in summer months even for a south facing collector. Choudhury studied the influence of asymmetry in solar radiation distribution also in obtaining $(\overline{\tau\alpha})_b$.

Methods to calculate $\bar{\eta}_o$ for concentrating collectors are very limited. Gaul and Rabl [45] investigated the incidence angle modifier for parabolic trough collectors and presented the results in two forms: a) a polynomial fit to data and b) a single number, the all day average optical efficiency for typical operating conditions. Further studies in obtaining $\bar{\eta}_o$ for concentrating collectors tracked in the five principal modes are needed.

b) Annual Models

To further reduce computational effort, Barley and Winn [99], Lameiro and Bendt [100] and Ward [101] have proposed methods which are correlations obtained from f-chart results to predict the annual load fraction directly. Annual models to predict the yearly solar load fraction are also available in Satyamurty and Beckman [102], Satyamurty, Visalakhsi and Sastri [103] and Satyamurty and Visalakhsi [104, 105] for space heating systems and Visalakhsi [44] which includes industrial process heating systems as well. The annual models described particularly, in Satyamurty and Beckman [102] and further extensions [103, 104, 105, 44] require yearly average solar radiation received by the collector, $\bar{H}_{T,y}$, yearly average utilizability, $\bar{\phi}_y$ and yearly average transmittance-absorptance product, $(\overline{\tau\alpha})_y$. Visalakhsi [44] developed a method to estimate the yearly average solar radiation received by south facing flat plate collectors from the yearly average solar radiation on a horizontal surface valid for $-15^o \leq (\phi - \beta) \leq 15^o$ which is more general than Gordon and Zarmi's [106] method. Visalakhsi's approach correctly accounts for number of hours of solar radiation as received by the collector in the year. Visalakhsi also developed an expression for the yearly average transmittance-absorptance product under extra-terrestrial conditions. Satyamurty and Visalakhsi [105] calculated the yearly average utilizability for south facing flat plate collectors accurately using Klein's [84] correlaltion for the monthly average daily utilizability assuming the critical radiation level to be constant for all the

months in the year. This constant value has been chosen as the average of the monthly values. Other parameters in Klein's correlation such as $\bar{R}$ are replaced by corresponding yearly values. Lahiri [67] generalized the method to estimate yearly average solar radiation received by principal solar collectors by taking winter ($\delta < 0$) and summer ($\delta > 0$) averages separately. Similar concept has been validated by Lahiri to calculate the yearly average utilizability also. Approach described in Lahiri is valid for flat plate collectors with no restriction on the azimuthal angle, slope and concentrating collectors tracked in the five principal modes.

c) Simplified analytical approach

Owing to the input forcing functions (insolation, ambient temperature, load, etc.) varying on all (hourly, daily and seasonal) time scales, and the presence of control functions for changing the mode of operation of the system, solar energy systems do not permit simple analytical solutions. However, with a set of simplifying assumptions, performance estimates of simple solar energy systems have been represented analytically. Gordon and Rabl [107] have proposed a design method for open-loop industrial process heating systems without storage, which is applicable when the thermal load is uniform over the time scale of operation, usually a year. The design procedure proposed by Collares-Pereira, Gordon, Rabl and Zarmi [108] includes a well mixed storage. Similar methodology has been applied by Baer, Gordon and Zarmi [109] for solar steam generating systems. Analytical models for liquid systems with well mixed-storage (Gordon and Zarmi [110]) and air systems with stratified pebble-bed storage (Ajona and Gordon [111]) have been reported assuming a constant radiation model, where the diurnal variation of solar radiation has been replaced by a constant value over the time scale of operation.

1.2 Passive Solar Energy Systems

Several concepts for passive solar heating or cooling have been developed that are sufficiently distinct in principles and functions. These are direct gain windows, collector-storage-walls (also called Trombe wall) and sunspaces. In direct gain systems, energy through windows can meet part of the building heating loads. The window acts as a collector and the building itself provides some storage. Overhangs, wingwalls or other architectural devices are used to shade the windows during times when heating is not wanted. Collector-storage-wall combines the functions of a collector and storage into a single unit and is a part of the building structure. Part of a south wall may be single or double glazed; inside the glazing is a massive wall of masonry material or water tanks, finished black to absorb solar radiation. Heat is transferred from the storage wall to the

room by radiation and by convection from the room side of the wall. Room air is circulated by a fan (or natural circulation) through the space between the glazing and the wall. Room air may enter this space through openings in the bottom of the wall and return to the room through openings in the top. Sunspace attachments (which are green-house like structures) to buildings have been used as solar collectors, with storage in walls, floors, or pebble beds. Forced air circulation to the rooms is an option to improve the utilization of absorbed energy. In cold climates, energy losses from sunspaces may exceed the absorbed energy, and care must be taken to ensure that net gain accrues from such a system.

The calculation of solar radiant heat gain through fenestration system is an important component for cooling load calculations. In the terminology of Heating Ventilating and Air Conditioning (HVAC) engineering, solar heat gain coefficient (SHGC) defined as the fraction of incident solar radiation on a fenestration aperture that enters the building as heat [112, 113] is an important parameter. The solar heat gain coefficient, F can be estimated as a function of the transmittance and absorptance of the glazing and the fraction of absorbed solar radiation that enters the building. This calculation calls for estimating the incident solar radiation on the fenestration system. Methods reported in [112, 113] for the fraction of absorbed solar radiation are essentially thumb rules. For energy analyses including hourly building performance simulation calculations, it is suggested that further studies on angle-dependent values of solar heat gain coefficient (SHGC) be developed [112].

In almost all passive devices, solar radiation is absorbed, conducted, radiated or convected into the space. The absorbing surface may be a part of a heat loosing surface of the structure. In general, net energy transfer due to a receiver comprises of energy gain from the solar radiation and the thermal loss from the receiver. The specific transmittance or absorptance associated with the receiver differ from system to system. Over a short period of time (say, 1 hour), net energy transfer, Q_r, from a receiver of area, A_r, can be expressed as,

$$Q_r = A_r \left[I_b R_b f_i \eta_1 + K_2 I_d \eta_2 + K_3 I \eta_3 \right] - A_r U_L \left(T_r - T_a \right) \tag{1.12}$$

In Eq. (1.12), I_b, I_d and I are hourly direct, diffuse and global solar radiation values on a horizontal surface; R_b is the tilt factor for direct radiation; f_i is the instantaneous shading factor defined as the ratio of direct solar radiation received by a shaded receiver to that on an unshaded receiver ($f_i = 1$, if the window is unshaded); f_i can be estimated from the algorithm developed by Tseng-Yao Sun [114]. K_2 and K_3 are constants already defined in Eqs. (1.4) and (1.5); U_L is the heat loss coefficient for the receiver; T_r is the room temperature and T_a is the ambient temperature; η_1, η_2 and η_3 are the optical factors associated with direct, diffuse and ground reflected components of solar radiation which

depend on the specific receiver. For example, for direct gain window,

$$\eta_1 = \alpha_e \tau_b \qquad \eta_2 = \alpha_e \tau_d \qquad \text{and} \qquad \eta_3 = \alpha_e \tau_g \tag{1.13}$$

where, α_e is the effective absorptance of the window-room combination; τ_b, τ_d and τ_g are respectively the transmittance for direct, diffuse and ground reflected components of solar radiation at appropriate angles of incidence; The effective absorptance, α_e can be estimated according to Duffie and Beckman (see Chapter 5, Section 5.11). For collector-storage-wall, η_1, η_2 and η_3 are given by,

$$\eta_1 = (\tau\alpha)_b \qquad \eta_2 = (\tau\alpha)_d \qquad \text{and} \qquad \eta_3 = (\tau\alpha)_g \tag{1.14}$$

It may be noted that $(\tau\alpha)_b$ is a function of the angle of incidence which varies with time during the day.

Just as in the case of active solar energy systems, method to predict long term performance of passive solar energy systems also may be classified as simulations and design methods. A brief review of these is presented in the following.

1.2.1 Simulations

Although experiments are the best tools to determine long term performance of solar energy systems, system scale experiments are very limited in the literature for passive solar energy systems. Like active solar energy systems, methods have been developed to simulate the components of passive solar energy systems. Eq. (1.12) forms the basis for simulations for passive solar energy devices. It may be noted that Eq. (1.12) gives the net energy transfer across the receiver (a passive device) and not the useful energy gain. Eq. (1.12), when combined with the load on the system and performance of other components (storage etc.), determines the useful energy gain from the passive system. PASOLE [115] is one simulation program developed by McFarland of Los Alamos National Laboratory. Later versions (Version 12.1 and above) of TRNSYS [5] can also be used for simulating building energy systems. Numerous building simulation programs for commonly employed components in the building have been developed. The widely used ones are: ESP – Building energy simulation systems [116], is used to simulate coupled heat and mass flows in integrated building and plant systems; BLAST [117], The Building Loads Analysis and System Thermodynamics uses heat balance method and is used to simulate building mechanical systems like fans; WINDOW [118] and VISSION [119], are used to simulate solar optical and heat transfer calculations to arrive at centre-glass U-factors and solar heat gain values.

1.2.2 Design Methods

To estimate the long term (monthly) average net energy transfer, Eq. (1.12) can be summed up over a month for all hours and all days. Such calculations are conveniently replaced (though some accuracy may be lost) by monthly average calculations. Monthly average net energy transfer, $\bar{Q}_r$, as given in [6] is expressed as,

$$\begin{aligned} \bar{Q}_r &= A_r \left[\bar{H}_b \bar{R}_b \bar{f}_i \bar{\eta}_1 + K_2 \bar{H}_d \bar{\eta}_2 + K_3 \bar{H} \bar{\eta}_3\right] - 24 A_r \bar{U}_L \left(\bar{T}_r - \bar{T}_a\right) \\ &= A_r \bar{S} - 24 A_r \bar{U}_L \left(\bar{T}_r - \bar{T}_a\right) \end{aligned} \tag{1.15}$$

where, $\bar{H}_b$, $\bar{H}_d$ and $\bar{H}$ are the monthly average daily direct, diffuse and global solar radiation values on a horizontal surface; $\bar{R}_b$ is the monthly average tilt factor for direct radiation; $\bar{f}_i$ is the monthly average daily shading factor; $\bar{\eta}_1$, $\bar{\eta}_2$ and $\bar{\eta}_3$ are the monthly average optical factors for direct, diffuse and ground reflected components of solar radiation respectively; $\bar{U}_L$ is the monthly average loss coefficient; $\bar{T}_r$ and $\bar{T}_a$ are respectively the monthly average receiver and ambient temperatures. $\bar{S}$ is the monthly average energy absorbed by the receiver per unit receiver area. Eq. (1.15) becomes available to estimate $\bar{Q}_r$ through a single calculation when $\bar{f}_i$ can be calculated. Other monthly average parameters in Eq. (1.15) have already been discussed.

The energy balance on a building as a whole or a passive solar energy system in general, shows four major energy flow terms across the boundaries. The two input streams are the solar energy absorbed in the building, $A_r \bar{S}$ and the auxiliary energy added, L_A. The outputs are the excess that cannot be used or stored without driving the room temperature to unacceptably high (the 'dumped' energy, Q_D) and the load, L (comprising of the skin losses and infiltration losses minus the internal energy generation). The auxiliary energy required for a month, neglecting differences in stored energy at the beginning and end of the month, will be,

$$L_A = A_r \bar{S} - Q_D - L \tag{1.16}$$

Similar to the useful energy gain from solar collectors employed in active systems, Eq. (1.15) gives the energy available for heating/cooling by passive means. Eq. (1.15) is the analogous of long term useful energy gain for active systems, except, that the loss is for 24 hours in the case of passive systems.

The Solar Load Ratio (SLR) method [120, 121], is widely used for designing direct gain, collector-storage-wall and sunspace systems. The SLR method is a means of calculating annual requirements for auxiliary energy based on extensive simulation studies of performance of many passive heating systems done with the simulation program PASOLE [115]. Although SLR method gives annual requirements for auxiliary energy within an

accuracy of 3%, monthly values can be erroneous.

Empirical correlations of simulation results have proved their applicability in designing standard passive solar heating systems as well. The unutilizability method (also called UU-method) of Monsen, Klein and Beckman [122, 123] is another design method applicable to direct gain and collector-storage-wall systems based on the concept that a passively heated building can be viewed as a collector with finite heat capacity. Correlations are developed for estimating the auxiliary energy requirement of two limiting cases, i.e., an infinite capacitance structure that can store all energy in excess of loads and a zero capacitance structure that can store no energy. Then the correlations are used to determine the auxiliary energy requirement of a real structure which lies between these limits.

Depending on the monthly energy flow streams entering and leaving a passive structure, at times there will be insufficient solar energy to meet the loads and auxiliary energy must be supplied to the system. There will also be times when there is excess solar energy absorbed that is not used to meet the losses and can not be stored and hence the excess energy must be dumped or vented. In case of infinite capacity structure, all absorbed energy in excess of the load is stored in the structure, maintaining a constant temperature of the conditioned space. A monthly energy balance gives the auxiliary energy requirement for infinite capacity structure, $L_{A,i}$, as,

$$L_{A,i} = (L - A_r \bar{S} N)^+ \tag{1.17}$$

where, N is the number of days in the month. The superscript plus sign indicates that only positive differences are considered, i.e., when $(L - A_r \bar{S} N) < 0$, $(L - A_r \bar{S} N) = 0$.

In the case of zero capacity structure, since there is no storage capacity, energy deficits must be made up by auxiliary energy supply and excess solar energy is dumped. The temperature of the conditioned space is maintained fixed by addition or removal of energy rather than by the storage. An instantaneous energy balance on the structure gives the rate at which energy must be dumped from the structure, $\dot{Q}_D$, as,

$$\dot{Q}_D = [\, A_r I_T(\tau\alpha) - (UA)_h(T_b - T_a)\,]^+ \tag{1.18}$$

where, T_b is the building temperature and $(UA)_h$ is building load coefficients and can be calculated by standard methods e.g., ASHRAE [124].

A critical solar radiation level can be defined as that level at which the solar gain just offsets the losses and can be expressed as,

$$I_{T,c} = \frac{(UA)_h\,(T_b - T_a)}{A_r(\tau\alpha)} \tag{1.19}$$

In this case, absorbed radiation above the critical level must be dumped and is unutilizable. The dumped energy for the month, Q_D, can be estimated by summing up Eq. (1.18) over the month as,

$$Q_D = A_r(\overline{\tau\alpha}) \int_{month} (I_T - I_{T,c})^+ \, dt \tag{1.20}$$

Eq. (1.20) can be expressed in terms of the monthly average daily utilizability, ϕ, as,

$$Q_D = A_r \bar{S} N \bar{\phi} \tag{1.21}$$

The auxiliary energy requirement of a zero capacity structure is thus, load plus dumped energy minus absorbed solar energy and can be expressed as,

$$L_{A,z} = L\,(1 - \bar{\phi}) A_r \bar{S} N \tag{1.22}$$

It is warranted from Eq. (1.15) that evaluation of the monthly average shading factor, $\bar{f}_i$, is necessary for the calculation of average solar energy gains from a direct gain system. Shading by horizontal overhangs for vertical windows have been studied by different researchers. Utzinger and Klein [125] defined instantaneous shading factor, f_i, as the fraction of beam irradiated area (the ratio of beam irradiated area of the window to the total area of the window) and suggested expressions for the monthly average daily shading factor, $\bar{f}_i$. Utzinger and Klein [125] evaluated the shading factor numerically under extra-terrestrial condition using the algorithm developed by Tseng Yao Sun [114] and presented the results in graphical form, for only south facing surfaces with different overhang parameters. Jones [126] developed a method to evaluate the total radiation over a surface shaded by an overhang of infinitely long extent so that the end effect can be neglected. But Jones' [126] calculation was based on, evaluation of the tilt factor, $\bar{R}_b$, under extra-terrestrial condition. Sharp [127] presented an analytical solution to the calculation of monthly average insolation on shaded surface at any tilt and azimuth under extra-terrestrial condition. Yanda and Jones [128] presented analytical methods for calculating monthly average insolation on a vertical surface facing towards the equator with overhang shading of finite lateral extent, also under extra-terrestrial conditions. Studies on monthly average shading factor due to wingwalls in conjunction with the overhang which is commonly referred to as egg-crate structures have been reported by Barozzi and Grossa [129]. Another study by Delsante and Spencer [130] dealt with the estimation of the proportion of sky seen by windows shaded by horizontal or vertical projections which can be used to calculate the diffuse radiation incident on the shaded window. Works carried out by Acharya [94] and Lahiri [67] showed that there is a considerable difference in the value of monthly average tilt factor, $\bar{R}_b$, evaluated under extra-terrestrial and terrestrial conditions for both south facing and non-south facing surfaces. So, a similar trend can be expected in the case of monthly average shading factor, $\bar{f}_i$ also.

1.3 Summary of drawbacks and limitations of existing methods

From the review presented in § 1.1 on active solar energy systems it is evident that long term system performance is assessed based on simulations or design methods that make use of one calculation for each month or one yearly calculation. Third approach pertains to analytical calculations with varying degrees of limitations. Simulations require, in addition to the component models, a large body of meteorological information typically on hourly time scales, calling for enormous computational resources. When the data is not available, use of synthetic data is resorted to with an associated penalty on accuracy. Thus, simulations are, in general, not ideal for routine design and small scale systems.

Design methods, particularly, the f-chart and $\bar{\phi}$, f-chart methods to a certain extent fulfil the need to make available quick and inexpensive means for sizing active solar energy systems. However, they are valid for standard system configurations. Also, the correlations are composite in terms of the performance of the solar collectors and other components in the system. Thus, it is desirable to re-examine methods to estimate long term useful energy gain for principal types of solar collectors. It appears, within the framework of available models for diffuse sky radiation, methods to estimate monthly solar radiation received by the solar collectors are general enough. Similarly, monthly average daily utilizability for principal solar collectors can be estimated within a few percent of accuracy through several correlations or by single day calculation. The single day is the equivalent mean day (EMD) as defined in the studies of Acharya [94], Lahiri [67] and Choudhury [39]. However, a limitation on all the methods to estimate $\bar{\phi}$ is that the critical radiation level is assumed to be constant. Accounting for variable critical level calls for details of the operational strategy of the system, making thereby calculation of $\bar{\phi}$ iterative and not a simple meteorologic and critical level statistic.

Estimation of the monthly average useful energy gain for principal types of solar collectors also needs an appropriately defined long term average optical efficiency. Though, methods to estimate $(\overline{\tau\alpha})$ for flat plate collectors are available as a weighted average of incident solar radiation, a further examination on this definition is warranted particularly, since Collares-Pereira and Rabl [68, 69] defined an average optical efficiency during the operational time period of the collectors. Explicit methods to estimate even the monthly operating time period for solar collectors is not available. Expressions to evaluate monthly average optical efficiency for concentrating collectors need to be developed. The methods to evaluate $(\overline{\tau\alpha})/(\tau\alpha)_n$ need to be general enough to include non-south facing collectors also, in view of it's applicability for passive structures.

Monthly average performance of passive systems critically depends on the solar radiation falling on the receiver. It may be noted in general, the receivers that form part of a passive system are shaded by overhangs, wingwalls or a combination of both and even by adjacent structures. In view of the importance of the SHGC for architects and in applications such as direct heat gain systems, trombe walls methods to estimate solar radiation falling on shaded surfaces of general orientation need to be further studied. A key parameter in such estimates is the monthly average shading factor. The methods reported in the literature evaluate the shading factor under extra-terrestrial conditions.

1.4 Scope and Objectives

The review of the literature given in §1.1 and §1.2 and the drawbacks summarized in §1.3 motivated the studies on the following aspects. The studies pertain to arriving at a definition for the long term (monthly) average optical efficiency for flat plate collectors and concentrating collectors and develop methods to evaluate the same. The monthly average optical efficiency is defined so as to be consistent with the definition of monthly average daily utilizability and yields the monthly average daily useful energy delivered by the collector per unit area as a product of heat removal factor, monthly average daily solar radiation falling on the collector aperture, monthly average daily utilizability and monthly average optical efficiency. The second study pertains to obtaining monthly average shading factors for surfaces shaded by overhangs and wingwalls. In order to develop an understanding and methods to evaluate the aforementioned parameters the following topics which form the subject matter of chapters 2 to 6 have been studied.

1. Monthly useful energy gain and a definition of transmittance-absorptance product for flat plate collectors.
2. Evaluation of monthly average transmittance-absorptance product during the operational time period for flat plate collectors.
3. Evaluation of monthly average optical efficiency during the operational time period for parabolic trough concentrators.
4. Evaluation of monthly average shading factor for surfaces shaded by overhangs under terrestrial conditions.
5. Evaluation of monthly average shading factor for surfaces shaded by wingwalls under terrestrial conditions.

Chapter 2 is devoted to studies on calculating the daily and the monthly average daily useful energy gain for flat plate collectors. The study reported in Chapter 2 is

aimed to establish validity or otherwise of calculating monthly average daily transmittance-absorptance product, $(\overline{\tau\alpha})$, as a mean day calculation (as defined by Klein [95]). When a flat plate collector is supplying energy above a minimum temperature, T_{min}, the critical radiation level, I_c, is given by,

$$I_c = \frac{F_R U_L (T_i - T_a)}{F_R(\tau\alpha)} \tag{1.23}$$

Useful energy gain for a day, $Q_{u,day}$, per unit area of the collector is evaluated according to,

$$Q_{u,day} = F_R \sum_{hours} (I_T - I_c)^+ (\tau\alpha) \tag{1.24}$$

If $(\tau\alpha)_{day}$ is the transmittance-absorptance product defined as,

$$(\tau\alpha)_{day} = \sum_{hours} I_T (\tau\alpha) / \sum_{hours} I_T \tag{1.25}$$

Let $Q'_{u,day}$ be given by,

$$Q'_{u,day} = F_R H_T (\tau\alpha)_{day} \phi_{day} \tag{1.26}$$

where, ϕ_{day} is the utilizability for a single day and is defined by,

$$\phi_{day} = \frac{\sum (I_T - I_c)^+}{\sum I_T} \tag{1.27}$$

If $Q_{u,day}$ given by Eq. (1.24) is equal to $Q'_{u,day}$ given by Eq. (1.26), defining $(\tau\alpha)_{day}$ according to Eq. (1.25) is correct. Chapter 2 examines the validity of defining $(\tau\alpha)_{day}$. In order that Eq. (1.26) yields useful energy gain correctly [equal to the energy gain given by Eq. (1.24)], $(\tau\alpha)_{day}$ needs to be defined as,

$$(\tau\alpha)^*_{day} = \frac{\sum (I_T - I_c)^+ (\tau\alpha)}{\sum (I_T - I_c)^+} \tag{1.28}$$

It may be noted that, the notation $(\tau\alpha)^*_{day}$ has been employed to designate the present transmittance-absorptance product. Numerical results for $Q_{u,day}$ and $Q'_{u,day}$, given by Eqs. (1.24) and (1.26) are presented in Chapter 2 for $\phi = 20^o$, 40^o and 60^o; $(\phi - \beta) = -15^o$, 0^o, 15^o and $\beta = 90^o$; $\gamma = 0^o$, 30^o, 60^o and 90^o; for $K_T = 0.3$, 0.5 and 0.7, for non-dimensional critical levels $0 \leq X_c \leq 1$. The ratio of $Q'_{u,day}$ to $Q_{u,day}$ is also equal to the ratio of $(\tau\alpha)^*_{day}$ to $(\tau\alpha)_{day}$. Normalized difference defined by, $[(\tau\alpha)^*_{day} - (\tau\alpha)_{day}]/(\tau\alpha)_{day}$ increases as X_c, ϕ and γ increase and in general, the azimuthal angle has a significant influence.

A similar numerical examination, performed on the monthly average useful energy gain and transmittance-absorptance product, reveals that $[(\overline{\tau\alpha})^* - (\overline{\tau\alpha})]/(\overline{\tau\alpha})$ is higher than the corresponding single day value, i.e. when K_T for the day is numerically equal to

$\bar{K}_T$ of the month and for a fixed I_c. Thus, the studies reported in Chapter 2 establish the need to develop method to evaluate $(\overline{\tau\alpha})^*$ according to Eq. (1.28) written for the month.

Chapter 3 is devoted to develop methods to evaluate the monthly average transmittance-absorptance product, $(\overline{\tau\alpha})^*/(\tau\alpha)_n$, defined as a weighted average over all hours and all days in a month, the weighting function being the solar radiation on the collector surface above the critical radiation level. An expression valid for the transmittance-absorptance product for the single day $(\tau\alpha)^*_{day}/(\tau\alpha)_n$ has been developed using integral equivalent of Eq. (1.28). I_T has been expressed in terms of r_t [12] and r_d [16] correlations. Numerical values obtained employing the expressions for $(\tau\alpha)^*_{day}/(\tau\alpha)_n$ have been validated by comparing with the hour by hour calculations according to Eq. (1.28) employing solar radiation data.

In order to obtain the monthly average transmittance-absorptance product, $(\overline{\tau\alpha})^*/(\tau\alpha)_n$, equivalent mean day (EMD) approach as explained in §1.1.4, has been adapted. Basically, the procedure involves calculating $(\tau\alpha)^*_{day}/(\tau\alpha)_n$ on the EMD which is characterized by $\delta = \delta_m$ and $K_T = \bar{K}^*_T$. $\bar{K}^*_T$ is the average clearness index of the days that contribute to useful energy. $(\overline{\tau\alpha})^*/(\tau\alpha)_n$ values obtained according to the EMD calculation have been validated by comparing with the values obtained by detailed hour by hour calculations.

Monthly average optical efficiency for concentrating collectors also has been defined as a weighted average over all hours and all days in the month, the weighting function being the solar radiation on the collector aperture above the critical radiation level. Following the procedure similar to that for flat plate collectors, studies to evaluate the monthly average optical efficiency for concentrating collectors tracked in five principal modes have been reported in Chapter 4. Expressions developed for $(\eta^*_{o,day}/\eta_{o,n})$ have been validated against hour by hour computations employing solar radiation data. The results include evaluating the influence of the diffuse fraction, cut-off time and dependence on latitude. The monthly average optical efficiency, $(\bar{\eta}^*_o/\eta_{o,n})$ has been obtained by following the EMD approach and validated by comparing against the values obtained by hour by hour computations. The numerical results and the validation have been discussed for a wide range of the parameters, latitudes, declination, clearness index, critical radiation level for concentrating collectors tracked in the five principal modes.

The importance of estimating the solar radiation received by shaded surfaces has already been emphasised in §1.2. The methods reported in the literature deal with estimating monthly average shading factor, $\bar{f}_i$, under extra-terrestrial conditions. Even under extra-terrestrial conditions, for finite overhangs, Yanda and Jones' [128] method of shading plane concept is available for south facing surfaces only. Studies available in the literature

[66, 67] show that the monthly average daily tilt factor for direct radiation depends significantly on the atmospheric transmittance, particularly, for non-south facing surfaces. Since, the shaded windows can have a general orientation (not facing the equator only) it can be expected that the monthly average shading factor values, taking atmospheric transmittance into account, differ from the values under extra-terrestrial conditions. Studies on evaluating the monthly average shading factors for receivers shaded by infinite or finite overhangs are reported in Chapter 5. The monthly average shading factor for infinite overhangs, $\bar{f}_{i\infty}$ under terrestrial condition has been evaluated, on the mean day of the month, according to,

$$\bar{f}_{i\infty} = \frac{\int I_b R_b f_i \, d\omega}{\int I_b R_b \, d\omega} \tag{1.29}$$

I_b in Eq. (1.29) has been expressed employing the correlations for r_t [12] and r_d [16]. Eq. (1.29) is integrable when the overhang is infinite and yields expressions which are equivalent to the expressions obtained by Jones [126] using the shading plane concept. Also, formalization of $\bar{f}_{i\infty}$ according to Eq. (1.29) allowed generalization for non-vertical receivers. Numerical values obtained for $\bar{f}_{i\infty}$ have been validated by comparing with the values obtained employing solar radiation data. The influence of including atmospheric transmittance in evaluating $\bar{f}_{i\infty}$ is significant, particularly, for low latitudes in summer months and when the receivers are non-south facing. $\bar{f}_{i\infty}$ differs from the corresponding extra-terrestrial value by 30 % when $\phi = 30^o$, $\gamma = 30^o$ and $D_f = 0.4$ for typical overhang parameters, the non-dimensional projection $p = 0.3$ and height of the window being equal to the width.

Eq. (1.29) is not amenable for integration when the overhang is finite. In order to alleviate this difficulty, monthly average shading factor values for finite overhangs, $\bar{f}_i$ have been related to the infinite overhang shading factor values as a function of the extension of the overhang. The correlations and the procedure developed to obtain $\bar{f}_i$ values from $\bar{f}_{i\infty}$ values have been validated for a wide range of latitudes and climatic conditions as indicated by the monthly average daily diffuse fractions for south as well as for non-south facing receivers.

Starting from an equation similar to Eq. (1.29), expressions for $f_{i\infty}$, for receivers shaded by infinite wingwalls have been developed and are reported in Chapter 6. $f_{i\infty}$ for wingwalls also can be interpreted in terms of the shading plane concept with the following differences.

1. Eq. (1.29) needs to be integrated piece-wise from ω_{sr} to ω_o and from ω_o to ω_{ss}. ω_{sr} and ω_{ss} are the apparent sunrise and sunset hour angles. ω_o is the hour angle when solar azimuthal angle equal to the receiver azimuthal angle.

2. Shading plane for the wingwall is the plane joining the outer edge of the wingwall to the opposite side of the receiver. Thus, the shading plane for the wingwall is characterized with an azimuthal angle different for the receiver azimuthal angle.

Tabulated values of the shading factor for wingwalls for a wide range of latitudes, clearness indices and projection of the wingwalls are also given in Appendix D.

Chapter 7 summarizes the significant results of the present study.

Chapter 2

Monthly Useful Energy Gain and a Definition of Transmittance-Absorptance Product for Flat Plate Collectors

2.1 Introduction

It is perceived that the monthly average daily useful energy gain for a flat plate collector of unit area can be obtained as a product of heat removal factor, monthly average daily solar radiation falling on the collectors, monthly average daily utilizability and an appropriate average transmittance-absorptance product. Klein [95] introduced a monthly average transmittance-absorptance product, $(\overline{\tau\alpha})$, calculated on the average day of the month, which is also a key parameter in calculating the non-dimensional absorbed energy (one of the variables in f-chart [54, 55, 56] and $\bar{\phi}$, f-chart [61, 62] correlations). Collares-Pereira and Rabl [68, 69], however, used the terminology of average optical efficiency pertinent to the collector operating time period, though no method to obtain the same is available.

In the present chapter, it is proposed to evaluate, first, daily useful energy gain as summation of hour by hour calculations. Daily useful energy gain is proposed to be obtained as a product of heat removal factor, daily solar radiation falling on the collectors, daily utilizability and an appropriate average transmittance-absorptance product. From the useful energy gain for the day obtained by hour by hour calculation, an effective transmittance-absorptance product has been evaluated. This transmittance-absorptance product has been shown to be differing from the transmittance-absorptance product evaluated following Klein's [95] procedure for the day. This difference is found to be dependent on clearness index and critical radiation level, in addition to the latitude, declination, slope and azimuth angle.

Calculations similar to those described above for the single day have also been performed to obtain the monthly average daily useful energy gain and a monthly average transmittance-absorptance product, to be associated with the product of F_R, $\bar{H}_T$ and $\bar{\phi}$, so that the correct monthly average daily useful energy gain can be obtained. Like the transmittance-absorptance product for a day, monthly average transmittance-absorptance product which yields the correct monthly average daily useful energy gain differs from the monthly average daily transmittance-absorptance product obtained by Klein's [95] procedure.

2.2 Daily Useful Energy Gain

Consider a flat plate collector characterized by $F_R(\tau\alpha)_n$ and $F_R U_L$, where, F_R is the collector heat removal factor; $(\tau\alpha)_n$ is the transmittance-absorptance product at normal incidence and U_L is the overall heat loss coefficient of the collector. The flat plate collector is delivering energy at or above a minimum temperature of T_{min}, which corresponds to a critical radiation level of I_c. Let, K_T be the daily clearness index. For such a collector of unit area, daily useful energy gain can be obtained from,

$$Q_{u,day} = F_R(\tau\alpha)_n \sum_{hour} [I_T - I_c]^+ (\tau\alpha)/(\tau\alpha)_n \tag{2.1}$$

where, $(\tau\alpha)$ is the transmittance-absorptance product for the collector-cover system at the hour angle, ω, centered for the hour in question. The superscript plus sign is used to mean that only the positive differences will be considered in the summation process and when $(I_T - I_c) < 0$, $(I_T - I_c) = 0$. I_T in Eq. (2.1) can be expressed, comprising of direct, diffuse and ground reflected components as,

$$I_T = I_b R_b + K_2 I_d + K_3 I \tag{2.2}$$

where, K_2 and K_3 are constants as defined by Eqs. (1.4) and (1.5) of Chapter 1. I, I_b and I_d are the hourly global, direct and diffuse components of solar radiation on a horizontal surface. R_b is the tilt factor for direct radiation and is evaluated from,

$$R_b = \frac{\cos\theta}{\cos\theta_z} \tag{2.3}$$

The angle of incidence, θ, for a surface of general orientation can be expressed as,

$$\cos\theta = A + B\cos\omega + C\sin\omega \tag{2.4}$$

where, the constants A, B and C are given by,

$$A = \sin\delta(\sin\phi\cos\beta - \cos\phi\sin\beta\cos\gamma) \tag{2.5}$$

$$B = \cos\delta(\cos\phi\cos\beta + \sin\phi\sin\beta\cos\gamma) \tag{2.6}$$

$$C = \cos\delta\sin\beta\sin\gamma \tag{2.7}$$

In Eq. (2.3), θ_z is the angle of incidence for a horizontal surface (β=0), also called the zenith angle and is given by,

$$\begin{aligned} \cos\theta_z &= \cos\phi\cos\delta\cos\omega + \sin\phi\sin\delta \\ &= A' + B'\cos\omega \\ &= B'(\cos\omega - \cos\omega_s) \end{aligned} \tag{2.8}$$

where,

$$A' = \sin\phi\sin\delta \qquad \text{and} \qquad B' = \cos\phi\cos\delta \tag{2.9}$$

In Eqs. (2.5) to (2.8), ϕ is the latitude (north positive) of the location, δ is the declination and γ is the surface azimuthal angle, '-ve' towards east. δ can be obtained [see, Duffie and Beckman [6]] from,

$$\delta = 23.45 \sin\left(360\,\frac{284+n}{365}\right) \tag{2.10}$$

The ratio of the transmittance-absorptance product at any incidence angle to that at normal incidence, $(\tau\alpha)/(\tau\alpha)_n$, can be expressed as,

$$\frac{(\tau\alpha)}{(\tau\alpha)_n} = \frac{I_b R_b (\tau\alpha)_b/(\tau\alpha)_n + K_2 I_d (\tau\alpha)_d/(\tau\alpha)_n + K_3 I (\tau\alpha)_g/(\tau\alpha)_n}{I_b R_b + K_2 I_d + K_3 I} \tag{2.11}$$

where, $(\tau\alpha)_b/(\tau\alpha)_n$, $(\tau\alpha)_d/(\tau\alpha)_n$ and $(\tau\alpha)_g/(\tau\alpha)_n$ are the transmittance-absorptance product ratios for the direct, diffuse and ground-reflected components of solar radiation. $(\tau\alpha)_b/(\tau\alpha)_n$ is evaluated corresponding to the angle of incidence θ. $(\tau\alpha)_d/(\tau\alpha)_n$ and $(\tau\alpha)_g/(\tau\alpha)_n$ are evaluated at θ_d and θ_g, the effective angles of incidence for sky diffuse and ground reflected components of solar radiation respectively. θ_d and θ_g have been correlated to β by Brandemuehl and Beckman [98] as,

$$\theta_d = 59.7 - 0.1388\beta + 0.001497\beta^2 \tag{2.12}$$

$$\theta_g = 90 - 0.5788\beta + 0.002693\beta^2 \tag{2.13}$$

The variation of $(\tau\alpha)/(\tau\alpha)_n$ with incidence angle, valid in the range of $0^o \le \theta \le 60^o$, is obtained from ASHRAE [42] as,

$$\frac{(\tau\alpha)}{(\tau\alpha)_n} = 1 + b_o\left(\frac{1}{\cos\theta} - 1\right) \qquad \text{for} \quad 0^o \le \theta \le 60^o \tag{2.14}$$

Visalakhsi [44] presented an expression for $(\tau\alpha)/(\tau\alpha)_n$ for the range $60^o < \theta \le 90^o$ as,

$$\frac{(\tau\alpha)}{(\tau\alpha)_n} = 2\,(1 + b_o)\cos\theta \qquad \text{for} \quad 60^o < \theta \le 90^o \tag{2.15}$$

which agrees closely with the data values given in [43]. In Eqs. (2.14) and (2.15), b_o is the incidence angle modifier coefficient.

Since the objective of the present chapter has been to obtain an appropriate transmittance-absorptance product that yields daily useful energy gain, $Q_{u,day}$, as a product of F_R, H_T, ϕ_{day} and the appropriate transmittance-absorptance product, it is proposed to calculate $Q_{u,day}$ using Eq. (2.1) employing r_t and r_d correlations to obtain I, I_d and I_b. The correlations for r_t and r_d due to Collares-Pereira and Rabl [12] and Liu and Jordan [16] are given by,

$$r_t = I/H = K_1\,(a + b\cos\omega)(\cos\omega - \cos\omega_s) \tag{2.16}$$

$$r_d = I_d/H_d = K_1\,(\cos\omega - \cos\omega_s) \tag{2.17}$$

H and H_d are the daily global and diffuse radiation on a horizontal surface. ω_s is the sunset hour angle for a horizontal surface given by

$$\omega_s = \cos^{-1}\left[-\tan\phi\,\tan\delta\right] \tag{2.18}$$

The constants K_1, a and b are given by,

$$K_1 = \pi/[24(\sin\omega_s - \omega_s\cos\omega_s)] \tag{2.19}$$

$$a = 0.409 + 0.5016\sin(\omega_s - \pi/3) \tag{2.20}$$

$$b = 0.6609 - 0.4767\sin(\omega_s - \pi/3) \tag{2.21}$$

The correlation for r_d which takes in to account a climatic parameter, namely, the daily (or monthly average daily) diffuse fraction, $D_f = H_d/H$ (or $\bar{D}_f = \bar{H}_d/\bar{H}$), from [15] is given by,

$$r_d = K_1\,(a' + b'\cos\omega)(\cos\omega - \cos\omega_s) \tag{2.22}$$

where a' and b' are evaluated as

$$a' = \begin{cases} 0.4922 + 0.27/D_f & \text{for} \quad 0.1 \le D_f \le 0.7 \\ 0.76 + 0.113/D_f & \text{for} \quad 0.7 < D_f \le 0.9 \end{cases} \tag{2.23}$$

$$b' = 2(1 - a')(\sin\omega_s - \omega_s\cos\omega_s)\;/(\omega_s - 0.5\sin 2\omega_s) \tag{2.24}$$

When $a' = 1$ and $b' = 0$ is put in Eq. (2.22), Eq. (2.22) reduces to Eq. (2.17). In the present investigation correlations due to Collares-Pereira and Rabl [12] and Liu and Jordon [16] have been employed since most of the calculations are ratios and no significant difference is made when Eq. (2.17) is used instead of Eq. (2.22).

When the daily clearness index, K_T $(=H/H_o)$ is known, the hourly components of solar radiation, viz. I, I_d and I_b $(=I - I_d)$ can be expressed making use of the correlations for r_t and r_d given by Eqs. (2.16) and (2.17) as,

$$I = K_1 K_T H_o\,(a + b\cos\omega)(\cos\omega - \cos\omega_s) \tag{2.25}$$

$$I_d = K_1 K_T H_o D_f\,(\cos\omega - \cos\omega_s) \tag{2.26}$$

$$I_b = r_t H - r_d H_d = K_1 K_T H_o\,(a_1 + b\cos\omega)(\cos\omega - \cos\omega_s) \tag{2.27}$$

where,

$$a_1 = a - D_f \tag{2.28}$$

In Eqs. (2.25) to (2.27), H_o is the daily extraterrestrial radiation on a horizontal surface. D_f is the daily diffuse fraction. I_T given by Eq. (2.2), can now be expressed, using Eqs. (2.25) to (2.27) as,

$$\begin{aligned} I_T &= \frac{K_1 K_T H_o}{B'}\Big[(a_1 + b\cos\omega)\cos\theta + K_2 D_f B'(\cos\omega - \cos\omega_s) \\ &\quad + K_3 B'(a + b\cos\omega)(\cos\omega - \cos\omega_s)\Big] \end{aligned} \tag{2.29}$$

Critical radiation level of I_c corresponds to a non-dimensional critical level, X_c, for the day and is defined as,

$$X_c = \frac{I_c}{I_{T,m}} \tag{2.30}$$

It may be noted that, $I_{T,m}$ is the maximum solar radiation falling on the collector during the day which occurs at $\omega = \omega_m$. Generally, $\omega_m = 0.0$, for south facing collectors. $I_{T,m}$ is expressed as,

$$I_{T,m} = r_{t,m} R_m K_T H_o \tag{2.31}$$

In Eq. (2.31), R_m is to be evaluated from,

$$R_m = \left[1 - D_f\left(\frac{r_{d,m}}{r_{t,m}}\right)\right] R_{b,m} + K_2 D_f\left(\frac{r_{d,m}}{r_{t,m}}\right) + K_3 \tag{2.32}$$

$r_{t,m}$, $r_{d,m}$ and $R_{b,m}$ in Eqs. (2.31) and (2.32) are r_t, r_d and R_b at $\omega = \omega_m$. $I_{T,m}$ analogous to Eq. (2.29) can be written as,

$$\begin{aligned} I_{T,m} &= \frac{K_1 K_T H_o}{B'}\Big[(a_1 + b\cos\omega_m)\cos\theta_m + K_2 D_f B'(\cos\omega_m - \cos\omega_s) \\ &\quad + K_3 B'(a + b\cos\omega_m)(\cos\omega_m - \cos\omega_s)\Big] \end{aligned} \tag{2.33}$$

where, θ_m is the angle of incidence at $\omega = \omega_m$.

Eq. (2.1) can be re-written using Eqs. (2.16) and (2.17) for r_t and r_d and Eq. (2.30) for I_c as,

$$\begin{aligned} Q_{u,day} &= F_R K_T H_o (\tau\alpha)_n \sum [r_t R - r_{t,m} R_m X_c]^+ (\tau\alpha)/(\tau\alpha)_n \\ &= F_R K_1 K_T H_o (\tau\alpha)_n \sum [R(a + b\cos\omega)(\cos\omega - \cos\omega_s) - R_m X_c (a + b\cos\omega_m) \\ &\quad \times(\cos\omega_m - \cos\omega_s)]^+ (\tau\alpha)/(\tau\alpha)_n \end{aligned} \tag{2.34}$$

In Eq. (2.34), R is the tilt factor at ω which can be obtained from Eq. (2.32), re-written without the subscript m for r_t, r_d etc.

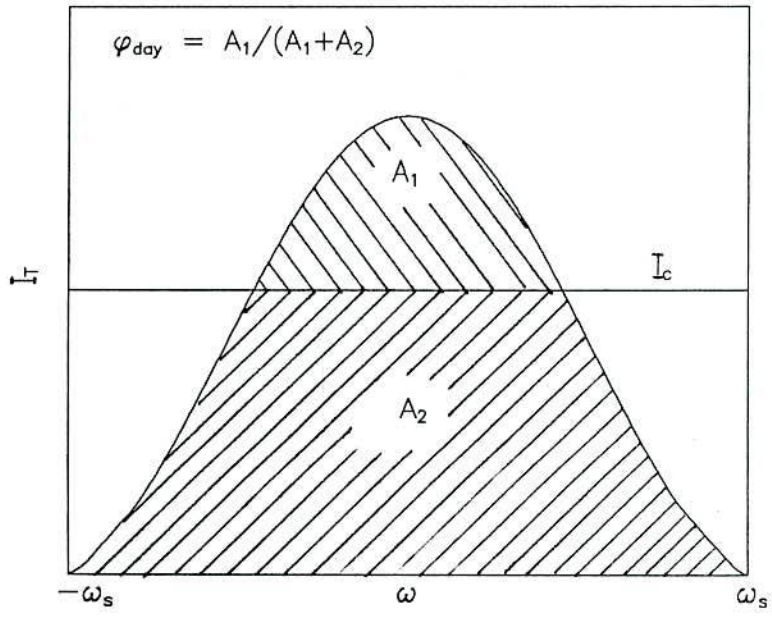

Figure 2.1: Graphical depiction of daily utilizability

Utilizability for a day, ϕ_{day} is defined as,

$$\phi_{day} = \sum_{-\omega_s}^{\omega_s} [I_T - I_c]^+ \Big/ \sum_{-\omega_s}^{\omega_s} I_T \tag{2.35}$$

Graphically, ϕ_{day} is depicted in Figure 2.1. It is desired that $Q_{u,day}$ is given by,

$$Q_{u,day} = F_R(\tau\alpha)^*_{day} H_T \phi_{day} \tag{2.36}$$

subject to a suitable evaluation of $(\tau\alpha)^*_{day}$. Not withstanding how $(\tau\alpha)^*_{day}$ is to be calculated, $(\tau\alpha)^*_{day}$ should be equal to,

$$(\tau\alpha)^*_{day} = \frac{Q_{u,day}}{F_R H_T \phi_{day}} \tag{2.37}$$

Using Eq. (2.1) for $Q_{u,day}$ and Eq. (2.35) for ϕ_{day} in Eq. (2.37), it follows,

$$(\tau\alpha)^*_{day} = \sum [I_T - I_c]^+ (\tau\alpha) \Big/ \sum [I_T - I_c]^+ \tag{2.38}$$

Eq. (2.38) yields $(\tau\alpha)^*_{day}$ to be used in conjunction with Eq. (2.36) to obtain $Q_{u,day}$ conveniently, when simple method to calculate the RHS of Eq. (2.38) is developed.

Let $Q'_{u,day}$ be the useful energy gain as obtained from,

$$Q'_{u,day} = F_R(\tau\alpha)_{day} H_T \phi_{day} \tag{2.39}$$

where, $(\tau\alpha)_{day}$ is obtained from an expression for the day analogous to Klein's [95] method. Thus,

$$\begin{aligned}(\tau\alpha)_{day} &= \sum_{-\omega_s}^{\omega_s} I_T(\tau\alpha) \Big/ \sum_{-\omega_s}^{\omega_s} I_T \\ &= \frac{\sum r_d\left[(a_1 + b\cos\omega)R_b(\tau\alpha)_b + K_2 D_f(\tau\alpha)_d + K_3(a + b\cos\omega)(\tau\alpha)_g\right]}{\sum r_d\left[(a_1 + b\cos\omega)R_b + K_2 D_f + K3(a + b\cos\omega)\right]}\end{aligned} \tag{2.40}$$

$(\tau\alpha)_{day}$ can be obtained without going through hour by hour calculation adapting the expressions given by Sfeir [96], Acharya [94] or Choudhury [39]. However, when simple methods to estimate $(\tau\alpha)^*_{day}$ defined by Eq. (2.38) are developed, $Q_{u,day}$ as given by Eq. (2.36) can be obtained. The present chapter is concerned with examining the differences between $Q_{u,day}$ and $Q'_{u,day}$ due to employing $(\tau\alpha)_{day}$ instead of $(\tau\alpha)^*_{day}$ in Eq. (2.36). Numerical results are discussed in §2.4.

2.3 Monthly Average Daily Useful Energy Gain

Consider the flat plate collector with the characteristics as described in §2.2 which delivers energy at or above a minimum temperature of T_{min}, corresponding to a critical radiation level of I_c. It is assumed that the critical radiation level is constant through out the month. The monthly average daily clearness index is $\bar{K}_T$. For such a system, the monthly average daily useful energy gain from a flat plate collector of unit area can be obtained from,

$$\bar{Q}_{u,m} = \frac{1}{N} F_R(\tau\alpha)_n \sum_{day}\sum_{hour} (I_T - I_c)^+ (\tau\alpha)/(\tau\alpha)_n \tag{2.41}$$

where, N is the number of days in the month. Since, the objective has been to obtain an appropriate monthly average transmittance-absorptance product that yields $Q_{u,m}$ as a product of F_R, $\bar{H}_T$, $\bar{\phi}$ and the appropriate transmittance-absorptance product, it is proposed to calculate $\bar{Q}_{u,m}$, using Eq. (2.41) employing r_t and r_d correlations to obtain I, I_d and I_b. A critical radiation level of I_c, corresponds to a monthly average non-dimensional critical level, $\bar{X}_c$, defined by,

$$\bar{X}_c = \frac{I_c}{\bar{I}_{T,m}} \tag{2.42}$$

It may be noted that $\bar{I}_{T,m}$ is the maximum solar radiation falling on the collector which occurs at $\omega = \omega_m$ on the monthly mean day i.e., $\delta = \delta_m$, $K_T = \bar{K}_T$. Using r_t and r_d correlations, similar to $I_{T,m}$ [Eq. (2.33)], $\bar{I}_{T,m}$ can be expressed as,

$$\begin{aligned}\bar{I}_{T,m} &= \bar{r}_{t,m}\bar{R}_m\bar{K}_T\bar{H}_o \\ &= K_1\bar{K}_T\bar{H}_o(\cos\omega_m - \cos\omega_s)\Big[(a + b\cos\omega_m - \bar{D}_f)\bar{R}_{b,m} + K_2\bar{D}_f \\ &\quad + K_3(a + b\cos\omega_m)\Big]\end{aligned} \tag{2.43}$$

In Eq. (2.43), overbars on $r_{t,m}$ and R_m indicate that they are evaluated on the mean day of the month.

Eq. (2.41) can be re-written using Eqs. (2.16) and (2.17) for r_t and r_d and Eq. (2.12) for I_c as,

$$\bar{Q}_{u,m} = \frac{1}{N} F_R(\tau\alpha)_n \sum_{day} K_T H_o \sum_{hour} [r_t R - r_{t,m} R_m X_c]^+ (\tau\alpha)/(\tau\alpha)_n \tag{2.44}$$

$$= \frac{1}{N} F_R(\tau\alpha)_n \sum_{day} K_1 K_T H_o \sum_{hour} \Big[R\,(a + b\cos\omega)(\cos\omega - \cos\omega_s) - R_m \bar{X}_c (a + b\cos\omega_m)(\cos\omega_m - \cos\omega_s) \Big]^+ (\tau\alpha)/(\tau\alpha)_n \tag{2.45}$$

Let $\bar{\phi}$ be the monthly average daily utilizability, defined as,

$$\bar{\phi} = \sum_{day} \sum_{hour} (I_T - I_c)^+ \Big/ \sum_{day} \sum_{hour} I_T \tag{2.46}$$

It is desired that $\bar{Q}_{u,m}$ is given by,

$$\bar{Q}_{u,m} = F_R(\overline{\tau\alpha})^* \bar{H}_T \bar{\phi} \tag{2.47}$$

subject to a suitable evaluation of $(\overline{\tau\alpha})^*$. Not withstanding how $(\overline{\tau\alpha})^*$ is to be calculated, $(\overline{\tau\alpha})^*$ should be equal to,

$$(\overline{\tau\alpha})^* = \frac{\bar{Q}_{u,m}}{F_R \bar{H}_T \bar{\phi}} \tag{2.48}$$

Using Eq. (2.41) for $\bar{Q}_{u,m}$ and Eq. (2.46) for $\bar{\phi}$ in Eq. (2.47), it follows,

$$(\overline{\tau\alpha})^* = \sum_{day} \sum_{hour} (I_T - I_c)^+ (\tau\alpha) \Big/ \sum_{day} \sum_{hour} (I_T - I_c)^+ \tag{2.49}$$

Eq. (2.49) yields $(\overline{\tau\alpha})^*$ to be used in conjunction with Eq. (2.47) to obtain $\bar{Q}_{u,m}$ conveniently, when a simple method to calculate the RHS of Eq. (2.49) is developed.

Let $\bar{Q}'_{u,m}$ be the monthly average daily useful energy gain as obtained from,

$$\bar{Q}'_{u,m} = F_R(\overline{\tau\alpha}) \bar{H}_T \bar{\phi} \tag{2.50}$$

where, $(\overline{\tau\alpha})$ is obtained, as proposed by Klein [95], from,

$$(\overline{\tau\alpha}) = \sum_{day} \sum_{hour} I_T(\tau\alpha) \Big/ \sum_{day} \sum_{hour} I_T$$

$$= \frac{\sum\sum r_d [(a_1 + b\cos\omega) R_b (\tau\alpha)_b + K_2 D_f (\tau\alpha)_d + K_3 (a + b\cos\omega)(\tau\alpha)_g]}{\sum\sum r_d [(a_1 + b\cos\omega) R_b + K_2 D_f + K_3 (a + b\cos\omega)]} \tag{2.51}$$

When a simple method to evaluate $(\overline{\tau\alpha})^*$ is developed $\bar{Q}_{u,m}$ can be obtained using Eq. (2.47). The present chapter is concerned with examining the difference between $\bar{Q}_{u,m}$ and $\bar{Q}'_{u,m}$ resulting from using $(\overline{\tau\alpha})$ instead of $(\overline{\tau\alpha})^*$ in Eq. (2.47).

2.4 Results and Discussion

$Q_{u,day}$, $Q'_{u,day}$, $(\tau\alpha)_{day}$ and $(\tau\alpha)^*_{day}$ for single day calculations and $\bar{Q}_{u,m}$, $\bar{Q}'_{u,m}$, $(\overline{\tau\alpha})$ and $(\overline{\tau\alpha})^*$ for the monthly average calculations have been obtained using Eqs. (2.31), (2.39), (2.40), (2.37) and (2.45), (2.50), (2.51), (2.48) respectively. The parameter values and their ranges are as follows:

$\phi = 20^o$, 40^o and 60^oN

$\beta = \phi + 15^o$, ϕ, $\phi - 15^o$ and 90^o

$\gamma = 0^o$, 30^o, 60^o and 90^o

$-23.45^o \leq \delta \leq 23.45^o$

$b_o = -0.1$ (applicable for flat plate collectors with a single glass cover)

$0.3 \leq K_T \leq 0.7, \quad 0.0 \leq X_c \leq 0.8$

$0.3 \leq \bar{K}_T \leq 0.7, \quad 0.0 \leq \bar{X}_c \leq 1.2.$

It may be noted that $\bar{Q}_{u,m} > 0$ for $\bar{X}_c < \bar{X}_{c,max}$, where $\bar{X}_{c,max}$ corresponds to monthly average daily utilizability, $\bar{\phi} = 0$. $\bar{X}_{c,max}$ will be approximately equal to $K_{T,max}/\bar{K}_T$, where $K_{T,max}$ is the maximum daily clearness index when the monthly average daily clearness index is $\bar{K}_T$. In this chapter numerical results are presented for $0.2 \leq \bar{X}_c \leq 1.2$ since $\bar{X}_{c,max}$ varies widely say, 1.2 for $\bar{K}_T = 0.7$ to 3.0 for $\bar{K}_T = 0.3$.

2.4.1 Single Day Useful Energy Gain and Transmittance-Absorptance Product

South Facing Collectors ($\gamma = 0$)

Values of $Q_{u,day}$ $(MJ/m^2\text{-}day)$, $Q'_{u,day}$ $(MJ/m^2\text{-}day)$, $(\tau\alpha)_{day}/(\tau\alpha)_n$, $(\tau\alpha)^*_{day}/(\tau\alpha)_n$ and the percentage differences in the useful energy gain and the transmittance-absorptance product are given in Tables A.1 to A.3 of Appendix A for $\phi = 20^o$, 40^o and 60^o respectively, for $\gamma = 0$, for different slopes, clearness indices and the non-dimensional critical radiation levels. Mean declination of the month has been chosen as the declination for the day. In Tables A.1 to A.3 $(\tau\alpha)_{day}/(\tau\alpha)_n$ and $(\tau\alpha)^*_{day}/(\tau\alpha)_n$ are designated by Z and Z^*. Summary of the Tables A.1 to A.3 giving only the percentage differences is given in Tables 2.1 to 2.3. The percentage differences, Δ_d, in the useful energy gain and transmittance-absorptance product are equal and is calculated as,

$$\Delta_d = \frac{Q_{u,day} - Q'_{u,day}}{Q'_{u,day}} \times 100 = \frac{(\tau\alpha)^*_{day} - (\tau\alpha)_{day}}{(\tau\alpha)_{day}} \times 100 \qquad (2.52)$$

It may noted that Δ_d has been normalized with respect to $(\tau\alpha)_{day}$, since this is the commonly employed definition in the literature. $Q'_{u,day}$ is the corresponding useful energy gain that would be obtained. When $X_c = 0$, obviously $\Delta_d = 0$ and $(\tau\alpha)^*_{day} = (\tau\alpha)_{day}$.

Table 2.1: Percentage difference Δ_d in useful energy gain and transmittance-absorptance product, $\phi = 20^o$N, $\delta = \delta_m$, $\gamma = 0^o$

β (deg.)	X_c	Percentage difference, Δ_d								
		$K_T = 0.3$			$K_T = 0.5$			$K_T = 0.7$		
		Mar	Jun	Dec	Mar	Jun	Dec	Mar	Jun	Dec
5	0.2	0.13	0.14	0.10	0.97	0.96	1.14	2.56	2.49	3.05
	0.4	0.28	0.30	0.22	1.51	1.53	1.90	3.63	3.57	4.71
	0.6	0.45	0.47	0.36	1.83	1.86	2.28	4.14	4.07	5.40
	0.8	0.62	0.64	0.51	2.10	2.13	2.56	4.52	4.45	5.85
20	0.2	0.14	0.11	0.14	0.95	0.91	0.97	2.47	2.50	2.35
	0.4	0.29	0.24	0.29	1.45	1.65	1.41	3.43	3.90	3.33
	0.6	0.46	0.39	0.46	1.76	2.03	1.70	3.92	4.49	3.80
	0.8	0.63	0.55	0.61	2.01	2.32	1.94	4.27	4.91	4.16
35	0.2	0.13	0.07	0.17	0.98	0.75	0.74	2.53	2.46	1.67
	0.4	0.28	0.16	0.35	1.48	1.71	1.07	3.53	4.45	2.36
	0.6	0.44	0.32	0.52	1.79	2.30	1.32	4.01	5.41	2.76
	0.8	0.60	0.46	0.67	2.04	2.62	1.53	4.37	5.92	3.07
90	0.2	−0.26	0.00	0.11	0.53	0.00	0.38	2.77	0.00	0.54
	0.4	−0.51	0.00	0.21	1.09	0.00	0.57	4.92	0.00	1.17
	0.6	−0.66	0.00	0.31	1.68	0.00	0.73	6.78	0.00	1.48
	0.8	−0.68	0.00	0.40	2.30	0.00	0.87	8.47	0.00	1.73

From the values given in Tables 2.1 to 2.3, Δ_d increases as X_c, ϕ and K_T increase. The percentage differences for different slopes will depend on the declination. For example, at low latitudes (say, $\phi = 20^o$N), when $\beta = 90^o$, the change is zero in June and is highest in March. Similarly, when the latitude is high (say, $\phi = 60^o$N), the highest differences, in general, are in the month of June.

Variation of Δ_d as defined by Eq. (2.52) with the non-dimensional critical level X_c is shown is Figure 2.2, for $\phi = 40^o$, $\delta = 23.09^o$, $\gamma = 0^o$ for $(\phi - \beta) = 0^o$ and $\beta = 90^o$ at $K_T = 0.3$, 0.5 and 0.7. It is evident from Figure 2.2 that Δ_d increases with K_T for $(\phi - \beta) = 0^o$. Δ_d is about 6 % at $X_c = 0.8$, when $K_T = 0.7$. When $\beta = 90^o$, Δ_d is negative for all clearness indices and $|\Delta_d|$ is higher for higher K_T. Similar plot for $\delta = -23.05^o$ with other parameters being the same is shown in Figure 2.3. It is evident from Figure 2.3 that Δ_d is always positive for all clearness indices for both $(\phi - \beta) = 0^o$ and $\beta = 90^o$.

Δ_d negative implies $(\tau\alpha)^*_{day}/(\tau\alpha)_n$ (a weighted average during part of the day, the operating time period) is lower than $(\tau\alpha)_{day}/(\tau\alpha)_n$, the weighted average over the entire day. This is due to instantaneous $(\tau\alpha)/(\tau\alpha)_n$ does not monotonically reach a maximum at $\omega = 0^o$, for $\gamma = 0^o$ when $\delta > 0$, in general. This feature is pronounced when $\beta = 90^o$, since ω'_s is considerably lower than ω_s. During $-\omega_s$ to $-\omega'_s$ (also during ω'_s to ω_s) only the

Table 2.2: Percentage difference Δ_d in useful energy gain and transmittance-absorptance product, $\phi = 40^o$N, $\delta = \delta_m$, $\gamma = 0^o$

β (deg.)	X_c	Percentage difference, Δ_d								
		$K_T = 0.3$			$K_T = 0.5$			$K_T = 0.7$		
		Mar	Jun	Dec	Mar	Jun	Dec	Mar	Jun	Dec
25	0.2	0.15	0.14	0.14	1.11	1.01	1.21	2.70	2.49	2.22
	0.4	0.32	0.31	0.28	1.68	1.81	1.78	3.82	3.83	3.63
	0.6	0.51	0.49	0.43	2.02	2.21	2.09	4.32	4.40	4.19
	0.8	0.68	0.68	0.58	2.28	2.51	2.34	4.70	4.82	4.60
40	0.2	0.18	0.12	0.21	1.12	0.92	0.70	2.59	2.48	1.12
	0.4	0.37	0.29	0.41	1.63	1.91	1.03	3.56	4.14	1.86
	0.6	0.57	0.49	0.59	1.96	2.41	1.28	4.04	4.84	2.28
	0.8	0.75	0.67	0.75	2.22	2.74	1.49	4.40	5.31	2.60
55	0.2	0.19	0.09	0.27	1.17	0.73	0.42	2.66	2.37	0.55
	0.4	0.39	0.24	0.50	1.70	1.89	0.69	3.66	4.60	1.07
	0.6	0.59	0.49	0.69	2.04	2.70	0.91	4.14	5.74	1.42
	0.8	0.78	0.68	0.86	2.30	3.09	1.10	4.50	6.30	1.69
90	0.2	0.10	−0.36	0.31	1.60	−1.38	0.26	3.63	−3.84	0.25
	0.4	0.25	−0.79	0.53	2.71	−2.73	0.48	5.91	−4.80	0.62
	0.6	0.41	−1.26	0.70	3.31	−3.23	0.66	7.02	−4.23	0.93
	0.8	0.57	−1.52	0.85	3.62	−3.10	0.81	7.53	−3.18	1.16

Table 2.3: Percentage difference Δ_d in useful energy gain and transmittance-absorptance product, $\phi = 60^o$N, $\delta = \delta_m$, $\gamma = 0^o$

β (deg.)	X_c	Percentage difference, Δ_d								
		$K_T = 0.3$			$K_T = 0.5$			$K_T = 0.7$		
		Mar	Jun	Dec	Mar	Jun	Dec	Mar	Jun	Dec
45	0.2	0.26	0.23	0.17	1.44	1.12	0.12	2.90	2.64	0.09
	0.4	0.51	0.56	0.31	2.02	2.36	0.36	3.97	4.36	0.26
	0.6	0.75	0.89	0.42	2.38	2.96	0.58	4.48	5.06	0.62
	0.8	0.96	1.14	0.52	2.67	3.36	0.77	4.86	5.55	0.96
60	0.2	0.33	0.21	0.19	1.43	1.00	0.07	2.75	2.52	0.06
	0.4	0.61	0.58	0.31	1.96	2.38	0.23	3.70	4.51	0.16
	0.6	0.86	0.98	0.41	2.32	3.17	0.39	4.18	5.39	0.41
	0.8	1.08	1.26	0.50	2.59	3.61	0.53	4.54	5.95	0.67
75	0.2	0.34	0.15	0.18	1.50	0.79	0.05	2.80	2.36	0.04
	0.4	0.65	0.48	0.30	2.05	2.29	0.17	3.79	4.86	0.12
	0.6	0.91	1.01	0.39	2.41	3.48	0.30	4.28	6.30	0.32
	0.8	1.14	1.35	0.48	2.69	4.02	0.42	4.65	6.93	0.53
90	0.2	0.34	−0.02	0.18	1.71	0.15	0.04	3.09	1.44	0.03
	0.4	0.63	0.12	0.28	2.36	1.41	0.13	4.33	4.47	0.10
	0.6	0.89	0.69	0.37	2.75	3.24	0.26	4.87	7.21	0.26
	0.8	1.12	1.41	0.45	3.04	4.71	0.36	5.27	9.01	0.46

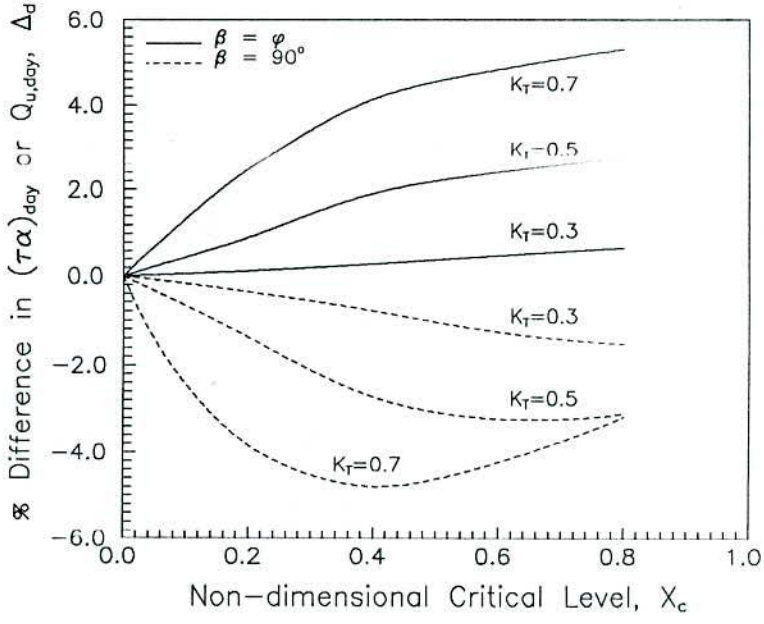

Figure 2.2: Variation of percentage difference in $(\tau\alpha)_{day}$ and $Q_{u,day}$ with non-dimensional critical level, $\phi = 40^o$, $\delta = 23.09^o$, $\gamma = 0^o$

sky diffuse and ground reflected components contribute to $(\tau\alpha)/(\tau\alpha)_n$. This contribution is included in $(\tau\alpha)_{day}/(\tau\alpha)_n$, whereas, $(\tau\alpha)^*_{day}/(\tau\alpha)_n$ depends upon X_c, which decides the operating time period. Thus, $(\tau\alpha)^*_{day}/(\tau\alpha)_n$ can be lower than $(\tau\alpha)_{day}/(\tau\alpha)_n$. This feature is demonstrated in Figure 2.4 where a plot of $(\tau\alpha)/(\tau\alpha)_n$ vs ω is shown for $\phi = 40^o$, $\beta = 90^o$, $\delta = 23.09$, $\gamma = 0^o$ for $K_T = 0.7$. Depending upon the value of X_c, $(\tau\alpha)^*_{day}/(\tau\alpha)_n$ is constituted during $-\omega_c$ to ω_c. If, $\omega_c > \omega^*_c$, $(\tau\alpha)^*_{day}/(\tau\alpha)_n$ will be higher than $(\tau\alpha)^*_{day}/(\tau\alpha)_n$ when $\omega_c < \omega^*_c$. As can be observed in Figure 2.2, this ω^*_c corresponds to $X_c \approx 0.4$, beyond which Δ_d starts increasing, implying $(\tau\alpha)^*_{day}/(\tau\alpha)_n$ is increasing.

Δ_d variation with latitude when $\gamma = 0^o$, for $(\phi - \beta) = 0^o$ and $\beta = 90^o$, for $\delta = 23.09^o$ is shown in Figure 2.5 for three values of non-dimensional critical level, $X_c = 0.2$, 0.6 and 0.8. Once again, when $\beta = 90^o$, Δ_d does not vary monotonically with ϕ. However, at high latitudes, say, $\phi = 60^o$, Δ_d goes up to 9 % when $\beta = 90^o$. Thus, it appears that difference in $Q_{u,day}$ obtained by hour by hour calculation and by using Eq. (2.34) is not insignificant for vertical collectors, which may be of importance in direct gain systems.

A plot of Δ_d vs declination for $\gamma = 0^o$, when $(\phi - \beta) = 15^o$ and $(\phi - \beta) = -15^o$ is shown in Figure 2.6 corresponding to a non-dimensional critical level, $X_c = 0.6$, for the three latitudes, $\phi = 20^o$, 40^o and 60^o when $K_T = 0.7$. It is interesting to note that Δ_d, when $(\phi - \beta) = 15^o$ is higher than the values when $(\phi - \beta) = -15^o$ for $\delta < 0$ and the opposite is true when $\delta > 0$. Also, the lines for a given ϕ, corresponding to $(\phi - \beta) = 15^o$

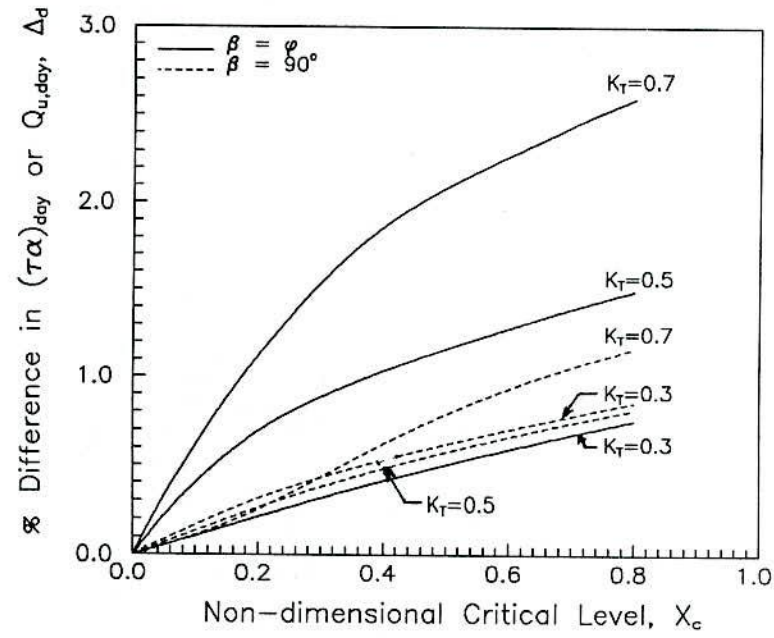

Figure 2.3: Variation of percentage difference in $(\tau\alpha)_{day}$ and $Q_{u,day}$ with non-dimensional critical level, $\phi = 40^o$, $\delta = -23.05^o$, $\gamma = 0^o$

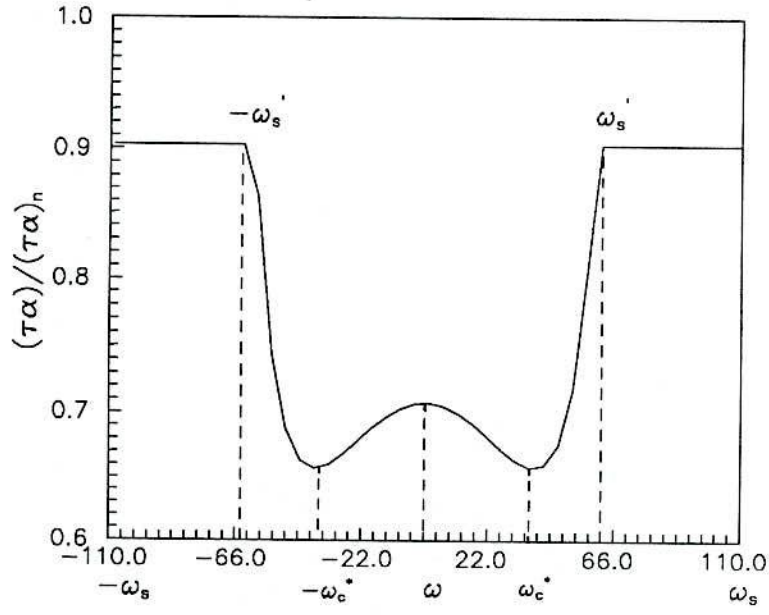

Figure 2.4: Variation of $(\tau\alpha)/(\tau\alpha)_n$ with ω, $\phi = 40^o$, $\beta = 90^o$, $\delta = 23.09^o$, $\gamma = 0^o$

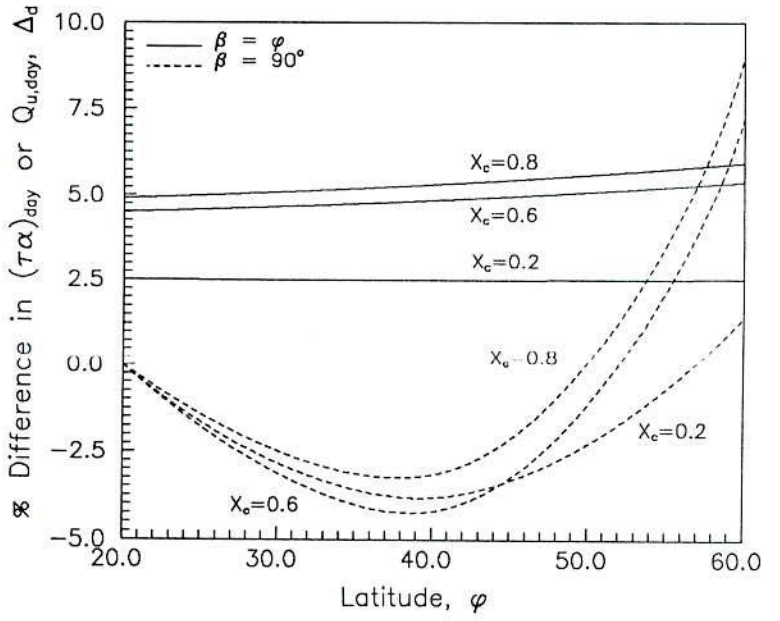

Figure 2.5: Variation of percentage difference in $(\tau\alpha)_{day}$ and $Q_{u,day}$ with latitude, $\delta = 23.09^o$, $K_T = 0.7$, $\gamma = 0^o$

and $(\phi - \beta) = -15^o$, intersect exactly at $\delta = 0$. This feature reveals the importance in developing a suitable method to estimate $(\tau\alpha)^*_{day}$, since Δ_d may not be insignificant depending on whether the system is summer optimized $[(\phi - \beta) = 15^o]$ or winter optimized $[(\phi - \beta) = -15^o]$. In order to further confirm the influence of β on $(\tau\alpha)_{day}$ and $(\tau\alpha)^*_{day}$, a plot of Δ_d vs declination is shown in Figure 2.7 for $\phi = 60^o$, $K_T = 0.7$, $X_c = 0.6$ for different slopes, $\beta = 0^o$, 15^o, 30^o, 45^o, 60^o, 75^o and 90^o. These values of β yield the variation of Δ_d with δ for $|\phi - \beta| = 0^o$, 15^o, 30^o, 45^o and 60^o. It is interesting to note that the curves for fixed $|\phi - \beta|$ ($\beta = 45^o$, 75^o and $\beta = 30^o$, 90^o) intersect at $\delta = 0^o$.

Δ_d as a function of clearness index when $X_c = 0.6$ is shown in Figures 2.8 and 2.9 for $(\phi - \beta) = 0^o$ and $\beta = 90^o$ respectively for $\phi = 20^o$, 40^o and 60^o, for $\delta = -23.05^o$ and $\delta = 23.09^o$. When $(\phi - \beta) = 0^o$ (Figure 2.8), Δ_d monotonically increase with K_T and is higher at higher ϕ when $\delta = 23.09$, whereas, when $\delta = -23.05$, Δ_d is higher at lower ϕ. As has been observed in Figures 2.2 and 2.5, Δ_d is negative for all clearness indices when $\beta = 90^o$ for $\delta = 23.09$ for low and moderate latitudes. However, when $\phi = 60^o$, Δ_d is positive and increases with K_T. In general, for $\beta = 90^o$, when $\delta = -23.1$, Δ_d is insignificant at all clearness indices and latitudes.

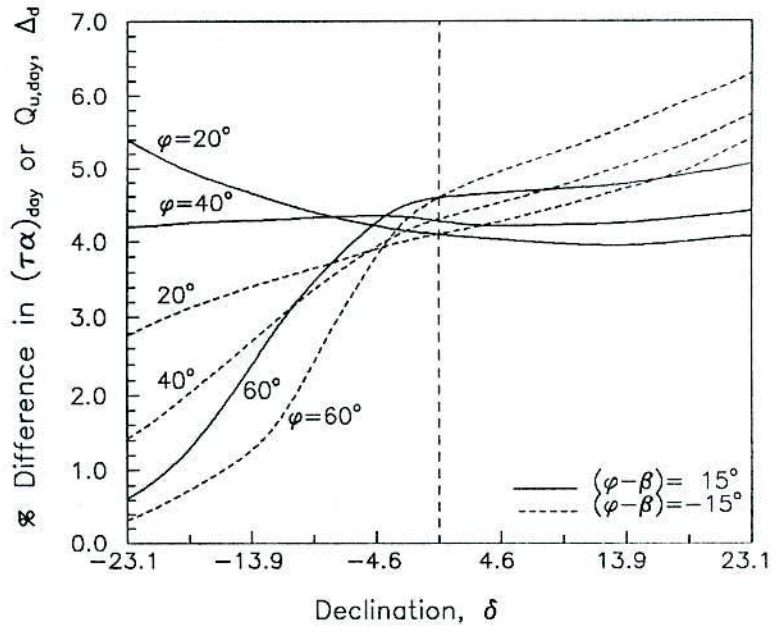

Figure 2.6: Variation of percentage difference in $(\tau\alpha)_{day}$ and $Q_{u,day}$ with declination, $K_T = 0.7$, $X_c = 0.6$, $\gamma = 0^o$

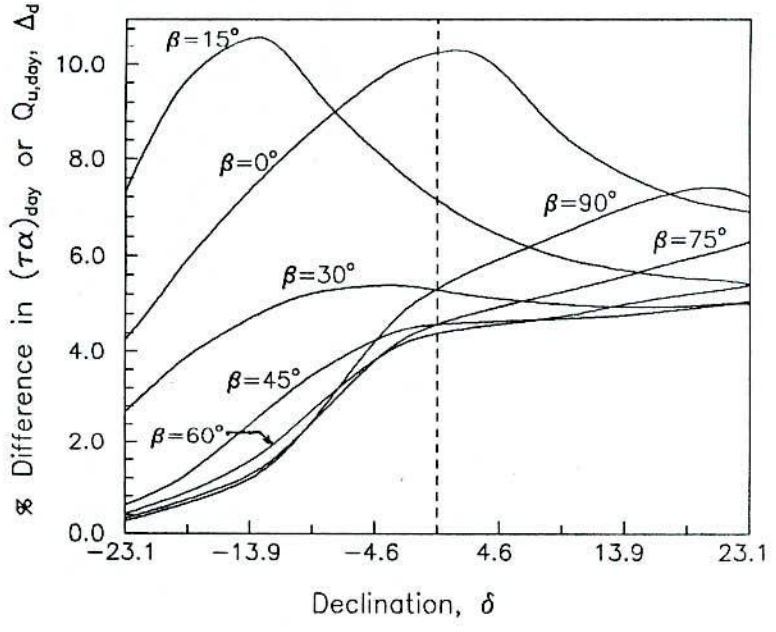

Figure 2.7: Variation of percentage difference in $(\tau\alpha)_{day}$ and $Q_{u,day}$ with declination, $\phi = 60^o$, $K_T = 0.7$, $X_c = 0.6$, $\gamma = 0^o$

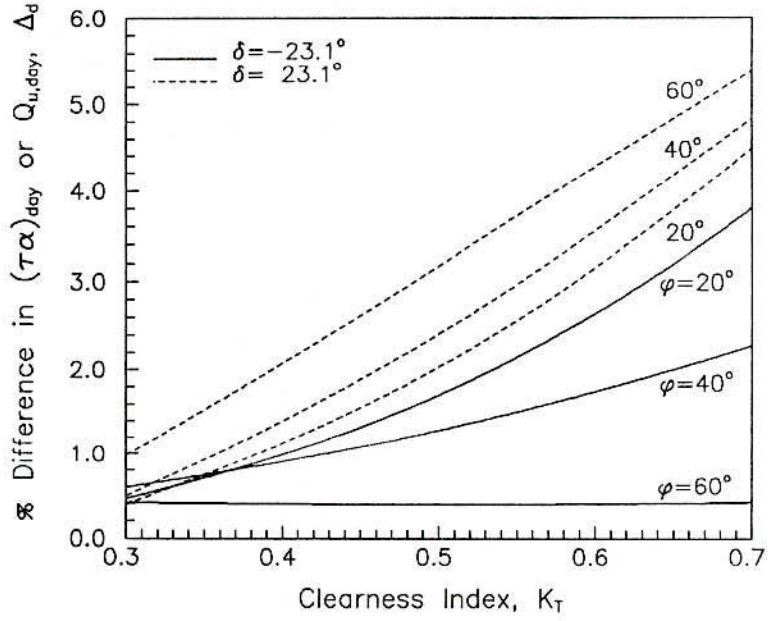

Figure 2.8: Variation of percentage difference in $(\tau\alpha)_{day}$ and $Q_{u,day}$ with clearness index, $(\phi - \beta) = 0^o$, $X_c = 0.6$, $\gamma = 0^o$

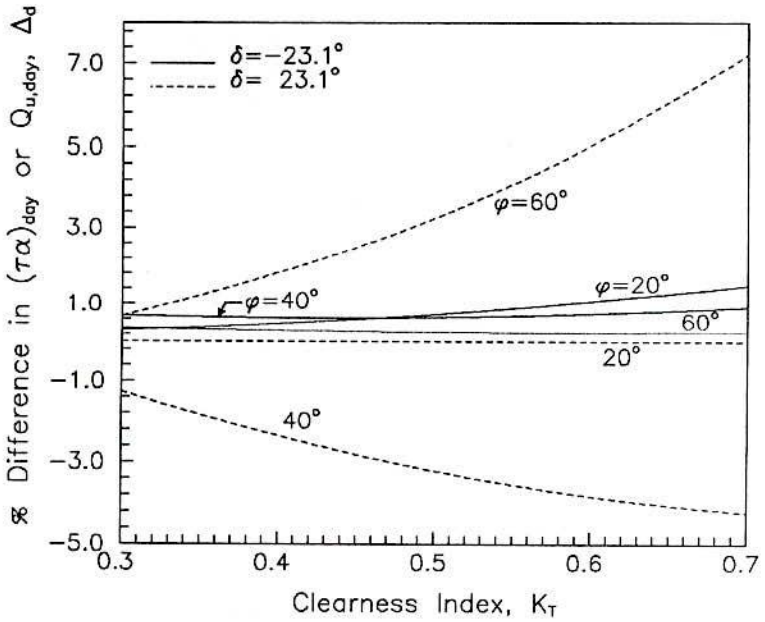

Figure 2.9: Variation of percentage difference in $(\tau\alpha)_{day}$ and $Q_{u,day}$ with clearness index, $\beta = 90^o$, $X_c = 0.6$, $\gamma = 0^o$

Table 2.4: Percentage difference Δ_d in useful energy gain and transmittance-absorptance product, $\phi = 20°$N, $(\phi - \beta) = 0°$

γ (deg.)	X_c	Percentage difference, Δ_d								
		$K_T = 0.3$			$K_T = 0.5$			$K_T = 0.7$		
		Mar	Jun	Dec	Mar	Jun	Dec	Mar	Jun	Dec
30	0.4	0.28	0.25	0.28	1.38	1.54	1.44	3.11	3.75	3.19
	0.8	0.62	0.57	0.59	1.96	2.24	2.00	3.97	4.75	4.07
60	0.4	0.27	0.26	0.23	1.24	1.32	1.38	2.80	3.19	3.17
	0.8	0.61	0.61	0.57	1.91	2.04	2.16	3.70	4.16	4.27
90	0.4	0.23	0.27	0.14	1.15	1.20	1.23	2.81	2.80	3.55
	0.8	0.59	0.62	0.55	1.93	1.90	2.42	3.80	3.72	5.22

Non-South Facing Collectors ($\gamma \neq 0$)

Even though flat plate collectors are seldom oriented non-south facing (generally, azimuthal angle is within $\pm 15°$ due south), investigating the difference in $(\tau\alpha)_{day}$ and $(\tau\alpha)^*_{day}$ is motivated since these results are indicative for direct gain windows as well and the azimuthal angle for such windows can be $-180° \leq \gamma \leq 180°$.

Values of $Q_{u,day}$, $Q'_{u,day}$, $(\tau\alpha)_{day}$, $(\tau\alpha)^*_{day}$ calculated according to Eqs. (2.34), (2.39), (2.40), (2.37) respectively and the percentage differences, Δ_d, in the useful energy gain and the transmittance-absorptance product [Eq. (2.52)] are given in Tables A.4 to A.9 of Appendix A for $\phi = 20°$, $40°$ and $60°$ respectively, for $\gamma = 30°$, $60°$ and $90°$, for two slopes, $(\phi - \beta) = 0°$ and $\beta = 90°$ for mean days of different months, clearness indices and the non-dimensional critical radiation levels. Summary of the Tables A.4 to A.9 giving only the percentage differences is given in Tables 2.4 to 2.9.

From the values given in Tables 2.4 to 2.9, Δ_d increases as X_c, ϕ and K_T increase. The percentage differences for different slopes will depend on the declination. When $(\phi - \beta) = 0°$, the maximum Δ_d is under 8 %, for low and moderate latitudes. However, at higher latitudes, say, $\phi = 60°$ (see Table 2.8), Δ_d is as high as 19 % in December, when $K_T = 0.7$ and $\gamma = 90°$. When $\beta = 90°$, $K_T = 0.7$ and $X_c = 0.8$, at lower latitudes, say, $\phi = 20°$ (see Table 2.5), Δ_d is negative and $|\Delta_d|$ is 11 %, when $\gamma = 30°$ in June. Whereas, at higher latitudes, say, $\phi = 60°$ (see Table 2.9), Δ_d increases sharply as γ increases and Δ_d is about 21 % when $\gamma = 90°$ in December.

Variation of Δ_d with the azimuth angle, γ, for $\beta = 90°$, $\delta = 23.09$, $K_T = 0.7$ is shown in Figure 2.10 for three latitudes, $\phi = 20°$, $40°$ and $60°$, for two non-dimensional

Table 2.5: Percentage difference Δ_d in useful energy gain and transmittance-absorptance product, $\phi = 20^o$N, $\beta = 90^o$

γ (deg.)	X_c	Percentage difference, Δ_d								
		$K_T = 0.3$			$K_T = 0.5$			$K_T = 0.7$		
		Mar	Jun	Dec	Mar	Jun	Dec	Mar	Jun	Dec
30	0.4	−0.44	−0.14	0.15	−0.96	0.26	1.36	0.60	−1.80	3.64
	0.8	−1.21	−0.09	0.85	−0.82	0.11	3.08	3.78	−11.22	5.47
60	0.4	−0.30	−0.26	−0.32	−0.72	−1.06	−0.22	1.57	−1.25	2.77
	0.8	−1.28	−0.83	−0.83	−0.52	−4.75	1.77	4.60	0.59	5.42
90	0.4	−0.24	−0.23	−0.34	−0.78	−0.79	−1.16	1.71	1.33	1.56
	0.8	−1.01	−0.94	−1.33	−1.60	−1.92	−2.62	5.03	4.45	5.71

Table 2.6: Percentage difference Δ_d in useful energy gain and transmittance-absorptance product, $\phi = 40^o$N, $(\phi - \beta) = 0^o$

γ (deg.)	X_c	Percentage difference, Δ_d								
		$K_T = 0.3$			$K_T = 0.5$			$K_T = 0.7$		
		Mar	Jun	Dec	Mar	Jun	Dec	Mar	Jun	Dec
30	0.4	0.36	0.28	0.38	1.44	1.62	1.63	2.81	3.95	2.89
	0.8	0.76	0.74	0.74	2.13	2.60	2.22	3.69	5.15	3.74
60	0.4	0.24	0.21	0.19	1.06	1.03	1.41	2.64	2.95	3.44
	0.8	0.82	0.74	0.94	2.20	2.17	3.02	3.80	4.15	5.10
90	0.4	−0.05	0.12	−0.56	0.30	0.65	−0.84	2.53	2.53	2.52
	0.8	0.30	0.61	−1.31	2.01	1.94	0.48	4.45	3.82	6.67

Table 2.7: Percentage difference Δ_d in useful energy gain and transmittance-absorptance product, $\phi = 40^o$N, $\beta = 90^o$

γ (deg.)	X_c	Percentage difference, Δ_d								
		$K_T = 0.3$			$K_T = 0.5$			$K_T = 0.7$		
		Mar	Jun	Dec	Mar	Jun	Dec	Mar	Jun	Dec
30	0.4	0.08	−0.53	0.59	0.88	−0.71	2.13	2.71	−0.64	3.51
	0.8	0.84	−1.64	1.09	2.84	−1.93	2.86	4.79	2.29	4.39
60	0.4	−0.27	−0.30	−0.20	−0.10	−0.75	1.10	2.47	0.63	3.86
	0.8	−0.74	−1.30	0.59	1.83	−1.24	3.78	4.79	3.84	6.18
90	0.4	−0.31	−0.23	−0.60	−0.80	−0.65	−1.68	2.34	1.77	2.47
	0.8	−1.31	−1.01	−2.46	−0.69	−0.90	−2.07	5.60	4.54	8.54

Table 2.8: Percentage difference Δ_d in useful energy gain and transmittance-absorptance product, $\phi = 60^o$N, $(\phi - \beta) = 0^o$

γ (deg.)	X_c	Percentage difference, Δ_d								
		$K_T = 0.3$			$K_T = 0.5$			$K_T = 0.7$		
		Mar	Jun	Dec	Mar	Jun	Dec	Mar	Jun	Dec
30	0.4	0.64	0.36	0.49	1.84	2.07	1.45	2.81	4.39	1.80
	0.8	1.25	1.13	0.80	2.66	3.46	1.94	3.73	5.86	2.58
60	0.4	0.17	0.11	1.07	1.31	1.39	4.42	3.13	3.97	6.39
	0.8	1.23	0.71	3.39	3.04	3.00	7.50	4.44	5.51	9.88
90	0.4	−0.48	−0.12	−2.42	−0.41	0.35	−3.68	3.32	2.77	6.21
	0.8	−1.66	−0.30	−8.14	1.70	2.04	−1.97	6.31	4.51	18.58

Table 2.9: Percentage difference Δ_d in useful energy gain and transmittance-absorptance product, $\phi = 60^o$N, $\beta = 90^o$

γ (deg.)	X_c	Percentage difference, Δ_d								
		$K_T = 0.3$			$K_T = 0.5$			$K_T = 0.7$		
		Mar	Jun	Dec	Mar	Jun	Dec	Mar	Jun	Dec
30	0.4	0.74	-0.06	0.47	2.04	1.37	1.16	3.05	4.37	1.39
	0.8	1.62	0.41	0.77	3.15	3.82	1.60	4.18	7.97	2.15
60	0.4	−0.12	−0.21	1.67	1.11	0.72	4.98	3.26	3.61	6.75
	0.8	0.76	−0.72	4.41	3.46	2.57	7.93	4.93	6.29	9.73
90	0.4	−0.53	−0.25	−3.07	−0.69	−0.16	−1.33	3.41	2.29	7.86
	0.8	−2.47	−1.17	−10.54	1.37	1.18	5.76	6.79	4.60	20.77

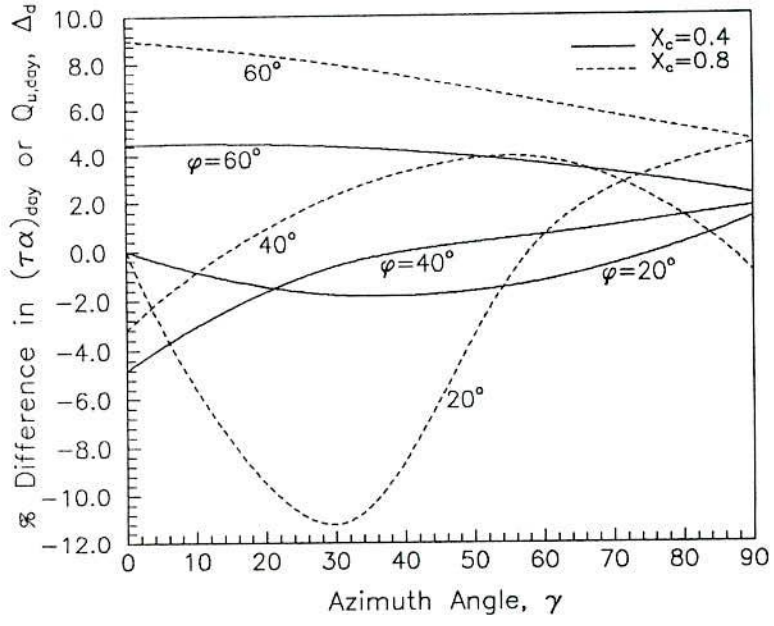

Figure 2.10: Variation of percentage difference in $(\tau\alpha)_{day}$ and $Q_{u,day}$ with azimuthal angle, $\beta = 90^o$, $\delta = 23.09^o$, $K_T = 0.7$

critical levels, $X_c = 0.4$ and 0.8. As observed for south facing collectors, Δ_d is negative for low latitudes when $\gamma < 50^o$. As latitude increases, Δ_d becomes positive for lower γ. Also, as ϕ increases, Δ_d is higher for all γ and is higher for higher X_c. Similar plot for $\delta = -23.1^o$ is shown in Figure 2.11. It may be readily seen from Figure 2.11, that Δ_d is always positive which has already been explained with reference to Figure 2.2 and 2.3. For higher latitudes and higher γ, Δ_d is significant.

Maximum Percentage Difference

In general, since Δ_d increases as X_c increases, it can be expected that $\Delta_d \rightarrow \Delta_{d,max}$ as $X_c \rightarrow 1.0$. When $X_c \rightarrow 1.0$, operating time period tends to zero. Considering operating time period to be small, let the collector operate from $-\epsilon_c$ to ϵ_c around $\omega = \omega_m$. During this small operating time period, $(\tau\alpha)^*_{day}/(\tau\alpha)_n$ from Eq. (2.38) can be expressed in integral form as,

$$\frac{(\tau\alpha)^*_{day}}{(\tau\alpha)_n} = \frac{\int_{-\epsilon_c}^{\epsilon_c} I_T\,(\tau\alpha)/(\tau\alpha)_n\,d\omega}{\int_{-\epsilon_c}^{\epsilon_c} (I_T - I_c)\,d\omega} - \frac{I_c \int_{-\epsilon_c}^{\epsilon_c} (\tau\alpha)/(\tau\alpha)_n\,d\omega}{\int_{-\epsilon_c}^{\epsilon_c} (I_T - I_c)\,d\omega} \tag{2.53}$$

Considering the intensity of solar radiation to be constant during $-\epsilon_c$ to ϵ_c, Eq. (2.53) can

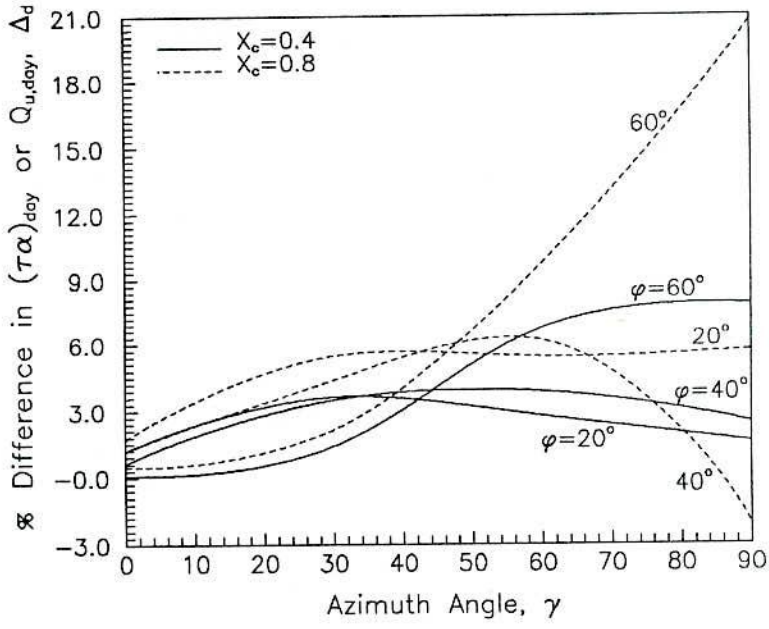

Figure 2.11: Variation of percentage difference in $(\tau\alpha)_{day}$ and $Q_{u,day}$ with azimuthal angle. $\beta = 90^o$, $\delta = -23.05^o$, $K_T = 0.7$

be replaced by,

$$\frac{(\tau\alpha)^*_{day}}{(\tau\alpha)_n} = \frac{G_T \int_{-\epsilon_c}^{\epsilon_c} (\tau\alpha)/(\tau\alpha)_n \, d\omega}{2(G_T - G_c)\epsilon_c} - \frac{G_c \int_{-\epsilon_c}^{\epsilon_c} (\tau\alpha)/(\tau\alpha)_n \, d\omega}{2(G_T - G_c)\epsilon_c} \tag{2.54}$$

Eq. (2.54) reduces to,

$$\frac{(\tau\alpha)^*_{day}}{(\tau\alpha)_n} = \frac{(G_T - G_c) \int_{-\epsilon_c}^{\epsilon_c} (\tau\alpha)/(\tau\alpha)_n \, d\omega}{2(G_T - G_c)\epsilon_c} \tag{2.55}$$

$$= \frac{\int_{-\epsilon_c}^{\epsilon_c} (\tau\alpha)/(\tau\alpha)_n \, d\omega}{2\epsilon_c} \tag{2.56}$$

Eq. (2.56) can be approximated as,

$$\frac{(\tau\alpha)^*_{day}}{(\tau\alpha)_n} = \frac{\left[\frac{(\tau\alpha)}{(\tau\alpha)_n}\Big|_{\omega=\omega_m}\right] 2\epsilon_c}{2\epsilon_c} \tag{2.57}$$

As $X_c \to 1$, $\epsilon_c \to 0$ and $(\tau\alpha)^*_{day}/(\tau\alpha)_n$ approaches a limiting value given by,

$$\frac{(\tau\alpha)^*_{day}}{(\tau\alpha)_n} = \frac{(\tau\alpha)}{(\tau\alpha)_n}\Big|_{\omega=\omega_m} \qquad \text{as} X_c \to 1 \tag{2.58}$$

When $(\tau\alpha)^*_{day}/(\tau\alpha)_n \to (\tau\alpha)/(\tau\alpha)_n|_{\omega=\omega_m}$ as $X_c \to 1$, Δ_d in Eq. (2.52) becomes $\Delta_{d,max}$ given by,

$$\Delta_{d,max} = \frac{\frac{(\tau\alpha)}{(\tau\alpha)_n}\Big|_{\omega=\omega_m} - \frac{(\tau\alpha)_{day}}{(\tau\alpha)_n}}{\frac{(\tau\alpha)_{day}}{(\tau\alpha)_n}} \tag{2.59}$$

$\Delta_{d,max}$ values are given in Table 2.10 for $\phi = 20^o$, 40^o and 60^o, $\beta = \phi$ and $\beta = 90^o$, for $\gamma = 0^o$, 30^o, 60^o and 90^o, with $K_T = 0.3$, 0.5 and 0.7 for mean days for the months of March, June and December. It is realized that when $X_c \rightarrow 1.0$, $Q_{u,day} \rightarrow 0$. However, the $\Delta_{d,max}$ values are indicative of the differences that can be expected in the monthly average values.

2.4.2 Monthly Average Daily Useful Energy Gain and Transmittance-Absorptance Product

South Facing Collectors ($\gamma = 0$)

Values of $\bar{Q}_{u,m}$, $\bar{Q}'_{u,m}$, $(\overline{\tau\alpha})$ and $(\overline{\tau\alpha})^*$ have been calculated using Eqs. (2.45), (2.50), (2.51), and (2.48) respectively, for $\phi = 20^o$, 40^o and 60^o, $\gamma = 0^o$, $\bar{K}_T = 0.3$, 0.5 and 0.7, and the non-dimensional critical level $0 \leq \bar{X}_c \leq 2.0$. Depending on the value of $\bar{K}_T$, $\bar{Q}_{u,m} \rightarrow 0$ for $\bar{X}_c \rightarrow \bar{X}_{c,max}$, a finite value. $\bar{X}_{c,max}$ will be approximately equal to $K_{T,max}/\bar{K}_T$, when $K_{T,max}$ is the maximum daily clearness index in a month whose monthly average clearness index is $\bar{K}_T$. The percentage difference $\bar{\Delta}_d$, in the monthly average daily useful energy gain and transmittnce-absorptance product is calculated according to,

$$\bar{\Delta}_d = \frac{\bar{Q}_{u,m} - \bar{Q}'_{u,m}}{Q'_{u,m}} \times 100 = \frac{(\overline{\tau\alpha})^* - (\overline{\tau\alpha})}{(\overline{\tau\alpha})} \times 100 \qquad (2.60)$$

It may be noted that as in Eq. (2.52), difference in $(\overline{\tau\alpha})$ and $(\overline{\tau\alpha})^*$ has been normalized with $(\overline{\tau\alpha})$, since, $(\overline{\tau\alpha})$ as given by Eq. (2.51), is the commonly employed definition in the literature. $\bar{Q}'_{u,m}$ [from Eq. (2.50)] is the corresponding monthly average daily useful energy gain that would be obtained.

A plot of $\bar{\Delta}_d$ vs $\bar{X}_c$ is shown in Figure 2.12, for $\phi = 40^o$, $\delta = 23.09^o$, $(\phi - \beta) = 0^o$ and $\beta = 90^o$, for $\bar{K}_T = 0.3$, 0.5 and 0.7. Also, shown in the figure is the corresponding plot of Δ_d vs X_c numerically equal to the value of $\bar{X}_c$ which is a re-plot from Figure 2.2 for $K_T = 0.5$, $(\phi - \beta) = 0^o$ and $\beta = 90^o$. It can be seen from Figure 2.12 that $|\bar{\Delta}_d|$ increases as $\bar{K}_T$ increases. $|\Delta_d|$ is lower than $|\bar{\Delta}_d|$ for equal values of X_c and $\bar{X}_c$. It may be noted, $\bar{Q}_{u,m} > 0$ for $\bar{X}_c > 1.0$, whereas, $Q_{u,day} = 0$ for $X_c \geq 1.0$. Thus, it can be expected $\bar{Q}'_{u,m}$ estimated with Eq. (2.50) which employs Eq. (2.51) for $(\overline{\tau\alpha})$ differs more from $\bar{Q}_{u,m}$ obtained from hour by hour calculations than the corresponding difference between $Q'_{u,day}$ and $Q_{u,day}$.

Variation of $\bar{\Delta}_d$ with latitude for $(\phi - \beta) = 0^o$ and $\beta = 90^o$ is shown in Figure 2.13, for a fixed $\bar{X}_c = 0.8$, for three declinations, $\delta = -23.05^o$, -2.4^o and 23.09^o. The trend is similar to that shown in Figure 2.5 for the single day for $\delta = 23.09^o$.

Table 2.10: Maximum percentage difference Δ_d in useful energy gain and transmittance-absorptance product for south facing and non-south facing collectors, $\phi = 20^o$, 40^o and 60^oN, $\beta = \phi$ and $\beta = 90^o$

ϕ	β	γ	Percentage difference, $\Delta_{d,max}$								
			$K_T = 0.3$			$K_T = 0.5$			$K_T = 0.7$		
(deg)	(deg)	(deg)	Mar	Jun	Dec	Mar	Jun	Dec	Mar	Jun	Dec
20	20	0	0.77	0.69	0.75	2.22	2.54	2.13	4.54	5.23	4.44
		30	0.77	0.72	0.73	2.16	2.46	2.22	4.25	5.07	4.35
		60	0.76	0.76	0.72	2.13	2.28	2.36	3.98	4.46	4.58
		90	0.73	0.77	0.70	2.14	2.12	2.67	4.09	4.00	5.59
	90	0	−0.62	0.00	0.48	2.89	0.00	0.99	9.96	0.00	1.92
		30	−1.62	0.52	1.09	−0.02	−3.45	3.37	6.19	−12.47	5.78
		60	−2.57	−2.61	−0.11	1.50	−6.36	2.84	5.05	3.56	5.88
		90	−3.40	−3.30	−4.01	0.43	0.54	−0.59	5.63	4.99	6.78
40	40	0	0.91	0.84	0.89	2.42	3.01	1.66	4.66	5.66	2.83
		30	0.93	0.90	0.88	2.36	2.86	2.42	3.97	5.49	4.04
		60	1.01	0.93	1.19	2.46	2.43	3.28	4.10	4.47	5.46
		90	0.77	0.83	−1.53	2.47	2.21	2.57	4.86	4.13	8.52
	90	0	0.71	−1.55	0.97	3.86	−2.68	0.94	7.90	−1.94	1.35
		30	1.27	−2.29	1.29	3.17	−1.74	3.05	5.15	4.02	4.61
		60	0.33	−2.80	1.84	2.88	0.84	4.23	5.09	4.91	6.49
		90	−3.96	−3.39	−5.65	1.73	1.23	0.65	6.12	5.05	9.48
60	60	0	1.27	1.48	0.60	2.81	3.95	0.65	4.82	6.35	0.86
		30	1.45	1.36	1.01	2.87	3.82	2.10	3.99	6.27	2.83
		60	1.60	1.14	4.27	3.32	3.35	7.88	4.75	5.88	10.28
		90	−1.50	0.55	−9.65	3.25	2.52	−3.18	6.78	4.86	27.76
	90	0	1.30	1.72	0.52	3.28	5.21	0.46	5.58	9.67	0.61
		30	1.87	1.19	0.98	3.46	4.57	1.76	4.49	8.60	2.32
		60	1.90	0.47	5.38	3.80	3.41	8.45	5.29	6.80	10.22
		90	−4.79	−2.55	−13.12	3.55	2.33	8.51	7.29	5.03	25.61

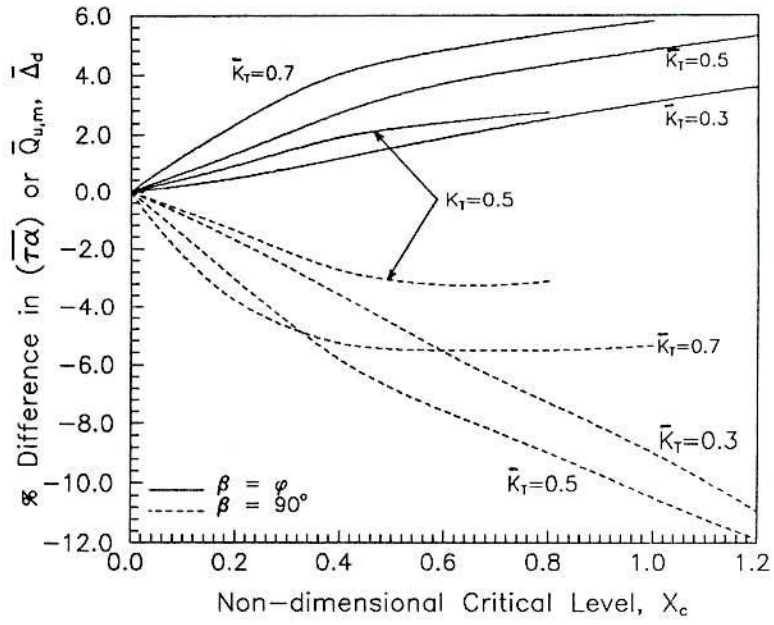

Figure 2.12: Variation of percentage difference in $(\overline{\tau\alpha})$ and $\bar{Q}_{u,m}$ with non-dimensional critical level, $\phi = 40^o$, $\delta = 23.09^o$, $\gamma = 0^o$

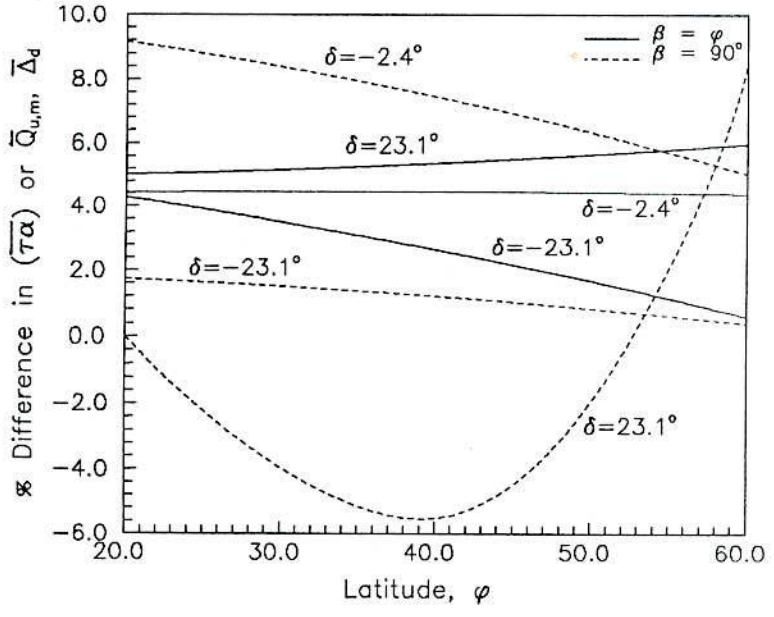

Figure 2.13: Variation of percentage difference in $(\overline{\tau\alpha})$ and $\bar{Q}_{u,m}$ with latitude, $\bar{K}_T = 0.7$, $\bar{X}_c = 0.8$, $\gamma = 0^o$

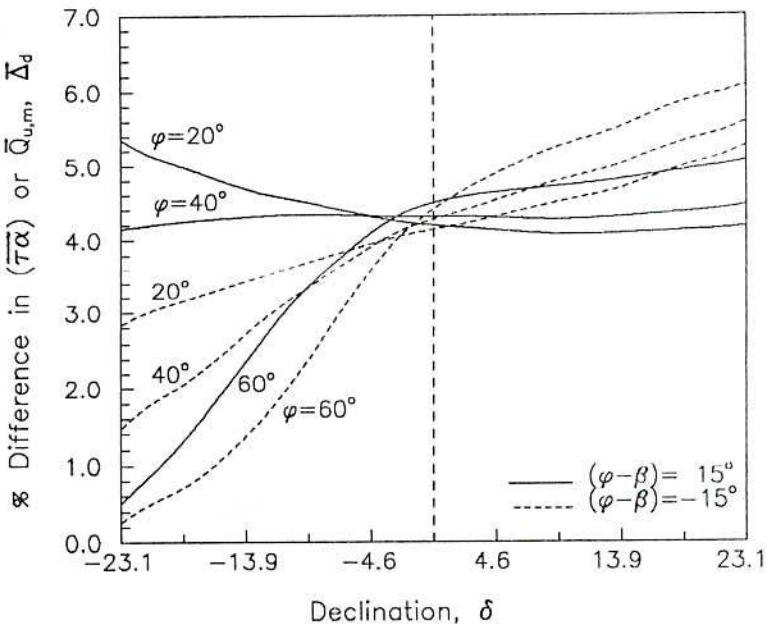

Figure 2.14: Variation of percentage difference in $(\overline{\tau\alpha})$ and $Q_{u,m}$ with declination, $\bar{K}_T = 0.7$, $\bar{X}_c = 0.6$, $\gamma = 0^o$

Percentage difference in $(\overline{\tau\alpha})$ or $\bar{Q}_{u,m}$ plotted against declination is shown in Figure 2.14, for three latitudes, $\phi = 20^o$, 40^o and 60^o, for $(\phi - \beta) = -15^o$ and 15^o, for a fixed $\bar{X}_c = 0.6$ and $\bar{K}_T = 0.7$. Variation of $\bar{\Delta}_d$ with δ is exactly similar to the corresponding plots for the single day shown in Figure 2.6. It may be noted from Figure 2.14 also, that $\bar{\Delta}_d$, when $(\phi - \beta) = 15^o$ is higher than the values when $(\phi - \beta) = -15^o$ for $\delta < 0$ and the opposite is true when $\delta > 0$. The lines for a given ϕ, corresponding to $(\phi - \beta) = 15^o$ and $(\phi - \beta) = -15^o$, intersect exactly at $\delta = 0^o$.

Variation of $\bar{\Delta}_d$ with the monthly average daily clearness index, $\bar{K}_T$ is shown in Figure 2.15 for $\phi = 20^o$, 40^o and 60^o, $\delta = -23.05^o$ and $\delta = 23.09^o$, for a fixed $\bar{X}_c = 0.6$. $\bar{\Delta}_d$ continuously increases with $\bar{K}_T$ and is higher at higher latitudes. Also, $\bar{\Delta}_d$ is higher when $\delta = 23.09^o$ compared to the value for $\delta = -23.05^o$.

Non-South Facing Collectors ($\gamma \neq 0$)

A plot of $\bar{\Delta}_d$ vs γ for $\phi = 20^o$, 40^o and 60^o, $\beta = 90^o$ and $\delta = -23.05^o$, is shown in Figure 2.16 corresponding to two non-dimensional critical levels, $\bar{X}_c = 0.4$ and 0.8, for $\bar{K}_T = 0.7$. It may be seen from Figure 2.16, that the dependence of $\bar{\Delta}_d$ on γ is similar to the dependence of Δ_d for single day as shown in Figure 2.11. The difference $\bar{\Delta}_d$ is higher than the corresponding Δ_d for a single day. $\bar{\Delta}_d$ is not monotonic with γ, owing to differing changes for ω_{sr} and ω_{ss} from ω_s' and getting limited to ω_s beyond a certain γ.

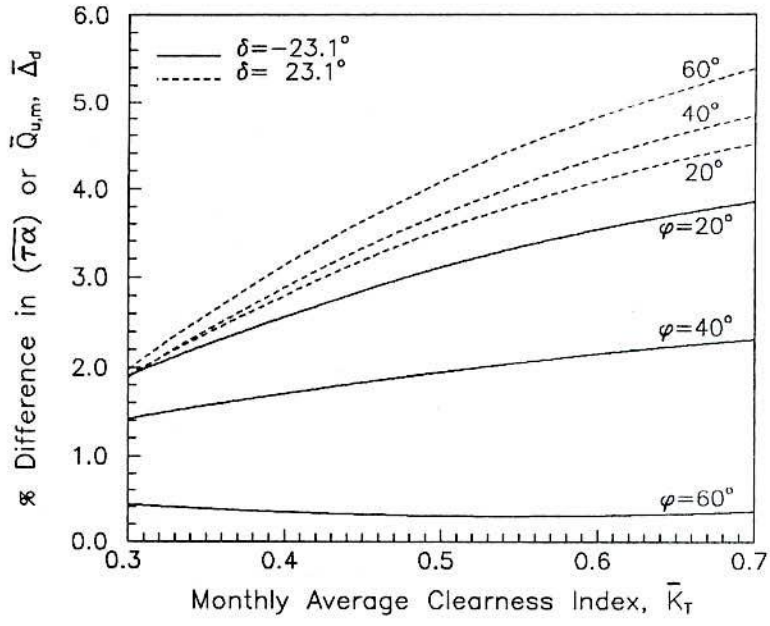

Figure 2.15: Variation of percentage difference in $(\overline{\tau\alpha})$ and $\bar{Q}_{u,m}$ with clearness index, $(\phi - \beta) = 0^o$, $\bar{X}_c = 0.6$, $\gamma = 0^o$

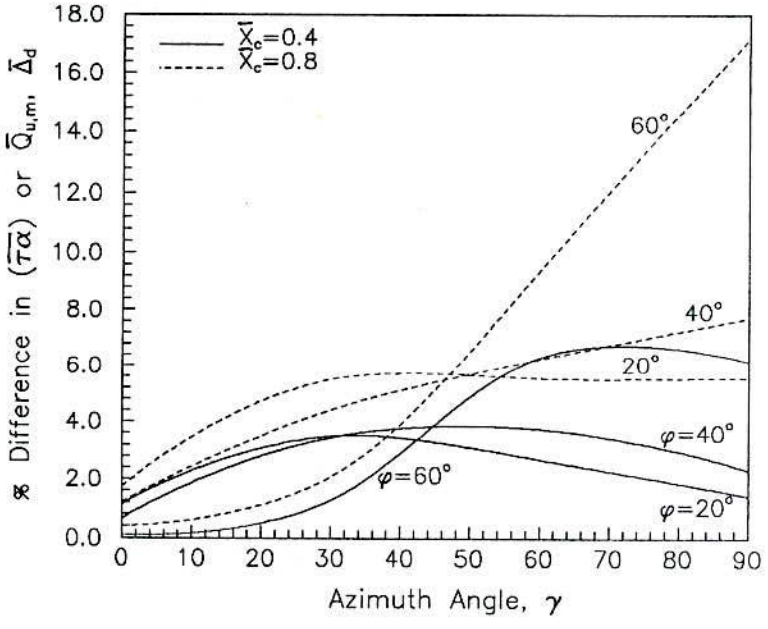

Figure 2.16: Variation of percentage difference in $(\overline{\tau\alpha})$ and $\bar{Q}_{u,m}$ with azimuth angle, $\beta = 90^o$, $\delta = -23.05^o$, $\bar{K}_T = 0.7$

2.5 Conclusions

In order to estimate the daily useful energy gain or the monthly average daily useful energy gain for flat plate collectors, using the utilizability concept, an appropriately averaged transmittance-absorptance product has been defined. The average transmittance-absorptance product applicable for the day or the month are the weighted average of the instantaneous values, the weighting function being the solar radiation above the critical level. The differences between $(\tau\alpha)_{day}$ and $(\tau\alpha)^*_{day}$ or $(\overline{\tau\alpha})$ and $(\overline{\tau\alpha})^*$ have been estimated for a wide range of latitudes, declinations, slopes of the collectors, azimuthal angles, clearness indices and non-dimensional critical radiation levels. It has been found that the percentage differences in the aforementioned quantities are not insignificant. In general, the differences are significant for higher latitudes and clearness indices, particularly at $\beta = 90°$. Also, Δ_d and $\bar{\Delta}_d$ are higher when $\gamma \neq 0$. Though, flat plate collectors generally are not oriented with $\gamma \neq 0$, the results are relevant for direct gain systems. $(\overline{\tau\alpha})^*$ differs more from $(\overline{\tau\alpha})$ compared to the corresponding differences in $(\tau\alpha)^*_{day}$ and $(\tau\alpha)_{day}$. Also, these differences are higher at higher non-dimensional critical levels. Changes at higher critical levels are relevant for designing direct gain systems.

Noting that methods to estimate $\bar{H}_T$ or $\bar{\phi}$ are widely reported in the literature, estimating $Q_{u,day}$ or $\bar{Q}_{u,m}$ according to Eqs. (2.34) and (2.45) will be straight forward when methods to calculate $(\tau\alpha)^*_{day}$ or $(\overline{\tau\alpha})^*$ conveniently are developed. Chapter 3 is devoted to such studies.

Chapter 3

Evaluation of Monthly Average Transmittance-Absorptance Product during the Operational Time Period for Flat Plate Collectors

3.1 Introduction

The monthly average daily useful energy gain from flat plate collector is commonly evaluated as a product of F_R, $\bar{H}_T$, $\bar{\phi}$ and a monthly average transmittance-absorptance product. Studies reported in Chapter 2 established that the appropriately defined monthly average transmittance-absorptance product, $(\overline{\tau\alpha})^*$, is a weighted average of the instantaneous $(\tau\alpha)$ and the solar radiation on the collector above the critical radiation level. Numerical results discussed in Chapter 2 show that the difference between $(\overline{\tau\alpha})$ and $(\overline{\tau\alpha})^*$ is not insignificant. This difference is significant, particularly, for non-south facing vertical collectors. Direct gain systems, in general, comprise non-south facing collection devices. Methods to estimate $\bar{\phi}$ and $\bar{H}_T$ are widely available in the literature. Eq. (2.47) to calculate $\bar{Q}_{u,m}$ becomes available when methods to evaluate $(\overline{\tau\alpha})^*$ have been developed. The usefulness of these methods is enhanced when they become applicable for collectors of general orientation.

In the present chapter, an expression for $(\tau\alpha)^*_{day}$, defined by Eq. (2.38), applicable for a single day, has been developed, assuming critical radiation to be constant. Eq. (2.38) has been rewritten in terms of corresponding integrals. The instantaneous solar radiation falling on the collector surface, I_T, [Eq. (2.2)] has been expressed using the correlations due to Collares-Pereira and Rabl [12] for r_t and Liu and Jordan [16] for r_d. It has been

shown that the appropriate monthly average transmittance-absorptance product, $(\overline{\tau\alpha})^*$, can be calculated with the expressions developed for a single day, the single day being the equivalent mean day (EMD). Equivalent mean day approach has been successful [94, 67, 39] in calculating the monthly average daily utilizability from the expressions developed for utilizability for a single day. Numerical values obtained for $(\tau\alpha)^*_{day}$ and $(\overline{\tau\alpha})^*$, using the expressions developed in the present chapter, have been validated against hour by hour calculations, as obtained in Chapter 2, as well as, by comparing with the values obtained using solar radiation data.

3.2 Evaluation of Daily Transmittance-Absorptance Product during the Operational Time Period for Flat Plate Collectors

3.2.1 Mathematical Formulation

The effective transmittance-absorptance product for a day, $(\tau\alpha)^*_{day}$, given by Eq. (2.38), after normalizing with the transmittance-absorptance product at normal incidence, can be expressed in an integral form by,

$$\frac{(\tau\alpha)^*_{day}}{(\tau\alpha)_n} = \int_{-\omega_s}^{\omega_s} [I_T - I_c]^+ \frac{(\tau\alpha)}{(\tau\alpha)_n}\, d\omega \Big/ \int_{-\omega_s}^{\omega_s} [I_T - I_c]^+\, d\omega \tag{3.1}$$

It may be noted that replacing Eq. (2.38) by Eq. (3.1) requires I_T to be a continuous function. Also, I_T has been treated as a rate in writing Eq. (3.1), though, the commonly employed notation (for example, in Duffie and Beckman [6]) is that it is the solar radiation over a short time interval, say, an hour. In Eq. (3.1), the superscript '+' indicates that when $(I_T - I_c)$ is negative, it will be considered as zero. Assuming that I_T has a single maximum value during $-\omega_s \leq \omega \leq \omega_s$, Eq. (3.1) can be re-written dropping the superscript '+' as,

$$\frac{(\tau\alpha)^*_{day}}{(\tau\alpha)_n} = \int_{\omega_{c1}}^{\omega_{c2}} [I_T - I_c] \frac{(\tau\alpha)}{(\tau\alpha)_n}\, d\omega \Big/ \int_{\omega_{c1}}^{\omega_{c2}} [I_T - I_c]\, d\omega \tag{3.2}$$

In Eq. (3.2), ω_{c1} and ω_{c2} are the hour angles corresponding to I_T equal to I_c. Eq. (3.2) when expanded leads to,

$$\frac{(\tau\alpha)^*_{day}}{(\tau\alpha)_n} = \int_{\omega_{c1}}^{\omega_{c2}} I_T \frac{(\tau\alpha)}{(\tau\alpha)_n}\, d\omega \Big/ \int_{\omega_{c1}}^{\omega_{c2}} [I_T - I_c]\, d\omega - I_c \int_{\omega_{c1}}^{\omega_{c2}} \frac{(\tau\alpha)}{(\tau\alpha)_n}\, d\omega \Big/ \int_{\omega_{c1}}^{\omega_{c2}} [I_T - I_c]\, d\omega \tag{3.3}$$

Eq. (3.3) is equivalent to Eq. (2.38) which is obtained by equating the daily useful energy gain to the product of $(\tau\alpha)^*_{day}$, F_R, H_T and ϕ_{day} [Eq. (2.35)]. It may be noted that Eq. (3.3) is different from Collares-Pereira and Rabl's [68, 69] definition for $\bar{\eta}_o$. When the

definition of Collares-Pereira and Rabl for $\bar{\eta}_o$ is adapted for a single day, designated as $\eta_{o,day}$, in the present notation becomes,

$$\eta_{o,day} = \int_{\omega_{c1}}^{\omega_{c2}} I_T\,(\tau\alpha)\,d\omega \Big/ \int_{\omega_{c1}}^{\omega_{c2}} I_T\,d\omega \tag{3.4}$$

Eq. (3.3) when integrated yields $(\tau\alpha)^*_{day}$. The expressions thus obtained will become determined when explicit methods to evaluate ω_{c1} and ω_{c2} are made available. ω_{c1} and ω_{c2} can be found by equating I_T to I_c and solving for ω. The relevant equations have been developed by Lahiri [67] and are given in Appendix B.

In the case of flat plate collectors, the solar radiation incident on the collector at any time can be estimated from,

$$I_T = I_b\,R_b + K_2\,I_d + K_3\,I \tag{3.5}$$

where, the constants K_2 and K_3 are as given by Eqs. (1.4) and (1.5) of Chapter 1 and are reproduced here for flat plate collectors for ready reference.

$$K_2 = (1+\cos\beta)/2 \tag{3.6}$$

$$K_3 = \rho\,(1-\cos\beta)/2 \tag{3.7}$$

The instantaneous tilt factor for direct radiation, R_b, at an hour angle ω is defined by.

$$R_b = \frac{\cos\theta}{\cos\theta_z} \tag{3.8}$$

θ is the angle of incidence for direct radiation which is given in Chapter 2 by Eq. (2.1). θ_z is the angle of incidence for a horizontal surface (β=0), also called the zenith angle and is given by,

$$\begin{aligned}\cos\theta_z &= \cos\phi\cos\delta\cos\omega + \sin\phi\sin\delta \\ &= A' + B'\cos\omega \\ &= B'(\cos\omega - \cos\omega_s)\end{aligned} \tag{3.9}$$

where,

$$A' = \sin\phi\sin\delta \qquad \text{and} \qquad B' = \cos\phi\cos\delta \tag{3.10}$$

$(\tau\alpha)/(\tau\alpha)_n$ in Eq. (3.3) is given by Eq. (2.11) of Chapter 2 which is reproduced here for ready reference.

$$\frac{(\tau\alpha)}{(\tau\alpha)_n} = \frac{I_b\,R_b(\tau\alpha)_b/(\tau\alpha)_n + K_2\,I_d(\tau\alpha)_d/(\tau\alpha)_n + K_3\,I(\tau\alpha)_g/(\tau\alpha)_n}{I_b\,R_b + K_2\,I_d + K_3\,I} \tag{3.11}$$

Using Eq. (3.5) for I_T and Eq. (3.11) for $(\tau\alpha)/(\tau\alpha)_n$ in Eq. (3.3), Eq. (3.3) becomes,

$$\frac{(\tau\alpha)^*_{day}}{(\tau\alpha)_n} = \left[\int_{\omega'_{c1}}^{\omega'_{c2}} I_b R_b \frac{(\tau\alpha)_b}{(\tau\alpha)_n}\, d\omega + K_2 \int_{\omega_{c1}}^{\omega_{c2}} I_d \frac{(\tau\alpha)_d}{(\tau\alpha)_n}\, d\omega + K_3 \int_{\omega_{c1}}^{\omega_{c2}} I \frac{(\tau\alpha)_g}{(\tau\alpha)_n}\, d\omega - I_c \int_{\omega_{c1}}^{\omega_{c2}} \frac{(\tau\alpha)}{(\tau\alpha)_n}\, d\omega\right] \div \left[\int_{\omega'_{c1}}^{\omega'_{c2}} I_b R_b\, d\omega + K_2 \int_{\omega_{c1}}^{\omega_{c2}} I_d\, d\omega + K_3 \int_{\omega_{c1}}^{\omega_{c2}} I\, d\omega - I_c \int_{\omega_{c1}}^{\omega_{c2}} d\omega\right] \quad (3.12)$$

Eq. (3.12) can be written in a compact form as,

$$\frac{(\tau\alpha)^*_{day}}{(\tau\alpha)_n} = \left[I_{1N} + I_{2N} + I_{3N} - I_{4N}\right] \div \left[I_{1D} + I_{2D} + I_{3D} - I_{4D}\right] \quad (3.13)$$

where,

$$I_{1N} = \int_{\omega'_{c1}}^{\omega'_{c2}} I_b\, R_b\, \frac{(\tau\alpha)_b}{(\tau\alpha)_n}\, d\omega \quad (3.14)$$

$$I_{2N} = K_2 \int_{\omega_{c1}}^{\omega_{c2}} I_d\, \frac{(\tau\alpha)_d}{(\tau\alpha)_n}\, d\omega \quad (3.15)$$

$$I_{3N} = K_3 \int_{\omega_{c1}}^{\omega_{c2}} I\, \frac{(\tau\alpha)_g}{(\tau\alpha)_n}\, d\omega \quad (3.16)$$

$$I_{4N} = I_c \int_{\omega_{c1}}^{\omega_{c2}} \frac{(\tau\alpha)}{(\tau\alpha)_n}\, d\omega \quad (3.17)$$

and

$$I_{1D} = \int_{\omega'_{c1}}^{\omega'_{c2}} I_b R_b\, d\omega \quad (3.18)$$

$$I_{2D} = K_2 \int_{\omega_{c1}}^{\omega_{c2}} I_d\, d\omega \quad (3.19)$$

$$I_{3D} = K_3 \int_{\omega_{c1}}^{\omega_{c2}} I\, d\omega \quad (3.20)$$

$$I_{4D} = I_c \int_{\omega_{c1}}^{\omega_{c2}} d\omega \quad (3.21)$$

It may be noted that the limits of integration for the direct radiation part given by I_{1N} and I_{1D} [Eqs. (3.14) and (3.18)] are designated as ω'_{c1} and ω'_{c2}. The critical hour angles, ω_{c1} and ω_{c2}, for low critical radiation levels may extend beyond the apparent sunrise and sunset hour angles ω_{sr} and ω_{ss} and less than the sunset hour angle for a horizontal surface, ω_s. In this situation I_{1N} and I_{1D} are to be evaluated from ω_{sr} to ω_{ss} only. ω'_{c1} and ω'_{c2} thus are given by,

$$\omega'_{c1} = \max\left[\omega_{c1}, \omega_{sr}\right] \quad (3.22)$$

$$\omega'_{c2} = \min\left[\omega_{c2}, \omega_{ss}\right] \quad (3.23)$$

Methods to evaluate ω_{sr} and ω_{ss} are available from Duffie and Beckman [6] or Klein and Theilacker [66] and in Lahiri [67] for more general situations, such as, double sunshine. The equations needed to calculate ω_{sr} and ω_{ss} are given in Appendix B.

3.2.2 Expressions for $(\tau\alpha)^*_{day}/(\tau\alpha)_n$

Eq. (3.13) in terms of the integrals defined by Eqs. (3.14) to (3.21) becomes available for evaluating $(\tau\alpha)^*_{day}/(\tau\alpha)_n$ when specific expressions for the integrals are developed. It may be noted that the critical hour angles ω_{c1} and ω_{c2} can be readily evaluated from Eqs. (B.27) to (B.35) of Appendix B.

Using Eqs. (2.25), (2.26) and (2.27) from Chapter 2, for I, I_d and I_b respectively, and Eq. (3.8) for R_b with Eq. (2.4) for $\cos\theta$ and Eq. (3.11) for $(\tau\alpha)/(\tau\alpha)_n$, the integrals in Eqs. (3.14) to (3.17) for I_{1N} to I_{4N} are given by,

$$I_{1N} = \left(\frac{K_1 K_T H_o}{B'}\right) \int_{\omega'_{c1}}^{\omega'_{c2}} (a_1 + b\cos\omega)\cos\theta \frac{(\tau\alpha)_b}{(\tau\alpha)_n} d\omega \tag{3.24}$$

$$I_{2N} = \left(\frac{K_1 K_T H_o}{B'}\right) K_2 D_f B' \int_{\omega_{c1}}^{\omega_{c2}} (\cos\omega - \cos\omega_s) \frac{(\tau\alpha)_d}{(\tau\alpha)_n} d\omega \tag{3.25}$$

$$I_{3N} = \left(\frac{K_1 K_T H_o}{B'}\right) K_3 B' \int_{\omega_{c1}}^{\omega_{c2}} (a + b\cos\omega)(\cos\omega - \cos\omega_s) \frac{(\tau\alpha)_g}{(\tau\alpha)_n} d\omega \tag{3.26}$$

$$I_{4N} = I_c(\overline{\overline{\tau\alpha}})/(\tau\alpha)_n \tag{3.27}$$

It follows from Eq. (3.17), $(\overline{\overline{\tau\alpha}})/(\tau\alpha)_n$ is defined as,

$$\frac{(\overline{\overline{\tau\alpha}})}{(\tau\alpha)_n} = \int_{\omega_{c1}}^{\omega_{c2}} \frac{(\tau\alpha)}{(\tau\alpha)_n} d\omega \tag{3.28}$$

Similarly Eqs. (3.18) to (3.21) for I_{1D} to I_{4D} are given by,

$$I_{1D} = \left(\frac{K_1 K_T H_o}{B'}\right) \int_{\omega'_{c1}}^{\omega'_{c2}} (a_1 + b\cos\omega)\cos\theta \, d\omega \tag{3.29}$$

$$I_{2D} = \left(\frac{K_1 K_T H_o}{B'}\right) K_2 D_f B' \int_{\omega_{c1}}^{\omega_{c2}} (\cos\omega - \cos\omega_s) \, d\omega \tag{3.30}$$

$$I_{3D} = \left(\frac{K_1 K_T H_o}{B'}\right) K_3 B' \int_{\omega_{c1}}^{\omega_{c2}} (a + b\cos\omega)(\cos\omega - \cos\omega_s) \, d\omega \tag{3.31}$$

$$I_{4D} = I_c \int_{\omega_{c1}}^{\omega_{c2}} d\omega \tag{3.32}$$

It may be noted that $(\tau\alpha)_d/(\tau\alpha)_n$ in Eq. (3.25) and $(\tau\alpha)_g/(\tau\alpha)_n$ in Eq. (3.26) are independent of the hour angle ω. $(\tau\alpha)_d/(\tau\alpha)_n$ and $(\tau\alpha)_g/(\tau\alpha)_n$ can be obtained employing Eqs. (2.14) and (2.15), using $\theta = \theta_d$ or θ_g, the effective angle of incidence for sky diffuse and ground reflected components of solar radiation. θ_d and θ_g have been correlated to the slope of the collector by Brandemuehl and Beckman [98] and are given by Eqs. (2.12) and (2.13). $(\tau\alpha)_b/(\tau\alpha)_n$ in Eq. (3.24) depends on the angle of incidence. Dependence of $(\tau\alpha)/(\tau\alpha)_n$ on θ as described by Eqs. (2.14) and (2.15) of Chapter 2 has been employed in evaluating Eq. (3.24). $(\tau\alpha)/(\tau\alpha)_n$ variation with θ as given by Eqs. (2.14) and (2.15)

is piece-wise continuous. Let ω_1 and ω_2 be the hour angles corresponding to $\theta = 60^o$. ω_1 and ω_2 can be obtained by setting $\theta = 60^o$ in Eq. (2.4) for $\cos\theta$. The relevant equations to determine ω_1 and ω_2 are also given in Appendix B. Thus, I_{1N} needs to be evaluated as,

$$\begin{aligned} I_{1N} &= \left(\frac{K_1 K_T H_o}{B'}\right)\left[\int_{\omega'_{c1}}^{\omega_1}(a_1 + b\cos\omega)\,2(1+b_o)\cos^2\theta\,d\omega\right. \\ &\quad + \int_{\omega_1}^{\omega_2}(a_1 + b\cos\omega)\,\cos\theta\left[1 + b_o\left(\frac{1}{\cos\theta} - 1\right)\right]d\omega \\ &\quad \left. + \int_{\omega_2}^{\omega'_{c2}}(a_1 + b\cos\omega)\,2(1+b_o)\cos^2\theta\,d\omega\right] \end{aligned} \tag{3.33}$$

Integrating Eqs. (3.25) to (3.33), I_{1N} etc. are expressed as,

$$\begin{aligned} I_{1N} &= K_4\Big[2(1+b_o)\left\{a_1 I_{P3}(\omega_1,\omega'_{c1}) + bI_{P4}(\omega_1,\omega'_{c1})\right\} + a_1(1-b_o)I_{P1}(\omega_2,\omega_1) \\ &\quad + a_1 b_o(\omega_2 - \omega_1) + b(1-b_o)I_{P2}(\omega_2,\omega_1) + b\,b_o I_{P5}(\omega_2,\omega_1) + \\ &\quad 2(1+b_o)\left\{a_1 I_{P3}(\omega'_{c2},\omega_2) + bI_{P4}(\omega'_{c2},\omega_2)\right\}\Big] \end{aligned} \tag{3.34}$$

$$I_{2N} = K_4 K_2 D_f B' \frac{(\tau\alpha)_d}{(\tau\alpha)_n}\Big[I_{P5}(\omega_{c2},\omega_{c1}) - \cos\omega_s(\omega_{c2} - \omega_{c1})\Big] \tag{3.35}$$

$$\begin{aligned} I_{3N} &= K_4 K_3 B' \frac{(\tau\alpha)_g}{(\tau\alpha)_n}\Big[K_5 I_{P5}(\omega_{c2},\omega_{c1}) - a\cos\omega_s(\omega_{c2} - \omega_{c1}) \\ &\quad + bI_{P6}(\omega_{c2},\omega c1)\Big] \end{aligned} \tag{3.36}$$

$$I_{4N} = I_c \frac{(\overline{\overline{\tau\alpha}})}{(\tau\alpha)_n} \tag{3.37}$$

and

$$I_{1D} = K_4\Big[a_1 I_{P1}(\omega'_{c2},\omega'_{c1}) + bI_{P2}(\omega'_{c2},\omega'_{c1})\Big] \tag{3.38}$$

$$I_{2D} = K_4 K_2 D_f B'\Big[I_{P5}(\omega_{c2},\omega_{c1}) - \cos\omega_s(\omega_{c2} - \omega_{c1})\Big] \tag{3.39}$$

$$I_{3D} = K_4 K_3 B'\Big[K_5 I_{P5}(\omega_{c2},\omega_{c1}) - a\cos\omega_s(\omega_{c2} - \omega_{c1}) + bI_{P6}(\omega_{c2},\omega c1)\Big] \tag{3.40}$$

$$I_{4D} = I_c(\omega_{c2} - \omega c1) \tag{3.41}$$

where, K_4 and K_5 are constants given by,

$$K_4 = K_1 K_T H_o / B' \tag{3.42}$$

$$K_5 = (a - b\cos\omega_s) \tag{3.43}$$

The primitives I_{P1}, I_{P2}, I_{P3}, I_{P4}, I_{P5} and I_{P6} appearing in Eqs. (3.34) to (3.40) are defined by,

$$I_{P1}(\omega) = \int \cos\theta\,d\omega \tag{3.44}$$

$$I_{P2}(\omega) = \int \cos\theta \cos\omega \, d\omega \tag{3.45}$$

$$I_{P3}(\omega) = \int \cos^2\theta \, d\omega \tag{3.46}$$

$$I_{P4}(\omega) = \int \cos^2\theta \cos\omega \, d\omega \tag{3.47}$$

$$I_{P5}(\omega) = \int \cos\omega \, d\omega \tag{3.48}$$

$$I_{P6}(\omega) = \int \cos^2\omega \, d\omega \tag{3.49}$$

Detailed procedure to evaluate $(\overline{\overline{\tau\alpha}})/(\tau\alpha)_n$ in Eq. (3.37), defined by Eq. (3.28), is presented after evaluating the primitives for non-south facing and south facing collectors.

Non-South Facing Collectors

Using Eqs. (3.34) to (3.41) in Eq. (3.13), $(\tau\alpha)^*_{day}/(\tau\alpha)_n$ is expressed as,

$$\begin{aligned}
\frac{(\tau\alpha)^*_{day}}{(\tau\alpha)_n} = {} & \Big[2(1+b_o)\Big\{a_1 I_{P3}(\omega_1,\omega'_{c1}) + bI_{P4}(\omega_1,\omega'_{c1})\Big\} + a_1(1-b_o)I_{P1}(\omega_2,\omega_1) \\
& + a_1 b_o(\omega_2-\omega_1) + b(1-b_o)I_{P2}(\omega_2,\omega_1) + bb_o I_{P5}(\omega_2,\omega_1) + \\
& 2(1+b_o)\Big\{a_1 I_{P3}(\omega'_{c2},\omega_2) + bI_{P4}(\omega'_{c2},\omega_2)\Big\} + \\
& K_2 D_f B' \frac{(\tau\alpha)_d}{(\tau\alpha)_n}\Big[I_{P5}(\omega_{c2},\omega_{c1}) - \cos\omega_s(\omega_{c2}-\omega_{c1})\Big] + \\
& K_3 B' \frac{(\tau\alpha)_g}{(\tau\alpha)_n}\Big[K_5 I_{P5}(\omega_{c2},\omega_{c1}) - a\cos\omega_s(\omega_{c2}-\omega c1) + bI_{P6}(\omega_{c2},\omega_{c1})\Big] \\
& - \frac{I_c}{K_4}\frac{(\overline{\overline{\tau\alpha}})}{(\tau\alpha)_n}\Big] \div \Big[a_1 I_{P1}(\omega'_{c2},\omega'_{c1}) + bI_{P2}(\omega'_{c2},\omega'_{c1}) + \\
& K_2 D_f B'\Big[I_{P5}(\omega_{c2},\omega_{c1}) - \cos\omega_s(\omega_{c2}-\omega_{c1})\Big] + K_3 B'\Big[K_5 I_{P5}(\omega_{c2},\omega_{c1}) - \\
& a\cos\omega_s(\omega_{c2}-\omega_{c1}) + bI_{P6}(\omega_{c2},\omega_{c1})\Big] - \frac{I_c}{K_4}(\omega_{c2}-\omega_{c1})\Big]
\end{aligned} \tag{3.50}$$

The primitives I_{P1} to I_{P6}, in Eq. (3.50), on evaluating Eqs. (3.44) to (3.49), are given by,

$$I_{P1}(\omega) = A\omega + B\sin\omega - C\cos\omega \tag{3.51}$$

$$I_{P2}(\omega) = A\sin\omega + B\left(\frac{\omega}{2} + \frac{\sin 2\omega}{4}\right) - C\frac{\cos 2\omega}{4} \tag{3.52}$$

$$\begin{aligned}
I_{P3}(\omega) = {} & \left[A^2 + \frac{B^2+C^2}{2}\right]\omega + 2AB\sin\omega + \frac{B^2-C^2}{4}\sin 2\omega \\
& - 2AC\cos\omega - \frac{BC}{2}\cos 2\omega
\end{aligned} \tag{3.53}$$

$$I_{P4}(\omega) = AB\,\omega + (A^2 + B^2)\sin\omega + \frac{AB}{2}\sin 2\omega - \frac{B^2 - C^2}{3}\sin^3\omega - \frac{AC}{2}\cos 2\omega - \frac{2BC}{3}\cos^3\omega \quad (3.54)$$

$$I_{P5}(\omega) = \sin\omega \quad (3.55)$$

$$I_{P6}(\omega) = \left(\frac{\omega}{2} + \frac{\sin 2\omega}{4}\right) \quad (3.56)$$

A, B and C appearing in Eqs. (3.51) to (3.56) are already defined by Eqs. (2.5) to (2.7).

South Facing Collectors

The expression for $(\tau\alpha)^*_{day}/(\tau\alpha)_n$ for south facing collectors is obtained from Eq. (3.50) when the limits of the integrals are changed suitably. For south facing flat plate collectors $|\omega_{c1}| = |\omega_{c2}|$. Let the critical hour angles thus be $-\omega_c$ and ω_c. Similarly, ω'_{c1} and ω'_{c2} are replaced by $-\omega'_c$ and ω'_c. Also, ω_1 and ω_2 are replaced by $-\omega'$ and ω'. Thus, for south facing collectors,

$$\begin{aligned}\frac{(\tau\alpha)^*_{day}}{(\tau\alpha)_n} = {} & \Big[2(1+b_o)\Big[a_1 I_{P3}(\omega'_c,\omega') + bI_{P4}(\omega'_c,\omega')\Big] + a_1(1-b_o)I_{P1}(\omega',0) \\ & + a_1 b_o(\omega' - 0) + b(1-b_o)I_{P2}(\omega',0) + bb_o I_{P5}(\omega',0) + \\ & K_2 D_f B' \frac{(\tau\alpha)_d}{(\tau\alpha)_n}\Big[I_{P5}(\omega_c,0) - \cos\omega_s(\omega_c - 0)\Big] + \\ & K_3 B' \frac{(\tau\alpha)_g}{(\tau\alpha)_n}\Big[K_5 I_{P5}(\omega_c,0) - a\cos\omega_s(\omega_c - 0) + bI_{P6}(\omega_c,0)\Big] \\ & - \frac{I_c}{K_4}\frac{(\overline{\overline{\tau\alpha}})}{(\tau\alpha)_n}\Big] \div \Big[a_1 I_{P1}(\omega'_c,0) + bI_{P2}(\omega'_c,0) + \\ & K_2 D_f B'\Big[I_{P5}(\omega_c,0) - \cos\omega_s(\omega_c - 0)\Big] + K_3 B'\Big[K_5 I_{P5}(\omega_c,0) - \\ & a\cos\omega_s(\omega_c - 0) + bI_{P6}(\omega_c,0)\Big] - \frac{I_c}{K_4}(\omega_c - 0)\Big]\end{aligned} \quad (3.57)$$

The primitives I_{P1} to I_{P6} in Eq. (3.57) become,

$$I_{P1}(\omega) = A\,\omega + B\sin\omega \quad (3.58)$$

$$I_{P2}(\omega) = A\sin\omega + B\left(\frac{\omega}{2} + \frac{\sin 2\omega}{4}\right) \quad (3.59)$$

$$I_{P3}(\omega) = \left[A^2 + \frac{B^2}{2}\right]\omega + 2AB\sin\omega + \frac{B^2}{4}\sin 2\omega \quad (3.60)$$

$$I_{P4}(\omega) = AB\,\omega + (A^2 + B^2)\sin\omega + \frac{AB}{2}\sin 2\omega - \frac{B^2}{3}\sin^3\omega \quad (3.61)$$

$$I_{P5}(\omega) = \sin\omega \quad (3.62)$$

$$I_{P6}(\omega) = \left(\frac{\omega}{2} + \frac{\sin 2\omega}{4}\right) \quad (3.63)$$

It may be noted that the constant C, defined by Eq. (2.7) of Chapter 2, is zero for south facing surfaces and the constants A and B, obtained by putting $\gamma = 0$ in Eqs. (2.5) and (2.6), are given by,

$$A = \sin\delta(\sin\phi\cos\beta - \cos\phi\sin\beta) \tag{3.64}$$

$$B = \cos\delta(\cos\phi\cos\beta + \sin\phi\sin\beta) \tag{3.65}$$

Evaluation of $(\overline{\overline{\tau\alpha}})/(\tau\alpha)_n$

Eqs. (3.50) and (3.57) shall become available when $(\overline{\overline{\tau\alpha}})/(\tau\alpha)_n$ defined by Eq. (3.28) is evaluated. Expressing $(\tau\alpha)/(\tau\alpha)_n$ in terms of the total absorbed radiation by the collector and the incident radiation, $(\overline{\overline{\tau\alpha}})/(\tau\alpha)_n$ can be expressed as,

$$\frac{(\overline{\overline{\tau\alpha}})}{(\tau\alpha)_n} = \int_{\omega_{c1}}^{\omega_{c2}} \frac{I_b\, R_b(\tau\alpha)_b/(\tau\alpha)_n + K_2\, I_d(\tau\alpha)_d/(\tau\alpha)_n + K_3\, I(\tau\alpha)_g/(\tau\alpha)_n}{I_b\, R_b + K_2\, I_d + K_3\, I}\, d\omega \tag{3.66}$$

Eq. (3.66) after splitting leads to,

$$(\overline{\overline{\tau\alpha}})/(\tau\alpha)_n = \overline{\overline{T}}_1 + \overline{\overline{T}}_2 + \overline{\overline{T}}_3 \tag{3.67}$$

where,

$$\overline{\overline{T}}_1 = \int_{\omega_{c1}}^{\omega_{c2}} \frac{I_b\, R_b(\tau\alpha)_b/(\tau\alpha)_n}{I_b\, R_b + K_2\, I_d + K_3\, I}\, d\omega \tag{3.68}$$

$$\overline{\overline{T}}_2 = K_2 \int_{\omega_{c1}}^{\omega_{c2}} \frac{I_d(\tau\alpha)_d/(\tau\alpha)_n}{I_b\, R_b + K_2\, I_d + K_3\, I}\, d\omega \tag{3.69}$$

$$\overline{\overline{T}}_3 = K_3 \int_{\omega_{c1}}^{\omega_{c2}} \frac{I(\tau\alpha)_g/(\tau\alpha)_n}{I_b\, R_b + K_2\, I_d + K_3\, I}\, d\omega \tag{3.70}$$

Using Eqs. (2.25), (2.26) and (2.27) for I, I_d and I_b respectively and Eq. (2.3) for R_b in Eq. (3.68), and using ω'_{c1} and ω'_{c2} instead of ω_{c1} and ω_{c2} as has been done in Eq. (3.14), $\overline{\overline{T}}_1$ can be written as,

$$\begin{aligned}
\overline{\overline{T}}_1 = & \int_{\omega'_{c1}}^{\omega_1} \frac{(a_1 + b\cos\omega)\dfrac{\cos\theta}{\cos\theta_z}\left[2(1+b_o)\cos\theta\right]}{(a_1 + b\cos\omega)\dfrac{\cos\theta}{\cos\theta_z} + K_2 D_f + K_3(a + b\cos\omega)}\, d\omega \\
& + \int_{\omega_1}^{\omega_2} \frac{(a_1 + b\cos\omega)\dfrac{\cos\theta}{\cos\theta_z}\left[1 + b_o\left(\dfrac{1}{\cos\theta} - 1\right)\right]}{(a_1 + b\cos\omega)\dfrac{\cos\theta}{\cos\theta_z} + K_2 D_f + K_3(a + b\cos\omega)}\, d\omega \\
& + \int_{\omega_2}^{\omega'_{c2}} \frac{(a_1 + b\cos\omega)\dfrac{\cos\theta}{\cos\theta_z}\left[2(1+b_o)\cos\theta\right]}{(a_1 + b\cos\omega)\dfrac{\cos\theta}{\cos\theta_z} + K_2 D_f + K_3(a + b\cos\omega)}\, d\omega
\end{aligned} \tag{3.71}$$

On simplification, after some what lengthy algebra, $\overline{\overline{T}}_1$ in Eq. (3.71) is given by,

$$\overline{\overline{T}}_1 = 2(1+b_o)T_{11}(\omega_1,\omega'_{c1})+(1-b_o)T_{12}(\omega_2,\omega_1)+b_oT_{13}(\omega_2,\omega_1)+2(1+b_o)T_{11}(\omega'_{c2},\omega_2) \quad (3.72)$$

The primitives T_{11}, T_{12} and T_{13} in Eq. (3.72) are defined by,

$$T_{11}(\omega) = \int \frac{(a_1 + b\cos\omega)\cos^2\theta\, d\omega}{(a_1 + b\cos\omega)\cos\theta + K_2D_f\cos\theta_z + K_3(a + b\cos\omega)\cos\theta_z} \quad (3.73)$$

$$T_{12}(\omega) = \int \frac{(a_1 + b\cos\omega)\cos\theta\, d\omega}{(a_1 + b\cos\omega)\cos\theta + K_2D_f\cos\theta_z + K_3(a + b\cos\omega)\cos\theta_z} \quad (3.74)$$

$$T_{13}(\omega) = \int \frac{(a_1 + b\cos\omega)\, d\omega}{(a_1 + b\cos\omega)\cos\theta + K_2D_f\cos\theta_z + K_3(a + b\cos\omega)\cos\theta_z} \quad (3.75)$$

Using similar procedure, $\overline{\overline{T}}_2$ and $\overline{\overline{T}}_3$ can be expressed as,

$$\overline{\overline{T}}_2 = K_2D_f(\tau\alpha)_d/(\tau\alpha)_n\, T_2(\omega_{c2},\omega_{c1}) \quad (3.76)$$

$$\overline{\overline{T}}_3 = K_3(\tau\alpha)_g/(\tau\alpha)_n\, T_3(\omega_{c2},\omega_{c1}) \quad (3.77)$$

where, the primitives $T_2(\omega)$ and $T_3(\omega)$ are defined as,

$$T_2(\omega) = \int \frac{\cos\theta_z\, d\omega}{(a_1 + b\cos\omega)\cos\theta + K_2D_f\cos\theta_z + K_3(a + b\cos\omega)\cos\theta_z} \quad (3.78)$$

$$T_3(\omega) = \int \frac{(a + b\cos\omega)\cos\theta_z\, d\omega}{(a_1 + b\cos\omega)\cos\theta + K_2D_f\cos\theta_z + K_3(a + b\cos\omega)\cos\theta_z} \quad (3.79)$$

$\overline{\overline{T}}_1$, $\overline{\overline{T}}_2$ and $\overline{\overline{T}}_3$, as given by Eqs. (3.72), (3.76) and (3.77), where the primitives are defined by Eqs. (3.73) – (3.75), (3.78) and (3.79), are not integrable for non-south facing collectors. In what follows a simple procedure to calculate $(\overline{\overline{\tau\alpha}})/(\tau\alpha)_n$ for non-south facing collectors (which is valid for south facing collectors also) and analytical evaluation for south facing collectors is described.

Non-South Facing Collectors: In order to evaluate $(\overline{\overline{\tau\alpha}})/(\tau\alpha)_n$ for non-south facing collectors, a simple procedure which yields accurate results is suggested. Let, θ_1, θ_m and θ_2 be the angles of incidence for direct radiation at the hour angles ω_{c1}, ω_m and ω_{c2} respectively. It may be noted that ω_m corresponds to the hour angle for maximum radiation on the collector surface. Let, $\bar{\theta}$ be the effective angle of incidence defined by,

$$\bar{\theta} = \frac{\theta_1 + \theta_m + \theta_2}{3} \quad (3.80)$$

Let, $\bar{\omega}$ be the hour angle corresponding to $\bar{\theta}$. $\bar{\omega}$ can be obtained from Eqs. (B.12) to (B.18) of Appendix B, by replacing the numerical value of 0.5 with the value of $\cos\bar{\theta}$ given by

Eq. (3.80). It is suggested that $(\overline{\overline{\tau\alpha}})/(\tau\alpha)_n$ be calculated from,

$$\frac{(\overline{\overline{\tau\alpha}})}{(\tau\alpha)_n} = \frac{I_b(\bar{\bar{\omega}})R_b(\bar{\bar{\omega}})\frac{(\tau\alpha)_b}{(\tau\alpha)_n} + K_2 I_d(\bar{\bar{\omega}})\frac{(\tau\alpha)_d}{(\tau\alpha)_n} + K_3 I(\bar{\bar{\omega}})\frac{(\tau\alpha)_g}{(\tau\alpha)_n}}{I_b(\bar{\bar{\omega}})R_b(\bar{\bar{\omega}}) + K_2 I_d(\bar{\bar{\omega}}) + K_3 I(\bar{\bar{\omega}})}(\omega_{c2} - \omega_{c1}) \qquad (3.81)$$

It may be noted that in Eq. (3.81), the value of $(\tau\alpha)_b/(\tau\alpha)_n$ is the corresponding value at $\bar{\bar{\theta}}$, from Eq. (2.14) or (2.15).

South Facing Collectors: For south facing collectors, $\overline{\overline{T}}_1$, $\overline{\overline{T}}_2$ and $\overline{\overline{T}}_3$ as given by Eqs. (3.68), (3.69) and (3.70), reduce to,

$$\overline{\overline{T}}_1 = 2\int_o^{\omega_c'} \frac{I_b\, R_b(\tau\alpha)_b/(\tau\alpha)_n}{I_b\, R_b + K_2\, I_d + K_3\, I}\, d\omega \qquad (3.82)$$

$$\overline{\overline{T}}_2 = 2K_2\int_o^{\omega_c} \frac{I_d(\tau\alpha)_d/(\tau\alpha)_n}{I_b\, R_b + K_2\, I_d + K_3\, I}\, d\omega \qquad (3.83)$$

$$\overline{\overline{T}}_3 = 2K_3\int_o^{\omega_c} \frac{I(\tau\alpha)_g/(\tau\alpha)_n}{I_b\, R_b + K_2\, I_d + K_3\, I}\, d\omega \qquad (3.84)$$

On simplification, $\overline{\overline{T}}_1$ is expressed as,

$$\overline{\overline{T}}_1 = 2\Big[2(1+b_o)T_{11}(\omega_c', \omega') + (1-b_o)T_{12}(\omega', 0) + b_o T_{13}(\omega', 0)\Big] \qquad (3.85)$$

where the primitives T_{11}, T_{12} and T_{13} are as defined by Eqs. (3.73) to (3.75), and for south facing collectors $\cos\theta$ is given by Eq. (2.4) with $C = 0$ and A and B are given by Eqs. (3.64) and (3.65).

On evaluating the primitives which involves lengthy algebra T_{11}, T_{12} and T_{13} can be expressed as,

$$T_{11} = D_1 I_{P5}(\omega_c', \omega') + C_1 D_1(\omega_c' - \omega') + C_1 D_1 P_5 I_{P7}(\omega_c', \omega') + C_1 D_1 Q_5 I_{P8}(\omega_c', \omega') \qquad (3.86)$$

$$T_{12} = E_1(\omega' - 0) + E_1 P_2 I_{P7}(\omega', 0) + E_1 Q_2 I_{P8}(\omega', 0) \qquad (3.87)$$

$$T_{13} = E_2 P_1 I_{P7}(\omega', 0) + E_2 Q_1 I_{P8}(\omega', 0) \qquad (3.88)$$

Similarly, $\overline{\overline{T}}_2$ and $\overline{\overline{T}}_3$ can be expressed as,

$$\overline{\overline{T}}_2 = \frac{(\tau\alpha)_d}{(\tau\alpha)_n}\Big[P_3 I_{P7}(\omega_c, 0) + Q_3 I_{P8}(\omega_c, 0)\Big] \qquad (3.89)$$

$$\overline{\overline{T}}_3 = \frac{(\tau\alpha)_g}{(\tau\alpha)_n}\Big[E_3(\omega_c - 0) + E_3 P_4 I_{P7}(\omega_c, 0) + E_3 Q_4 I_{P8}(\omega_c, 0)\Big] \qquad (3.90)$$

Using Eqs. (3.85) to (3.90) in Eq. (3.67), $(\overline{\overline{\tau\alpha}})/(\tau\alpha)_n$ can be expressed as,

$$\frac{(\overline{\overline{\tau\alpha}})}{(\tau\alpha)_n} = 2\Bigg[2(1+b_o)\Big\{D_1 I_{P5}(\omega_c',\omega') + C_1 D_1(\omega_c' - \omega') + C_1 D_1 P_5 I_{P7}(\omega_c',\omega') + C_1 D_1 Q_5 I_{P8}(\omega_c',\omega')\Big\} + E_1(\omega' - 0) + (E_1 P_2 + E_2 P_1) I_{P7}(\omega',0) + (E_1 Q_2 + E_2 Q_1) I_{P8}(\omega',0) + \frac{(\tau\alpha)_d}{(\tau\alpha)_n}\Big[P_3 I_{P7}(\omega_c,0) + Q_3 I_{P8}(\omega_c,0)\Big] + \frac{(\tau\alpha)_g}{(\tau\alpha)_n}\Big[E_3(\omega_c - 0) + E_3 P_4 I_{P7}(\omega_c,0) + E_3 Q_4 I_{P8}(\omega_c,0)\Big]\Bigg] \quad (3.91)$$

$I_{P5}(\omega)$ appearing in Eq. (3.91) is already given by Eq. (3.62). The primitives $I_{P7}(\omega)$ and $I_{P8}(\omega)$ in Eq. (3.91) are defined as,

$$I_{P7}(\omega) = \int \frac{1}{P + \cos\omega}\, d\omega \quad (3.92)$$

$$I_{P8}(\omega) = \int \frac{1}{Q + \cos\omega}\, d\omega \quad (3.93)$$

with

$$P = \frac{B_2'}{2} \mp \frac{1}{2}\sqrt{B_2'^2 - 4A_2'} \quad (3.94)$$

$$Q = \frac{B_2'}{2} \pm \frac{1}{2}\sqrt{B_2'^2 - 4A_2'} \quad (3.95)$$

In Eqs. (3.94) and (3.95), A_2' and B_2' are given by,

$$A_2' = \frac{Aa_1 + K_2 D_f A' + K_3 A' a}{Bb + K_3 B' b} \quad (3.96)$$

$$B_2' = \frac{Ab + a_1 B + K_2 D_f B' + K_3 A' b + K_3 a B'}{Bb + K_3 B' b} \quad (3.97)$$

$I_{P7}(\omega)$ and $I_{P8}(\omega)$ defined by Eqs. (3.92) and (3.93) are standard integrals. $I_{P7}(\omega)$ is given by,

$$I_{P7}(\omega) = \frac{1}{\sqrt{P^2 - 1}} \cos^{-1}\left(\frac{1 + P\cos\omega}{P + \cos\omega}\right) \quad \text{if} \quad P > 1 \quad (3.98)$$

$$= \frac{1}{\sqrt{1 - P^2}} \log_e \frac{\sqrt{1+P} + \sqrt{1-P}\tan(\omega/2)}{\sqrt{1+P} - \sqrt{1-P}\tan(\omega/2)} \quad \text{if} \quad P < 1 \quad (3.99)$$

$I_{P8}(\omega)$ can be obtained from Eqs. (3.98) and (3.99) by replacing P with Q.

The constants C_1, D_1, etc., appearing in Eq. (3.91) are defined as follows:

$$C_1 = \frac{a_1 B + 2Ab}{Bb} - B_2' \quad (3.100)$$

$$D_1 = \frac{B^2}{B + K_3 B'} \quad (3.101)$$

$$E_1 = \frac{(1-b_o)Bb}{Bb + K_3B'b} \tag{3.102}$$

$$E_2 = \frac{b_o}{Bb + K_3B'b} \tag{3.103}$$

$$P_1 = \frac{bP - a_1}{P - Q} \tag{3.104}$$

$$Q_1 = \frac{a_1 - bQ}{P - Q} \tag{3.105}$$

$$P_2 = \frac{(Ab + a_1B - BbB_2')P - (Aa_1 - A_2'Bb)}{Bb(P - Q)} \tag{3.106}$$

$$Q_2 = \frac{(Aa_1 - A_2'Bb) - (Ab + a_1B - BbB_2')Q}{Bb(P - Q)} \tag{3.107}$$

$$P_3 = \frac{K_2D_f(B'P - A')}{(Bb + K_3B'b)(P - Q)} \tag{3.108}$$

$$Q_3 = \frac{K_2D_f(A' - B'Q)}{(Bb + K_3B'b)(P - Q)} \tag{3.109}$$

$$P_4 = \frac{(A'b + aB' - B'bB_2')P - (A'a - A_2'B'b)}{B'b(P - Q)} \tag{3.110}$$

$$Q_4 = \frac{(A'a - A_2'B'b) - (A'b + aB' - B'bB_2')Q}{B'b(P - Q)} \tag{3.111}$$

$$\begin{aligned} P_5 = {} & \Big[\Big\{2ABa_1 + A^2b - A_2'B^2b - B_2'(a_1B^2 + 2ABb - B_2'B^2b)\Big\}P \\ & - \Big\{A^2a_1 - A_2'(a_1B^2 + 2ABb - B_2'B^2b)\Big\}\Big] \\ & \div \Big[(P - Q)(a_1B^2 + 2ABb - B_2'B^2b)\Big] \end{aligned} \tag{3.112}$$

$$\begin{aligned} Q_5 = {} & \Big[\Big\{A^2a_1 - A_2'(a_1B^2 + 2ABb - B_2'B^2b)\Big\} \\ & - \Big\{2ABa_1 + A^2b - A_2'B^2b - B_2'(a_1B^2 + 2ABb - B_2'B^2b)\Big\}Q\Big] \\ & \div \Big[(P - Q)(a_1B^2 + 2ABb - B_2'B^2b)\Big] \end{aligned} \tag{3.113}$$

Though, $(\overline{\overline{\tau\alpha}})/(\tau\alpha)_n$ for south facing surfaces has been obtained after integrating Eq. (3.66), the resulting expression is some what lengthy. However, adapting an effective angle of incidence, $\bar{\bar{\theta}}$, as has been done for non-south facing collectors [Eq. (3.80)], $(\overline{\overline{\tau\alpha}})/(\tau\alpha)_n$ can be evaluated easily. $\bar{\bar{\theta}}$ is now defined as,

$$\bar{\bar{\theta}} = \frac{2\theta_1 + \theta_n}{3} \tag{3.114}$$

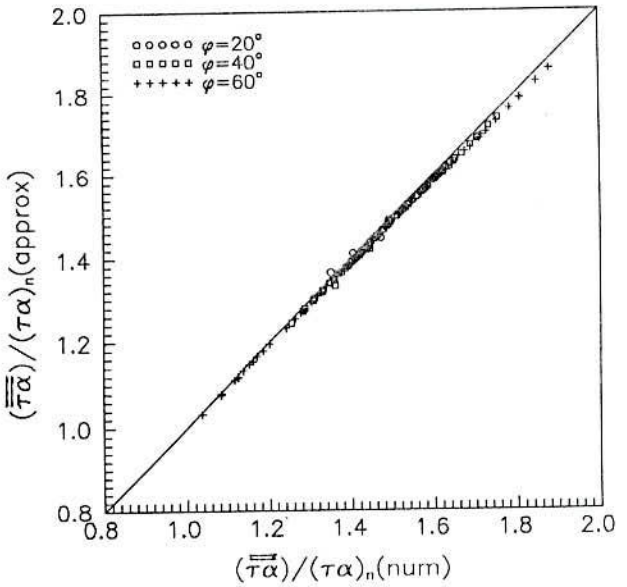

Figure 3.1: Validation of the approximate procedure to calculate $(\overline{\overline{\tau\alpha}})/(\tau\alpha)_n$ for south facing collectors

where, θ_n is the angle of incidence at noon time. Let, $\bar{\omega}$ be the hour angle corresponding to $\bar{\bar{\theta}}$. $\bar{\omega}$ can be obtained from Eqs. (B.12) to (B.18) of Appendix B, replacing the numerical value of 0.5, with the value of $\cos\bar{\bar{\theta}}$ given by Eq. (3.114). Thus, $(\overline{\overline{\tau\alpha}})/(\tau\alpha)_n$ for south facing collectors is given by,

$$\frac{(\overline{\overline{\tau\alpha}})}{(\tau\alpha)_n} = \frac{I_b(\bar{\omega})R_b(\bar{\omega})\frac{(\tau\alpha)_b}{(\tau\alpha)_n} + K_2 I_d(\bar{\omega})\frac{(\tau\alpha)_d}{(\tau\alpha)_n} + K_3 I(\bar{\omega})\frac{(\tau\alpha)_g}{(\tau\alpha)_n}}{I_b(\bar{\omega})R_b(\bar{\omega}) + K_2 I_d(\bar{\omega}) + K_3 I(\bar{\omega})} \times 2\,\omega_c \qquad (3.115)$$

It may be noted that $(\tau\alpha)_b/(\tau\alpha)_n$ in Eq. (3.115) is the value obtained from Eq. (2.14) or (2.15) with $\theta = \bar{\bar{\theta}}$ given by Eq. (3.114).

Validation: Calculating $(\overline{\overline{\tau\alpha}})/(\tau\alpha)_n$ using Eq. (3.81) for non-south facing surfaces and Eq. (3.115) for south facing surfaces has been validated by comparing with the values obtained by numerically integrating Eq. (3.66) for $\gamma = 0^o$, 30^o, 60^o and 90^o; $\phi = 20^o$, 40^o and 60^o; $-23.05^o \leq \delta \leq 23.09^o$; $K_T = 0.5$ and $X_c = 0.6$, with $\beta = \phi - 15^o$, ϕ, $\phi + 15^o$ and $\beta = 90^o$. The comparison between $(\overline{\overline{\tau\alpha}})/(\tau\alpha)_n$, obtained with Eqs. (3.81) and (3.115), designated as $(\overline{\overline{\tau\alpha}})/(\tau\alpha)_n$(approx) with the value obtained by numerically integrating Eq. (3.66) designated as $(\overline{\overline{\tau\alpha}})/(\tau\alpha)_n$(num) is shown in Figure 3.1 for south facing surfaces and in Figure 3.2 for non-south facing surfaces. The agreement is excellent and the values differ by less than 1.0 %.

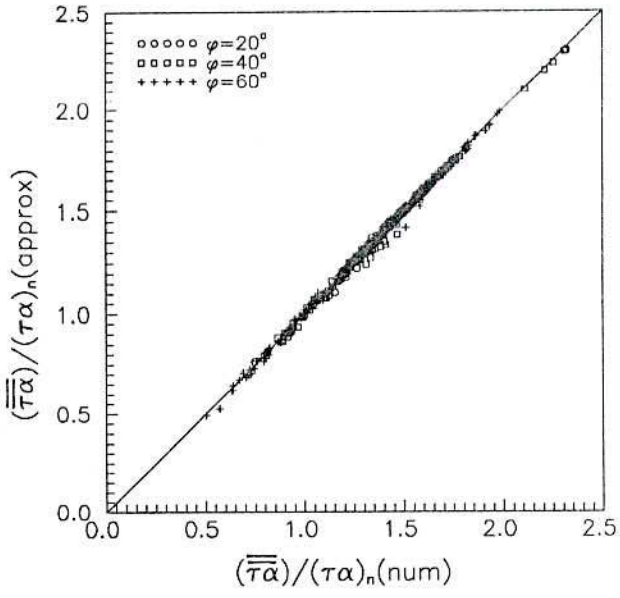

Figure 3.2: Validation of the approximate procedure to calculate $(\overline{\overline{\tau\alpha}})/(\tau\alpha)_n$ for non-south facing collectors

3.3 Evaluation of Monthly Average Transmittance-Absorptance Product during the Operational Time Period for Flat Plate Collectors

3.3.1 Equivalent Mean Day (EMD)

In order to obtain the monthly average transmittance-absorptance product during the period of operation of the collector, it is proposed that $(\overline{\tau\alpha})^*/(\tau\alpha)_n$ be obtained employing the expressions developed for a single day given by Eqs. (3.50) and (3.57), along with Eq. (3.81) (for non-south facing collectors) and Eq. (3.115) (for south facing collectors) for $(\overline{\overline{\tau\alpha}})/(\tau\alpha)_n$ on a suitably chosen day. The single day chosen, designated as equivalent mean day (EMD), is characterized by the following features:

1. Declination for the equivalent mean day is the mean declination, δ_m, for the month.

2. Has clearness index of K_T^*. K_T^* is the average of the clearness indices of the days that contribute to the useful energy.

3. Days that contribute to the useful energy are described by $K_T > K_{T,min}$, where $K_{T,min}$ is the clearness index of the day for which the maximum solar radiation on the collector surface is equal to the critical radiation level. Let, N_c be the number

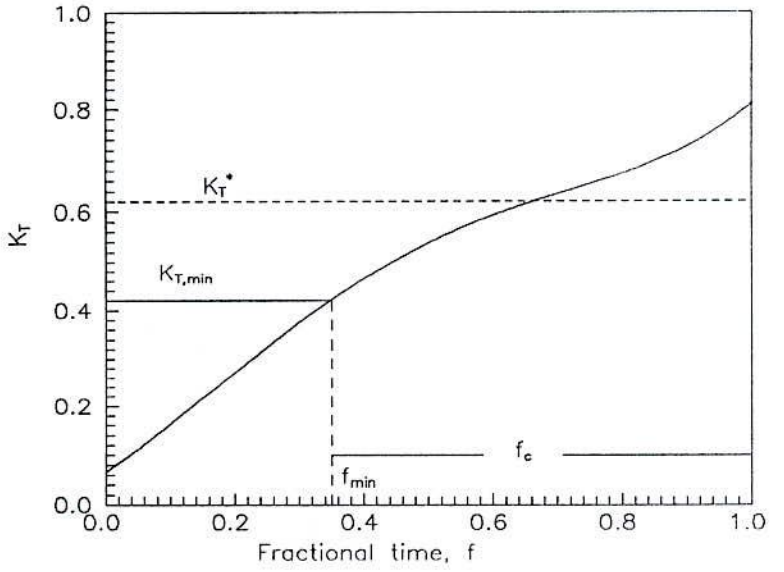

Figure 3.3: Depiction of $K_{T,min}$ from the generalized distribution curves of K_T due to Liu and Jordan [16] for $\bar{K}_T = 0.5$

of days with $K_T > K_{T,min}$. $\bar{K}_T^*$, thus is obtained from,

$$\bar{K}_T^* = \frac{1}{N_c} \sum_{i=1}^{N_c} K_{T_i} \qquad (K_T > K_{T,min}) \tag{3.116}$$

$\bar{K}_T^*$ is depicted in Figure 3.3. Distribution of clearness indices for $\bar{K}_T = 0.5$ from Liu and Jordan [16] is shown in Figure 3.3. For a certain I_c, $K_{T,min}$ is the clearness index below which there is no useful energy gain for the collector. This corresponds to a certain fractional time of f_{min}. $\bar{K}_T^*$ is the average of K_T values during $f = f_{min}$ to 1. N_c, the number of contributing days is obtained from,

$$N_c = N\,(1 - f_{min}) \tag{3.117}$$

where, N is the number of days in a month.

Evaluation of $K_{T,min}$

Let $\bar{X}_c$ be the non-dimensional critical radiation level which corresponds to a critical radiation level of I_c and is given by,

$$I_c = \bar{X}_c\, \bar{I}_{T,m} \tag{3.118}$$

where, $\bar{I}_{T,m}$ can be obtained from Eq. (2.33), replacing K_T with $\bar{K}_T$ and D_f with $\bar{D}_f$. It may be noted that $\bar{I}_{T,m}$ is the maximum radiation on the collector surface on the mean day of the month which occurs at ω_m.

Equating I_c to the maximum radiation on the collector surface for a day with clearness index $K_{T,min}$,

$$I_c = r_{t,m} R_m K_{T,min} H_o \tag{3.119}$$

R_m in Eq. (3.119), given by Eq. (2.32), is reproduced here,

$$R_m = \left[1 - D_f \left(\frac{r_{d,m}}{r_{t,m}}\right)\right] R_{b,m} + K_2 D_f \left(\frac{r_{d,m}}{r_{t,m}}\right) + K_3 \tag{3.120}$$

where, $(r_{d,m}/r_{t,m})$ is given by,

$$\left(\frac{r_{d,m}}{r_{t,m}}\right) = \frac{1}{(a + b\cos\omega_m)} \tag{3.121}$$

In Eq. (3.120), D_f corresponds to $K_{T,min}$. $R_{b,m}$ is the instantaneous tilt factor for direct radiation at $\omega = \omega_m$.

The correlations due to Collares-Periera and Rabl [12] for daily diffuse fraction, D_f, have been linearized for explicit evaluation of $K_{T,min}$ and the following form is suggested.

$$D_f = L_1 + L_2 K_{T,min} \tag{3.122}$$

The constants L_1 and L_2 in Eq. (3.122) assume the values according to $K_{T,min}$ divided into three bins as,

$$L_1 = 1 \qquad L_2 = 0 \qquad \text{if} \quad K_{T,min} \leq 0.24 \tag{3.123}$$

$$L_1 = 1.37 \qquad L_2 = -1.54 \qquad \text{if} \quad 0.24 < K_{T,min} < 0.74 \tag{3.124}$$

$$L_1 = 0.23 \qquad L_2 = 0 \qquad \text{if} \quad K_{T,min} \geq 0.74 \tag{3.125}$$

In Eqs. (3.123) to (3.125), $K_{T,min}$ is used instead of K_T to signify that these approximate relations are used to determine the daily diffuse fraction to obtain $K_{T,min}$ only.

Using Eq. (3.122) for D_f along with R_m given by Eq. (3.120) in Eq. (3.119), $K_{T,min}$ can now be obtained from the generalized quadratic equation,

$$s_1 K_{T,min}^2 + s_2 K_{T,min} + s_3 = 0 \tag{3.126}$$

where,

$$s_1 = \frac{1}{(a + b\cos\omega_m)} L_2 (K_2 - R_{b,m}) \tag{3.127}$$

$$s_2 = \frac{1}{(a + b\cos\omega_m)} L_1 (K_2 - R_{b,m}) + R_{b,m} + K_3 \tag{3.128}$$

$$s_3 = -I_c/(r_{t,m} H_o) \tag{3.129}$$

If $K_{T,min}$ is either ≤ 0.24 or ≥ 0.74, $L_2 = 0$, giving $s_1 = 0$ from Eq. (3.127). $s_1 = 0$ for a horizontal surface also, since $K_2 = (1 + \cos\beta)/2 = 1$, $R_{b,m} = 1$. Thus, when $s_1 = 0$.

$$K_{T,min} = -s_3/s_2 \tag{3.130}$$

The procedure followed to determine the appropriate value of $K_{T,min}$ is to use all the three equations, Eqs. (3.123) to (3.125), to get the respective coefficients s_1 and s_2 from Eqs. (3.127) and (3.128) and subsequently calculate $K_{T,min}$ from Eqs. (3.126) or Eq. (3.130) when $s_1 = 0$. Out of the four values of $K_{T,imin}$ (obtained one each when Eqs. (3.123) and Eq. (3.125) are used and two when Eq. (3.124) is used) obtained, only one value falling in the range for which the equation employed [Eq. (3.123), (3.124) or (3.125)] is valid, is to be accepted.

The difficulty of solving Eq. (3.126) three times corresponding to the three sets of values for L_1 and L_2 as given by Eqs. (3.123) to (3.125) can be alleviated by realizing that,

$$I_c = r_{t,m} R_m K_{T,min} H_o = r_{t,m} R_m K_T H_o X_c \tag{3.131}$$

In Eq. (3.131), $\bar{r}_{t,m}$, $\bar{R}_m$, $\bar{H}_o$ correspond to the values on the average day of the month. Assuming that $r_{t,m} R_m H_o \approx \bar{r}_{t,m} \bar{R}_m \bar{H}_o$, approximate value for $K_{T,min}$, to determine the relevant equation from Eqs. (3.123) to (3.125) for D_f is given by,

$$K_{T,min,a} = X_c K_T \tag{3.132}$$

where, $K_{T,min,a}$ is the approximate value of $K_{T,min}$. It may be noted that Eq. (3.126) in conjunction with Eq. (3.124) for L_1 and L_2 still yields two values of $K_{T,min}$. The value of $K_{T,min}$ nearer to $K_{T,min,a}$ is to be accepted as the value of $K_{T,min}$.

When $K_{T,min}$ is determined, N_c and $\bar{K}_T^*$ can be obtained from Table 3.1, prepared from K_T distribution curves of Liu and Jordan [16]. Alternately, $\bar{K}_T^*$ can be obtained from analytical representation for the Liu and Jordan curves given by Bendt et al. [17].

3.3.2 Evaluating $(\overline{\tau\alpha})^*/(\tau\alpha)_n$ from the Single Day Expressions

It is proposed that $(\overline{\tau\alpha})^*/(\tau\alpha)_n$ be obtained using Eq. (3.57) for south facing flat plate collectors and Eq. (3.50) for non-south facing flat plate collectors which have been developed for a single day. The value thus obtained is designated as $(\overline{\tau\alpha})^*_{cmd}/(\tau\alpha)_n$. The single day expressions, to obtain $(\overline{\tau\alpha})^*_{cmd}/(\tau\alpha)_n$, are used with,

1. $\delta = \delta_m$
2. $K_T = \bar{K}_T^*$ and

Table 3.1: Daily clearness index distribution from Liu and Jordan's [16] curves, number of contributing days and average clearness index for the contributing days

$\bar{K}_T$	0.3			0.4			0.5			0.6			0.7		
Day	K_T	N_c	$\bar{K}_T^*$	K_T	N_c	$\bar{K}_T^*$	K_T	N_c	$\bar{K}_T^*$	K_T	N_c	$\bar{K}_T^*$	K_T	N_c	$\bar{K}_T^*$
1	0.01	30	0.30	0.05	30	0.40	0.08	30	0.50	0.12	30	0.60	0.37	30	0.70
2	0.02	29	0.31	0.07	29	0.41	0.12	29	0.51	0.19	29	0.62	0.47	29	0.71
3	0.04	28	0.32	0.09	28	0.42	0.16	28	0.53	0.25	28	0.63	0.52	28	0.72
4	0.06	27	0.33	0.12	27	0.43	0.21	27	0.54	0.31	27	0.64	0.57	27	0.73
5	0.07	26	0.34	0.14	26	0.45	0.24	26	0.55	0.32	26	0.66	0.60	26	0.73
6	0.09	25	0.35	0.16	25	0.46	0.28	25	0.57	0.37	25	0.67	0.63	25	0.74
7	0.11	24	0.36	0.18	24	0.47	0.31	24	0.58	0.43	24	0.68	0.65	24	0.74
8	0.13	23	0.37	0.20	23	0.48	0.35	23	0.59	0.47	23	0.70	0.66	23	0.75
9	0.15	22	0.38	0.23	22	0.50	0.37	22	0.60	0.50	22	0.71	0.67	22	0.75
10	0.17	21	0.40	0.25	21	0.51	0.40	21	0.61	0.54	21	0.72	0.69	21	0.76
11	0.19	20	0.41	0.29	20	0.52	0.43	20	0.62	0.56	20	0.73	0.69	20	0.76
12	0.20	19	0.42	0.32	19	0.54	0.46	19	0.63	0.59	19	0.73	0.70	19	0.76
13	0.22	18	0.43	0.34	18	0.55	0.49	18	0.64	0.61	18	0.74	0.71	18	0.77
14	0.23	17	0.45	0.36	17	0.56	0.52	17	0.65	0.64	17	0.75	0.72	17	0.77
15	0.27	16	0.46	0.39	16	0.57	0.54	16	0.66	0.66	16	0.76	0.73	16	0.77
16	0.29	15	0.47	0.41	15	0.59	0.56	15	0.67	0.68	15	0.76	0.73	15	0.77
17	0.31	14	0.48	0.44	14	0.60	0.57	14	0.68	0.69	14	0.77	0.73	14	0.78
18	0.34	13	0.49	0.46	13	0.61	0.59	13	0.69	0.71	13	0.77	0.74	13	0.78
19	0.36	12	0.51	0.49	12	0.62	0.61	12	0.69	0.72	12	0.78	0.75	12	0.79
20	0.38	11	0.52	0.51	11	0.64	0.63	11	0.70	0.73	11	0.79	0.76	11	0.79
21	0.41	10	0.54	0.54	10	0.65	0.64	10	0.71	0.74	10	0.79	0.76	10	0.79
22	0.43	9	0.55	0.57	9	0.66	0.65	9	0.72	0.75	9	0.80	0.77	9	0.79
23	0.45	8	0.56	0.59	8	0.67	0.66	8	0.72	0.76	8	0.80	0.77	8	0.80
24	0.47	7	0.58	0.61	7	0.68	0.67	7	0.73	0.77	7	0.81	0.78	7	0.80
25	0.50	6	0.60	0.63	6	0.70	0.69	6	0.74	0.78	6	0.82	0.79	6	0.81
26	0.53	5	0.62	0.65	5	0.71	0.71	5	0.75	0.78	5	0.82	0.79	5	0.81
27	0.56	4	0.64	0.67	4	0.73	0.72	4	0.76	0.80	4	0.83	0.80	1	0.81
28	0.60	3	0.67	0.70	3	0.75	0.75	3	0.78	0.82	3	0.84	0.81	3	0.81
29	0.66	2	0.70	0.75	2	0.77	0.77	2	0.80	0.84	2	0.85	0.81	2	0.82
30	0.75	1	0.75	0.79	1	0.79	0.82	1	0.82	0.87	1	0.87	0.83	1	0.83

3. $X_c = X_c^*$

where, X_c^* is the single day (now the equivalent mean day) non-dimensional critical radiation level corresponding to I_c and is given by,

$$X_c^* = \frac{I_c}{r_{t,m}^* \bar{K}_T^* \bar{R}_m^* H_o} \tag{3.133}$$

From Eq. (3.118), it may be noted that X_c^* is related to $\bar{X}_c$ by,

$$\begin{aligned} X_c^* &= \bar{X}_c \frac{\bar{r}_{t,m} \bar{K}_T \bar{R}_m}{r_{t,m}^* \bar{K}_T^* \bar{R}_m^*} \\ &= \bar{X}_c \frac{\bar{I}_{t,m}}{I_{t,m}^*} \end{aligned} \tag{3.134}$$

when, $\bar{I}_{T,m}^*$ is obtained, by rewriting Eq. (2.33) for the equivalent mean day, as,

$$\begin{aligned} \bar{I}_{T,m}^* = \frac{K_1 \bar{K}_T^* H_o}{B'} \Big[& (a_1 + b\cos\omega_m)\cos\theta_m + K_2 D_f B'(\cos\omega_m - \cos\omega_s) \\ & + K_3 B'(a + b\cos\omega_m)(\cos\omega_m - \cos\omega_s) \Big] \end{aligned} \tag{3.135}$$

D_f in Eq. (3.135) is the daily diffuse fraction corresponding to $\bar{K}_T^*$.

This methodology becomes available to calculate $(\overline{\tau\alpha})^*/(\tau\alpha)_n$ when validated against the defining equation [Eq. (2.49)] which is reproduced here,

$$(\overline{\tau\alpha})^*/(\tau\alpha)_n = \frac{\sum\sum(I_T - I_c)^+(\tau\alpha)/(\tau\alpha)_n}{\sum\sum(I_T - I_c)^+} \tag{3.136}$$

$\bar{Q}_{u,m}$ can thus be calculated from,

$$\bar{Q}_{u,m} = F_R(\tau\alpha)_n \bar{H}_T \bar{\phi} \frac{(\overline{\tau\alpha})_{emd}^*}{(\tau\alpha)_n} \tag{3.137}$$

3.4 Results and Discussion

Numerical values for $(\tau\alpha)_{day}^*/(\tau\alpha)_n$ obtained using Eqs. (3.50) and (3.57) and $(\overline{\tau\alpha})^*/(\tau\alpha)_n$ using the EMD approach have been validated against the values reported in Chapter 2, obtained by hour by hour numerical integration. The validation has been carried out for the following values of the parameters.

$\phi = 20^o$, 40^o and 60^oN
$\beta = \phi + 15^o$, ϕ, $\phi - 15^o$ and 90^o
$\gamma = 0^o$, 30^o, 60^o and 90^o
$-23.45^o \leq \delta \leq 23.45^o$

$b_o = -0.1$ (applicable for flat plate collectors with a single glass cover)

$0.3 \leq K_T \leq 0.7, \quad 0.0 \leq Xc \leq 0.8$

$0.3 \leq \bar{K}_T \leq 0.7 \quad 0.0 \leq \bar{X}_c \leq \bar{X}_{c,max}.$

It may be noted that when $\bar{X}_c \geq \bar{X}_{c,max}$, the monthly average daily utilizability, $\bar{\phi} = 0$. $\bar{X}_{c,max}$ will be approximately equal to $K_{T,max}/K_T$, where $K_{T,max}$ is the maximum daily clearness index in a month of average daily clearness index K_T.

3.4.1 Transmittance-Absorptance Product for a Single Day, $(\tau\alpha)^*_{day}/(\tau\alpha)_n$

South Facing Collectors

Even though, in principle, numerically integrated values as obtained in Chapter 2 and the values obtained from integrated expressions should not differ, (except for a small difference due to numerical integration) this validation has been undertaken since the analytically obtained expression involved certain intricacies, such as, employing ω_{c1} and ω_{c2} instead of ω_{sr} and ω_{ss} and determining the same. $(\tau\alpha)^*_{day}/(\tau\alpha)_n$ values have been obtained using Eq. (3.57), along with Eq. (3.115) for $(\overline{\tau\alpha})/(\tau\alpha)_n$. $(\tau\alpha)^*_{day}/(\tau\alpha)_n$ obtained following hour by hour summation according to Eq. (2.38) of Chapter 2 is designated as $(\tau\alpha)^*_{day}/(\tau\alpha)_n$(num). A plot of $(\tau\alpha)^*_{day}/(\tau\alpha)_n$ vs $(\tau\alpha)^*_{day}/(\tau\alpha)_n$(num) is shown in Figure 3.4 for $\phi = 20^o$, 40^o and 60^o, for $-23.05^o \leq \delta \leq 23.09^o$, $\beta = \phi - 15^o$, ϕ, $\phi + 15^o$ and $\beta = 90^o$ for $\gamma = 0^o$ at $X_c = 0.6$ and $\bar{K}_T = 0.5$. The agreement is near perfect even though Eq. (3.115), which yields $(\overline{\tau\alpha})/(\tau\alpha)_n$ somewhat approximately, is used, the differences are in the fourth decimal place in $(\tau\alpha)^*_{day}/(\tau\alpha)_n$.

Non-South Facing Surfaces

Plots of $(\tau\alpha)^*_{day}/(\tau\alpha)_n$ vs $(\tau\alpha)^*_{day}/(\tau\alpha)_n$(num) are shown in Figures 3.5, 3.6 and 3.7 for $\gamma = 30^o$, 60^o and 90^o respectively, for $\phi = 20^o$, 40^o and 60^o, for $-23.05^o \leq \delta \leq 23.09^o$, $\beta = \phi - 15^o$, ϕ, $\phi + 15^o$ and $\beta = 90^o$, at $X_c = 0.6$ and $K_T = 0.5$. The agreement between $(\tau\alpha)^*_{day}/(\tau\alpha)_n$ and $(\tau\alpha)^*_{day}/(\tau\alpha)_n$(num) is as good as the agreement for south facing collectors in all the three figures for non-south facing collectors.

Validation Against Data

$(\tau\alpha)^*_{day}/(\tau\alpha)_n$ values as obtained using Eq. (3.57) for south facing and Eq. (3.50) for non-south facing collectors respectively have been compared with the values obtained employing monthly average hourly solar radiation data for 3 locations, Ahmedabad ($\phi = 23.07^o$), New Delhi ($\phi = 28.58^o$) in India and Madison, WI ($\phi = 43.10^o$) in USA. The data have been taken from [132], for the Indian locations and the TMY data for Madison

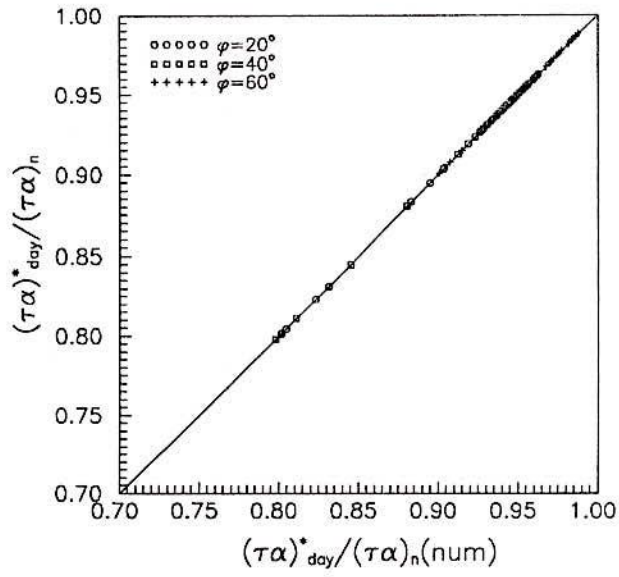

Figure 3.4: Validation of $(\tau\alpha)^*_{day}/(\tau\alpha)_n$ and $(\tau\alpha)^*_{day}/(\tau\alpha)_n(\text{num})$ for single day calculation for south facing collectors

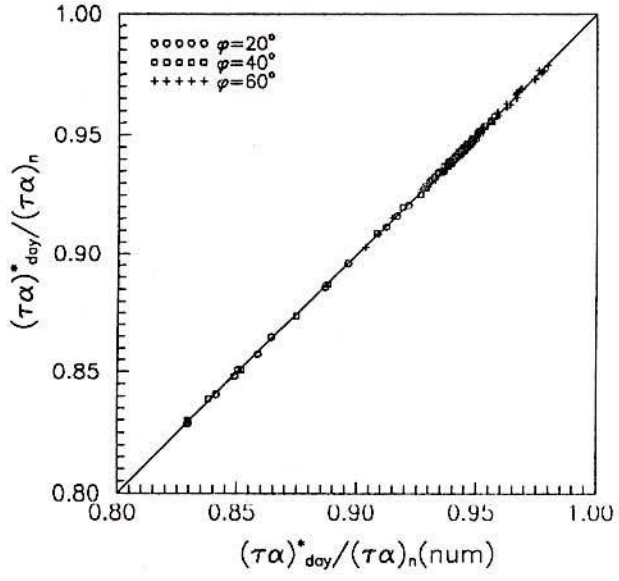

Figure 3.5: Validation of $(\tau\alpha)^*_{day}/(\tau\alpha)_n$ and $(\tau\alpha)^*_{day}/(\tau\alpha)_n(\text{num})$ for single day calculation for non-south facing collectors, $\gamma = 30^o$

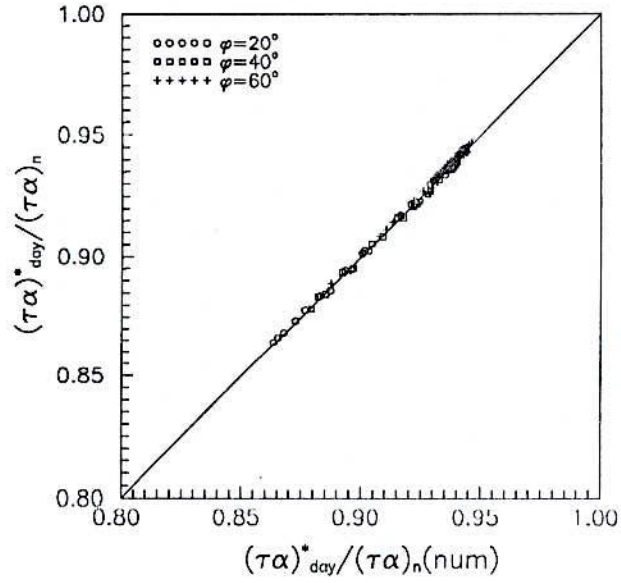

Figure 3.6: Validation of $(\tau\alpha)^*_{day}/(\tau\alpha)_n$ and $(\tau\alpha)^*_{day}/(\tau\alpha)_n(\text{num})$ for single day calculation for non-south facing collectors, $\gamma = 60^o$

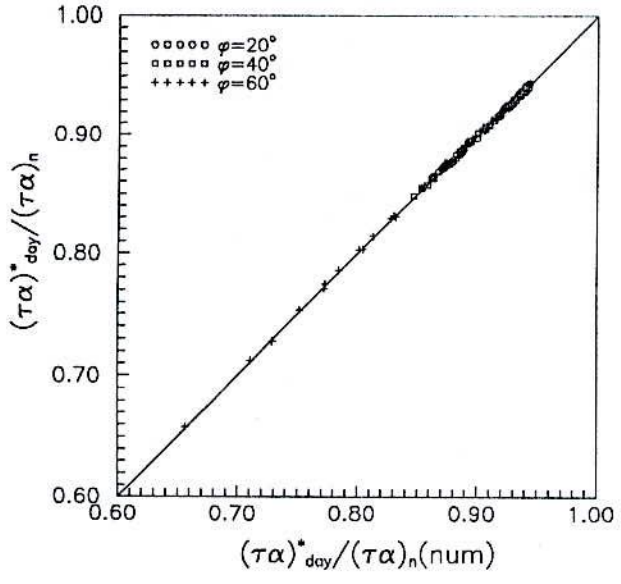

Figure 3.7: Validation of $(\tau\alpha)^*_{day}/(\tau\alpha)_n$ and $(\tau\alpha)^*_{day}/(\tau\alpha)_n(\text{num})$ for single day calculation for non-south facing collectors, $\gamma = 90^o$

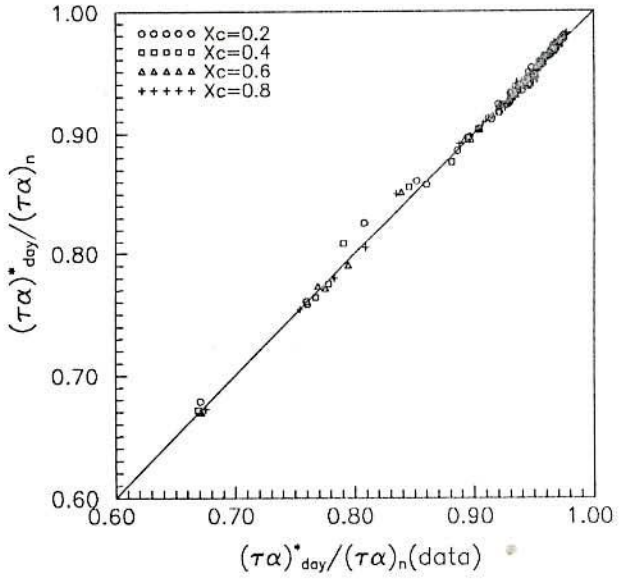

Figure 3.8: Validation of $(\tau\alpha)^*_{day}/(\tau\alpha)_n$ with $(\tau\alpha)^*_{day}/(\tau\alpha)_n$(data) for south facing collectors for Ahmedabad ($\phi = 23.07^o$)

[133]. $(\tau\alpha)^*_{day}/(\tau\alpha)_n$ obtained using Eq. (2.38) employing the data is designated as $(\tau\alpha)^*_{day}/(\tau\alpha)_n$(data). Plots of $(\tau\alpha)^*_{day}/(\tau\alpha)_n$ vs $(\tau\alpha)^*_{day}/(\tau\alpha)_n$(data) are shown in Figures 3.8, 3.9 and 3.10 for the three locations, Ahmedabad, New Delhi and Madison respectively. Figures 3.8 to 3.10 are drawn for $\gamma = 0$, for all the 12 months with $\beta = \phi - 15^o$, ϕ, $\phi + 15^o$ and $\beta = 90^o$ for $X_c = 0.2$, 0.4, 0.6 and 0.8. The agreement is good. The differences seen in Figures 3.8 and 3.9 are due to employing r_t [12] and r_d [16] correlations in obtaining Eq. (3.57) for $(\tau\alpha)^*_{day}/(\tau\alpha)_n$. However, these differences are small. Somewhat larger differences in Figure 3.10 between $(\tau\alpha)^*_{day}/(\tau\alpha)_n$ and $(\tau\alpha)^*_{day}/(\tau\alpha)_n$(data) for Madison, WI, USA is due to low $\bar{K}_T$ values for the months of November, December and January.

Similar plot of $(\tau\alpha)^*_{day}/(\tau\alpha)_n$ vs $(\tau\alpha)^*_{day}/(\tau\alpha)_n$(data) is shown in Figure 3.11 for New Delhi ($\phi = 28.58^o$), India, for $\beta = \phi - 15^o$, ϕ, $\phi + 15^o$ and $\beta = 90^o$, for $X_c = 0.2$, 0.4, 0.6 and 0.8, for all the 12 months, for $\gamma = 30^o$, 60^o and 90^o. It is evident from Figure 3.11 that the agreement is good. The rms difference for indian locations between $(\tau\alpha)^*_{day}/(\tau\alpha)_n$ and $(\tau\alpha)^*_{day}/(\tau\alpha)_n$(data) is less than 1 % for south facing as well as non-south facing collectors. For Madison, WI the rms difference is 1.4 %. It may be noted that the only information required to calculate $(\tau\alpha)^*_{day}/(\tau\alpha)_n$ is the daily diffuse fraction or alternately the clearness index K_T.

Transmittance-absorptance product for the day as defined in Eqs. (2.38), (2.40) and (3.4), using the solar radiation data for the 3 locations (Ahmedabad, New Delhi and

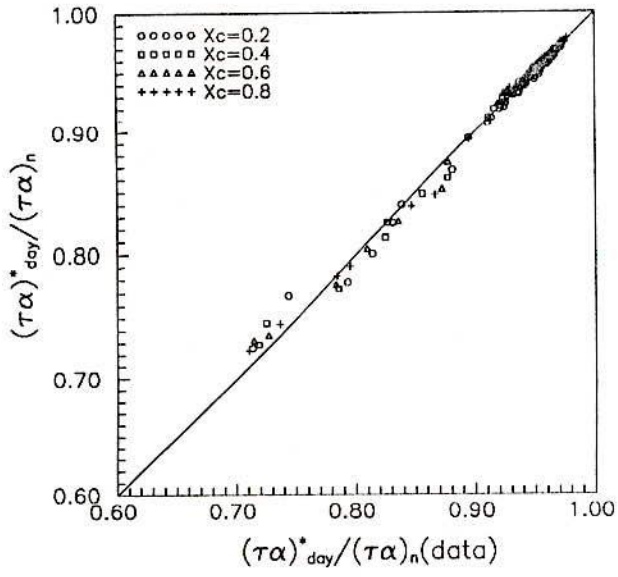

Figure 3.9: Validation of $(\tau\alpha)^*_{day}/(\tau\alpha)_n$ with $(\tau\alpha)^*_{day}/(\tau\alpha)_n$(data) for south facing collectors for New Delhi ($\phi = 28.58^o$)

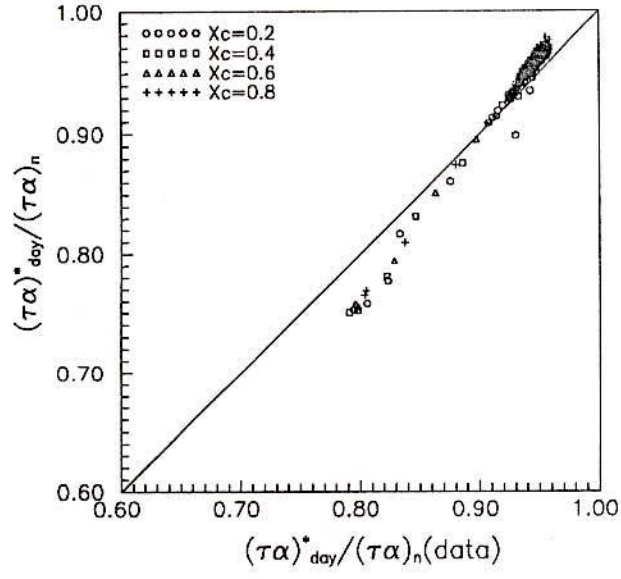

Figure 3.10: Validation of $(\tau\alpha)^*_{day}/(\tau\alpha)_n$ with $(\tau\alpha)^*_{day}/(\tau\alpha)_n$(data) for south facing collectors for Madison, WI ($\phi = 43.10^o$)

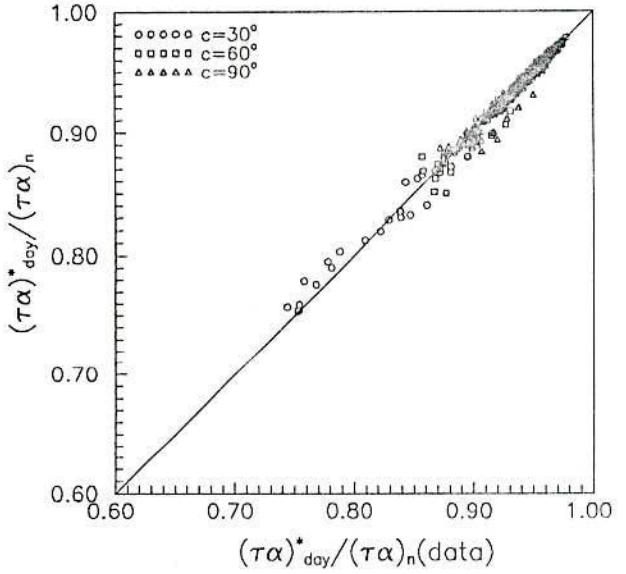

Figure 3.11: Validation of $(\tau\alpha)^*_{day}/(\tau\alpha)_n$ with $(\tau\alpha)^*_{day}/(\tau\alpha)_n$(data) for non-south facing collectors for New Delhi, India ($\phi = 28.58^o$)

Madison, WI), designated respectively as $(\tau\alpha)^*_{day}/(\tau\alpha)_n$(data), $(\tau\alpha)_{day}/(\tau\alpha)_n|_{KL}$ and $(\eta_{o,day}/\eta_{o,n})|_{CPR}$ have been calculated. Plot of $(\tau\alpha)_{day}/(\tau\alpha)_n|_{KL}$ and $(\eta_{o,day}/\eta_{o,n})|_{CPR}$ vs $(\tau\alpha)^*_{day}/(\tau\alpha)_n$(data) is shown in Figure 3.12 for $\beta = \phi - 15^o$, ϕ, $\phi + 15^o$ and 90^o, $-23.05^o \leq \delta \leq 23.09^o$, for $X_c = 0.2$, 0.4, 0.6 and 0.8, for $\gamma = 0^o$. It is evident from Figure 3.12 that $(\tau\alpha)_{day}/(\tau\alpha)_n|_{KL}$ values deviate more than $(\eta_{o,day}/\eta_{o,n})|_{CPR}$ values from the $(\tau\alpha)^*_{day}/(\tau\alpha)_n$(data) values and the deviations are not insignificant. $(\eta_{o,day}/\eta_{o,n})|_{CPR}$ being closer to $(\tau\alpha)^*_{day}/(\tau\alpha)_n$(data) is due to $(\eta_{o,day}/\eta_{o,n})|_{CPR}$ being defined as the average for the operating period.

3.4.2 Validation of EMD Calculation of Monthly Average Transmittance-Absorptance Product

The values of $(\overline{\tau\alpha})^*/(\tau\alpha)_n$ as given by Eq. (2.49) have already been reported in Chapter 2, §2.3, for $\phi = 20^o$, 40^o and 60^o, $\beta = \phi - 15^o$, ϕ, $\phi + 15^o$ and 90^o, $\bar{K}_T = 0.3$, 0.5 and 0.7, and $0.2 \leq \bar{X}_c \leq 2.0$. The values thus obtained by hour by hour numerical integration for all the hours and days are designated by $(\overline{\tau\alpha})^*/(\tau\alpha)_n$(num). As proposed in the present Chapter, §3.3, monthly average transmittance-absorptance product, obtained employing the EMD method, designated as $(\overline{\tau\alpha})^*_{emd}/(\tau\alpha)_n$, has also been calculated for the aforementioned parameters. It may be recalled that the EMD calculation employs the expression for $(\tau\alpha)^*_{day}/(\tau\alpha)_n$ developed for a single day with $\delta = \delta_m$, $X_c = X^*_c$ and $\bar{K}_T = \bar{K}^*_T$.

In what follows, $(\overline{\tau\alpha})^*_{emd}/(\tau\alpha)_n$ values have been compared with $(\overline{\tau\alpha})^*/(\tau\alpha)_n$ values,

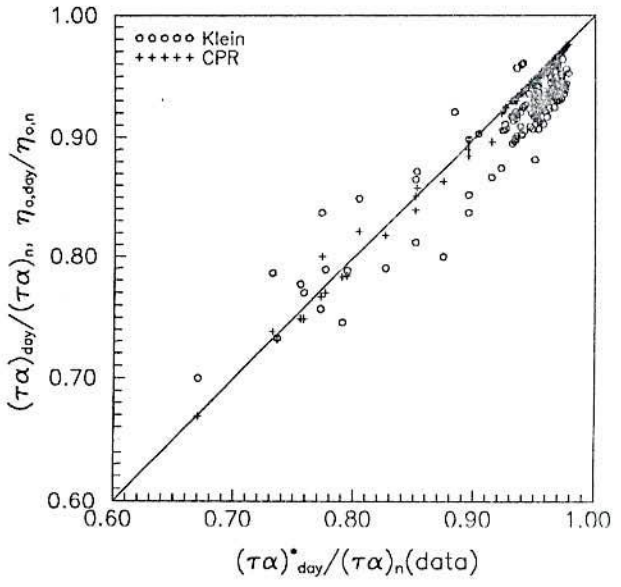

Figure 3.12: Comparison of $(\tau\alpha)_{day}/(\tau\alpha)_n|_{KL}$ and $(\eta_{o,day}/\eta_{o,n})|_{CPR}$ against $(\tau\alpha)^*_{day}/(\tau\alpha)_n$(data) for south facing collectors

calculated according to Eq. (2.49).

Plots of $(\overline{\tau\alpha})^*_{emd}/(\tau\alpha)_n$ vs $(\overline{\tau\alpha})^*/(\tau\alpha)_n$(num) are shown in Figures 3.13 to 3.16 for $\gamma = 0^o$, 30^o, 60^o and 90^o respectively, for $\phi = 20^o$, 40^o and 60^o; $\beta = \phi$, for all the 12 months for $0.2 \leq \bar{X}_c \leq 2.0$, for $\bar{K}_T = 0.3$, 0.5 and 0.7. It is evident from Figures 3.13 to 3.16 that the EMD approach yields values which agree well with $(\overline{\tau\alpha})^*/(\tau\alpha)_n$ obtained by hour by hour calculation for the month. The rms differences are 0.50 %, 0.53 %, 0.61 % and 1.03 % for $\gamma = 0^o$, 30^o, 60^o and 90^o respectively.

$(\overline{\tau\alpha})^*_{emd}/(\tau\alpha)_n$ values have also been compared with $(\overline{\tau\alpha})^*/(\tau\alpha)_n$(num) values for $\beta = 90^o$ for $\gamma = 0^o$ and 90^o, for the same parameters as stated in the preceding paragraph. The comparisons are shown in Figures 3.17 and 3.19. The agreement between $(\overline{\tau\alpha})^*_{emd}/(\tau\alpha)_n$ and $(\overline{\tau\alpha})^*/(\tau\alpha)_n$ is within a rms difference of 1.76 % and 1.23 %.

Thus, the EMD approach predicts the monthly average transmittance-absorptance product, $(\overline{\tau\alpha})^*/(\tau\alpha)_n$, defined as a weighted average of instantaneous $(\tau\alpha)$ and the solar radiation above the critical radiation level over all the hours and days in the month within a small rms difference.

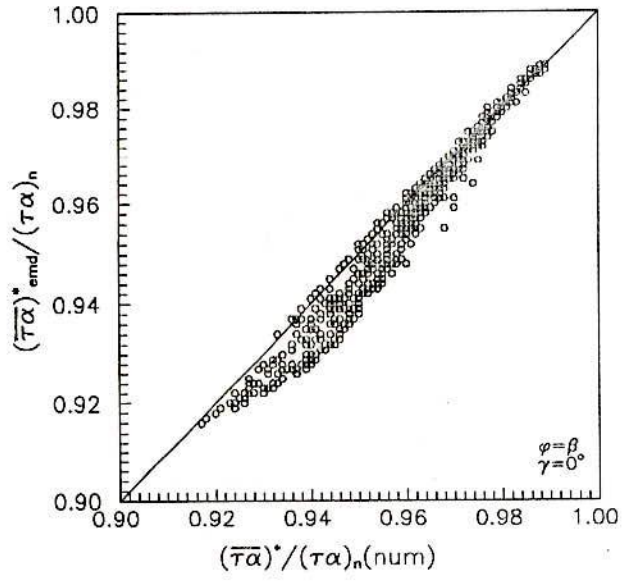

Figure 3.13: Validation of $(\overline{\tau\alpha})^*_{cmd}/(\tau\alpha)_n$ against $(\overline{\tau\alpha})^*/(\tau\alpha)_n$ for $\beta = \phi$ for south facing collectors

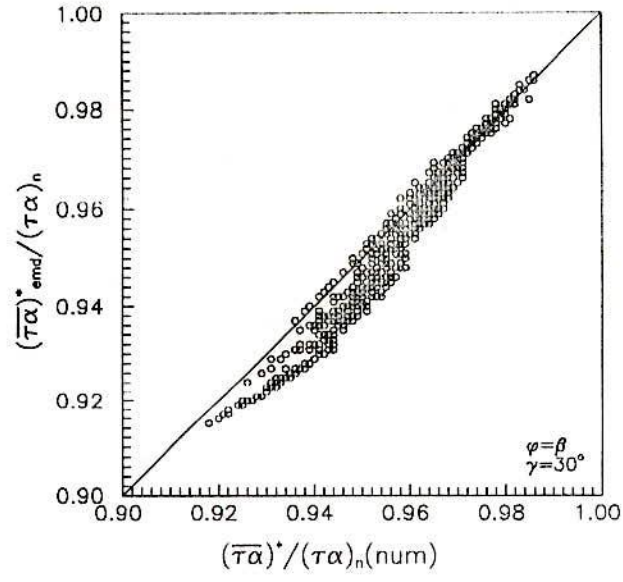

Figure 3.14: Validation of $(\overline{\tau\alpha})^*_{cmd}/(\tau\alpha)_n$ against $(\overline{\tau\alpha})^*/(\tau\alpha)_n$ for $\beta = \phi$ for $\gamma = 30°$

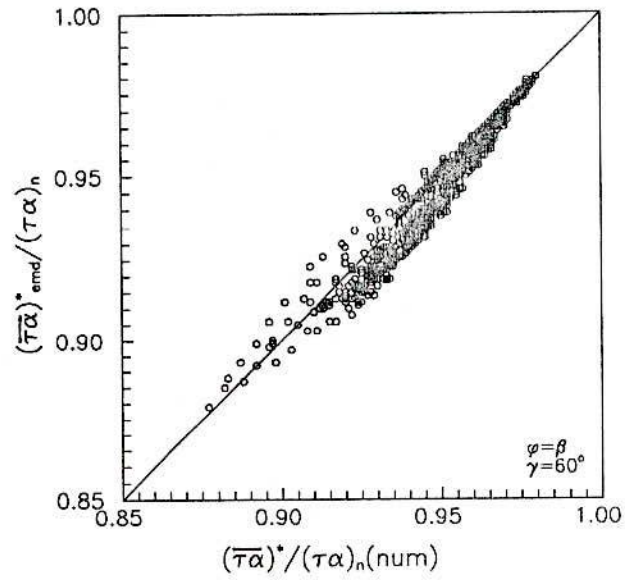

Figure 3.15: Validation of $(\overline{\tau\alpha})^*_{emd}/(\tau\alpha)_n$ against $(\overline{\tau\alpha})^*/(\tau\alpha)_n$ for $\beta = \phi$ for $\gamma = 60°$

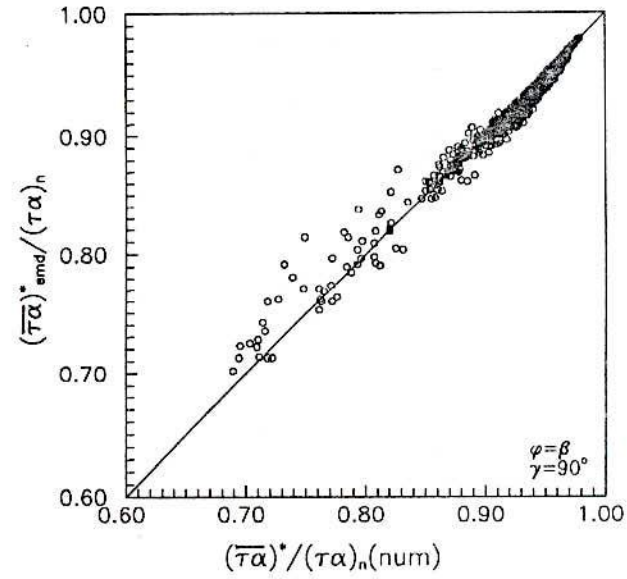

Figure 3.16: Validation of $(\overline{\tau\alpha})^*_{emd}/(\tau\alpha)_n$ against $(\overline{\tau\alpha})^*/(\tau\alpha)_n$ for $\beta = \phi$ for $\gamma = 90°$

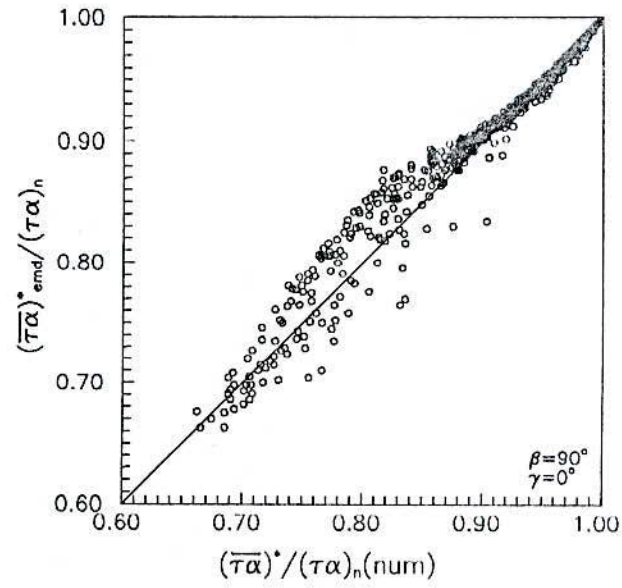

Figure 3.17: Validation of $(\overline{\tau\alpha})^*_{emd}/(\tau\alpha)_n$ against $(\overline{\tau\alpha})^*/(\tau\alpha)_n$ for vertical collectors for $\gamma = 0^o$

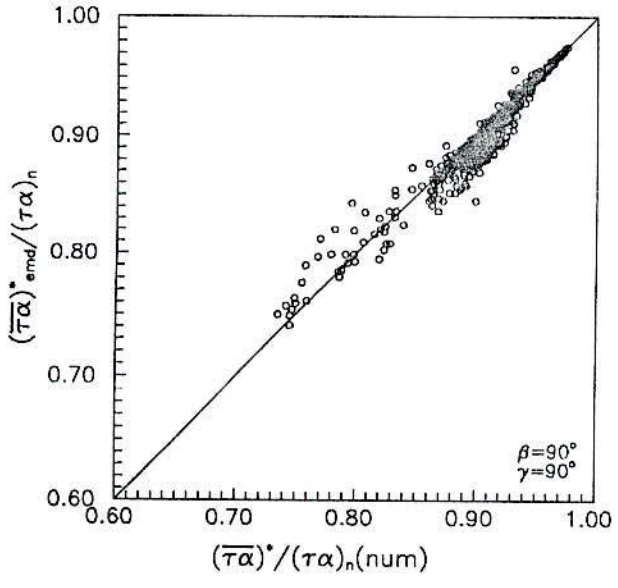

Figure 3.18: Validation of $(\overline{\tau\alpha})^*_{emd}/(\tau\alpha)_n$ against $(\overline{\tau\alpha})^*/(\tau\alpha)_n$ for vertical collectors for $\gamma = 90^o$

3.5 Conclusions

An expression to evaluate the transmittance-absorptance product for a single day, defined as a weighted average of instantaneous $(\tau\alpha)$ and the solar radiation above the critical radiation level has been developed. The approach followed involves integrating the defining equation during the period of operation. The period of operation from ω_{c1} to ω_{c2} has been related to the critical radiation level. Numerical values obtained for $(\tau\alpha)^*_{day}/(\tau\alpha)_n$ have been compared with the values obtained employing hour by hour solar radiation data for south facing as well as non-south facing collectors. The agreement is good, within a rms difference of 1.0 % except for a few months when $\bar{K}_T < 0.4$. $(\tau\alpha)^*_{day}/(\tau\alpha)_n$(data) values differ to a significant extent from the all day and operational time period averaged values calculated as per the procedure of Klein [95] and Collares-Pereira and Rabl [68] respectively.

A procedure has been developed to obtain the monthly average transmittance-absorptance product, $(\overline{\tau\alpha})^*/(\tau\alpha)_n$, defined as a weighted average of instantaneous $(\tau\alpha)$ and the solar radiation above the critical radiation level over all the hours in the month. The procedure involves employing the expression developed for a single day in the present study on the equivalent mean day (EMD). The EMD is characterized be $\delta = \delta_m$, $\bar{K}_T = \bar{K}^*_T$, where $\bar{K}^*_T$ is the average daily clearness index of the days that contribute to useful energy. Values of $(\overline{\tau\alpha})^*/(\tau\alpha)_n$ obtained according to the EMD calculation differ from the values obtained by hour by hour numerical calculations by less than 1.8 % rms.

Chapter 4

Evaluation of Monthly Average Optical Efficiency during the Operational Time Period for Parabolic Trough Concentrators

4.1 Introduction

Studies reported in Chapter 2 have established that the product of F_R, H_T, ϕ and $(\overline{\tau\alpha})^*$ yields the monthly average daily useful energy gain per unit area for flat plate collectors, when $(\overline{\tau\alpha})^*$ is defined as a weighted average of the instantaneous transmittance-absorptance product, $(\tau\alpha)$ and the solar radiation on the collector surface above the critical radiation level. A procedure to calculate $(\overline{\tau\alpha})^*$, using an expression developed considering a single day and applied on the equivalent mean day (EMD), has been developed and validated in Chapter 3.

Neither the graphical presentation of Klein [95] (with its own limitations, such as, does not account for diffuse fraction or the operating time period) nor the analytical approach similar to that of Sfeir [96] is available for concentrating collectors. Studies reported by Gaul and Rabl [45] provide a polynomial expression for the incidence angle modifier for five different brands of parabolic trough concentrators. Gaul and Rabl also suggested a procedure to obtain the all-day average optical efficiency, η_o, and presented tabulated information for two cut-off times, one or two hours before sunset. The applicability of all-day average optical efficiency values in place of monthly average values to obtain monthly average useful energy gain has not been established. Also, certain equations in Gaul and Rabl's work appear to be inconsistent. For the sake of clarity §5 *All-Day Average*, of Gaul and Rabl's article is reproduced here in the box that follows. In this reproduction, equation numbers refer to the numbers as appeared in Gaul and Rabl's article.

From Gaul and Rabl's [45] article, Transactions of the ASME, Journal of Solar Energy Engineering, Vol. 102, Page–16-21, 1980.

5 All-Day Average

Use of a single number, the all-day average optical efficiency $\bar{\eta}_o$, is far more convenient than the function $\eta_o(\theta)$ for short-hand prediction of performance. To be consistent with the utilizability method [10], the all-day average must be calculated with the beam irradiance I_b as a weighting factor. For this purpose, the long-term average meteorological correlations of the Liu and Jordan type [11] are appropriate (see [8], Appendix). The beam irradiance corresponding to hour angle ω and sunset hour angle ω_s is given by the equation (for latitudes between 45 deg N and 45 deg S)

$$I_b(\omega, \omega_s) = \left(a + b\cos\omega - H_d/H_h\right) K_h I_o \qquad (11)$$

where,

a $= 0.409 + 0.5016\sin(\omega_s - 1.047),$ (12)

b $= 0.6609 - 0.4767\sin(\omega_s - 1.047),$ (13)

I_o = solar constant,

K_h = clearness index (ratio of terrestrial to extraterrestrial daily total irradiation on the horizontal surface), and

H_d/H_h = ratio of diffuse to hemispherical daily total irradiation on the horizontal surface.

Since concentrating collectors operate primarily during sunny periods, one can assume $H_d/H_h = 0.23$ and $K_h = 0.75$ (the values of K_h and I_o do not matter for the calculations in this paper). The all-day average is defined by the formula

$$\bar{y} = \int_o^{\omega_c} I_b(\omega)\,\cos\theta\, y(\theta)\, d\omega \Big/ \int_o^{\omega_c} I_b(\omega)\,\cos\theta\, d\omega \qquad (14)$$

where, y can be K, Γ, $K\Gamma$, or η_o, and ω is the hour angle corresponding to time of day t. The incidence angle is a function of time of day and time of year given by

$$\cos\theta_{EW} = \cos\delta\,(\cos^2\omega + \tan^2\delta)^{1/2} \qquad (15)$$

where δ= solar declination for a collector with horizontal tracking axis aligned in the east-west direction. For a collector with horizontal tracking axis aligned in the north-south direction, it is given by

$$\cos\theta_{NS} = \cos\delta\,[\sin^2\omega + (\cos\lambda\cos\omega + \tan\delta\sin\lambda)^2]^{1/2} \qquad (16)$$

with λ= geographic latitude.

For polar mount, the incidence angle equals the declination,

$$\cos\theta_{polar} = \cos\delta \qquad (17)$$

at all times and is so small that the incidence-angle modifier can be neglected in most cases.

Strictly speaking, one should calculate $\overline{K\Gamma}$; however, the presentation of the results is greatly simplified by the approximation

$$\eta_o = \eta_o(\theta = 0)\overline{K\Gamma} \approx \eta_o(\theta = 0)\bar{K}\,\bar{\Gamma} \qquad (18)$$

Therefore, we first investigate (see Table 2) the ratio of $\overline{K\Gamma}$ and $\bar{K}\,\bar{\Gamma}$ for three different values of the ratio of the collector length to focal length, l/f, corresponding to a Hexcel collector operating as a single module or as two or four modules joined in a row. For this table, as well as the next two tables, the following format has been adopted; all values are calculated for summer solstice, equinox, and winter solstice for both east-west and north-south mounts, and for each case, values are entered for two cut-off times [$t_c = t_s - 1h$ (top row) and $t_c = t_s - 2h$ (bottom row)], based on the assumption that the collector operates from t_c hours before noon until t_c hours afternoon (t_s is the sunset hour time). The difference between the average of the product and the product of the averages is seen to be small enough to be neglected, since collectors with horizontal tracking axes will usually be installed in long rows.
Therefore, two tables suffice to present the all-day averages. Table 3 lists $\bar{\Gamma}$ as a function of l/f, and Table 4 lists $\bar{K}$ for each of the collectors that have been tested. Comparison of the entries for different cut-off times, t_c, indicates variation on the order of 1 percent. This implies that an all-day average interpolated from these tables is quite acceptable for use in calculations of long-term energy delivery.

Conclusion

The incidence angle modifiers for several commercially available parabolic trough collectors have been calculated from test data. The results have been presented in two forms: analytical curve fits and all-day averages.

Not withstanding how Eq. (14) of Gaul and Rabl [15] has been integrated, Eq. (11), from which Eq. (14) follows, does not appear to be correct. I_o in Eq. (11) of [15] should be the hourly extra-terrestrial radiation (KJ/m^2-hr) over a horizontal surface centered around the hour angle ω. As mentioned in Gaul and Rabl [15], I_o is not the solar constant. Indeed, I_o does depend on ω in addition to latitude, ϕ and declination, δ. Also, though concentrating collectors operate during sunny days and Eq. (14) of Gaul and Rabl does not depend on daily clearness index explicitly, I_b appearing in Eq. (11), when evaluated from r_t [12] and r_d [16] correlations, depends on H_d/H, either a data value or a value correlated to K_T. It may also be noted that the cut-off times depend on the critical radiation level and one or two hours before sunset do not imply same dimensional or non-dimensional critical level for different tracking modes, latitudes and declination. Thus, for a given critical radiation level and monthly average daily clearness index K_T, since the cut-off time differs from day to day, optical efficiency of a single day can be expected to differ from the monthly average value. Further, one or two hours cut-off time before sunset corresponds to operating periods differing by a factor of more than two depending on the latitude and the month. For example, for 1-hr cut-off time before sunset, the operating

periods for $\phi = 60^o$ is 16.3 hours for June and 3.7 hours for December. Also, the influence of clearness index needs to be examined. In this context, it may be noted that the solar radiation incident on the aperture consists of diffuse component as well, though small when concentration ratio is high. The effect of including the diffuse component of solar radiation in I_T can be expected to be important when concentration ratio is lower and K_T is not very high. $K_T \approx 0.6$ can be considered moderate, when a concentrating collector can be operated satisfactorily. Indeed, a few locations have an an yearly average K_T greater than 0.5. Further, as has been shown in Chapter 2 of the present study, to be consistent with the definition of utilizability, average optical efficiency is a weighted average of the solar radiation on the collector aperture above the critical radiation level. Eq. (14) of Gaul and Rabl, though takes into account the cut-off time in principle, is a weighted average of the incident beam radiation only. In this context, Gaul and Rabl's calculation implicitly assumes that the collector operates continuously from a certain cut-off period after sunrise to a certain cut-off period before sunset. This is not true for tracking mode **c**, since the solar radiation distribution can be bimodal even within the frame work of r_t and r_d correlations. This is explained in Figure 4.1. I_{bT} variation with ω for tracking mode **c** for $K_T = 0.7$, for $\phi = 40^o$, in December is shown. Also, shown is the 1/2-hr cut-off time. The collector actually operates from $-\omega_c$ to $-\omega_{cb}$ and ω_{cb} to ω_c and not from $-\omega_c$ to ω_c. If the cut-off time is 3-hrs, according to Gaul and Rabl, the optical efficiency is estimated from $-\omega_{cb}$ and ω_{cb} whereas, in reality the collector does not operate during this time interval. In terms of critical radiation level, I_c (also shown in Figure 4.1), both 1/2-hr and 3-hrs cut-off times correspond to the same critical level and the period of operation is discontinuous.

As has been reported in Gaul and Rabl [45] to apply test results from a collector module to collector arrays of arbitrary length, it is necessary to seperate the end loss from the optical loss. The end loss factor, defined as one minus the fraction of the rays incident on the aperture that spill out the end of a receiver of finite length, is strictly a geometric quantity. In the present study also, as proposed by Gaul and Rabl [45], it is assumed that $\overline{K\Gamma}$ can be calculated as product of $\bar{K}$ and $\bar{\Gamma}$.

As a first step, the dependence of optical efficiency for a single day, defined as a weighted average of incident radiation (comprising of direct radiation only and direct radiation and diffuse component) on latitude, clearness index and bimodal nature of solar radiation distribution has been examined. This part of the study is essentially along the lines of Gaul and Rabl [45] as far as the weighting function in defining the optical efficiency is concerned. Present study is concerned with developing a method to calculate monthly average $\bar{K}$, i.e., the monthly average optical efficiency, $(\bar{\eta}_o^\star/\eta_{o,n})$ with a modified

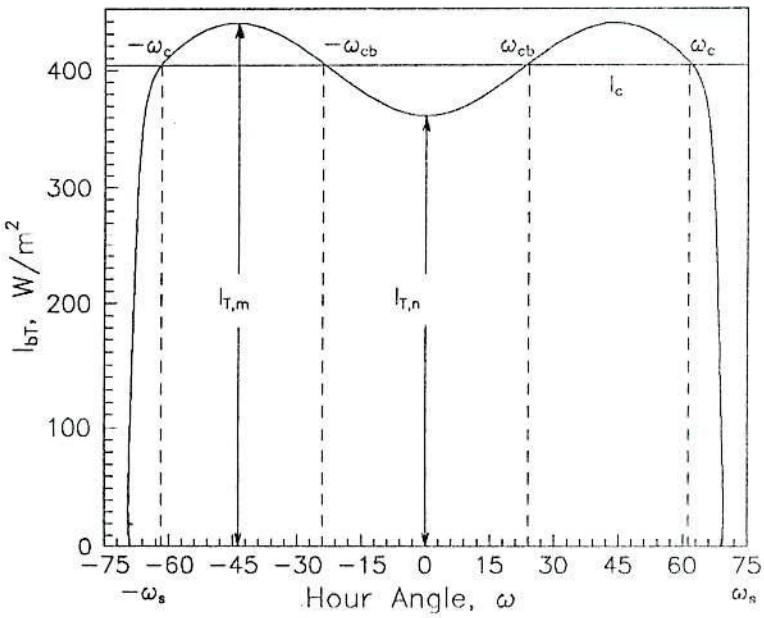

Figure 4.1: Bimodal distribution of direct radiation on collector surface tracked in mode **c** for $\phi = 40^o$ in December

definition consistent with the definition of utilizability. In order to be consistent with the definition of utilizability, expressions for optical efficiency, defined as a weighted average of incident solar radiation above the critical level, have been developed for a single day for parabolic trough concentrators tracked in the five principal modes. To facilitate the present approach, a suitable form for the incidence angle modifier, amenable for analytical treatment, has been chosen. Finally, the monthly average optical efficiency calculated employing the EMD approach has been validated.

4.2 Incidence Angle Modifier

The incidence angle modifier $\eta_o(\theta)/\eta_o(\theta = 0)$ for infinitely long parabolic trough collectors for the five[1] brands of parabolic concentrators studied by Gaul and Rabl [15] are as following:

$$\left(\frac{\eta_o}{\eta_{o,n}}\right)_1 = 1 + 3.81 \times 10^{-5}\theta^2 - 1.18 \times 10^{-6}\theta^3 - 6.85 \times 10^{-9}\theta^4 \qquad (4.1)$$

$$\left(\frac{\eta_o}{\eta_{o,n}}\right)_2 = 1 - 2.02 \times 10^{-5}\theta^2 + 4.69 \times 10^{-7}\theta^3 - 1.80 \times 10^{-8}\theta^4 \qquad (4.2)$$

[1]subscript 1 to 5 in the LHS of Eqs. (4.1) to (4.5) refer to the brands: 1=Solar Kinetics; 2=SERI Hexcel; 3=Sandia Hexcel; 4=Del; 5=Acurex.

$$\left(\frac{\eta_o}{\eta_{o,n}}\right)_3 = 1 - 6.74 \times 10^{-5}\theta^2 + 1.64 \times 10^{-6}\theta^3 - 2.51 \times 10^{-8}\theta^4 \quad (4.3)$$

$$\left(\frac{\eta_o}{\eta_{o,n}}\right)_4 = 1 - 8.45 \times 10^{-5}\theta^2 + 1.72 \times 10^{-6}\theta^3 - 2.40 \times 10^{-8}\theta^4 \quad (4.4)$$

$$\left(\frac{\eta_o}{\eta_{o,n}}\right)_5 = 1 + 1.69 \times 10^{-4}\theta^2 - 8.92 \times 10^{-6}\theta^3 + 6.30 \times 10^{-8}\theta^4 \quad (4.5)$$

In Eqs. (4.1) to (4.5), η_o refers to the value at any incidence angle, θ and $\eta_{o,n}$ refers to the value at normal incidence, i.e., $\theta = 0$.

Eqs. (4.1) to (4.5) for $(\eta_o/\eta_{o,n})$ are not suitable for analytical treatment to obtain all-day average optical efficiency employing equations similar to Eq. (3.4) or Eq. (3.1). $(\eta_o/\eta_{o,n})_1$, $(\eta_o/\eta_{o,n})_2$, $(\eta_o/\eta_{o,n})_3$, $(\eta_o/\eta_{o,n})_4$ and $(\eta_o/\eta_{o,n})_5$, given by Eqs. (4.1) to (4.5), have been rewritten as,

$$\left(\frac{\eta_o}{\eta_{o,n}}\right) = P_i + \frac{Q_i}{\cos\theta} + R_i \cos\theta \quad \text{if} \quad 0^o \le \theta \le 60^o \quad (4.6)$$

$$= S_i \cos\theta \quad \text{if} \quad 60^o \le \theta \le 90^o \quad (4.7)$$

where, $S_i = (2\,P_i + 4\,Q_i + R_i)$. Eq. (4.7) satisfies $(\eta_o/\eta_{o,n})_i|_{Eq.(4.7)} = (\eta_o/\eta_{o,n})_i|_{Eq.(4.6)}$ at $\theta = 60^o$ and $(\eta_o/\eta_{o,n})_i = 0$, at $\theta = 90^o$. The accuracy of Eq. (4.7) has not been examined, since it satisfies the conditions for $\theta = 60^o$ and 90^o and monotonically decreases with θ. Even if a minor deviation occurs from the polynomial fits (it may be noted that no data exists for $\theta > 60^o$ from which the polynomial fits have been derived), $(\eta^*_{o,day}/\eta_{o,n})$ accuracy does not suffer since concentrating collectors tracked in the five principal modes seldom encounter $\theta > 60^o$ during the operating time period.

The coefficients P_i, Q_i, R_i and S_i for the five types of parabolic trough concentrators are determined from the data given in Gaul and Rabl [45]. The values of P_i, Q_i, R_i and S_i for the five collectors are given in Table 4.1.

A plot of $(\eta_o/\eta_{o,n})$ using Eqs. (4.2) and (4.6) for SERI Hexcel parabolic trough collector is shown in Figure 4.2. The proposed functional form yields values sufficiently close to the values given by the polynomial fit [Eq. (4.2)] differing in the fourth decimal place. A plot of $(\eta_o/\eta_{o,n})$ values obtained from Eqs. (4.1) to (4.5) and Eq. (4.6) using the values of the coefficients given in Table 4.1, is shown in Figure 4.3, for all the five brands of parabolic trough concentrators. Values of $(\eta_o/\eta_{o,n})_i$ obtained from Eq. (4.6), yield values differing by less than 0.5% (rms) from the values given by Eqs. (4.1) to (4.4). For the Acurex collector, $(\eta_o/\eta_{o,n})_5$ obtained from Eq. (4.6), differs with the values given by Eq. (4.5) by 1.57% (rms). However, the values given by Eq. (4.6) actually are close to the data values fortuitously.

Table 4.1: Coefficients P_i, Q_i, R_i and S_i for the incidence angle modifier for different types of parabolic trough concentrators

Coefficient.	Solar kinetics	SERI Hexcel	Sandia Hexcel	Del	Acurex
P_i	1.73557	1.45292	1.18929	1.03257	1.59799
Q_i	−0.389908	−0.289961	−0.204709	−0.171925	−0.558666
R_i	−0.339366	−0.161671	0.013020	0.136490	−0.012018
S_i	1.572142	1.584325	1.572764	1.513930	0.949298

The advantage of the present functional form for $(\eta_o/\eta_{o,n})$ [Eqs. (4.6) and (4.7)], is that it is amenable for analytical integration to yield expressions similar to Eq. (3.57) for concentrating collectors as well. Further, the constants P_i, Q_i, R_i and S_i appear as parameters in the expressions. For different collector brands (other than the five considered in the studies of Gaul and Rabl and the present study) or types, suitable values for P_i, Q_i, R_i and S_i can be inserted in the final expression, to calculate $(\eta^*_{o,day}/\eta_{o,n})$. It may also be noted that, Rabl [91] suggested using a single polynomial [Eq. (4.2)], as a compromise, to all types of collectors. The present form can be employed for other collector types as well by altering the values of the constants P_i, Q_i R_i etc. For example, Eqs. (4.6) and (4.7) reduce to Eqs. (2.14) and (2.15) for flat plate collectors with $P_i = (1 - b_o)$, $Q_i = b_o$ $R_i = 0$ and $S_i = 2(1 + b_o)$.

4.3 Evaluation of Daily Optical Efficiency during the Operational Time Period for Concentrating Collectors

4.3.1 Mathematical Formulation

Analogous to $(\tau\alpha)^*_{day}/(\tau\alpha)_n$, given by Eq. (2.38) of Chapter 2, optical efficiency valid for a single day, $(\eta^*_{o,day}/\eta_{o,n})$, for concentrating collectors when defined as a weighted average of solar radiation incident on the collector aperture above the critical radiation level, is expressed as follows:

$$\left(\frac{\eta^*_{o,day}}{\eta_{o,n}}\right) = \sum_{-\omega_s}^{\omega_s} [I_T - I_c]^+ \left(\frac{\eta_o}{\eta_{o,n}}\right) \Big/ \sum_{-\omega_s}^{\omega_s} [I_T - I_c]^+$$

$$= \int_{-\omega_s}^{\omega_s} [I_T - I_c]^+ \left(\frac{\eta_o}{\eta_{o,n}}\right) d\omega \Big/ \int_{-\omega_s}^{\omega_s} [I_T - I_c]^+ \, d\omega \qquad (4.8)$$

In Eq. (4.8), the superscript '+' indicates that when $(I_T - I_c)$ is negative, it will be considered as zero. In Eq. (4.8), I_T and $(\eta_o/\eta_{o,n})$ are the instantaneous solar radiation on

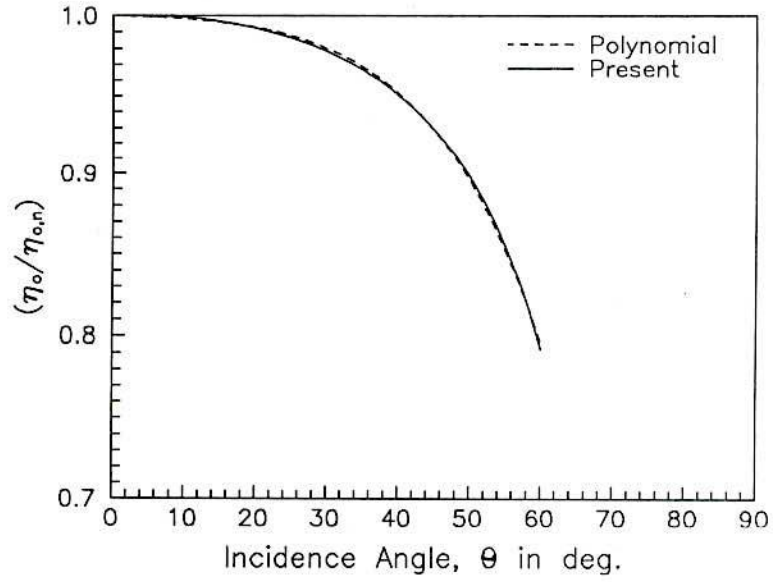

Figure 4.2: Comparison of incidence angle modifier from polynomial form and the present functional form for SERI Hexcel Concentrator

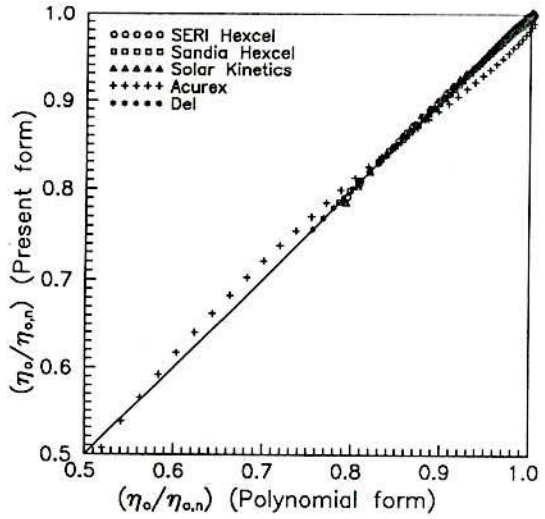

Figure 4.3: Validation of incidence angle modifier obtained from polynomial form and the present functional form for SERI Hexcel, Sandia Hexcel, Solar Kinetics, Del and Acurex Concentrators

the collector aperture and the corresponding optical efficiency which comprises of direct and diffuse components. In Eq. (4.8), I_c is the critical radiation level defined by,

$$I_c = \frac{F_R A_r U_L (T_i - T_a)}{F_R A_a \eta_o} = \frac{F_R U_L (T_i - T_a)}{F_R C_r \eta_o} \tag{4.9}$$

In Eq. (4.9), A_a and A_r are the aperture and receiver areas and C_r is the area concentration ratio, defined as,

$$C_r = \frac{A_a}{A_r} \tag{4.10}$$

If I_T has a single maximum value during $-\omega_s \leq \omega \leq \omega_s$ and ω_{c1} and ω_{c2} are the angles corresponding to $I_T = I_c$, Eq. (4.8) can be re-written dropping the superscript '+'. Making use of symmetry around $\omega = 0$ and recognizing $|\omega_{c1}| = |\omega_{c2}| = \omega_c$ say, Eq. (4.8) takes the form,

$$\left(\frac{\eta^*_{o,day}}{\eta_{o,n}}\right) = \int_0^{\omega_c} [I_T - I_c] \left(\frac{\eta_o}{\eta_{o,n}}\right) d\omega \Big/ \int_0^{\omega_c} [I_T - I_c]\, d\omega \tag{4.11}$$

Indeed Eq. (4.8) can be replaced by Eq. (4.11) as long as $I_T > I_c$ for $-\omega_c < \omega < \omega_c$. For a concentrating collector this is satisfied except when tracked in mode **c**. For mode **c** tracking, maximum solar radiation on the aperture may not occur at $\omega = 0$. Thus, when $I_c > I_{T,n}$ (referring to Figure 4.1), for tracking mode **c**, Eq. (4.11) needs to be modified as,

$$\left(\frac{\eta^*_{o,day}}{\eta_{o,n}}\right) = \int_{\omega_{cb}}^{\omega_c} [I_T - I_c] \left(\frac{\eta_o}{\eta_{o,n}}\right) d\omega \Big/ \int_{\omega_{cb}}^{\omega_c} [I_T - I_c]\, d\omega \tag{4.12}$$

Methods to evaluate ω_c and ω_{cb} (where applicable) will be discussed in the following section.

Non-dimensionalizing I_c with respect to solar radiation on the collector aperture at noon time, the non-dimensional critical level X_c is defined as,

$$X_c = \frac{I_c}{I_{T,n}} = \frac{I_c}{r_{t,n} R_n K_T H_o} \tag{4.13}$$

For concentrating collectors, I_T and $(\eta_o/\eta_{o,n})$ in Eqs. (4.8) and (4.11), are given by,

$$I_T = I_b R_b + \frac{1}{C_r} I_d \tag{4.14}$$

$$\left(\frac{\eta_o}{\eta_{o,n}}\right) = \frac{I_b R_b (\eta_{o,b}/\eta_{o,n}) + \frac{I_d}{C_r}(\eta_{o,d}/\eta_{o,n})}{I_b R_b + \frac{I_d}{C_r}} \tag{4.15}$$

where, R_b is the tilt factor for direct radiation given by,

$$R_b = \frac{\cos\theta}{\cos\theta_z} \tag{4.16}$$

$\cos\theta_z$, in Eq. (4.16), is given by Eq. (2.13) of Chapter 2. The different expressions for $\cos\theta$, for concentrating collectors tracked in the five principal modes, can be obtained from,

$$\cos\theta = A_1 + B_1\cos\omega + C_1\sin\omega \tag{4.17}$$

where, A_1, B_1 and C_1 for the five tracking modes take the expressions given in Table 4.2.

Using Eq. (4.14) for I_T, Eq. (4.11) becomes,

$$\left(\frac{\eta^*_{o,day}}{\eta_{o,n}}\right) = \left[\int_o^{\omega'_c} I_b R_b \left(\frac{\eta_{o,b}}{\eta_{o,n}}\right) d\omega + \frac{1}{C_r}\int_o^{\omega_c} I_d \left(\frac{\eta_{o,d}}{\eta_{o,n}}\right) d\omega - I_c \int_o^{\omega_c} \left(\frac{\eta_o}{\eta_{o,n}}\right) d\omega\right] \div \left[\int_o^{\omega'_c} I_b R_b\, d\omega + \frac{1}{C_r}\int_o^{\omega_c} I_d\, d\omega - I_c\int_o^{\omega_c} d\omega\right] \tag{4.18}$$

It may be noted that the upper limit of integration for the direct component of radiation in Eq. (4.11) is specified as ω'_c instead of ω_c due to reasons explained in Chapter 3, §3.2.1. Thus, ω'_c is given by,

$$\omega'_c = \min\left[\omega_c, \omega'_s\right] \tag{4.19}$$

where ω'_s is the apparent sunset hour angle. ω'_s for the five tracking modes are given by,

$$\omega'_s = \begin{cases} \min\left[\omega_s, \cos^{-1}\left(-\tan^2\delta\right)\right] & : \quad \text{for tracking mode } \mathbf{a} \\ \min\left[\omega_s, \pi/2\right] & : \quad \text{for tracking mode } \mathbf{b} \\ \omega_s & : \quad \text{for tracking modes } \mathbf{c}, \mathbf{d} \text{ and } \mathbf{e} \end{cases} \tag{4.20}$$

Eq. (4.18) can be written in a compact form, analogous to Eq. (3.13) of Chapter 3, as,

$$\left(\frac{\eta^*_{o,day}}{\eta_{o,n}}\right) = \left[I_{1NC} + I_{2NC} - I_{4NC}\right] \div \left[I_{1DC} + I_{2DC} - I_{4DC}\right] \tag{4.21}$$

where,

$$I_{1NC} = \int_o^{\omega'_c} I_b\, R_b \left(\frac{\eta_{o,b}}{\eta_{o,n}}\right) d\omega \tag{4.22}$$

$$I_{2NC} = \frac{1}{C_r}\int_o^{\omega_c} I_d \left(\frac{\eta_{o,d}}{\eta_{o,n}}\right) d\omega \tag{4.23}$$

$$I_{4NC} = I_c \int_o^{\omega_c} \left(\frac{\eta_o}{\eta_{o,n}}\right) d\omega \tag{4.24}$$

Table 4.2: Expressions to be used for A_1, B_1, C_1 in $\cos\theta = A_1 + B_1\cos\omega + C_1\sin\omega$ for different tracking modes

Tracking Mode	Quantity	Expression
Mode **a**	A_1	$\sin^2\delta$
	B_1	$\cos^2\delta$
	C_1	0
Mode **b**	A_1	$\sin\delta\tan\delta/\sqrt{\cos^2\omega+\tan^2\delta}$
	B_1	$\cos\delta\cos\omega/\sqrt{\cos^2\omega+\tan^2\delta}$
	C_1	0
Mode **c**	A_1	$[\sin^2\phi\sin^2\delta+\sin(2\phi)\sin(2\delta)\cos\omega/2]/\sqrt{D}$
	B_1	$[\sin(2\phi)\sin(2\delta)/2+\cos^2\phi\cos^2\delta\cos\omega]/\sqrt{D}$
	C_1	$(\cos^2\delta\sin\omega)/\sqrt{D}$
		where,
		$D=\sin^2\phi\sin^2\delta+\sin(2\phi)\sin(2\delta)\cos\omega/2+$
		$\cos^2\phi\cos^2\delta\cos^2\omega+\cos^2\delta\sin^2\omega$
Mode **d**	A_1	$\cos\delta$
	B_1	0
	C_1	0
Mode **e**	A_1	1
	B_1	0
	C_1	0

and

$$I_{1DC} = \int_o^{\omega_c'} I_b\, R_b\, d\omega \tag{4.25}$$

$$I_{2DC} = \frac{1}{C_r}\int_o^{\omega_c} I_d\, d\omega \tag{4.26}$$

$$I_{4DC} = I_c \int_o^{\omega_c} d\omega \tag{4.27}$$

In defining I_{1NC} etc., in Eqs. (4.22) to (4.27), symmetry around solar noon, $\omega = 0^o$, has been invoked, i.e., integration from $-\omega_c$ to ω_c has been replaced by twice of 0 to ω_c. It may be noted that, integrals such as, I_{3N} and I_{3D} [in Eq. (3.13)] do not appear for concentrating collectors since ground reflected component of solar radiation is not a part of I_T as defined by Eq. (4.14).

4.3.2 Expressions for $(\eta^*_{o,day}/\eta_{o,n})$

Eq. (4.21), in terms of the integrals defined by Eqs. (4.22) to (4.27), becomes available for evaluating $(\eta^*_{o,day}/\eta_{o,n})$ when specific expressions for the integrals and method to calculate ω_c are developed. Expressions to evaluate the critical hour angle ω_c for different tracking modes are given after deriving the expressions for $(\eta^*_{o,day}/\eta_{o,n})$ for all the five tracking modes.

Using Eqs. (2.26) and (2.27) from Chapter 2, for I_d and I_b respectively and Eqs. (4.16) and (4.17) along with the expressions for A_1, B_1 and C_1 given in Table 4.2 and using Eqs. (4.6) and (4.7) for $(\eta_o/\eta_{o,n})$, the integrals in Eqs. (4.22) to (4.24) for I_{1NC}, I_{2NC} and I_{4NC} are given by,

$$I_{1NC} = \left(\frac{K_1 K_T H_o}{B'}\right)\int_o^{\omega_c'} (a_1 + b\cos\omega)\cos\theta \left(\frac{\eta_{o,b}}{\eta_{o,n}}\right) d\omega \tag{4.28}$$

$$I_{2NC} = \left(\frac{K_1 K_T H_o}{B'}\right)\left(\frac{B' D_f}{C_r}\right)\int_o^{\omega_c} (\cos\omega - \cos\omega_s)\left(\frac{\eta_{o,d}}{\eta_{o,n}}\right) d\omega \tag{4.29}$$

$$I_{4NC} = I_c\left(\frac{\bar{\bar{\eta}}_o}{\eta_{o,n}}\right) \tag{4.30}$$

In Eq. (4.30), $(\bar{\bar{\eta}}_o/\eta_{o,n})$ is defined as,

$$\left(\frac{\bar{\bar{\eta}}_o}{\eta_{o,n}}\right) = \int_o^{\omega_c}\left(\frac{\eta_o}{\eta_{o,n}}\right) d\omega \tag{4.31}$$

Similarly Eqs. (4.25) to (4.27) for I_{1DC}, I_{2DC} and I_{4DC} are given by,

$$I_{1DC} = \left(\frac{K_1 K_T H_o}{B'}\right)\int_o^{\omega_c'} (a_1 + b\cos\omega)\cos\theta\, d\omega \tag{4.32}$$

$$I_{2DC} = \left(\frac{K_1 K_T H_o}{B'}\right) \frac{B' D_f}{C_r} \int_o^{\omega_c} (\cos\omega - \cos\omega_s)\, d\omega \tag{4.33}$$

$$I_{4DC} = I_c \int_o^{\omega_c} d\omega \tag{4.34}$$

It may be noted that $(\eta_{o,d}/\eta_{o,n})$ in Eq. (4.29) is independent of the hour angle ω. $(\eta_{o,d}/\eta_{o,n})$ can be obtained employing Eq. (4.6), using $\theta = \theta_d$ [Eq. (2.12) with $\beta = 0$], the effective angle of incidence for sky diffuse component of solar radiation. $(\eta_{o,b}/\eta_{o,n})$ in Eq. (4.28) depends on the angle of incidence for direct radiation and is described by Eqs. (4.6) and (4.7). $(\eta_{o,b}/\eta_{o,n})$ variation with θ as given by Eqs. (4.6) and (4.7) is piece-wise continuous. Let ω_1 and ω_2 be the hour angles corresponding to $\theta = 60^o$. ω_1 and ω_2 can be obtained by setting $\theta = 60^o$ in Eq. (4.17) for $\cos\theta$ with the appropriate expressions for A_1, B_1 and C_1 from Table 4.2. By virtue of symmetry, for tracking collectors, $|\omega_1| = |\omega_2| = \omega'$ (say). Expressions for ω' for different tracking modes will be presented after deriving the expressions for $(\eta^*_{o,day}/\eta_{o,n})$. Thus, I_{1NC} [Eq. (4.28)] needs to be evaluated as,

$$I_{1NC} = K_4 \left[\int_o^{\omega'} (a_1 + b\cos\omega) \left[P_i + \frac{Q_i}{\cos\theta} + R_i \cos\theta\right] \cos\theta\, d\omega + \int_{\omega'}^{\omega'_c} (a_1 + b\cos\omega)\, S_i \cos\theta\, d\omega \right] \tag{4.35}$$

Integrating Eqs. (4.29) to (4.35), I_{1NC} etc. are expressed as,

$$I_{1NC} = K_4 \Big[a_1 P_i I_{P1}(\omega', 0) + a_1 Q_i(\omega' - 0) + a_1 R_i I_{P3}(\omega', 0) + b P_i I_{P2}(\omega', 0) + bQ_i I_{P5}(\omega', 0) + bR_i I_{P4}(\omega', 0) + S_i \left\{ a_1 I_{P3}(\omega'_c, \omega') + b I_{P4}(\omega'_c, \omega') \right\} \Big] \tag{4.36}$$

$$I_{2NC} = K_4 \left(\frac{B' D_f}{C_r}\right) \left(\frac{\eta_{o,d}}{\eta_{o,n}}\right) \left[I_{P5}(\omega_c, 0) - \cos\omega_s(\omega_c - 0) \right] \tag{4.37}$$

$$I_{4NC} = I_c \left(\frac{\bar{\bar{\eta}}_o}{\eta_{o,n}}\right) \tag{4.38}$$

and

$$I_{1DC} = K_4 \left[a_1 I_{P1}(\omega'_c, 0) + b I_{P2}(\omega'_c, 0) \right] \tag{4.39}$$

$$I_{2DC} = K_4 \left(\frac{B' D_f}{C_r}\right) \left[I_{P5}(\omega_c, 0) - \cos\omega_s(\omega_c - 0) \right] \tag{4.40}$$

$$I_{4DC} = I_c(\omega_c - 0) \tag{4.41}$$

where, the constant K_4 is given by Eq. (3.42). The primitives I_{P1}, I_{P2}, I_{P3}, I_{P4}, and I_{P5} appearing in Eqs. (4.36) to (4.41) are defined by Eqs. (3.44) to (3.48) which are reproduced here.

$$I_{P1}(\omega) = \int \cos\theta\, d\omega \tag{4.42}$$

$$I_{P2}(\omega) = \int \cos\theta \cos\omega \, d\omega \tag{4.43}$$

$$I_{P3}(\omega) = \int \cos^2\theta \, d\omega \tag{4.44}$$

$$I_{P4}(\omega) = \int \cos^2\theta \cos\omega \, d\omega \tag{4.45}$$

$$I_{P5}(\omega) = \int \cos\omega \, d\omega \tag{4.46}$$

Using Eqs. (4.36) to (4.41), along with the primitives as given by Eqs. (4.42) to (4.46), $(\eta^*_{o,day}/\eta_{o,n})$ for concentrating collectors tracked in the five principal modes can be expressed as,

$$\begin{aligned}\left(\frac{\eta^*_{o,day}}{\eta_{o,n}}\right) = & \Bigg[a_1 P_i I_{P1}(\omega',0) + a_1 Q_i(\omega'-0) + a_1 R_i I_{P3}(\omega',0) + b P_i I_{P2}(\omega',0) \\ & + bQ_i I_{P5}(\omega',0) + bR_i I_{P4}(\omega',0) + S_i\Big\{a_1 I_{P3}(\omega'_c,\omega') + bI_{P4}(\omega'_c,\omega')\Big\} \\ & + \left(\frac{B'D_f}{C_r}\right)\left(\frac{\eta_{o,d}}{\eta_{o,n}}\right)\Big\{I_{P5}(\omega_c,0) - \cos\omega_s(\omega_c-0)\Big\} - I_c\left(\frac{\bar{\bar{\eta}}_o}{\eta_{o,n}}\right)\Bigg] \div \\ & \Bigg[a_1 I_{P1}(\omega'_c,0) + bI_{P2}(\omega'_c,0) + \left(\frac{B'D_f}{C_r}\right)\Big\{I_{P5}(\omega_c,0) - \cos\omega_s(\omega_c-0)\Big\} \\ & - I_c(\omega_c-0)\Bigg]\end{aligned} \tag{4.47}$$

Eq. (4.47) become available to evaluate $(\eta^*_{o,day}/\eta_{o,n})$, when specific expression for the primitives I_{P1} etc. are obtained for the different tracking modes. Also, a procedure to obtain $(\bar{\eta}_o/\eta_{o,n})$ is required.

The expressions for the primitives I_{P1} to I_{P5}, appearing in Eq. (4.47), for the five principal tracking modes are given in Table 4.3.

Evaluation of $(\bar{\bar{\eta}}_o/\eta_{o,n})$

Eq. (4.47), for evaluating $(\eta^*_{o,day}/\eta_{o,n})$ along with the primitives presented in Table 4.3, becomes available when a procedure to evaluate $(\bar{\bar{\eta}}_o/\eta_{o,n})_i$, defined by Eq. (4.31), is devised. Since the approximate procedure for evaluating $(\overline{\overline{\tau\alpha}})/(\tau\alpha)_n$ described in Chapter 3 has been successful, the same procedure has been adapted to obtain $(\bar{\bar{\eta}}_o/\eta_{o,n})_i$. Let, $\bar{\bar{\theta}}$ analogous to Eq. (3.114) be an effective angle of incidence obtained from,

$$\bar{\bar{\theta}} = \frac{2\,\theta_1 + \theta_n}{3} \tag{4.48}$$

In Eq. (4.48), θ_1 and θ_n are the angles of incidence at $\omega = \omega_c$ and $\omega = 0^o$ respectively.

Corresponding to $\bar{\bar{\theta}}$ determined from Eq. (4.48), if $\bar{\omega}$ is the hour angle, obtained from Eq. (4.17) along with the expressions for A_1, B_1 and C_1 given in Table 4.2 for the five

Table 4.3: Expressions for the primitives I_{P1}, I_{P2}, I_{P3}, I_{P4} and I_{P5} for different tracking modes

Mode	Primitive	Expression
Mode **a**	$I_{P1}(\omega)$	$A_1\,\omega + B_1\,\sin\omega$
	$I_{P2}(\omega)$	$A_1\,\sin\omega + B_1\,(\omega/2 + \sin 2\omega/4)$
	$I_{P3}(\omega)$	$[A_1^2 + (B_1^2/2)]\,\omega + 2A_1B_1\sin\omega + (B_1^2/4)\,\sin 2\omega$
	$I_{P4}(\omega)$	$A_1B_1\,\omega + (A_1^2 + B_1^2)\sin\omega + (A_1B_1/2)\,\sin 2\omega$ $-(B^2/3)\,\sin^3\omega$
	$I_{P5}(\omega)$	$\sin\omega$
Mode **b**	$I_{P1}(\omega)$	Approximate, Eq. (C.3) of Appendix C
	$I_{P2}(\omega)$	Approximate, Eq. (C.4) of Appendix C
	$I_{P3}(\omega)$	$(1 - \cos^2\delta/2)\omega + (\cos^2\delta\,\sin 2\omega)/4$
	$I_{P4}(\omega)$	$\sin\omega - (\cos^2\delta\,\sin^3\omega)/3$
	$I_{P5}(\omega)$	$\sin\omega$
Mode **c**	$I_{P1}(\omega)$	Approximate, Eq. (C.32) of Appendix C
	$I_{P2}(\omega)$	Approximate, Eq. (C.33) of Appendix C
	$I_{P3}(\omega)$	$(A'^2 + B'^2/2 + \cos^2\delta/2)\omega + 2A'\,B'\sin\omega + (B'^2 - \cos^2\delta)\sin 2\omega/4$
	$I_{P4}(\omega)$	$(A'^2 + B'^2)\sin\omega + A'B'(\omega + \sin 2\omega/2) - (B'^2 - \cos^2\delta)\sin^3\omega/3$
	$I_{P5}(\omega)$	$\sin\omega$
Mode **d**	$I_{P1}(\omega)$	$A_1\,\omega$
	$I_{P2}(\omega)$	$A_1\,\sin\omega$
	$I_{P3}(\omega)$	$A_1^2\,\omega$
	$I_{P4}(\omega)$	$A_1^2\,\sin\omega$
	$I_{P5}(\omega)$	$\sin\omega$
Mode **e**	$I_{P1}(\omega)$	ω
	$I_{P2}(\omega)$	$\sin\omega$
	$I_{P3}(\omega)$	ω
	$I_{P4}(\omega)$	$\sin\omega$
	$I_{P5}(\omega)$	$\sin\omega$

Note: Expressions for A_1, B_1 and C_1 for the five tracking modes are given in Table 4.2.

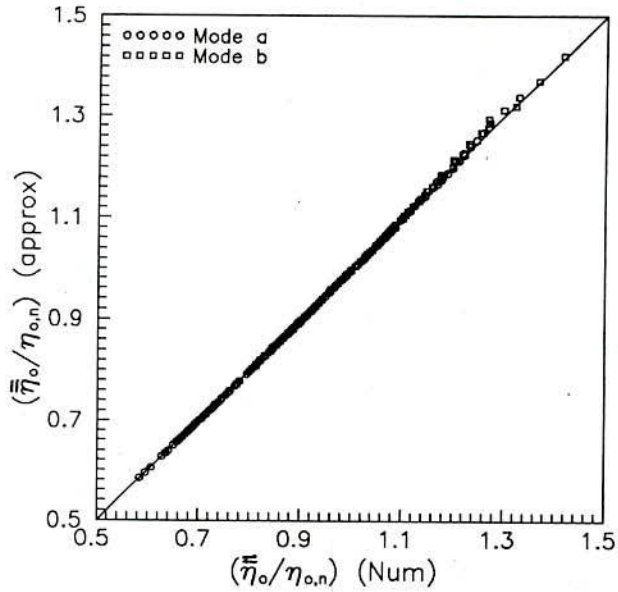

Figure 4.4: Validation of $(\bar{\bar{\eta}}_o/\eta_{o,n})$(approx) against $(\bar{\bar{\eta}}_o/\eta_{o,n})$(num) for tracking mode **a** and **b** for $20^o \leq \phi \leq 60^o$, $0.3 \leq K_T \leq 0.7$ and $0.2 \leq X_c \leq 0.6$

tracking modes, $I_T(\bar{\omega})$ is obtained from,

$$I_T(\bar{\omega}) = I_b(\bar{\omega})R_b(\bar{\omega}) + \frac{1}{C_r}I_d(\bar{\omega}) \tag{4.49}$$

where I_d and I_b are given by Eqs. (2.26) and (2.27). $(\bar{\bar{\eta}}_o/\eta_{o,n})$ is now obtained from,

$$\left(\frac{\bar{\bar{\eta}}_o}{\eta_{o,n}}\right) = \left(\frac{\eta_o(\bar{\omega})}{\eta_{o,n}}\right)(\omega_c - 0) = \frac{I_b(\bar{\omega})R_b(\bar{\omega})(\eta_{o,b}/\eta_{o,n}) + \frac{1}{C_r}I_d(\bar{\omega})(\eta_{o,d}/\eta_{o,n})}{I_b(\bar{\omega})R_b(\bar{\omega}) + \frac{1}{C_r}I_d(\bar{\omega})}(\omega_c - 0) \tag{4.50}$$

Though, analytical expressions for $(\bar{\bar{\eta}}_o/\eta_{o,n})_i$ can be obtained for tracking modes **a**, **d** and **e**, it is felt that it is unnecessary, since the values of $(\bar{\bar{\eta}}_o/\eta_{o,n})_i$, given by Eq. (4.50), differ by less than 1 % (rms) from the values obtained by numerical integration according to,

$$\left(\frac{\bar{\bar{\eta}}_o}{\eta_{o,n})}\right) = \sum_o^{\omega_c}\left(\frac{\eta_o}{\eta_{o,n}}\right)\Delta\omega \tag{4.51}$$

Values of $(\bar{\bar{\eta}}_o/\eta_{o,n})$ given by Eq. (4.50), designated as $(\bar{\bar{\eta}}_o/\eta_{o,n})$(approx) have been plotted against the values obtained from Eq. (4.51), designated as $(\bar{\bar{\eta}}_o/\eta_{o,n})$(num). The plot is shown in Figure 4.4, for tracking modes **a** and **b**, for $\phi = 20^o$, 40^o and 60^o, $-23.05^o \leq \delta \leq 23.09^o$, $K_T = 0.3$, 0.5 and 0.7 and $X_c = 0.2$, 0.4 and 0.6.

For the tracking mode **c**, the rms error between $(\bar{\bar{\eta}}_o/\eta_{o,n})$(num) and $(\bar{\bar{\eta}}_o/\eta_{o,n})$(approx) is relatively large and is equal to 5.28 % for the same values of the parameters mentioned

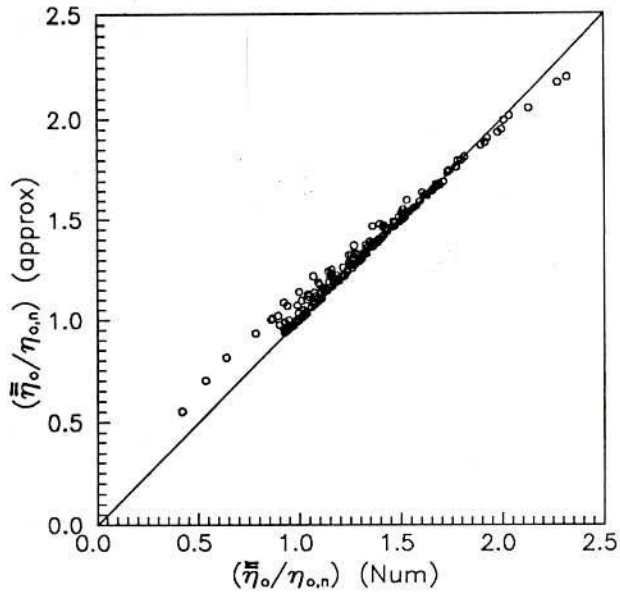

Figure 4.5: Validation of $(\bar{\bar{\eta}}_o/\eta_{o,n})$(approx) against $(\bar{\bar{\eta}}_o/\eta_{o,n})$(num) for tracking mode **c** for $20^o \leq \phi \leq 60^o$, $0.3 \leq K_T \leq 0.7$ and $0.2 \leq X_c \leq 0.6$

.

above. The plot is shown in Figure 4.5. It may be attributed as due to, for mode **c**, the range of θ variation is relatively high and hence a large variation in the instantaneous optical efficiency. Therefore, for mode **c**, particularly at higher latitudes, this approximation gives a larger error. However, it may be noted that $(\bar{\bar{\eta}}_o/\eta_{o,n})$ is only a part in the expression for $(\eta^*_{o,day}/\eta_{o,n})$ and the error in $(\eta^*_{o,day}/\eta_{o,n})$ has been examined and found to be less than 1 %.

4.3.3 Evaluation of Different Hour Angles needed for Evaluating $\eta^*_{o,day}/\eta_{o,n}$ for Concentrating Collectors

Critical Hour Angle, ω_c

Using Eq. (4.17), for $\cos\theta(= A_1 + B_1\cos\omega + C_1\sin\omega)$ along with the expressions for A_1, B_1 and C_1, from Table 4.2, the critical hour angles for concentrating collectors, ω_{c1} and ω_{c2}, in general, are obtained by setting $I_T = I_c$. For tracking collectors, by virtue of symmetry, $|\omega_{c1}| = |\omega_{c2}| = \omega_c$. The expression for I_T given by Eq. (4.14) can be rewritten for concentrating collectors in the form,

$$I_T \doteq K_4[(a_1 + b\cos\omega)\cos\theta + K_6(\cos\omega - \cos\omega_s)] \tag{4.52}$$

where, the constant K_6 is given by,

$$K_6 = \left(\frac{B' D_f}{C_r}\right) \tag{4.53}$$

By setting $I_T = I_c$ and solving for ω the equations to determine ω_c for the five tracking modes are as follows.

Tracking Mode **a:** For a concentrating collector tracked in mode **a**, $(\phi - \beta = \delta)$, using Eq. (4.52), I_T will be equal to I_c when,

$$d'_1 \cos^2 \omega_c + d'_2 \cos \omega_c + d'_3 = 0 \tag{4.54}$$

where the coefficients d'_1, d'_2 and d'_3 are given by,

$$d'_1 = b \cos^2 \delta \tag{4.55}$$

$$d'_2 = a_1 \cos^2 \delta + b \sin^2 \delta + K_6 \tag{4.56}$$

$$d'_3 = a_1 \sin^2 \delta - K_6 \cos \omega_s - I_c / K_4 \tag{4.57}$$

Solving Eq. (4.54) yields,

$$\omega_c = \cos^{-1} \left(\frac{-d'_2 \pm \sqrt{{d'_2}^2 - 4\, d'_1 d'_3}}{2\, d'_1} \right) \tag{4.58}$$

Out of the four roots given by Eq. (4.58), the two roots equal in magnitude and opposite in sign obtained by considering the positive sign of the radical are relevant.

Tracking Mode **b:** Using Eq. (4.17) for $\cos\theta$ along with the expressions from Table 4.2 for A_1 etc. for tracking mode **b** in Eq. (4.52) and upon simplifying a quartic equation in $\cos \omega_c$ of the following form results,

$$\cos^4 \omega_c + q_3 \cos^3 \omega_c + q_2 \cos^2 \omega_c + q_1 \cos \omega_c + q_o = 0 \tag{4.59}$$

where,

$$q_4 = [b \cos \delta]^2 \tag{4.60}$$

$$q_3 = 2\, a_1\, b \cos^2 \delta \,/\, q_4 \tag{4.61}$$

$$q_2 = [(b \sin \delta)^2 + (a_1 \cos \delta)^2 - K_6^2] \,/\, q_4 \tag{4.62}$$

$$q_1 = 2\,[a_1\, b \sin^2 \delta + K_6\,(K_6 \cos \omega_s + I_c / K_4)] \,/\, q_4 \tag{4.63}$$

$$q_o = [(a_1 \sin \delta)^2 - (I_c / K_4 + K_6 \cos \omega_s)^2] \,/\, q_4 \tag{4.64}$$

Eq. (4.59) can be solved explicitly by the algorithm given in Appendix B or by trial and error. Out of the four possible roots for $\cos \omega_c$, only one is relevant. The value which

yields ω_c in the range $0 \leq \omega_c \leq \omega_s$ is to be accepted. The correctness of the value of ω_c is ensured if the value of I_T calculated using Eq. (4.52) at $\omega = \omega_c$ is equal to I_c.

Tracking Mode **c:** Using Eq. (4.17) for $\cos\theta$ along with the expressions from Table 4.2 for A_1, etc. for tracking mode **c** in Eq. (4.52) and upon simplifying a quartic equation in $\cos\omega_c$ of the following form results,

$$\cos^4\omega_c + q'_3\cos^3\omega_c + q'_2\cos^2\omega_c + q'_1\cos\omega_c + q'_o = 0 \tag{4.65}$$

where,

$$q'_4 = b^2 C_c \tag{4.66}$$

$$q'_3 = [2\,a_1\,b\,C_c + b^2\,B_c]\,/\,q'_4 \tag{4.67}$$

$$q'_2 = [2\,a_1\,b\,B_c + A_c\,b^2 + a_1^2\,C_c - K_6^2]\,/\,q'_4 \tag{4.68}$$

$$q'_1 = 2\,[a_1\,A_c\,b + 0.5\,a_1^2\,B_c + K_6\,(K_6\cos\omega_s + I_c/K_4)]\,/\,q'_4 \tag{4.69}$$

$$q'_o = [A_c\,a_1^2 - (I_c/K_4 + K_6\cos\omega_s)^2]\,/\,q'_4 \tag{4.70}$$

The constants A_c, B_c and C_c in Eqs. (4.66) to (4.70) are given by,

$$A_c = 1 - \sin^2\delta\cos^2\phi \tag{4.71}$$

$$B_c = 2\sin\phi\sin\delta\cos\phi\cos\delta \tag{4.72}$$

$$C_c = -\cos^2\delta\sin^2\phi \tag{4.73}$$

Values for $\cos\omega_c$ governed by Eq. (4.65) can be evaluated employing the algorithm given in Appendix B or a trial and error method can be adapted. Out of the four possible values for $\cos\omega_c$, the values of ω_c in the range $0 \leq \omega_c \leq \omega_s$ are relevant.

Tracking Mode **d:** Using Eq. (4.52) for I_T along with Eq. (4.17) for $\cos\theta$, ω_c for tracking mode **d** can be obtained from,

$$\omega_c = \cos^{-1}\left(\frac{I_c/K_4 + K_6\cos\omega_s - a_1\cos\delta}{K_6 + b\cos\delta}\right) \tag{4.74}$$

Tracking Mode **e:** Upon using Eq. (4.52) along with Eq. (4.17) for $\cos\theta$, ω_c for tracking mode **e** can be obtained from,

$$\omega_c = \cos^{-1}\left(\frac{I_c/K_4 + K_6\cos\omega_s - a_1}{K_6 + b}\right) \tag{4.75}$$

Hour Angle Corresponding to $\theta = 60^o$, ω'

The hour angles ω_1 and ω_2 corresponding to $\theta = 60^o$ can be obtained by setting $\cos\theta = 0.5$ in the expressions for incidence angle for the five tracking modes. For tracking collectors,

by virtue of symmetry, $|\omega_1| = |\omega_2| = \omega'$. In what follows the equations to evaluate ω' for different tracking modes are given.

Tracking Mode **a :** Using Eq. (4.17) for $\cos\theta$ along with the expressions for A_1, B_1 and C_1 given in Table 4.2 and on inverting, ω is given by,

$$\omega = \cos^{-1}\left[\frac{\cos\theta - \sin^2\delta}{\cos^2\delta}\right] \tag{4.76}$$

ω' corresponding to $\theta = \pi/3$ is obtained from,

$$\omega' = \cos^{-1}\left[\frac{\cos(\pi/3) - \sin^2\delta}{\cos^2\delta}\right] \tag{4.77}$$

Tracking Mode **b :** Using Eq. (4.17) for $\cos\theta$ along with the expressions for A_1, B_1 and C_1 given in Table 4.2 and upon simplifying, ω can be obtained as,

$$\omega = \cos^{-1}\left[\pm\left(1 - \frac{1-\cos^2\theta}{\cos^2\delta}\right)^{1/2}\right] \tag{4.78}$$

Putting $\theta = \pi/3$ in Eq. (4.78) and upon solving ω' is given by,

$$\omega' = \cos^{-1}\left[\pm\left(1 - \frac{1-\cos^2(\pi/3)}{\cos^2\delta}\right)^{1/2}\right] \tag{4.79}$$

Correct values for ω or ω' are obtained by taking the positive sign in the radical of Eqs. (4.78) and (4.79).

Tracking Mode **c :** Using the expressions for A_1 etc. from Table 4.2, the angle of incidence θ for tracking mode **c** can be written as,

$$\cos\theta = \left[(A' + B'\cos\omega)^2 + \cos^2\delta\sin^2\omega\right]^{1/2} \tag{4.80}$$

Eq. (4.80) can be rewritten as a quadratic equation in terms of $\cos\omega$ as,

$$\cos^2\omega + B_1'\cos\omega + C_1' = 0 \tag{4.81}$$

where,

$$B_1' = \frac{2A'B'}{(B'^2 - \cos^2\delta)} \tag{4.82}$$

$$C_1' = \frac{A'^2 + \cos^2\delta - \cos^2\theta}{(B'^2 - \cos^2\delta)} \tag{4.83}$$

In Eqs. (4.82) and (4.83), A' and B' are as given by Eq. (3.10) of Chapter 3. Solving the quadratic equation, the hour angle ω can be found as,

$$\omega = \cos^{-1}\left[\frac{-B_1'}{2} \pm 0.5\sqrt{(B_1'^2 - 4C_1')}\right] \tag{4.84}$$

The value of ω' can be obtained from Eq. (4.84) by putting $\cos\theta = 0.5$ in Eq. (4.83) for C_1'. Out of the four possible values of ω, the two equal in magnitude and opposite in sign, are to be accepted as the correct value.

ω' is irrelevant for tracking modes **d** and **e**, since the incidence angle is always less than 60^o.

4.4 Evaluation of Monthly Optical Efficiency during the Operational Time Period for Concentrating Collectors: Equivalent Mean Day Calculation

In order to obtain the monthly average optical efficiency applicable for the period of operation of the collector, corresponding to a monthly average non-dimensional critical radiation level, $\bar{X}_c$, it is proposed that $(\bar{\eta}_o^*/\eta_{o,n})$ be evaluated employing the expressions developed for a single day given by Eq. (4.47), along with Eq. (4.50) for $(\bar{\bar{\eta}}_o/\eta_{o,n})$ on a suitably chosen day. $\bar{X}_c$ is defined by,

$$\bar{X}_c = \frac{I_c}{\bar{r}_{t,n}\bar{R}_n\bar{K}_T\bar{H}_o} \tag{4.85}$$

when $\bar{R}_n$ is the noon-time tilt factor on the average day of the month. For concentrating collectors $\bar{R}_n$ is given by,

$$\bar{R}_n = \left[1 - D_f\left(\frac{r_{d,n}}{r_{t,n}}\right)\right] R_{b,n} + \frac{D_f}{C_r}\left(\frac{r_{d,n}}{r_{t,n}}\right) \tag{4.86}$$

To obtain $(\bar{\eta}_o^*/\eta_{o,n})$, the single day chosen, as described in Chapter 3, is the equivalent mean day (EMD). The characteristics of the equivalent mean day have been described in Chapter 3, §3.3.1. The value thus obtained is designated as $(\bar{\eta}_{o,emd}^*/\eta_{o,n})$. Eq. (4.47) valid for a single day thus has been used to obtain $(\bar{\eta}_{o,emd}^*/\eta_{o,n})$ employing

$$\delta = \delta_m \qquad K_T = \bar{K}_T^* \qquad \text{and} \qquad X_c = X_c^* \tag{4.87}$$

It may be recalled from Chapter 3, §3.3.1 that $\bar{K}_T^*$ is the average daily clearness index of the contributing days. $\bar{K}_T^*$ has been obtained as the average clearness index of the days with $K_T > K_{T,min}$, where $K_{T,min}$ is the daily clearness index for which the maximum solar radiation on the collector surface is equal to the critical radiation level. Procedure and relevant equations to obtain $K_{T,min}$ and the number of contributing days, N_c, are

given in Chapter 3, §3.3.1. Eqs. (3.118) to (3.132) become applicable for concentrating collectors when $r_{t,m}$, $r_{d,m}$, $R_{b,m}$ and R_m are now the noon time values $r_{t,n}$, $r_{d,n}$, $R_{b,n}$ and R_n since $\bar{X}_c$ is defined with reference to the noon time solar radiation. X_c^* is the single day (equivalent mean day) non-dimensional critical radiation level corresponding to I_c. Applying Eq. (4.13) for the EMD, X_c^* is given by,

$$X_c^* = \frac{I_c}{r_{t,n}^* \bar{K}_T^* \bar{R}_n^* \bar{H}_o} = \bar{X}_c \frac{\bar{r}_{t,n} \bar{K}_T \bar{R}_n}{r_{t,n}^* \bar{K}_T^* \bar{R}_n^*} = \bar{X}_c \frac{\bar{I}_{t,n}}{\bar{I}_{t,n}^*} \tag{4.88}$$

In Eq. (4.88), $\bar{I}_{T,n}^*$ is obtained from,

$$\bar{I}_{T,n}^* = \frac{K_1 \bar{K}_T^* H_o}{B'} \left[(a_1 + b \cos\omega_n) \cos\theta_n + \left(\frac{B' D_f}{C_r} \right) (\cos\omega_n - \cos\omega_s) \right] \tag{4.89}$$

This methodology becomes available to calculate $(\bar{\eta}_o^*/\eta_{o,n})$ when validated against the defining equation,

$$\left(\frac{\bar{\eta}_o^*}{\eta_{o,n}} \right) = \sum \sum_{-\omega_s}^{\omega_s} [I_T - I_c]^+ \left(\frac{\eta_o}{\eta_{o,n}} \right) \Big/ \sum \sum_{-\omega_s}^{\omega_s} [I_T - I_c]^+ \tag{4.90}$$

$\bar{Q}_{u,m}$ can thus be calculated from,

$$\bar{Q}_{u,m} = F_R \eta_{o,n} \bar{H}_T \bar{\phi} \left(\frac{\bar{\eta}_{o,emd}^*}{\eta_{o,n}} \right) \tag{4.91}$$

4.5 Results and Discussion

4.5.1 Values of All-Day Average Optical Efficiency According to Gaul and Rabl [45]

All-day average optical efficiency according to Gaul and Rabl [45] designated in the present study as $(\eta_{o,day}/\eta_{o,n})_{GR}$ is given by,

$$\left(\frac{\eta_{o,day}}{\eta_{o,n}} \right)_{GR} = \sum_{-\omega_c}^{\omega_c} I_T \left(\frac{\eta_o}{\eta_{o,n}} \right) \Big/ \sum_{-\omega_c}^{\omega_c} I_T \tag{4.92}$$

$$= \int_{-\omega_c}^{\omega_c} I_T \left(\frac{\eta_o}{\eta_{o,n}} \right) d\omega \Big/ \int_{-\omega_c}^{\omega_c} I_T \, d\omega \tag{4.93}$$

It may be noted that, Eqs. (4.92) and (4.93) have been written consistent with the notation employed in the present study. In Gaul and Rabl [45], $-\omega_c$ corresponds to the hour angle 1 or 2 hours after the sunrise and ω_c corresponds to the hour angle 1 or 2 hours before the sunset.

In Eqs. (4.92) and (4.93), Gaul and Rabl expressed I_T as,

$$I_T = I_b R_b = K_T H_o (r_t - r_d D_f) R_b \tag{4.94}$$

Table 4.4: Values of $(\eta_{o,day}/\eta_{o,n})_{GR}$ for 1-hr and 2-hrs cut-off time

Cut-off times, hrs.	ϕ (deg.)	K_T	$(\eta_{o,day}/\eta_{o,n})_{GR}$								
			Mode **a**			Mode **b**			Mode **c**		
			Mar	Jun	Dec	Mar	Jun	Dec	Mar	Jun	Dec
1	20	0.30	0.985	0.984	0.990	0.985	0.985	0.991	0.992	0.999	0.947
		0.50	0.956	0.953	0.973	0.956	0.957	0.975	0.994	0.999	0.954
		0.70	0.947	0.943	0.969	0.947	0.949	0.971	0.994	0.998	0.955
	40	0.30	0.985	0.978	0.993	0.985	0.979	0.993	0.957	0.997	0.810
		0.50	0.957	0.940	0.984	0.957	0.944	0.984	0.968	0.997	0.843
		0.70	0.949	0.929	0.982	0.949	0.934	0.982	0.970	0.997	0.849
	60	0.30	0.986	0.959	0.997	0.986	0.962	0.997	0.852	0.982	0.518
		0.50	0.960	0.929	0.996	0.960	0.922	0.996	0.898	0.986	0.536
		0.70	0.952	0.922	0.996	0.953	0.913	0.996	0.907	0.986	0.540
2	20	0.30	0.985	0.984	0.990	0.985	0.985	0.990	0.992	0.999	0.947
		0.50	0.972	0.967	0.985	0.972	0.969	0.985	0.993	0.999	0.950
		0.70	0.969	0.963	0.984	0.969	0.966	0.984	0.993	0.999	0.950
	40	0.30	0.985	0.978	0.994	0.985	0.979	0.994	0.957	0.997	0.805
		0.50	0.973	0.951	0.992	0.973	0.956	0.992	0.963	0.998	0.815
		0.70	0.971	0.945	0.992	0.971	0.950	0.992	0.964	0.998	0.817
	60	0.30	0.986	0.959	0.999	0.986	0.962	0.999	0.852	0.982	0.357
		0.50	0.976	0.929	0.999	0.976	0.927	0.999	0.878	0.987	0.358
		0.70	0.974	0.922	0.999	0.974	0.919	0.999	0.883	0.988	0.358

However, I_T can be expressed including the diffuse component of solar radiation, in terms of r_t and r_d as,

$$I_T = I_b R_b + I_d/C_r = K_T\, H_o\, [(r_t - r_d D_f)\, R_b + r_d D_f/C_r] \tag{4.95}$$

Using Eq. (4.94) for I_T in Eq. (4.93) $(\eta_{o,day}/\eta_{o,n})$ has been obtained from,

$$\left(\frac{\eta_{o,day}}{\eta_{o,n}}\right)_{GR} = \frac{\sum (r_t - r_d D_f)\, R_b\, (\eta_{o,b}/\eta_{o,n})}{\sum (r_t - r_d D_f)\, R_b} \tag{4.96}$$

Dependence on Latitude and Clearness Index

Numerical values of $(\eta_{o,day}/\eta_{o,n})_{GR}$, have been obtained employing Eq. (4.96), considering I_T to be comprising of only direct component of solar radiation. $(\eta_o/\eta_{o,n})$ as given by Eq. (4.2) for SERI Hexcel collector has been employed in evaluating $(\eta_{o,day}/\eta_{o,n})_{GR}$. $(\eta_{o,day}/\eta_{o,n})_{GR}$ values for the tracking modes **a, b** and **c**, for K_T = 0.3, 0.50 and 0.70 are given in Table 4.4 for $\phi = 20^o$, 40^o and 60^o and $\delta = -2.42^o$, 23.09^o and -23.05^o, for 1-hr and 2-hrs cut-off times before sunset. From the numerical values the following points emerge.

1. $(\eta_{o,day}/\eta_{o,n})_{GR}$ does depend on K_T, particularly for tracking modes **a** and **b**. Indeed, the change in $(\eta_{o,day}/\eta_{o,n})_{GR}$, when K_T changes from 0.3 to 0.7, is more than the change when δ changes from -23.1^o to 23.1^o, for lower latitudes, $\phi = 20^o$ and 40^o. However, at $\phi = 60^o$ and $\delta = -23.1^o$ for tracking modes **a** and **b** the changes due to K_T are negligible. For tracking mode **c**, $(\eta_{o,day}/\eta_{o,n})_{GR}$ varies with K_T in the month of December.

2. $(\eta_{o,day}/\eta_{o,n})_{GR}$ does not significantly depend on the latitude for tracking modes **a** and **b** in the months of March and December. However, in June the changes are not insignificant.

3. For tracking mode **c**, $(\eta_{o,day}/\eta_{o,n})_{GR}$ changes significantly with latitude, particularly in December. This is due to strong bimodal solar radiation distribution as shown in Figure 4.1.

4. $(\eta_{o,day}/\eta_{o,n})_{GR}$ values are almost identical for 1-hr and 2-hrs cut-off times for low K_T (0.3). This is due to direct radiation being a small fraction of the global radiation at low K_T. $(\eta_{o,day}/\eta_{o,n})_{GR}$ values for 1-hr and 2-hrs cut-off times differ for higher K_T values. This difference is higher at higher latitudes, particularly for mode **c** in December.

An examination of Eq. (4.96) readily reveals that $(\eta_{o,day}/\eta_{o,n})_{GR}$ is independent of latitude and clearness index for tracking modes **d** and **e**, since $(\eta_o/\eta_{o,n})$ remains constant throughout the operating period.

From these results, it may be concluded that latitude dependence is relevant for tracking mode **c** and influence of clearness index in not insignificant for tracking modes **a** and **b**. Numerical values presented in Table 4 of Gaul and Rabl [45] can be reproduced with $\phi = 35.0^o$ which is perhaps the latitude of Albuquerque, NM, USA. Since, 1-hr and 2-hrs cut-off times imply significantly differing critical radiation levels or operating period, as a fraction of the of day length for different latitudes, declinations and clearness index, a systematic examination in terms of cut-off time is warranted.

Dependence on Cut-off Time

Numerical values of $(\eta_{o,day}/\eta_{o,n})_{GR}$ according to Eq. (4.96) have been obtained for tracking modes **a, b** and **c**, for $\phi = 20^o$, 40^o and 60^o, for $\delta = -2.42^o$, 23.09^o and -23.05^o, for $K_T = 0.3$, 0.5 and 0.7. The cut-off time has been characterized by a non-dimensional operating period, O_p, defined by,

$$O_p = \frac{\omega_c}{\omega_s} \tag{4.97}$$

Table 4.5: Tabulated values of $(\eta_{o,day}/\eta_{o,n})_{GR}$ for $\phi = 20^o$

Tracking Mode	O_p	$(\eta_{o,day}/\eta_{o,n})_{GR}$								
		$K_T = 0.3$			$K_T = 0.5$			$K_T = 0.7$		
		Mar	Jun	Dec	Mar	Jun	Dec	Mar	Jun	Dec
a	0.20	0.998	0.998	0.999	0.998	0.998	0.999	0.998	0.998	0.999
	0.40	0.993	0.992	0.995	0.992	0.992	0.995	0.992	0.991	0.995
	0.60	0.985	0.985	0.991	0.978	0.977	0.987	0.976	0.975	0.986
	0.80	0.985	0.984	0.990	0.958	0.957	0.974	0.951	0.949	0.970
b	0.20	0.998	0.998	0.999	0.998	0.998	0.999	0.998	0.998	0.999
	0.40	0.993	0.993	0.995	0.992	0.992	0.995	0.992	0.992	0.995
	0.60	0.985	0.985	0.991	0.978	0.978	0.987	0.976	0.976	0.986
	0.80	0.985	0.985	0.991	0.959	0.961	0.976	0.951	0.954	0.972
c	0.20	0.991	1.000	0.940	0.991	1.000	0.940	0.991	1.000	0.940
	0.40	0.992	1.000	0.943	0.992	1.000	0.944	0.992	1.000	0.944
	0.60	0.992	0.999	0.946	0.993	0.999	0.949	0.993	0.999	0.949
	0.80	0.992	0.999	0.947	0.994	0.999	0.953	0.994	0.999	0.955

where ω_c is the cut-off hour angle which corresponds to $I_T = I_c$. It may be noted that cut-off time of Gaul and Rabl [45] is $\omega_c/15$ hrs when ω_c is in degrees. Numerical values of $(\eta_{o,day}/\eta_{o,n})_{GR}$ for the above mentioned parameters are given in Tables 4.5 to 4.7 for $\phi = 20^o$, 40^o and 60^o respectively.

The variation of $(\eta_{o,day}/\eta_{o,n})_{GR}$ with non-dimensional operating period, O_p is shown in Figures 4.6 (a) to 4.6 (f). Figures 4.6 (a) to (c) are plots of $(\eta_{o,day}/\eta_{o,n})_{GR}$ vs O_p for tracking mode **b** (results for tracking mode **a**, can be expected to be very similar) for the three latitudes $\phi = 20^o$, 40^o and 60^o respectively, at $K_T = 0.7$, for the three months, March, June and December. For tracking mode **b**, as operating period increases $(\eta_{o,day}/\eta_{o,n})_{GR}$ decreses. This is due to the weighted average being for longer time periods during which higher angles of incidence are included. From Figures 4.6 (a) to (c), it is evident that the change in $(\eta_{o,day}/\eta_{o,n})_{GR}$ with O_p is minimum in the month of December owing to favourable angle of incidence. The change in $(\eta_{o,day}/\eta_{o,n})_{GR}$ with O_p is maximum in June for $\phi = 40^o$ and 60^o, whereas, for $\phi = 20^o$, the change in the months of March and June is comparable.

The plots of $(\eta_{o,day}/\eta_{o,n})_{GR}$ vs O_p for tracking mode **c**, shown in Figures 4.6 (d) to 4.6 (f) for $\phi = 20^o$, 40^o and 60^o respectively, display an opposite trend compared to mode **b**, in the variation of $(\eta_{o,day}/\eta_{o,n})_{GR}$ with O_p. For mode **c** tracking, $(\eta_{o,day}/\eta_{o,n})_{GR}$ increases as O_p increases. This is due to the angle of incidence being relatively higher

Table 4.6: Tabulated values of $(\eta_{o,day}/\eta_{o,n})_{GR}$ for $\phi = 40^o$

Tracking Mode	O_p	$(\eta_{o,day}/\eta_{o,n})_{GR}$								
		$K_T = 0.3$			$K_T = 0.5$			$K_T = 0.7$		
		Mar	Jun	Dec	Mar	Jun	Dec	Mar	Jun	Dec
a	0.20	0.998	0.998	0.999	0.998	0.998	0.999	0.998	0.998	0.999
	0.40	0.993	0.990	0.997	0.992	0.989	0.996	0.992	0.988	0.996
	0.60	0.986	0.978	0.993	0.979	0.968	0.991	0.977	0.966	0.991
	0.80	0.985	0.978	0.993	0.960	0.944	0.983	0.953	0.935	0.980
b	0.20	0.998	0.998	0.999	0.998	0.998	0.999	0.998	0.998	0.999
	0.40	0.993	0.990	0.997	0.992	0.989	0.996	0.992	0.989	0.996
	0.60	0.986	0.979	0.993	0.979	0.970	0.991	0.977	0.968	0.991
	0.80	0.985	0.979	0.993	0.960	0.949	0.983	0.953	0.941	0.981
c	0.20	0.945	0.996	0.763	0.945	0.996	0.763	0.945	0.996	0.763
	0.40	0.952	0.997	0.787	0.953	0.997	0.789	0.953	0.997	0.790
	0.60	0.957	0.997	0.808	0.961	0.998	0.820	0.962	0.998	0.822
	0.80	0.957	0.997	0.810	0.967	0.998	0.845	0.969	0.998	0.852

Table 4.7: Tabulated values of $(\eta_{o,day}/\eta_{o,n})_{GR}$ for $\phi = 60^o$

Tracking Mode	O_p	$(\eta_{o,day}/\eta_{o,n})_{GR}$								
		$K_T = 0.3$			$K_T = 0.5$			$K_T = 0.7$		
		Mar	Jun	Dec	Mar	Jun	Dec	Mar	Jun	Dec
a	0.20	0.998	0.996	1.000	0.998	0.996	1.000	0.998	0.996	1.000
	0.40	0.993	0.982	0.999	0.993	0.980	0.999	0.993	0.979	0.999
	0.60	0.986	0.961	0.997	0.980	0.944	0.997	0.979	0.940	0.997
	0.80	0.986	0.959	0.996	0.962	0.929	0.994	0.956	0.922	0.994
b	0.20	0.998	0.996	1.000	0.998	0.996	1.000	0.998	0.996	1.000
	0.40	0.993	0.982	0.999	0.993	0.980	0.999	0.993	0.980	0.999
	0.60	0.986	0.964	0.997	0.980	0.950	0.997	0.979	0.946	0.997
	0.80	0.986	0.962	0.996	0.962	0.942	0.995	0.956	0.937	0.994
c	0.20	0.783	0.968	0.314	0.783	0.969	0.315	0.783	0.969	0.315
	0.40	0.824	0.978	0.409	0.829	0.979	0.413	0.830	0.979	0.413
	0.60	0.851	0.982	0.500	0.870	0.985	0.514	0.874	0.986	0.517
	0.80	0.852	0.982	0.560	0.896	0.987	0.599	0.904	0.988	0.606

around mid-day (small operating period) than the angle of incidence near sunrise and sunset, i.e., when the operating period is high.

Defining daily average optical efficiency in terms of a cut-off time results in misleading values when the solar radiation distribution is bimodal. Referring to Figure 4.1, when $I_{T,n} < I_c < I_{T,m}$, it has already been pointed out that the collector operates during $-\omega_{c1}$ to $-\omega_{cb}$ and ω_{cb} to ω_{c1}. When Gaul and Rabl's [45] integral for daily optical efficiency is evaluated, specified cut-off times may correspond to ω_{c1} or ω_{cb}. Typically, 1-hr and 2-hrs cut-off times for $\phi = 40^o$ fall in this category. When it corresponds to ω_{cb}, the all-day average will be obtained for the period $-\omega_{cb}$ to ω_{cb}. For $I_{T,n} < I_c < I_{T,m}$, the collector does not operate during this time period. When the cut-off time corresponds to ω_{c1}, Gaul and Rabl's definition includes non-operating period also. Thus, it is desirable to fix the cut-off time(s) depending on the critical radiation level. The difference arising in the all-day average optical efficiencies due to specifying a cut-off time, though I_c is same, is demonstrated in Table 4.8. For critical radiation level $I_{T,n} < I_c < I_{T,m}$, ω_{c1} and ω_{cb} values have been obtained for $\phi = 40^o$ and 60^o, for the month of December, for $K_T = 0.7$. All-day average optical efficiencies, as obtained from Gaul and Rabl for cut-off times corresponding to ω_{c1} and ω_{cb}, given in Table 4.8, differ considerably. Indeed, both the values are incorrect. Values obtained averaged during $-\omega_{c1}$ to $-\omega_{cb}$ and ω_{cb} to ω_{c1} by the present approach also have been given in Table 4.8. A further discussion of this is presented in the following section. Thus, $(\eta_{o,day}/\eta_{o,n})_{GR}$ in general, displays dependence on latitude, clearness index and of course, declination. This dependence is strong for tracking mode **c**. Also, it is important to identify the operating period correctly.

4.5.2 $(\eta^*_{o,day}/\eta_{o,n})$, Single Day Values

Numerical values for $(\eta^*_{o,day}/\eta_{o,n})$ have been obtained using Eq. (4.47), along with the expressions for the primitives given in Table 4.3 and Eq. (4.50) for $(\bar{\bar{\eta}}_o/\eta_{o,n})$, for the concentrating collectors with $C_r = 10$ tracked in the five principal modes for $\phi = 20^o$, 40^o and 60^o, $X_c = 0.2$, 0.4, 0.6 and 0.8, for representative values of declinations, $\delta = -2.42^o$, 23.09^o and -23.05^o which correspond to March, June and December months. Values of the non-dimensional critical level considered $0.2 \leq X_c \leq 0.8$ include a wide range of operating time periods. Numerical values of $(\eta^*_{o,day}/\eta_{o,n})$ for the range of parameters mentioned are given in Tables 4.9 to 4.11 for $\phi = 20^o$, 40^o and 60^o respectively.

Tracking Modes a and b

Values of $(\eta^*_{o,day}/\eta_{o,n})$ for a given ϕ, δ and X_c for the tracking modes **a** and **b** are almost the same. Thus, the dependence of $(\eta^*_{o,day}/\eta_{o,n})$ on X_c and K_T for different latitudes and

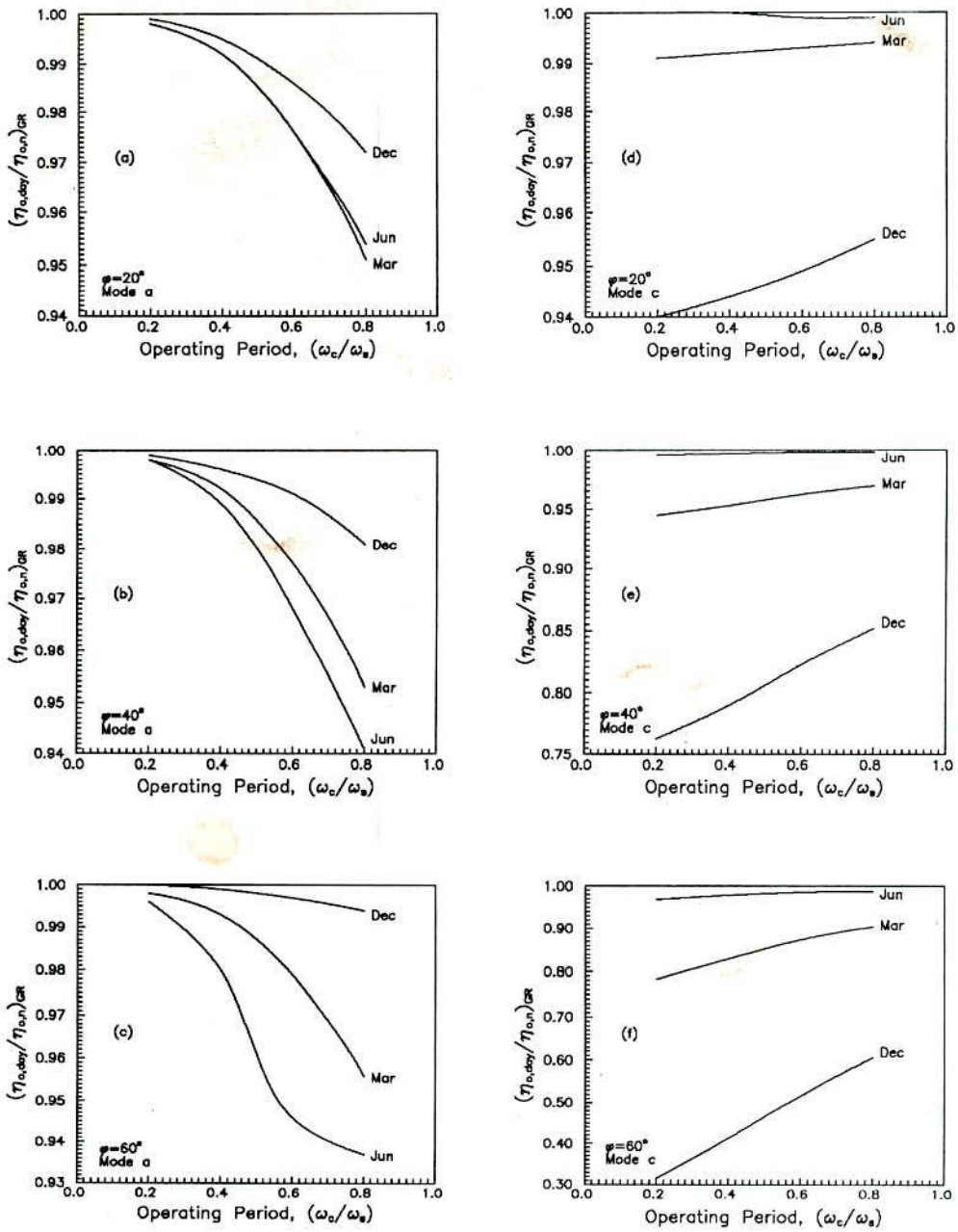

Figure 4.6: Dependence of $(\eta_{o,day}/\eta_{o,n})_{GR}$ on operating time period for tracking mode **b** (a, b, c) and tracking mode **c** (d, e, f) for $K_T = 0.7$, $\phi = 20^o$, 40^o and 60^o

Table 4.8: Values of $(\eta_{o,day}/\eta_{o,n})_{GR}$ (for different cut-off hour angles) and $(\eta^{*}_{o,day}/\eta_{o,n})$ for same critical radiation level

ϕ (deg.)	I_c W/m^2	Cut-off hour angle (deg.)	$(\eta_{o,day}/\eta_{o,n})_{GR}$	$(\eta^{*}_{o,day}/\eta_{o,n})$
40	380.50	67.10	0.872	0.899
		8.90	0.757	$(X_c = 1.02)$
	387.80	65.80	0.870	0.902
		12.80	0.762	$(X_c = 1.04)$
	395.30	64.24	0.867	0.903
		16.00	0.766	$(X_c = 1.06)$
	410.50	60.80	0.862	0.909
		22.00	0.777	$(X_c = 1.10)$
	425.30	56.70	0.855	0.912
		28.00	0.790	$(X_c = 1.14)$
60	147.30	*	*	0.708
		9.10	0.320	$(X_c = 1.50)$
	196.50	*	*	.736
		14.55	0.383	$(X_c = 2.00)$
	245.60	*	*	0.772
		20.10	0.451	$(X_c = 2.50)$
	294.50	*	*	0.812
		26.40	0.527	$(X_c = 3.00)$
	333.80	*	*	0.845
		33.10	0.598	$(X_c = 3.40)$

Note: $(\eta^{*}_{o,day}/\eta_{o,n})$, the present value is the average for the periods $-\omega_{c1}$ to $-\omega_{cb}$ and ω_{cb} to ω_{c1} since the collector does not operate during $-\omega_{cb}$ to ω_{cb}.

For $\phi = 60^{o}$, in columns 3 and 4, the '*' sign is used to mean that the cut-off hour angles are almost equal to the sunrise or sunset hour angles.

Table 4.9: Tabulated values of $(\eta^*_{o,day}/\eta_{o,n})$ for $\phi = 20^o$

Tracking Mode	X_c	$(\eta^*_{o,day}/\eta_{o,n})$								
		$K_T = 0.3$			$K_T = 0.5$			$K_T = 0.7$		
		Mar	Jun	Dec	Mar	Jun	Dec	Mar	Jun	Dec
a	0.20	0.922	0.919	0.935	0.954	0.952	0.964	0.960	0.958	0.966
	0.40	0.928	0.926	0.940	0.965	0.964	0.972	0.976	0.976	0.980
	0.60	0.934	0.931	0.944	0.972	0.970	0.978	0.986	0.985	0.988
	0.80	0.938	0.935	0.947	0.977	0.975	0.981	0.991	0.991	0.993
b	0.20	0.922	0.919	0.935	0.954	0.952	0.965	0.960	0.955	0.966
	0.40	0.928	0.926	0.940	0.965	0.964	0.972	0.976	0.976	0.980
	0.60	0.934	0.931	0.944	0.972	0.971	0.978	0.986	0.985	0.988
	0.80	0.938	0.935	0.947	0.977	0.975	0.981	0.991	0.991	0.993
c	0.20	0.923	0.930	0.893	0.973	0.978	0.937	0.990	0.994	0.954
	0.40	0.926	0.933	0.894	0.972	0.978	0.934	0.989	0.994	0.953
	0.60	0.928	0.935	0.894	0.971	0.978	0.931	0.988	0.995	0.950
	0.80	0.929	0.937	0.894	0.970	0.978	0.927	0.986	0.995	0.944
d	0.20	0.933	0.919	0.931	0.981	0.967	0.972	0.997	0.984	0.985
	0.40	0.936	0.922	0.933	0.980	0.967	0.972	0.996	0.984	0.985
	0.60	0.938	0.924	0.935	0.980	0.966	0.972	0.996	0.983	0.985
	0.80	0.939	0.925	0.936	0.980	0.966	0.972	0.996	0.983	0.985
e	0.20	0.933	0.930	0.943	0.981	0.980	0.985	0.997	0.996	0.998
	0.40	0.936	0.934	0.946	0.980	0.979	0.984	0.996	0.996	0.997
	0.60	0.938	0.936	0.947	0.980	0.979	0.984	0.996	0.996	0.997
	0.80	0.940	0.937	0.949	0.980	0.979	0.984	0.996	0.995	0.997

Table 4.10: Tabulated values of $(\eta^*_{o,day}/\eta_{o,n})$ for $\phi = 40^o$

Tracking Mode	X_c	$(\eta^*_{o,day}/\eta_{o,n})$								
		$K_T = 0.3$			$K_T = 0.5$			$K_T = 0.7$		
		Mar	Jun	Dec	Mar	Jun	Dec	Mar	Jun	Dec
a	0.20	0.932	0.919	0.954	0.958	0.948	0.974	0.961	0.954	0.974
	0.40	0.938	0.927	0.958	0.969	0.962	0.980	0.978	0.974	0.984
	0.60	0.943	0.933	0.961	0.976	0.971	0.985	0.987	0.984	0.991
	0.80	0.947	0.937	0.963	0.981	0.976	0.988	0.993	0.991	0.995
b	0.20	0.932	0.919	0.954	0.958	0.947	0.974	0.961	0.950	0.974
	0.40	0.938	0.927	0.958	0.969	0.962	0.980	0.978	0.974	0.984
	0.60	0.943	0.933	0.961	0.976	0.970	0.985	0.987	0.984	0.991
	0.80	0.947	0.937	0.963	0.981	0.976	0.988	0.993	0.991	0.995
c	0.20	0.901	0.930	0.796	0.950	0.978	0.846	0.969	0.993	0.869
	0.40	0.901	0.932	0.790	0.947	0.977	0.840	0.967	0.993	0.869
	0.60	0.901	0.934	0.783	0.943	0.977	0.832	0.966	0.993	0.870
	0.80	0.899	0.934	0.771	0.937	0.975	0.821	0.961	0.992	0.872
d	0.20	0.943	0.922	0.948	0.984	0.968	0.978	0.997	0.984	0.987
	0.40	0.946	0.925	0.950	0.984	0.968	0.978	0.997	0.984	0.987
	0.60	0.947	0.926	0.951	0.984	0.968	0.978	0.997	0.984	0.986
	0.80	0.949	0.928	0.952	0.984	0.967	0.978	0.997	0.983	0.986
e	0.20	0.943	0.934	0.960	0.985	0.981	0.991	0.998	0.997	0.999
	0.40	0.946	0.937	0.962	0.984	0.980	0.991	0.997	0.997	0.999
	0.60	0.947	0.938	0.963	0.984	0.980	0.990	0.997	0.996	0.999
	0.80	0.949	0.940	0.964	0.984	0.980	0.990	0.997	0.996	0.999

Table 4.11: Tabulated values of $(\eta^*_{o,day}/\eta_{o,n})$ for $\phi = 60^o$

Tracking Mode	X_c	$(\eta^*_{o,day}/\eta_{o,n})$								
		$K_T = 0.3$			$K_T = 0.5$			$K_T = 0.7$		
		Mar	Jun	Dec	Mar	Jun	Dec	Mar	Jun	Dec
a	0.20	0.950	0.920	0.985	0.965	0.943	0.990	0.963	0.950	0.991
	0.40	0.956	0.932	0.986	0.976	0.962	0.992	0.980	0.972	0.992
	0.60	0.960	0.940	0.987	0.982	0.972	0.994	0.989	0.984	0.994
	0.80	0.963	0.945	0.989	0.987	0.979	0.996	0.994	0.991	0.998
b	0.20	0.950	0.921	0.985	0.965	0.939	0.990	0.963	0.944	0.991
	0.40	0.956	0.932	0.986	0.976	0.961	0.992	0.980	0.971	0.992
	0.60	0.960	0.940	0.988	0.982	0.972	0.994	0.989	0.984	0.994
	0.80	0.963	0.945	0.989	0.987	0.979	0.996	0.994	0.991	0.998
c	0.20	0.828	0.924	0.550	0.893	0.969	0.624	0.919	0.980	0.637
	0.40	0.824	0.924	0.548	0.889	0.969	0.629	0.921	0.981	0.644
	0.60	0.817	0.922	0.546	0.885	0.967	0.637	0.924	0.983	0.653
	0.80	0.806	0.919	0.543	0.883	0.964	0.646	0.929	0.983	0.664
d	0.20	0.961	0.932	0.976	0.990	0.973	0.986	0.999	0.985	0.988
	0.40	0.962	0.934	0.977	0.990	0.972	0.986	0.999	0.985	0.988
	0.60	0.964	0.935	0.977	0.990	0.971	0.986	0.999	0.985	0.988
	0.80	0.965	0.936	0.977	0.990	0.971	0.986	0.998	0.984	0.988
e	0.20	0.961	0.944	0.989	0.990	0.985	0.999	0.999	0.998	1.000
	0.40	0.962	0.946	0.989	0.990	0.984	0.999	0.999	0.998	1.000
	0.60	0.964	0.947	0.989	0.990	0.984	0.998	0.999	0.997	1.000
	0.80	0.965	0.948	0.989	0.990	0.983	0.998	0.999	0.997	1.000

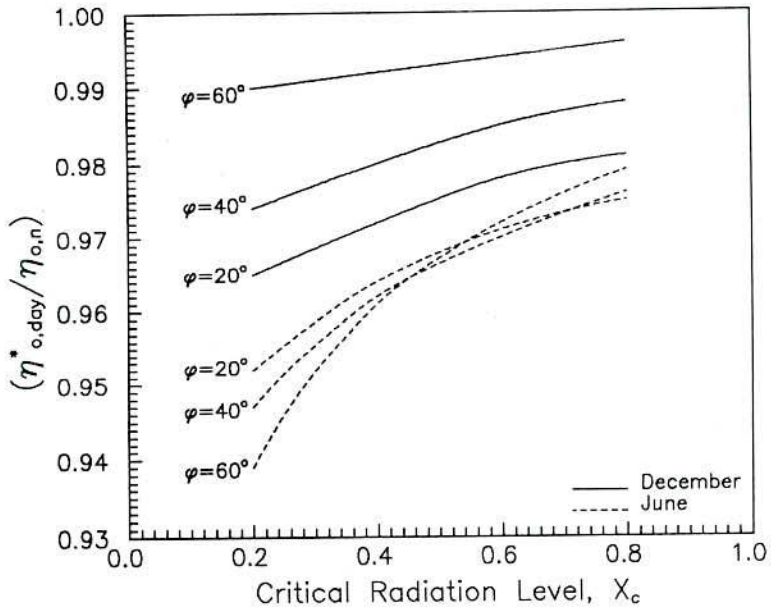

Figure 4.7: Variation of $(\eta^*_{o,day}/\eta_{o,n})$ with X_c for tracking mode **b** for $K_T = 0.5$, $\delta = -23.05^o$ and 23.09^o

.

months is discussed with the values corresponding to mode **b**. A plot of $(\eta^*_{o,day}/\eta_{o,n})$ vs the non-dimensional critical level X_c is shown in Figure 4.7, for $K_T = 0.5$, for the three latitudes, $\phi = 20^o$, 40^o and 60^o, for the months of June and December. From Figure 4.7, it is evident that, as X_c increases, $(\eta^*_{o,day}/\eta_{o,n})$ increases. The increase in $(\eta^*_{o,day}/\eta_{o,n})$ is higher in the month of June compared to the increase in December for a given latitude. The values of $(\eta^*_{o,day}/\eta_{o,n})$ are higher in December compared to the values in June. Also, it can be noticed from Figure 4.7, that as latitude increases, $(\eta^*_{o,day}/\eta_{o,n})$ increases with latitude in December whereas it decreases in June. This trend is similar to $\bar{R}_b$, the monthly average daily tilt factor for direct radiation when the orientation of the collector is optimum. For example, for a south facing flat plate collector, $(\phi - \beta) = \delta$ is the optimum. Mode **b** tracking is almost the same with additional adjustment of the slope throughout the day.

Variation of $(\eta^*_{o,day}/\eta_{o,n})$ with K_T corresponding to $X_c = 0.4$ is shown in Figure 4.8, for $\phi = 20^o$, 40^o and 60^o, for two months, June and December. As K_T increases, $(\eta^*_{o,day}/\eta_{o,n})$ increases. As can be expected $(\eta^*_{o,day}/\eta_{o,n})$ is higher at higher latitudes in December.

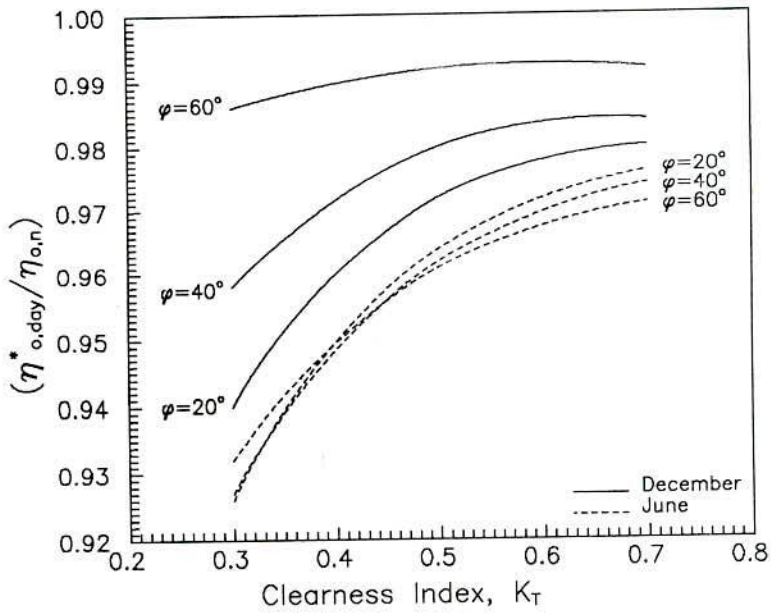

Figure 4.8: Variation of $(\eta^*_{o,day}/\eta_{o,n})$ with K_T for tracking mode **b**, $X_c = 0.4$, $\delta = -23.05^o$ and 23.09^o

.

Tracking Mode c

For tracking mode **c**, from the values given in Tables 4.9 to 4.11, it appears that $(\eta^*_{o,day}/\eta_{o,n})$ does not depend on X_c significantly for $X_c < 1.0$. This is due to the operating period not changing significantly as X_c increases, a consequence of the solar radiation distribution for tracking mode **c**. Even when the solar radiation is bimodal for tracking mode **c**, as shown in Figure 4.1, for $X_c < 1.0$, this feature is true. Significant changes in operating period and $(\eta^*_{o,day}/\eta_{o,n})$ occur for $X_c > 1.0$ which is relevant only when the solar radiation is bimodal.

In order to bring out the difference in the daily average optical efficiency when $X_c > 1.0$ i.e., $I_{T,n} < I_c < I_{T,m}$, when correct operational time period is employed, $(\eta^*_{o,day}/\eta_{o,n})$ values obtained as the averaged value during $-\omega_{c1}$ to $-\omega_{cb}$ and ω_{cb} to ω_{c1} (referring to Figure 4.1) have also been calculated for $\phi = 40^o$ and 60^o, $K_T = 0.7$, for concentrating collectors tracked in mode **c**. These values also are shown in the last column, along with the X_c values, of Table 4.8. It may be noted that as long as $I_c < I_{T,m}$, $(\eta^*_{o,day}/\eta_{o,n}) \neq 0$. Thus, cut-off time say, 2-hrs which corresponds to $-\omega_{cb}$ to ω_{cb} (referring Figure 4.1) is irrelevant. $(\eta^*_{o,day}/\eta_{o,n})$, if evaluated for $-\omega_{cb}$ to ω_{cb}, will be equal to zero since $I_T < I_c$ during $-\omega_{cb}$ to ω_{cb}. This feature is included in writting Eq. (4.8).

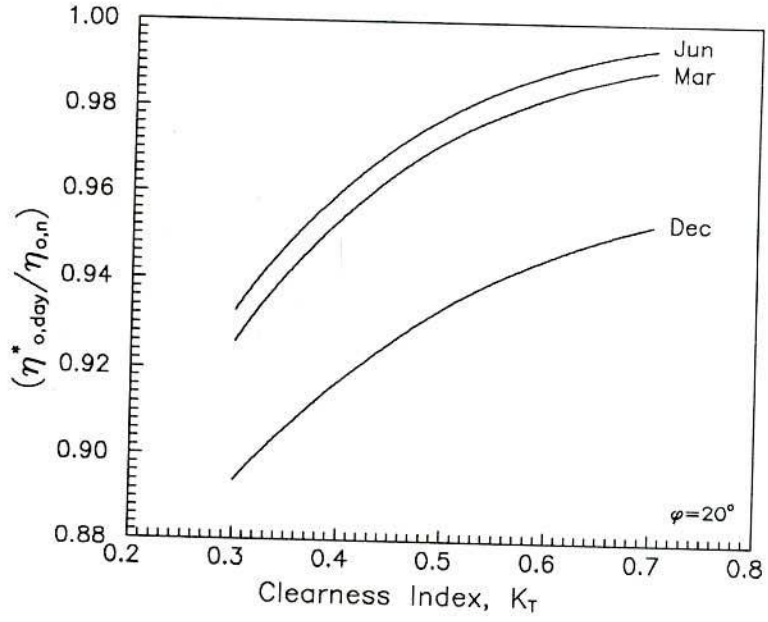

Figure 4.9: Variation of $(\eta^*_{o,day}/\eta_{o,n})$ with K_T for tracking mode **c**, $X_c = 0.4$, $\delta = -23.05^o$, -2.42^o and 23.09^o, $\phi = 20^o$

Plots of $(\eta^*_{o,day}/\eta_{o,n})$ vs K_T corresponding to $X_c = 0.4$, for three months, March, June and December are shown in Figures 4.9, 4.10 and 4.11 for $\phi = 20^o$, 40^o and 60^o respectively. As K_T increases $(\eta^*_{o,day}/\eta_{o,n})$ increases and the trend is same for the three latitudes considered. Also, the values of $(\eta^*_{o,day}/\eta_{o,n})$ increase as δ increases and decrease as ϕ increses.

Tracking Modes d and e

Owing to angle of incidence remaining constant ($\theta = \delta$ for mode **d** and $\theta = 0^o$ for mode **e**) through out the day, $(\eta_o/\eta_{o,n})$ does not vary during the operating period[2] and hence $(\eta^*_{o,day}/\eta_{o,n})$ does not depend on X_c.

Variation of $(\eta^*_{o,day}/\eta_{o,n})$ with K_T for tracking modes **d** and **e**, for the three latitudes, $\phi = 20^o$, 40^o and 60^o is shown in Figures 4.12 and 4.13, for the months of June and December respectively. As can be expected, $(\eta^*_{o,day}/\eta_{o,n})$ values are higher for tracking mode **e** compared to the values for tracking mode **d**. From the values given in Tables 4.9 to 4.11, it can also be seen that the values of $(\eta^*_{o,day}/\eta_{o,n})$ are almost same for modes **d** and **e** in the month of March which can be expected since the declination is small.

[2]except for small dependence arising due to including diffuse component of solar radiation

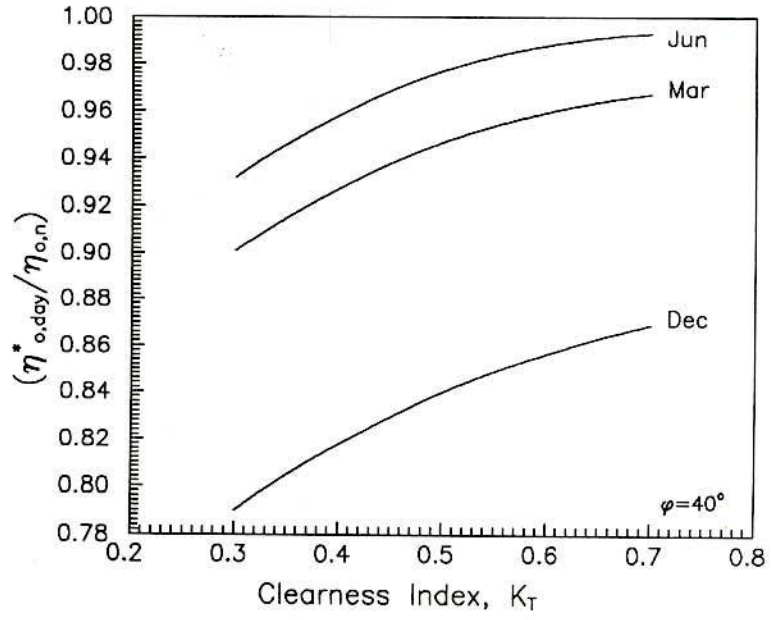

Figure 4.10: Variation of $(\eta^*_{o,day}/\eta_{o,n})$ with K_T for tracking mode **c**, $X_c = 0.4$, $\delta = -23.05^o$, -2.42^o and 23.09^o, $\phi = 40^o$

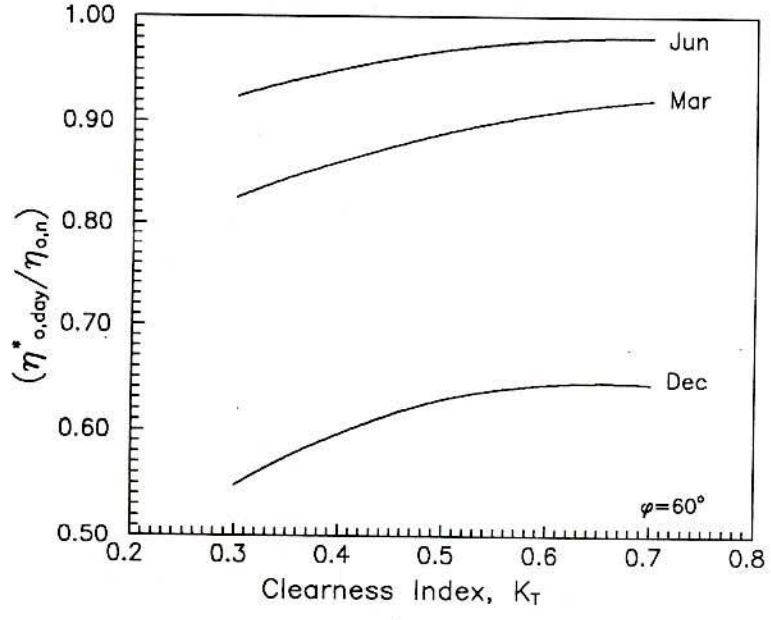

Figure 4.11: Variation of $(\eta^*_{o,day}/\eta_{o,n})$ with K_T for tracking mode **c**, $X_c = 0.4$, $\delta = -23.05^o$, -2.42^o and 23.09^o, $\phi = 60^o$

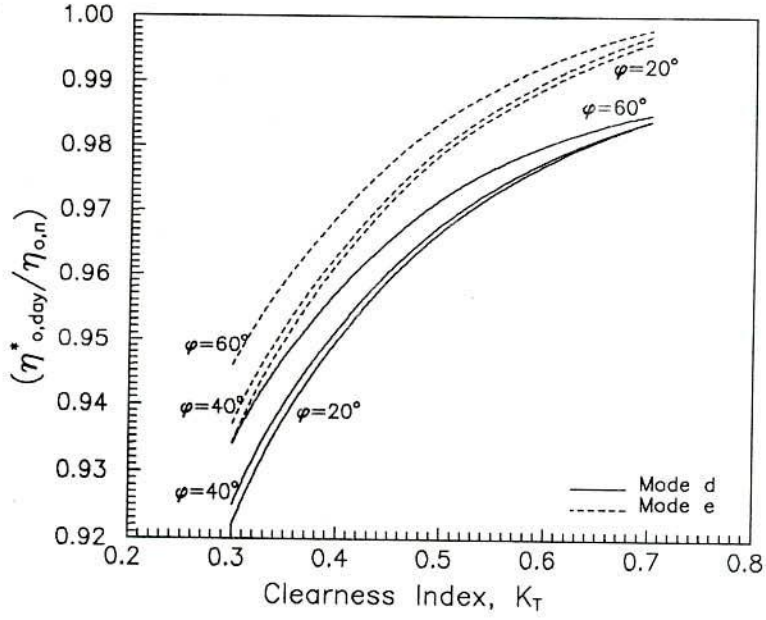

Figure 4.12: Variation of $(\eta^*_{o,day}/\eta_{o,n})$ with K_T for tracking modes **d** and **e**, $\phi = 20^o$, 40^o and 60^o, $\delta = 23.09^o$, $X_c = 0.4$

From Figures 4.12 and 4.13, it can be seen that $(\eta^*_{o,day}/\eta_{o,n})$ increases with K_T for both the modes **d** and **e**, for all latitudes in June as well as in December. As latitude increases, $(\eta^*_{o,day}/\eta_{o,n})$ increases at a given K_T. This is due to I_c, the critical radiation level remaining almost constant for different latitudes but the day length differing considerably. Also, it can be noted from Figures 4.12 and 4.13 that as K_T increases, the difference in $(\eta^*_{o,day}/\eta_{o,n})$ values for different latitudes decreases. This is due to the incident radiation becoming practically only the direct radiation which for mode e is independent of latitude (always the incident ray is normal to the aperture) and almost constant for mode **d**, the variation being by a factor of maximum 0.92 which is the value of $\cos\delta$ for $|\delta| = 23^o$.

Validation Against Data

$(\eta^*_{o,day}/\eta_{o,n})$ values as obtained using Eq. (4.47) have been compared with the values obtained employing monthly average hourly solar radiation data for three locations, Ahmedabad ($\phi = 23.07^o$), New Delhi ($\phi = 28.58^o$) in India and Madison, WI ($\phi = 43.10^o$) in the USA. The data have been taken from [132], for the Indian locations and the TMY data for Madison [133]. $(\eta^*_{o,day}/\eta_{o,n})$ obtained using Eq. (4.8) (as summation) employing the data is designated as $(\eta^*_{o,day}/\eta_{o,n})$(data). Plots of $(\eta^*_{o,day}/\eta_{o,n})$ vs $(\eta^*_{o,day}/\eta_{o,n})$(data) are shown in Figures 4.14, 4.15 and 4.16 for the three locations, Ahmedabad, New Delhi

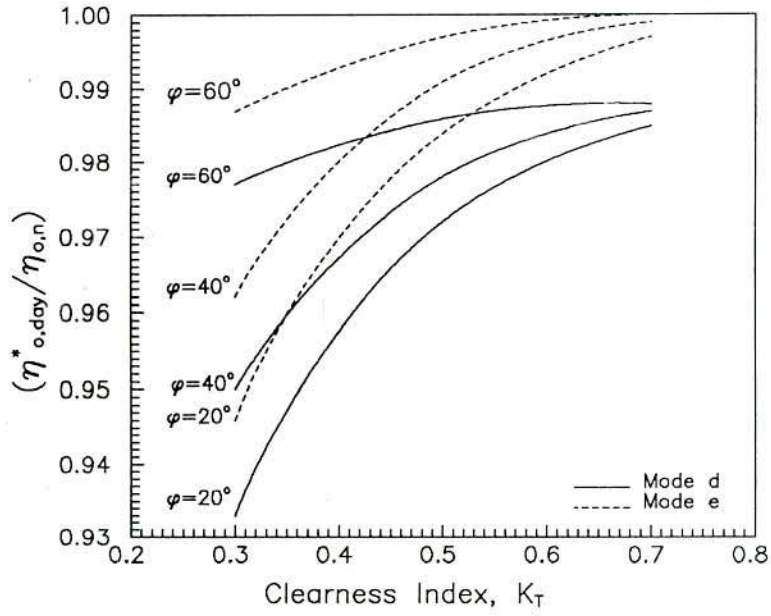

Figure 4.13: Variation of $(\eta^*_{o,day}/\eta_{o,n})$ with K_T for tracking modes **d** and **e**, $\phi = 20^o$, 40^o and 60^o, $\delta = -23.05^o$, $X_c = 0.4$

.

and Madison, WI respectively. Figures 4.14 to 4.16 include the comparison for all the 12 months, for X_c = 0.2, 0.4, 0.6 and 0.8, for tracking modes **a, b** and **c**. The three groups of four points each for which $(\eta^*_{o,day}/\eta_{o,n}) < 0.9$, in Figure 4.16, correspond to the months of November, December and January for tracking mode **c**. The larger differences are essentially due to low $\bar{K}_T$ value in these months for Madison, WI. In general, I, I_d and I_b predicted using r_t [12] and r_d [16] correlations may differ significantly from the data values for low $\bar{K}_T$ value. The agreement, in general, is good. The rms differences are 0.43 %, 0.49 % and 2.21 % respectively. Indeed the difference is due to employing r_t [12] and r_d [16] correlations in obtaining Eq. (4.47) for $(\eta^*_{o,day}/\eta_{o,n})$.

4.5.3 Monthly Average Optical Efficiency: Validation of EMD Calculation

Monthly average optical efficiency, $(\bar{\eta}^*_o/\eta_{o,n})$, defined by Eq. (4.90) has been evaluated using Eq. (4.95) for I_T for $\phi = 20^o$, 40^o and 60^o, for all the twelve months, for $\bar{K}_T = 0.5$ and 0.7, for $0.2 \leq \bar{X}_c \leq 2.0$. $\bar{X}_c$ is the monthly average non-dimensional critical radiation level, defined by Eq. (4.85). Summation process according to Eq. (4.90) has been carried out for all days and all hours for which $I_T > I_c$. Values of daily clearness indices corresponding to $\bar{K}_T = 0.5$ and 0.7 have been obtained from Liu and Jordan [16] distribution as presented

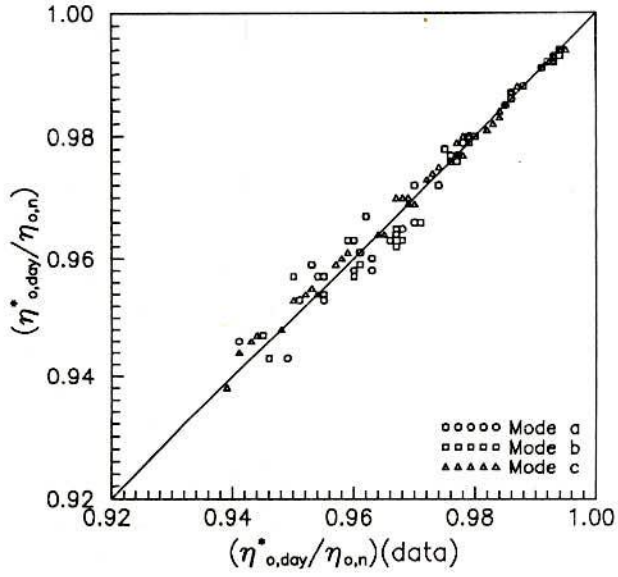

Figure 4.14: Validation of $(\eta^*_{o,day}/\eta_{o,n})$ against $(\eta^*_{o,day}/\eta_{o,n})$(data) for tracking modes **a**, **b** and **c** for Ahmedabad ($\phi = 23.07^o$); $-23.05^o \leq \delta \leq 23.09^o$, $0.2 \leq X_c \leq 0.8$

.

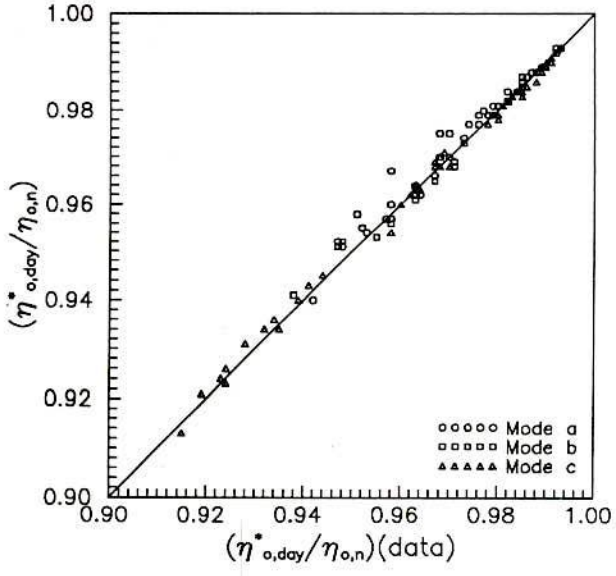

Figure 4.15: Validation of $(\eta^*_{o,day}/\eta_{o,n})$ against $(\eta^*_{o,day}/\eta_{o,n})$(data) for tracking mode **a**, **b** and **c** for New Delhi ($\phi = 28.58^o$); $-23.05^o \leq \delta \leq 23.09^o$, $0.2 \leq X_c \leq 0.8$

.

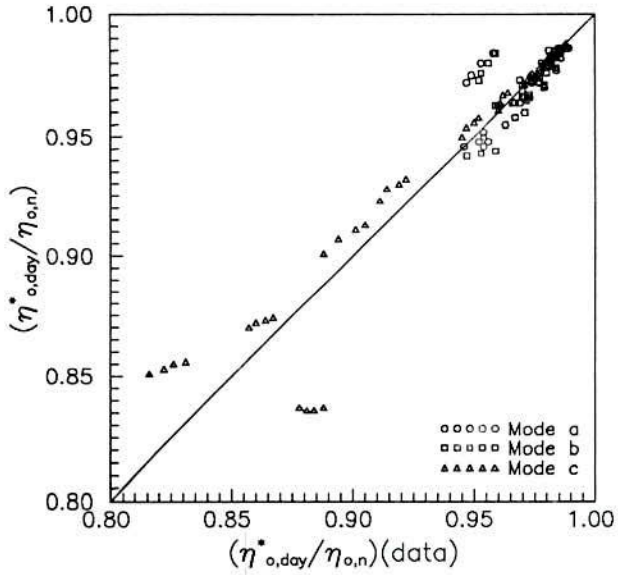

Figure 4.16: Validation of $(\eta^*_{o,day}/\eta_{o,n})$ against $(\eta^*_{o,day}/\eta_{o,n})$(data) for tracking modes **a**, **b** and **c** for Madison, WI ($\phi = 43.10^o$); $-23.05^o \leq \delta \leq 23.09^o$, $0.2 \leq X_c \leq 0.8$

in Table 3.1 of Chapter 3, §3.3.2. The values of $(\bar{\eta}^*_o/\eta_{o,n})$ so obtained are designated by $(\bar{\eta}^*_o/\eta_{o,n})$(num) which shall be compared with the values obtained using the expressions developed for single day given by Eq. (4.47) along with the primitives given in Table 4.3. Eq. (4.47) has been evaluated corresponding to $K_T = \bar{K}^*_T$ and $\delta = \delta_m$ and for I_c given by,

$$I_c = \bar{X}_c \, \bar{r}_{t,n} \, \bar{R}_n \, \bar{K}_T \, \bar{H}_o \tag{4.98}$$

Eq. (4.98) follows from Eq. (4.85). The value of $(\eta^*_{o,day}/\eta_{o,n})$ thus obtained for the equivalent mean day is designated as $(\bar{\eta}^*_{o,emd}/\eta_{o,n})$ which is the monthly average optical efficiency when validated against $(\bar{\eta}^*_o/\eta_{o,n})$(num) values.

Comparison for Tracking Modes a and b

Plots of $(\bar{\eta}^*_{o,emd}/\eta_{o,n})$ vs $(\bar{\eta}^*_o/\eta_{o,n})$(num) for the tracking modes **a** and **b** for the three latitudes, $\phi = 20^o$, 40^o and 60^o are shown in Figures 4.17 and 4.18 for $\bar{K}_T = 0.5$ and 0.7 respectively. The rms differences between $(\bar{\eta}^*_{o,emd}/\eta_{o,n})$ and $(\bar{\eta}^*_o/\eta_{o,n})$(num) are 0.4 % for $\bar{K}_T = 0.5$ and 0.3 % for $\bar{K}_T = 0.7$. Thus, the EMD calculation yields $(\bar{\eta}^*_o/\eta_{o,n})$ value very close to the value obtained by hour by hour numerical calculations.

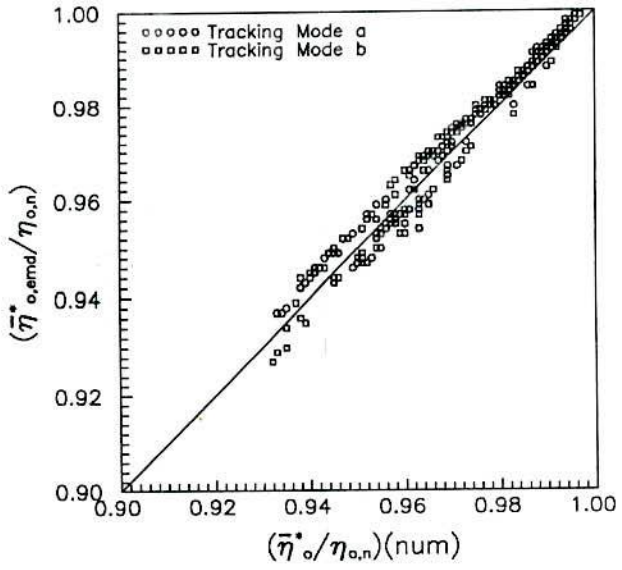

Figure 4.17: Validation of $(\bar{\eta}^*_{o,emd}/\eta_{o,n})$ against $(\bar{\eta}^*_{o}/\eta_{o,n})$(num) for tracking modes **a** and **b**, $\phi = 20^o$, 40^o and 60^o, $-23.05^o \leq \delta \leq 23.09^o$, $\bar{K}_T = 0.5$, $0.2 \leq \bar{X}_c \leq 2.0$

.

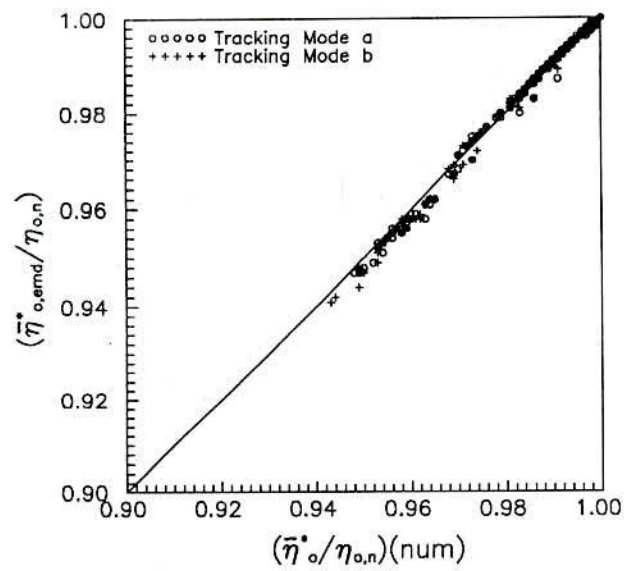

Figure 4.18: Validation of $(\bar{\eta}^*_{o,emd}/\eta_{o,n})$ against $(\bar{\eta}^*_{o}/\eta_{o,n})(num)$ for tracking modes **a** and **b**, $\phi = 20^o$, 40^o and 60^o, $-23.05^o \leq \delta \leq 23.09^o$, $\bar{K}_T = 0.7$, $0.2 \leq \bar{X}_c \leq 1.2$

.

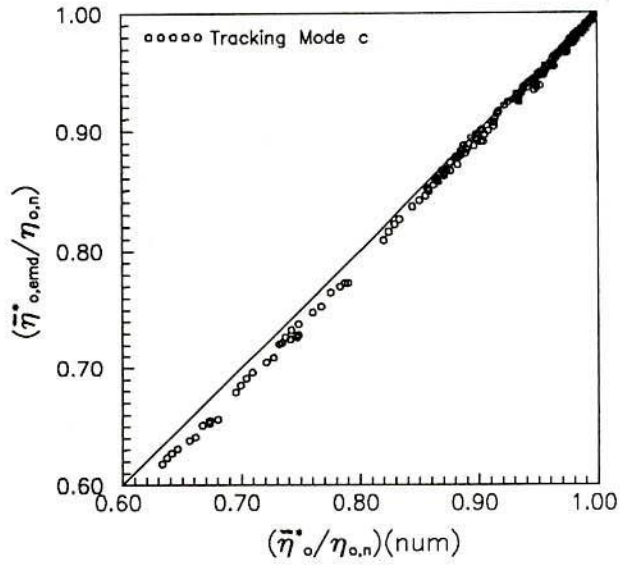

Figure 4.19: Validation of $(\bar{\eta}^*_{o,emd}/\eta_{o,n})$ against $(\bar{\eta}^*_o/\eta_{o,n})$(num) for tracking mode **c**, $\phi = 20^o$, 40^o and 60^o, $-23.05^o \leq \delta \leq 23.09^o$, $\bar{K}_T = 0.5$, $0.2 \leq \bar{X}_c \leq 2.0$

.

Comparison for Tracking Mode c

Plots of $(\bar{\eta}^*_{o,emd}/\eta_{o,n})$ vs $(\bar{\eta}^*_o/\eta_{o,n})$(num) for the tracking mode **c** for the three latitudes, $\phi = 20^o$, 40^o and 60^o are shown in Figures 4.19 and 4.20 for $\bar{K}_T = 0.5$ and 0.7 respectively. The rms differences between $(\bar{\eta}^*_{o,emd}/\eta_{o,n})$ and $(\bar{\eta}^*_o/\eta_{o,n})$(num) are 0.65 % for $\bar{K}_T = 0.5$ and 0.6 % for $\bar{K}_T = 0.7$. Slightly larger difference between $(\bar{\eta}^*_{o,emd}/\eta_{o,n})$ and $(\bar{\eta}^*_o/\eta_{o,n})$(num) for mode **c** compared to mode **a** and **b** are due to approximate calculation of $(\bar{\eta}_o/\eta_{o,n})$.

Comparison for Tracking Modes d and e

Similar plots of $(\bar{\eta}^*_{o,emd}/\eta_{o,n})$ vs $(\bar{\eta}^*_o/\eta_{o,n})$(num) for the tracking modes **d** and **e** for the three latitudes, $\phi = 20^o$, 40^o and 60^o are shown in Figures 4.21 and 4.22 for $\bar{K}_T = 0.5$ and 0.7 respectively. The rms differences between $(\bar{\eta}^*_{o,emd}/\eta_{o,n})$ and $(\bar{\eta}^*_o/\eta_{o,n})$(num) are 0.2 % for $\bar{K}_T = 0.5$ and 0.1 % for $\bar{K}_T = 0.7$. The plots shown in Figures 4.21 and 4.22 appear to display significant scatter due to the scale being large. 1 cm approximately corresponds to 0.005 in $(\bar{\eta}^*_{o,emd}/\eta_{o,n})$ or $(\bar{\eta}^*_o/\eta_{o,n})$(num).

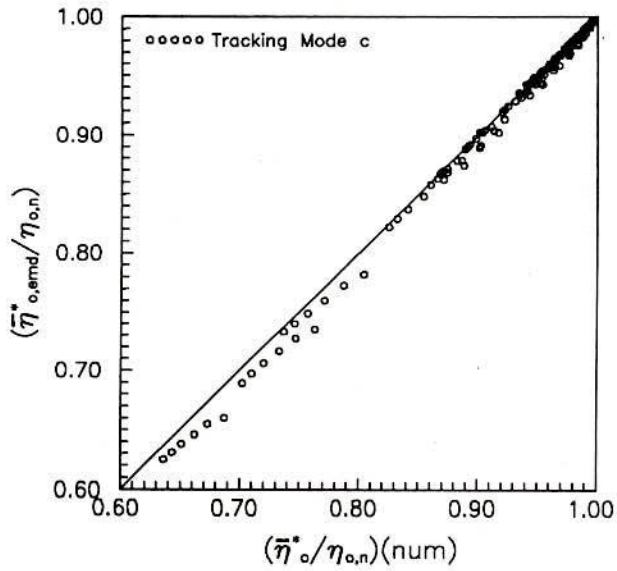

Figure 4.20: Validation of $(\eta^*_{o,emd}/\eta_{o,n})$ against $(\eta^*_o/\eta_{o,n})$(num) for tracking mode **c**, $\phi =$ 20°, 40° and 60°, $-23.05^o \leq \delta \leq 23.09^o$, $\bar{K}_T = 0.7$, $0.2 \leq \bar{X}_c \leq 1.2$

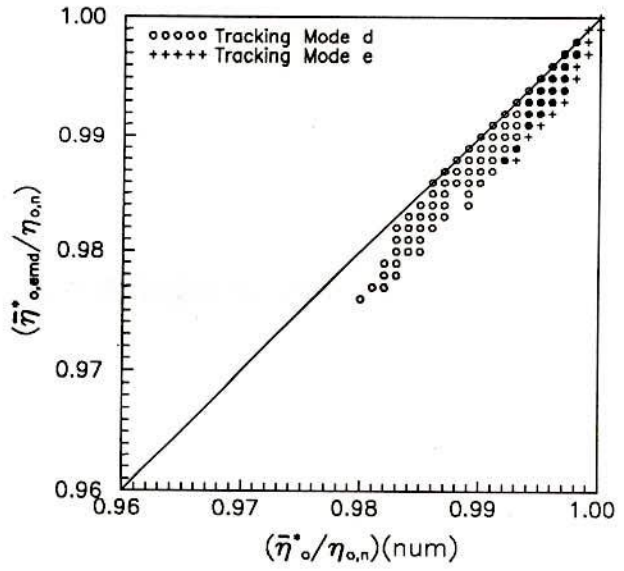

Figure 4.21: Validation of $(\bar{\eta}^*_{o,emd}/\eta_{o,n})$ against $(\bar{\eta}^*_o/\eta_{o,n})$(num) for tracking modes **d** and **e**, $\phi = 20^o$, 40° and 60°, $-23.05^o \leq \delta \leq 23.09^o$, $\bar{K}_T = 0.5$, $0.2 \leq \bar{X}_c \leq 2.0$

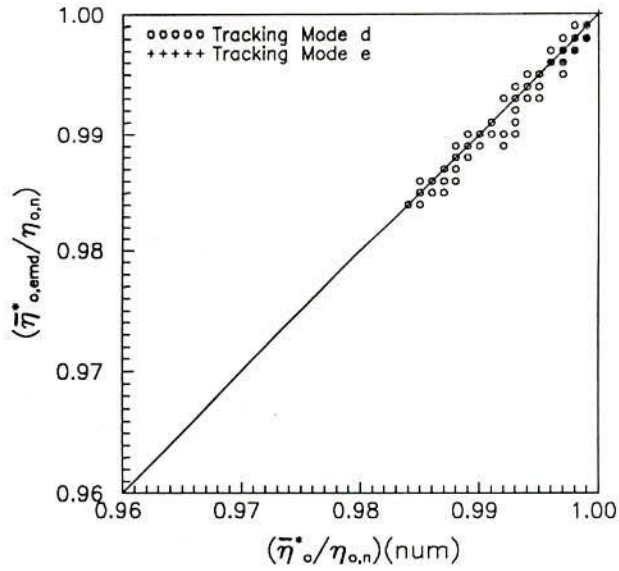

Figure 4.22: Validation of $(\bar{\eta}^*_{o,emd}/\eta_{o,n})$ against $(\bar{\eta}^*_o/\eta_{o,n})$(num) for tracking modes **d** and **e**, $\phi = 20^o$, 40^o and 60^o, $-23.05^o \leq \delta \leq 23.09^o$, $\bar{K}_T = 0.7$, $0.2 \leq \bar{X}_c \leq 1.2$

.

4.6 Conclusions

A method to calculate monthly average optical efficiency for parabolic trough concentrators, tracked in five principal modes, has been developed and validated. In order to be consistent with the definition of the monthly average daily utilizability, the monthly average optical efficiency has been defined as a weighted average of the instantaneous optical efficiency and the solar radiation above the critical level for all hours and days of the month. This some what tedious procedure to calculate the monthly average optical efficiency has been avoided by first obtaining a daily average optical efficiency defined as a weighted average of the instantaneous optical efficiency and the solar radiation above the critical level. Expressions for the daily optical efficiency have been obtained by integrating the defining equation, expressing the direct component of solar radiation in terms of r_t [12] and r_d [16] correlations. A convenient form of the instantaneous optical efficiency which fits the test data values, given in Gaul and Rabl [45], has been proposed. This representation has flexibility to describe instantaneous optical efficiency for other collectors by suitable choice of the constants. The single all-day average optical efficiency as defined by Gaul and Rabl [45] has been examined in detail. It has been shown that, indeed, even the single day optical efficiency depends on K_T and ϕ. Further, it has also been shown that it is desirable to define daily or monthly average daily optical efficiency for a given

critical level rather than a cut-off hour angle. It follows from this, though critical level and cut-off hour angle of Gaul and Rabl [45] can be related for a single day, to obtain monthly average value a single cut-off hour can not be associated for the given critical radiation level. Further, specifying a cut-off hour angle is misleading particularly when the solar radiation is bimodal, which is relevant for tracking mode **c**. Thus, single day approach is inadequate to obtain the monthly average value.

The single day optical efficiency value obtained using the equations developed in the present study have been compared with the values obtained using monthly average hourly solar radiation data. The rms difference is within 1 %.

Based on the expressions developed for the optical efficiency for a single day in the present study, it has been proposed and validated that the monthly average optical efficiency consistent with the definition of monthly average daily utilizability can be obtained by employing the expressions developed for the single day on the equavalent mean day (EMD). The monthly average optical efficiency values obtained using the equivalent mean day (EMD) approach agree with the hour by hour computations within a rms difference of less than 0.5 % when r_t and r_d correlations have been employed to generate hourly radiation values.

Chapter 5

Evaluation of Monthly Average Shading Factor for Surfaces Shaded by Overhangs under Terrestrial Conditions

5.1 Introduction

In estimating the monthly average daily solar radiation received by surfaces shaded by overhangs, the monthly average shading factor, $\bar{f}_i$, is a key parameter. As discussed in Chapter 1, §1.2.2, pp. 21-24, all the methods to estimate the monthly average shading factor yield values evaluated under extra-terrestrial conditions. Apart from Utzinger and Klein's [125] graphical presentation of the shading factors for south facing surfaces, attempts to provide algorithms [126, 128] to estimate $\bar{f}_i$ make use of the shading plane concept (applied under extra-terrestrial conditions only) which is valid for surfaces shaded by infinite overhangs. A method to obtain monthly average shading factor for surfaces shaded by finite overhangs, described in [128] is valid under extra-terrestrial conditions and for south facing surfaces only.

The objectives of the present chapter are as follows.

a) To examine the difference in the monthly average shading factor values evaluated under terrestrial and extra-terrestrial conditions.

b) Develop a method to estimate the monthly average shading factor under terrestrial conditions for receivers of arbitrary azimuthal angle and slope, shaded by infinite overhangs.

c) Develop methods to estimate the shading factor values for finite overhangs under terrestrial conditions for receivers with general azimuthal angle.

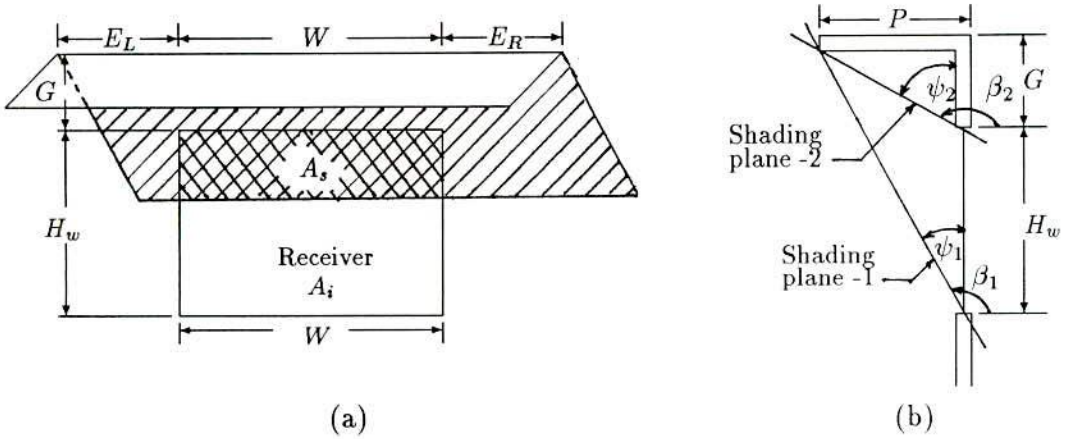

Figure 5.1: (a) Basic geometry of window shaded by overhang; (b) Resulting shading planes when gap is present.

5.2 Basic Geometry and Shading Factor

The basic geometry of a vertical shaded receiver (window) of height, H_w and width, W, is shown in Figure 5.1. The slope β, of the vertical receiver is equal to 90^o. Let the azimuthal angle of the receiver be γ. A horizontal overhang with projection P, extends by E_L and E_R to the left and to the right beyond the window width. The overhang is separated from the top of the receiver by a gap G. The non-dimensional width w, projection p, gap g and extensions e_L and e_R are obtained by referring the dimensional quantities to the height of the window. Thus,

$$w = \frac{W}{H_w}, \qquad p = \frac{P}{H_w}, \qquad g = \frac{G}{H_w} \qquad e_L = \frac{E_L}{H_w}, \qquad \text{and} \qquad e_R = \frac{E_R}{H_w} \tag{5.1}$$

If A_i is the irradiated area of the window and A_s is the shaded area of the window caused by the overhang, the shading factor at any instant, f_i, is given by,

$$f_i = \frac{A_i}{A_w} = 1 - \frac{A_s}{A_w} \tag{5.2}$$

where, A_w $(=WH_w)$ is the window area and $A_w = (A_i + A_s)$.

The solar radiation over a small period of time (say, 1-hr) per unit receiver area, I_s, according to Utzinger and Klein [125], is given by,

$$I_s = I_b R_b f_i + I_d \left(\frac{1}{2} - F_{r-o}\right) + \rho_1 I \left(\frac{1}{2} - \rho_2 F_{o-g} F_{r-o}\right) \tag{5.3}$$

where, ρ_1 and ρ_2 are the reflectivity of the ground and the underside of the overhang. F_{r-o} is the receiver radiation view factor of the overhang and F_{o-g} is the overhang view factor of the ground.

Summing Eq. (5.3) over all the hours and days in a month, the monthly average daily solar radiation per unit receiver area, $\bar{H}_s$, as given in Utzinger and Klein [125] can

be expressed as,

$$\bar{H}_s = \bar{H}_b \bar{R}_b \bar{f}_i + \bar{H}_d \left(\frac{1}{2} - F_{r-o}\right) + \rho_1 \bar{H} \left(\frac{1}{2} + \rho_2 F_{o-g} F_{r-o}\right) \tag{5.4}$$

where, $\bar{H}_b$, $\bar{H}_d$ and $\bar{H}$ are the monthly average daily direct, diffuse and global radiation on a horizontal surface of unit area. $\bar{R}_b$ is the monthly average daily tilt factor for direct radiation for the vertical receiver (window).

$\bar{f}_i$ and $\bar{R}_b$ in Eq. (5.4), strictly speaking, are to be evaluated as,

$$\bar{R}_b = \sum_{days} \sum_{hours} I_b R_b \Big/ \sum_{days} \sum_{hours} I_b \tag{5.5}$$

$$\bar{f}_i = \sum_{days} \sum_{hours} I_b R_b f_i \Big/ \sum_{days} \sum_{hours} I_b R_b \tag{5.6}$$

Utzinger and Klein [125] employed Eq. (5.4) but simplified Eqs. (5.5) and (5.6) by evaluating $\bar{R}_b$ and $\bar{f}_i$ on the monthly mean day. Thus, $\bar{R}_b$ and $\bar{f}_i$ are obtained from,

$$\bar{R}_b = \sum_{\overline{day}} I_b R_b \Big/ \sum_{\overline{day}} I_b = \int_{\overline{day}} I_b R_b \, dt \Big/ \int_{\overline{day}} I_b \, dt \tag{5.7}$$

$$\bar{f}_i = \sum_{\overline{day}} I_b R_b f_i \Big/ \sum_{\overline{day}} I_b R_b = \int_{\overline{day}} I_b R_b f_i \, dt \Big/ \int_{\overline{day}} I_b R_b \, dt \tag{5.8}$$

In Eqs. (5.7) and (5.8), $\overline{day}$ refers to summation or integration over the hours on the monthly mean day. Noting $dt = d\omega/(\pi/12)$, where ω is in radians, integral expressions in Eqs. (5.7) and (5.8) can be re-written as,

$$\bar{R}_b = \frac{\int_{\omega_{sr}}^{\omega_{ss}} I_b R_b \, d\omega}{\int_{-\omega_s}^{\omega_s} I_b \, d\omega} \tag{5.9}$$

$$\bar{f}_i = \frac{\int_{\omega_{sr}}^{\omega_{ss}} I_b R_b f_i \, d\omega}{\int_{\omega_{sr}}^{\omega_{ss}} I_b R_b \, d\omega} \tag{5.10}$$

where, ω_{sr} and ω_{ss} are the apparent sunrise and sunset hour angles for the receiver and ω_s is the sunset hour angle. Determining ω_{sr} and ω_{ss} for surfaces of general orientation unambiguously has been described in Appendix B of the present study.

Utzinger and Klein further simplified Eq. (5.10) by evaluating $\bar{f}_i$ under extra-terrestrial conditions i.e., by replacing I_b with I_o. This value designated as $\bar{f}_{io}$ in the present study is given by,

$$\bar{f}_{io} = \frac{\int_{\omega_{sr}}^{\omega_{ss}} I_o R_b f_i \, d\omega}{\int_{\omega_{sr}}^{\omega_{ss}} I_o R_b \, d\omega} \tag{5.11}$$

5.3 Conditions for Validity of Extra-terrestrial Calculation

Noting that $I_b = (I - I_d)$, I_b can be written as,

$$I_b = I\left(1 - \frac{I_d}{I}\right) = k_T I_o \left(1 - \frac{I_d}{I}\right) \tag{5.12}$$

where, k_T is the hourly clearness index.

Using Eq. (5.12) in Eq. (5.10), $\bar{f}_i$ can be expressed as,

$$\bar{f}_i = \frac{\int_{\omega_{sr}}^{\omega_{ss}} k_T I_o (1 - I_d/I) R_b f_i \, d\omega}{\int_{\omega_{sr}}^{\omega_{ss}} k_T I_o (1 - I_d/I) R_b \, d\omega} \tag{5.13}$$

Considering (I_d/I) to be a function of hourly clearness index, k_T only, Eq. (5.13) can be rewritten as,

$$\bar{f}_i = \frac{\int_{\omega_{sr}}^{\omega_{ss}} f(k_T) I_o R_b f_i \, d\omega}{\int_{\omega_{sr}}^{\omega_{ss}} f(k_T) I_o R_b \, d\omega} \tag{5.14}$$

If atmospheric transmittance or daily clearness index, $K_T = 1.0$, the hourly clearness index, k_T, also is unity throughout the day and $(I_d/I) = 0$, yielding $f(k_T) = 1.0$. Thereby, $\bar{f}_i$ from Eq. (5.14) reduces to,

$$\bar{f}_i = \frac{\int_{\omega_{sr}}^{\omega_{ss}} I_o R_b f_i \, d\omega}{\int_{\omega_{sr}}^{\omega_{ss}} I_o R_b \, d\omega} = \bar{f}_{io} \tag{5.15}$$

Thus, extra-terrestrial values and terrestrial values of the shading factor are identical when atmospheric transmittance is unity which can be expected. However, even if k_T remains constant throughout the day, Eq. (5.14) reduces to Eq. (5.15). Thus, shading factor calculation under extra-terrestrial condition is exact, not only when $K_T = 1.0$, but also when k_T is constant throughout the day, not necessarily equal to unity. In general, $\bar{f}_i$ and $\bar{f}_{io}$ values can be expected to differ since $K_T \neq 1.0$ and k_T is not uniform throughout the day.

5.4 Monthly Average Shading Factor for Receivers Shaded by Infinite Overhangs under Terrestrial Conditions

5.4.1 Infinite Overhang without Gap between Overhang and Window

From Sun's [114] algorithm, when the overhang extends to infinity on both sides of the receiver and the gap between the top of the receiver and the overhang base is zero (later

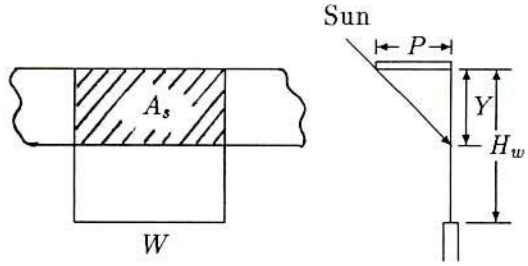

Figure 5.2: Shading of window caused by infinite overhang

in §5.4.2, the methodology has been generalized to include the gap between the receiver top and the overhang base), referring to Figure 5.2, the instantaneous shaded area, A_s is given by,

$$A_s = Y\,W \tag{5.16}$$

The projection of the shadow over the window, Y is related to the zenith angle, θ_z, the solar azimuth angle, γ_s and the surface azimuth angle, γ from [114] by,

$$Y = \frac{P}{\tan\theta_z \cos(\gamma_s - \gamma)} = \frac{P\cos\theta_z}{\sin\theta_z \cos(\gamma_s - \gamma)} \tag{5.17}$$

The the angle of incidence, θ, for a vertical surface of azimuthal angle γ from [6] is given by,

$$\cos\theta = \sin\theta_z \cos(\gamma_s - \gamma) \tag{5.18}$$

Using Eq. (5.18) in Eq. (5.17), the instantaneous shaded area A_s given by Eq. (5.16) can be expressed as,

$$A_s = \frac{P\,W\,\cos\theta_z}{\cos\theta} \tag{5.19}$$

Using Eq. (5.19) in Eq. (5.2) and noting that $A_w = H_w W$, the instantaneous shading factor f_i can be expressed as,

$$f_i = 1 - \frac{P\cos\theta_z}{H_w\cos\theta} = 1 - \tan\psi/R_b \tag{5.20}$$

where, ψ is the angle between the vertical and an imaginary plane passing through the outer edge of the overhang and the window base; R_b (=$\cos\theta/\cos\theta_z$) is the instantaneous tilt factor.

Using Eq. (5.20) for f_i, in Eq. (5.10), the monthly average shading factor, $\bar{f}_i$ for infinite overhangs designated as, $\bar{f}_{i\infty}$ for clarity can be expressed by,

$$\bar{f}_{i\infty} = \frac{\int_{\omega_{sr}}^{\omega_{ss}} I_b R_b \left[1 - \frac{\tan\psi}{R_b}\right] d\omega}{\int_{\omega_{sr}}^{\omega_{ss}} I_b R_b\, d\omega} = \frac{\int_{\omega_{sr}}^{\omega_{ss}} I_b \left[R_b - \tan\psi\right] d\omega}{\int_{\omega_{sr}}^{\omega_{ss}} I_b R_b\, d\omega} \tag{5.21}$$

Consider the integrand in the numerator of Eq. (5.21). Using Eq. (2.3) for R_b along with Eq. (2.4) for $\cos\theta$ and Eq. (2.8) for $\cos\theta_z$, the integrand of the numerator of Eq. (5.21) can be written as,

$$\begin{aligned} I_b R_b f_i &= I_b\,[R_b - \tan\psi] \\ &= I_b\left[\frac{A + B\cos\omega + C\sin\omega}{\cos\phi\cos\delta\cos\omega + \sin\phi\sin\delta} - \frac{\sin\psi}{\cos\psi}\right] \end{aligned} \tag{5.22}$$

Using Eqs. (2.5) to (2.7) for A, B and C and noting $\beta = \pi/2$, for the vertical receiver, after some what tedious but straight forward algebra, Eq. (5.22) simplifies to,

$$I_b\,[R_b - \tan\psi] = \left(\frac{I_b}{\cos\psi}\right)\left[\frac{A^* + B^*\cos\omega + C^*\sin\omega}{\cos\phi\cos\delta\cos\omega + \sin\phi\sin\delta}\right] \tag{5.23}$$

where, the constants A^*, B^* and C^* in Eq. (5.23) are given by,

$$A^* = \sin\delta(\sin\phi\cos\beta^* - \cos\phi\sin\beta^*\cos\gamma) \tag{5.24}$$

$$B^* = \cos\delta(\cos\phi\cos\beta^* + \sin\phi\sin\beta^*\cos\gamma) \tag{5.25}$$

$$C^* = \cos\delta\sin\beta^*\sin\gamma \tag{5.26}$$

β^* in Eqs. (5.24) to (5.26) is given by,

$$\beta^* = (\beta + \psi) \tag{5.27}$$

Comparing Eqs. (5.24), (5.25) and (5.26) for A^*, B^* and C^* with Eqs. (2.5), (2.6) and (2.7) for A, B and C, it can be readily noted that, A^*, B^* and C^* are nothing but the constants in the equation for $\cos\theta$ for a surface with slope $\beta^* = (\beta + \psi)$.

Thus, Eq. (5.23) takes the form,

$$I_b\,[R_b - \tan\psi] = \left(\frac{I_b}{\cos\psi}\right)\frac{\cos\theta^*}{\cos\theta_z} = \left(\frac{I_b}{\cos\psi}\right) R_b^* \tag{5.28}$$

where, θ^* is the angle of incidence for the imaginary plane joining the outer edge of the overhang to the base of the receiver (window) which has a slope of β^*. It may be noted that R_b^* is nothing but the instantaneous tilt factor for direct radiation of this imaginary plane which has been referred to as shading plane by Jones (1980).

Let ω_{sr}^* and ω_{ss}^* be the apparent sunrise and sunset hour angles for the shading plane. By noting that $|\omega_{sr}^*| \leq |\omega_{sr}|$ and $|\omega_{ss}^*| \leq |\omega_{ss}|$ and either I_b or R_b^* becomes zero for $|\omega| > |\omega_{sr}^*|$ and $|\omega| > |\omega_{ss}^*|$, it is sufficient to integrate the numerator of Eq. (5.21) between the limits ω_{sr}^* to ω_{ss}^*.

Using Eq. (5.28) in Eq. (5.21), the monthly average shading factor for infinite overhang is given by,

$$\bar{f}_{i\infty} = \left(\frac{1}{\cos\psi}\right) \frac{\int_{\omega_{sr}^*}^{\omega_{ss}^*} I_b R_b^* \, d\omega}{\int_{\omega_{sr}}^{\omega_{ss}} I_b R_b \, d\omega} \tag{5.29}$$

$\cos\psi$ in Eq. (5.29), related to the window geometry can be expressed as,

$$\cos\psi = \frac{H_w}{\sqrt{P^2 + H_w^2}} = \frac{W H_w}{W\sqrt{P^2 + H_w^2}} = \frac{A_w}{A_{shp}} \tag{5.30}$$

where, A_{shp} is the area of the shading plane.

Thus, Eq. (5.29) takes the form,

$$\bar{f}_{i\infty} = \left(\frac{A_{shp}}{A_w}\right) \frac{\int_{\omega_{sr}^*}^{\omega_{ss}^*} I_b R_b^* \, d\omega}{\int_{\omega_{sr}}^{\omega_{ss}} I_b R_b \, d\omega} \tag{5.31}$$

Recalling that the monthly average tilt factors for direct radiation, $\bar{R}_b$, and $\bar{R}_b^*$ for the receiver and the shading plane can be expressed by,

$$\bar{R}_b = \frac{\int_{\omega_{sr}}^{\omega_{ss}} I_b R_b \, d\omega}{\int_{-\omega_s}^{\omega_s} I_b \, d\omega} \tag{5.32}$$

$$\bar{R}_b^* = \frac{\int_{\omega_{sr}^*}^{\omega_{ss}^*} I_b R_b^* \, d\omega}{\int_{-\omega_s}^{\omega_s} I_b \, d\omega} \tag{5.33}$$

Eq. (5.31) now takes the form,

$$\bar{f}_{i\infty} = \left(\frac{A_{shp}}{A_w}\right) \frac{\bar{R}_b^*}{\bar{R}_b} \tag{5.34}$$

Eq. (5.34) is the same as the algorithm given by Jones [126] and Yanda and Jones [128]. However, $\bar{f}_{i\infty}$ values differ depending upon the manner in which $\bar{R}_b^*$ and $\bar{R}_b$ are evaluated. If Eqs. (5.32) and (5.33) are used, employing solar radiation data or r_t [12] and r_d [16] correlations for I_b, $\bar{R}_b^*$ and $\bar{R}_b$ are the values for the monthly average daily tilt factor under terrestrial conditions. When I_b is replaced by I_o in Eqs. (5.32) and (5.33) (approach of Liu and Jordan [16] and Klein [65]), the tilt factors are the extra-terrestrial values which have been employed by Jones [126] and Yanda and Jones [128]. Designating the monthly average shading factor for the infinite overhang obtained under extra-terrestrial conditions by $\bar{f}_{io\infty}$, $\bar{f}_{io\infty}$ can be expressed as,

$$\bar{f}_{io\infty} = \left(\frac{A_{shp}}{A_w}\right) \frac{\bar{R}_{bo}^*}{\bar{R}_{bo}} \tag{5.35}$$

$\bar{R}^*_{bo}$ and $\bar{R}_{bo}$ are the monthly average daily tilt factors for direct radiation for the shading plane and the receiver under extra-terrestrial conditions.

In the present investigation, $\bar{f}_{i\infty}$ has been evaluated using Eq. (5.34) along with Eqs. (5.32) and (5.33) for $\bar{R}^*_b$ and $\bar{R}_b$ employing r_t [12] and r_d [16] correlations to express I_b. This approach has been followed by Klein and Theilacker [66] to evaluate the monthly average tilt factor under terrestrial conditions. Lahiri [67] later generalized the algorithm to include asymmetry in the solar radiation distribution employing modified correlations for r_t and r_d [15]. For the sake of completeness, compact expression for $\bar{R}_b$ valid under terrestrial condition available in Lahiri [67] is reproduced below,

$$\bar{R}_b = \frac{\bar{R}_{bo} + b\,C_1\,I_2/(a - \bar{D}_f)}{1 + b\,C_2/(a - \bar{D}_f)} \tag{5.36}$$

where, $\bar{R}_{bo}$[1] is obtained from,

$$\bar{R}_{bo} = C_1 I_1 \tag{5.37}$$

In Eqs. (5.36) and (5.37), the constants C_1 and C_2 are given by,

$$C_1 = \frac{1}{2\,B'(\sin\omega_s - \omega_s\cos\omega_s)} \tag{5.38}$$

$$C_2 = \frac{(\omega_s/2 - \sin\,2\omega_s/4)}{(\sin\omega_s - \omega_s\cos\omega_s)} \tag{5.39}$$

The integrals I_1 and I_2 in Eqs. (5.36) and (5.37) are the definite integrals defined by,

$$I_1 = \int_{\omega_{sr}}^{\omega_{ss}} \cos\theta\,d\omega \tag{5.40}$$

$$I_2 = \int_{\omega_{sr}}^{\omega_{ss}} \cos\theta\cos\omega\,d\omega \tag{5.41}$$

Expressions for I_1 and I_2 can be derived easily and are available in Lahiri [67] which are reproduced here. I_1 and I_2 are given by,

$$\begin{aligned} I_1 &= I_{P1}(\omega_{ss}) - I_{P1}(\omega_{sr}) && \text{if } \omega_{sr} < \omega_{ss} \\ I_1 &= I_{P1}(\omega_{ss}) - I_{P1}(-\omega_s) + I_{P1}(\omega_s) - I_{P1}(\omega_{sr}) && \text{if } \omega_{sr} > \omega_{ss} \end{aligned} \tag{5.42}$$

$$\begin{aligned} I_2 &= I_{P2}(\omega_{ss}) - I_{P2}(\omega_{sr}) && \text{if } \omega_{sr} < \omega_{ss} \\ I_2 &= I_{P2}(\omega_{ss}) - I_{P2}(-\omega_s) + I_{P2}(\omega_s) - I_{P2}(\omega_{sr}) && \text{if } \omega_{sr} > \omega_{ss} \end{aligned} \tag{5.43}$$

[1] $\bar{R}_{bo}$ is the monthly average daily tilt factor for direct radiation under extra-terrestrial conditions defined by,

$$\bar{R}_{bo} = \int I_o R_b\,d\omega \Big/ \int I_o\,d\omega \tag{F5.1}$$

which on simplification becomes,

$$\bar{R}_{bo} = \int \cos\theta\,d\omega \Big/ \int \cos\theta_z\,d\omega \tag{F5.2}$$

Expressions given in Liu and Jordan [16] and Klein [65] are the result of evaluating Eq. (F5.2).

where, the primitives $I_{P1}(\omega)$ and $I_{P2}(\omega)$ are given by,

$$I_{P1}(\omega) = A\omega + B\sin\omega - C\cos\omega \tag{5.44}$$

$$I_{P2}(\omega) = A\sin\omega + B\left(\frac{\omega}{2} + \frac{\sin 2\omega}{4}\right) - C\frac{\cos 2\omega}{4} \tag{5.45}$$

It may be noted that I_1 and I_2 evaluated from Eqs. (5.42) and (5.43) can account for double sunshine period also, which may occur, particularly for the shading plane.

Eq. (5.36) can be used to evaluate $\bar{R}_b^*$ by replacing β with β^* in evaluating A^*, B^* and C^* in place of A, B and C appearing in the primitives $I_{P1}(\omega)$ and $I_{P2}(\omega)$ given by Eqs. (5.44) and (5.45).

5.4.2 Infinite Overhang with Gap between Overhang and Window

When a gap exists between the overhang and the window as described in Figure 5.1, the solar radiation reaching the receiver, following Yanda and Jones [128], is the difference between the solar radiation falling on the shading plane-1 of slope $\beta_1^* = (90^o + \psi_1)$ and the shading plane-2 with slope $\beta_2^* = (90^o + \psi_2)$. Shading factor for the receiver, when the overhang is infinite and a gap exists, under terrestrial and extra-terrestrial conditions can be expressed by,

$$\bar{f}_{i\infty} = \left(\frac{1}{\cos\psi_1}\right)\frac{\bar{R}_{b1}^*}{\bar{R}_b} - \left(\frac{1}{\cos\psi_2}\right)\frac{\bar{R}_{b2}^*}{\bar{R}_b} \tag{5.46}$$

$$\bar{f}_{io\infty} = \left(\frac{1}{\cos\psi_1}\right)\frac{\bar{R}_{bo1}^*}{\bar{R}_{bo}} - \left(\frac{1}{\cos\psi_2}\right)\frac{\bar{R}_{bo2}^*}{\bar{R}_{bo}} \tag{5.47}$$

In Eqs. (5.46) and (5.47), ψ_1 and ψ_2 characterizing the two imaginary planes are related to the receiver-overhang geometry by,

$$\cos\psi_1 = \left[1 + \left(\frac{P}{H_w + G}\right)^2\right]^{-1/2} \tag{5.48}$$

$$\cos\psi_2 = \left[1 + \left(\frac{P}{G}\right)^2\right]^{-1/2} \tag{5.49}$$

5.4.3 Infinite Overhangs for Non-vertical Receivers

When the receiver is non-vertical as shown in Figure 5.3, let the slope be β and the height measured along the receiver be H'. P' is the overhang projection. Let the vertical from the base of the receiver intersect the overhang at a point I. The vertical distance from the base of the receiver to the overhang is now (i.e. OI) H_w. The projection beyond I is P.

For both the actual receiver represented by the line OR and an imaginary vertical receiver represented by OI, OS represents the shading plane. Thus, the radiation received

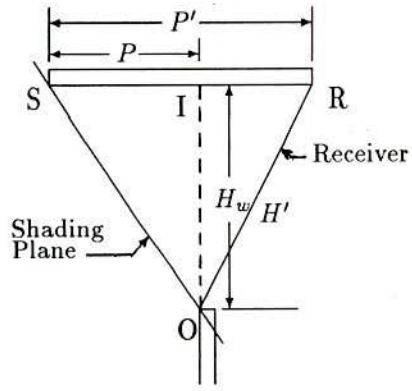

Figure 5.3: Non-vertical receiver and an infinite overhang

by the non-vertical receiver of slope β and projection P' is the same as the radiation received by the imaginary vertical receiver OI of projection P. H_w and P are related to H', P' and β by,

$$H_w = H' \cos(90^o - \beta) \tag{5.50}$$

$$P = P' - H' \sin(90^o - \beta) \tag{5.51}$$

Equating the direct radiation received by the shading plane, imaginary vertical receiver and the actual receiver over the mean day of the month, it follows,

$$H'_{sb}\, A'_w = H_{sb}\, A_w = A_{shp}\, \bar{H}_b \bar{R}^*_b \tag{5.52}$$

where, H'_{sb} and H_{sb} are the direct radiation on the actual receiver and the imaginary vertical receiver per unit receiver area respectively. A'_w is the area of the actual receiver.

Expressing in terms of the shading factor and the monthly average daily direct radiation on a horizontal surface of unit area, Eq. (5.52) can be re-written as,

$$\bar{H}_b \bar{R}'_b \bar{f}'_{i\infty} A'_w = \bar{H}_b \bar{R}_b \bar{f}_{i\infty} A_w = A_{shp} \bar{H}_b \bar{R}^*_b \tag{5.53}$$

where, $\bar{R}'_b$, $\bar{R}_b$ and $\bar{R}^*_b$ are the monthly average daily tilt factor for direct radiation for the actual receiver, the imaginary vertical receiver and the shading plane respectively. $\bar{f}'_{i\infty}$ and $\bar{f}_{i\infty}$ are respectively the shading factors for the actual receiver and the imaginary vertical receiver.

From Eq. (5.53),

$$\bar{f}'_{i\infty} = \left(\frac{A_{shp}}{A'_w}\right) \frac{\bar{R}^*_b}{\bar{R}'_b} = \left(\frac{A_{shp}}{A_w}\right) \frac{\bar{R}^*_b}{\bar{R}_b} \left[\frac{A_w}{A'_w} \frac{\bar{R}_b}{\bar{R}'_b}\right]$$

$$= \bar{f}_{i\infty}|_{\beta=90} \left(\frac{H_w}{H'} \frac{\bar{R}_b}{\bar{R}'_b} \right) \tag{5.54}$$

where, $\bar{f}_{i\infty}|_{\beta=90}$ indicates the shading factor for the imaginary vertical receiver. It may be noted that $\bar{f}_{i\infty}|_{\beta=90}$ can be evaluated by Eq. (5.34) along with Eqs. (5.30), (5.32) and (5.33) given in the preceding section §5.4.1.

By evaluating $\bar{f}_{i\infty}$ as an integral from the definitions of the instantaneous shading factor and tilt factor, equivalence of the formulation with the shading plane concept of Jones [126] has been established. The methodology allowed generalization for non-vertical receivers which has not been reported in the literature. By obtaining the monthly average shading factors for receivers shaded by infinite overhangs, it has been shown that $\bar{f}_{i\infty}$ under terrestrial conditions is a function of the diffuse fraction. The influence of the diffuse fraction can be assessed by examining the difference between $\bar{f}_{io\infty}$ and $\bar{f}_{i\infty}$ given by Eqs. (5.34) and (5.35) when there is no gap and Eqs. (5.46) and (5.47) when there is a gap between the overhang and the window and Eq.(5.54) when the receiver is non-vertical.

Numerical values for $\bar{f}_{i\infty}$ and $\bar{f}_{io\infty}$, obtained for different projections, latitudes, azimuthal angles and months for $0.0 \leq \bar{D}_f \leq 0.8$, have been discussed in the section on Results and Discussion §5.7.

5.5 Monthly Average Shading Factor for Finite Overhangs under Terrestrial Conditions

5.5.1 An Outline of the Approach

Monthly average shading factor for finite overhangs, in addition to the parameters which determine $\bar{f}_{i\infty}$, depends also on the value of e characterizing the finite extensions. Analytical treatment for finite overhangs similar to the one described for infinite overhangs in §5.4 is difficult since the shaded area, A_s does not remain rectangular throughout the day. Depending on the latitude, declination, slope of the receiver and the azimuthal angle, even if it is possible to characterize the shadow area, a priori, the integral in the numerator of Eq. (5.10), if integrable, needs to be evaluated piece-wise. In order to alleviate this difficulty to obtain the monthly average shading factor under terrestrial conditions for finite overhangs, the approach followed in the present study envisages that $\bar{f}_{i\infty}$ contains the information about the geometric parameters and the diffuse fraction. Thus, it can be expected that the shading factor for finite overhangs be related to the infinite values dominantly as a function of the extension only. Also, the difference between the shading factor values for finite and infinite overhangs vanishes (practically) for finitely large extensions, say $e > 0.8$.

5.5.2 Shading Factor for Finite Overhangs for South Facing Receivers

Relation between Monthly Average Shading Factor Values for Finite and Infinite Overhangs

When the shading factor values for finite overhangs are related to the infinite overhang values, finite overhang values also display dependence on diffuse fraction, since $\bar{f}_{i\infty}$ depends on the diffuse fraction as it has already been shown. Assuming the changes in $\bar{f}_{i\infty}$ and $\bar{f}_i$ values due to diffuse fraction to be similar, relations between finite and infinite monthly average shading factor values have been developed for $\bar{D}_f = 0.4$. The relations thus developed shall be validated for other diffuse fraction values in the section on Results and Discussion, §5.7. Based on the numerical results for $w = 1.0$, $\bar{D}_f = 0.4$, $\phi = 25^o$, 30^o, 40^o, 50^o and 60^o, declinations corresponding to all the 12 months, $e = 0.0$, 0.2, 0.4, 0.6 and 0.8 and $p = 0.2$, 0.3, 0.4 and 0.5 relations between $\bar{f}_i$ and $\bar{f}_{i\infty}$ have been developed. $\bar{f}_{i\infty}$ values have been calculated using Eq. (5.34) and $\bar{f}_i$ values have been obtained by numerical integration employing Eq. (5.8).

Plots of $\bar{f}_i$ vs $\bar{f}_{i\infty}$ are shown in Figures 5.4(a), 5.4(b) and 5.4(c) for $e = 0.0$, 0.4 and 0.8 respectively for $p = 0.2$ and in Figures 5.4(d), 5.4(e) and 5.4(f) for $p = 0.4$. From Figures 5.4(a) to 5.4(f), when $\bar{f}_{i\infty} > 0.0$, $\bar{f}_i$ can be related to $\bar{f}_{i\infty}$ by an equation of the form,

$$\bar{f}_i = M + N\,\bar{f}_{i\infty} \tag{5.55}$$

where, M and N are constants which depend, in general, on the extension e and the projection p.

If, according to Eq. (5.55), $\bar{f}_i < \bar{f}_{i\infty}$, $\bar{f}_i$ is to be evaluated as,

$$\bar{f}_i = \bar{f}_{i\infty} \tag{5.56}$$

It is interesting to note that $\bar{f}_i$ and $\bar{f}_{i\infty}$ values are linearly related (within a small difference) as shown in Figures 5.4(a) to 5.4(f). Each of Figures 5.4(a) to 5.4(f) include all latitudes and declinations. Dependence on latitude and declination is contained in $\bar{f}_{i\infty}$.

Best fit values for the constants M and N have been determined for $e = 0.0$, 0.2, 0.4, 0.6 and 0.8, and $p = 0.2$, 0.3, 0.4 and 0.5 and are given in Table 5.1. Thus, $\bar{f}_i$ values, using Eqs. (5.55) and (5.56) along with the values of the constants M and N given in Table 5.1 for different projections and extensions, can be estimated from $\bar{f}_{i\infty}$ which can be calculated from simple expressions.

Attempts to correlate M and N with p and e have not been successful. It may be noted that M and N are monotonically related to e but M and N vary some what

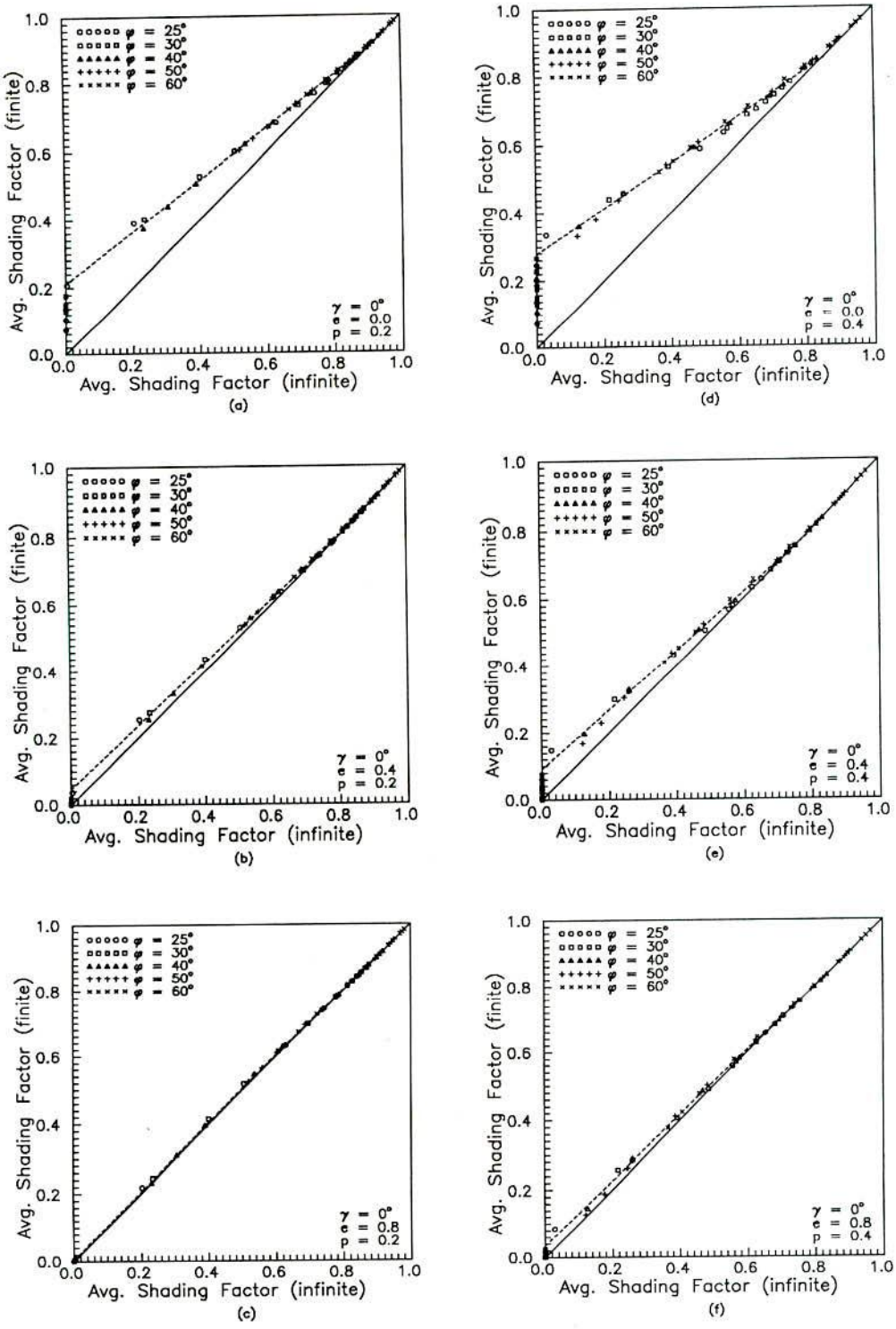

Figure 5.4: Relation between $\bar{f}_i$ and $\bar{f}_{i\infty}$ values for different overhang projections and extensions (a) $p = 0.2$, $e = 0.0$; (b) $p = 0.2$, $e = 0.4$; (c) $p = 0.2$, $e = 0.8$; (d) $p = 0.4$, $e = 0.0$, (e) $p = 0.4$, $e = 0.4$ and (f) $p = 0.4$, $e = 0.8$

Table 5.1: Values of the constants M and N in Eq. (5.55) to estimate $\bar{f}_i$ from $\bar{f}_{i\infty}$ (when $\bar{f}_{i\infty} > 0.0$)

p	Constants	Overhang Extension, e				
		0.00	0.20	0.40	0.60	0.80
0.2	M	0.210	0.097	0.046	0.021	0.005
	N	0.766	0.887	0.948	0.978	0.997
0.3	M	0.232	0.114	0.058	0.031	0.017
	N	0.740	0.863	0.932	0.964	0.981
0.4	M	0.277	0.155	0.092	0.056	0.035
	N	0.671	0.800	0.879	0.923	0.953
0.5	M	0.290	0.165	0.098	0.059	0.036
	N	0.655	0.784	0.866	0.918	0.950

irregularly with p. Also, the variation in M and N with p is small. A plot of $\bar{f}_i$ vs $\bar{f}_{i\infty}$ for all projections for $e = 0.0$, 0.2, 0.4 and 0.6 are shown in Figures 5.5(a) to 5.5(d). At some penalty of accuracy, $\bar{f}_i$ can be related to $\bar{f}_{i\infty}$ independent of p by,

$$\bar{f}_i = M_p + N_p \bar{f}_{i\infty} \tag{5.57}$$

Best fit values for M_p and N_p for different extensions are given in Table 5.2. M_p and N_p given in Table 5.2 are correlated to e by,

$$M_p = 0.258\, exp^{-2.90\, e} \tag{5.58}$$

$$N_p = 0.703 + 0.627\, e - 0.377\, e^2 \tag{5.59}$$

Using Eqs. (5.58) and (5.59) in Eq. (5.57), $\bar{f}_i$ is related to $\bar{f}_{i\infty}$ through a single equation by,

$$\bar{f}_i = 0.258\, exp^{-2.90\, e} + [0.703 + 0.627\, e - 0.377\, e^2]\, \bar{f}_{i\infty} \tag{5.60}$$

The relative accuracies in predicting $\bar{f}_i$ from $\bar{f}_{i\infty}$ using Eq. (5.55) along with the different constants for different extensions and projections vis-a-vis the single equation given by Eq. (5.60) will be discussed in the section on Results and Discussion §5.7.

$\bar{f}_i$ Values when $\bar{f}_{i\infty} = 0.0$

It can be noticed from Figures 5.4(a) to 5.4(f) that $\bar{f}_i$ values are non-zero, when $\bar{f}_{i\infty} = 0.0$ and differ depending on the latitude and declination. Non-zero $\bar{f}_i$ values corresponding

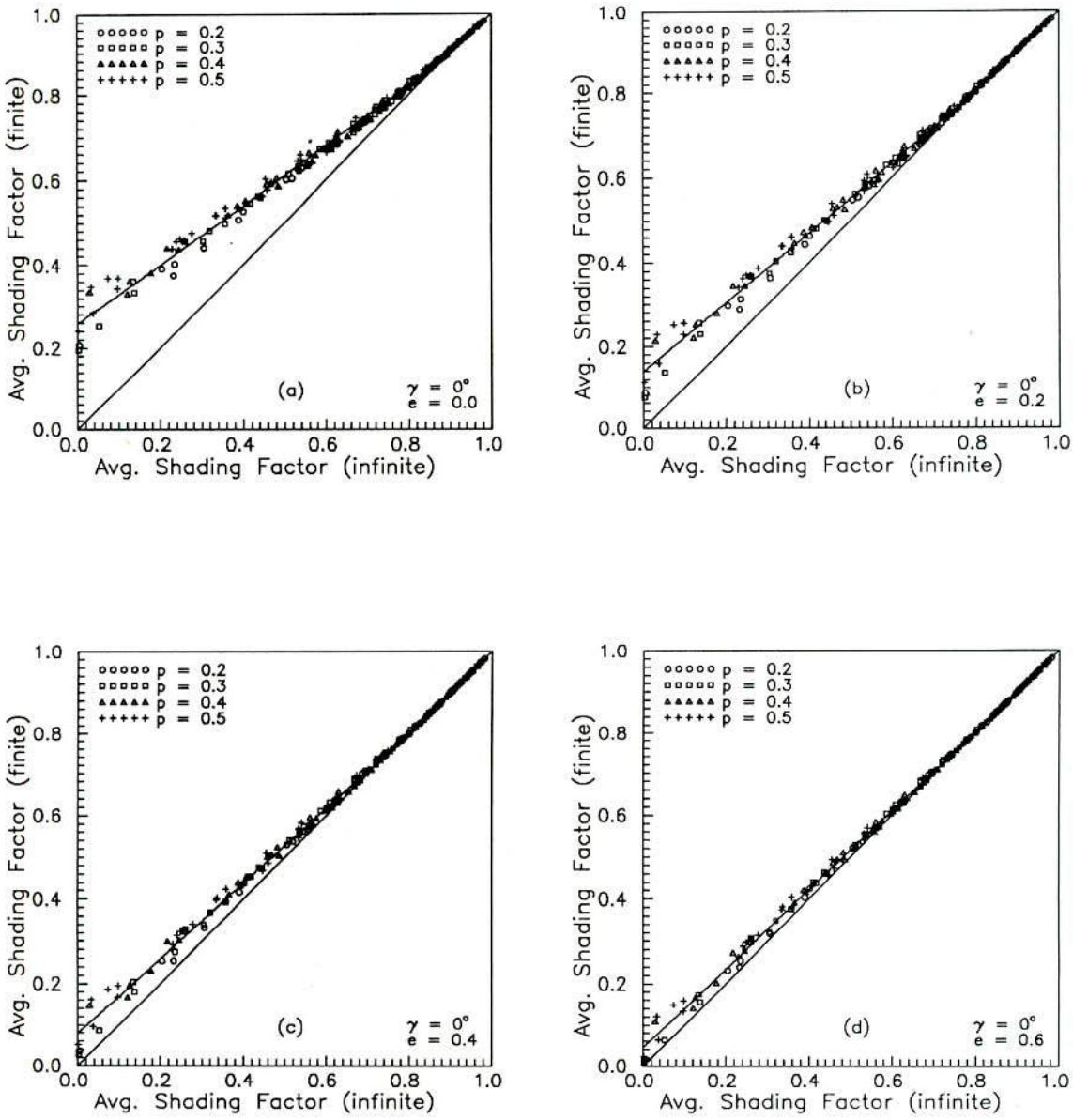

Figure 5.5: Relation between $\bar{f}_i$ and $\bar{f}_{i\infty}$ independent of projection for different overhang extensions (a) $e = 0.0$; (b) $e = 0.2$; (c) $e = 0.4$; and (d) $e = 0.6$

Table 5.2: Values of the constants M_p and N_p in Eq. (5.57) to estimate $\bar{f}_i$ from $\bar{f}_{i\infty}$ (when $\bar{f}_{i\infty} > 0.0$)

Constants	Overhang Extension, e				
	0.00	0.20	0.40	0.60	0.80
M_p	0.258	0.140	0.079	0.046	0.026
N_p	0.703	0.824	0.897	0.941	0.970

Table 5.3: Values of the constants m and n to estimate $\bar{f}_i^o$ from ω_s' for south facing receivers

e	0.00	0.20	0.40	0.60	0.80
m	0.245	0.174	0.160	0.153	0.169
n	1.018	1.569	1.917	1.801	1.539

to $\bar{f}_{i\infty} = 0.0$, designated as $\bar{f}_i^o$, result due to solar radiation reaching the receiver from the sides. In other words, when the projection of the overhang is such that the shadow length (Y is Figure 5.2) is greater than or equal to the window height throughout the day, $\bar{f}_{i\infty} = 0$. However, since the shaded area on the receiver (window) need not be rectangular when the overhang is finite, $\bar{f}_i \neq 0$. Also, it can be envisaged that $\bar{f}_i^o$ values for a given extension e, be independent of the projection p, since the radiation reaches the receiver from the sides only. This has been verified numerically and found to be true. In view of this, it is proposed that $\bar{f}_i^o$ values be correlated to ω_s', which describes the duration of the possible sunshine on the receiver.

A plot of $\bar{f}_i^o$ vs ω_s' for $w = 1.0$, $\bar{D}_f = 0.4$, $e = 0.0$, 0.2, 0.4, 0.6 and 0.8 for $25^o \leq \phi \leq 60^o$ and $-23.05 \leq \delta \leq 23.09^o$ is shown in Figure 5.6. $\bar{f}_i^o$ is remarkably well correlated to ω_s' for all latitudes and declinations and extension e will be a parameter in the relation between $\bar{f}_i^o$ and ω_s'. $\bar{f}_i^o$ is correlated to ω_s' by an equation of the form,

$$\bar{f}_i^o = m\left[\omega_s' - (e + 0.2)\right]^n \tag{5.61}$$

where ω_s' is in radians. Best fit values for m and n for $e = 0.0$, 0.2, 0.4, 0.6 and 0.8 are determined and are given is Table 5.3. It may be noted that the term $(e+0.2)$ in Eq. (5.61) has been arrived at by realizing that $\bar{f}_i^o \to 0$ for $\omega_s' > 0$. The value of ω_s' for which $\bar{f}_i^o \to 0$ depends on the extension.

It may be noted that Eq. (5.61) is valid for $25^o \leq \phi \leq 60^o$, $-23.05^o \leq \delta \leq 23.09^o$ and $0 \leq e \leq 0.8$. Eq. (5.61) predicts $\bar{f}_i^o$ values within a difference of 0.005 compared to the

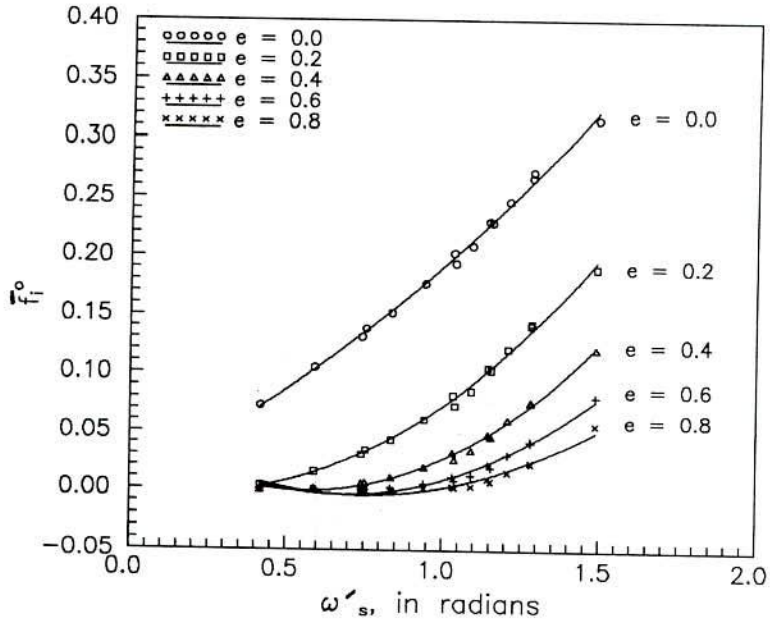

Figure 5.6: Relation between $\bar{f}_i^o$ and ω_s' for different overhang extensions for south facing receivers

values obtained by numerical integration. For $e > 0.8$ without significant loss of accuracy $\bar{f}_i^o = 0$. In otherwords, $\bar{f}_i = \bar{f}_{i\infty}$.

5.6 Shading Factor Values for Non-south Facing Receivers Shaded by Finite Overhangs

$\bar{f}_{i\infty}$ for non-south facing receivers can be calculated using Eq. (5.34) or Eq. (5.46) with no additional difficulty compared to that for south facing receivers. Fortunately, the relation between $\bar{f}_i$ and $\bar{f}_{i\infty}$ for a given p and e does not depend on ϕ and δ for south facing receivers. Even the apparent sunrise hour angle ω_s' does not explicitly appear in the relation between $\bar{f}_i$ and $\bar{f}_{i\infty}$ for south facing receivers. Thus, for non-south facing receivers, it can be expected that the relation between $\bar{f}_i$ and $\bar{f}_{i\infty}$ does not depend on the apparent sunrise and sunset hour angles, ω_{sr} and ω_{ss}. However, for non-south facing receivers, solar radiation falling on the receiver and the shading caused by the overhangs are not symmetric around $\omega = 0$. In view of this, relations between $\bar{f}_i$ and $\bar{f}_{i\infty}$ for non-south receivers will be dependent additionally on γ.

The difficulty arising owing to non-symmetric shading for receivers with $\gamma \neq 0$ is proposed to be alleviated by considering shading factors for two time intervals separately during ω_{sr} to ω_{ss}. To split ω_{sr} to ω_{ss} duration into two parts, the hour angle chosen is

the hour angle corresponding to $(\gamma_s - \gamma) = \gamma_d = 0$. This choice has been made realizing that, if the shading factor for south facing surfaces is split into two parts from $-\omega_s'$ to 0 and 0 to ω_s', the hour angle $\omega = 0$ corresponds to $\gamma_d = 0$. Of course, the shading factor values for forenoon and afternoon for south facing receivers will be equal.

When $\gamma \neq 0$, let the hour angle corresponding to $\gamma_d = 0$ be designated as ω_o. ω_o can be obtained by solving the equation (see, Duffie and Beckman [6], page-16),

$$\sin \gamma_s = \frac{\sin \omega \cos \delta}{\sin \theta_z} \tag{5.62}$$

Expressing $\sin \theta_z$ in Eq. (5.62) from Eq. (2.8) for $\cos \theta_z$ from Chapter 2, ω_o is governed by,

$$A_2 \cos^2 \omega_o + B_2 \cos \omega_o + C_2 = 0 \tag{5.63}$$

where, the constants A_2, B_2 and C_2 are given by,

$$A_2 = \sin^2 \gamma_s \cos^2 \phi \cos^2 \delta - \cos^2 \delta \tag{5.64}$$

$$B_2 = 2 \sin^2 \gamma_s \sin \phi \cos \phi \sin \delta \cos \delta \tag{5.65}$$

$$C_2 = \cos^2 \delta + \sin^2 \gamma_s \sin^2 \phi \sin^2 \delta - \sin^2 \gamma_s \tag{5.66}$$

ω_o is given by,

$$\omega_o = \cos^{-1} \left[\frac{-B_2 \pm \sqrt{B_2^2 - 4\, A_2 C_2}}{2\, A_2} \right] \tag{5.67}$$

The correct value of ω_o is obtained by considering positive sign for the radical in Eq. (5.67) and noting that $\omega_o > 0$ if $\gamma > 0$ and $\omega_o < 0$ if $\gamma < 0$.

Let H_{bT1} and H_{bT2} be the direct radiation reaching the unshaded non-south facing receiver during ω_{sr} to ω_o and ω_o to ω_{ss} respectively. If $\bar{f}_{i1}$ and $\bar{f}_{i2}$ are the shading factors for these two durations separately, the overall daily shading factor $\bar{f}_i$ is given by,

$$\bar{f}_i = \frac{H_{bT1}\, \bar{f}_{i1} + H_{bT2}\, \bar{f}_{i2}}{H_{bT}} \tag{5.68}$$

where, $H_{bT} = H_{bT1} + H_{bT2}$. $\bar{f}_{i1}$ and $\bar{f}_{i2}$ are defined by,

$$\bar{f}_{i1} = \frac{\sum_{\omega_{sr}}^{\omega_o} I_b R_b f_i}{\sum_{\omega_{sr}}^{\omega_o} I_b R_b} = \frac{\int_{\omega_{sr}}^{\omega_o} I_b R_b f_i \, d\omega}{\int_{\omega_{sr}}^{\omega_o} I_b R_b \, d\omega} \tag{5.69}$$

and

$$\bar{f}_{i2} = \frac{\sum_{\omega_o}^{\omega_{ss}} I_b R_b f_i}{\sum_{\omega_o}^{\omega_{ss}} I_b R_b} = \frac{\int_{\omega_o}^{\omega_{ss}} I_b R_b f_i \, d\omega}{\int_{\omega_o}^{\omega_{ss}} I_b R_b \, d\omega} \tag{5.70}$$

It may be noted that $\bar{f}_{i1}$ and $\bar{f}_{i2}$ are the shading factors for the two time intervals, when sunshine duration (ω_{sr} to ω_{ss}) is split according to a common feature qualitatively similar to that for south facing receivers. When the overhang is infinite, let $\bar{f}_{i\infty 1}$ and $\bar{f}_{i\infty 2}$ be the shading factor values for the durations ω_{sr} to ω_o and ω_o to ω_{ss} respectively. It is proposed that, $\bar{f}_{i1}$ and $\bar{f}_{i2}$ be correspondingly related to $\bar{f}_{i\infty 1}$ and $\bar{f}_{i\infty 2}$ by the same relations developed for south facing surfaces. Thus, when $\bar{f}_{i\infty 1,2} > 0$,

$$\bar{f}_{i1,2} = M + N\,\bar{f}_{i\infty 1,2} \tag{5.71}$$

where, M and N are the same constants given in Table 5.1 for different projections and extensions.

If $\bar{f}_{i1,2} < \bar{f}_{i\infty 1,2}$ according to Eq. (5.71), $\bar{f}_{i1,2}$ is to be evaluated as,

$$\bar{f}_{i1,2} = \bar{f}_{i\infty 1,2} \tag{5.72}$$

$\bar{f}_{i\infty 1}$ and $\bar{f}_{i\infty 2}$ are defined according to,

$$\bar{f}_{i\infty 1} = \left(\frac{A_{shp}}{A_w}\right)\frac{\bar{R}^*_{b1}}{\bar{R}_{b1}} \tag{5.73}$$

$$\bar{f}_{i\infty 2} = \left(\frac{A_{shp}}{A_w}\right)\frac{\bar{R}^*_{b2}}{\bar{R}_{b2}} \tag{5.74}$$

where, $\bar{R}^*_{b1}$, $\bar{R}_{b1}$, $\bar{R}^*_{b2}$ and $\bar{R}_{b2}$ are defined by,

$$\bar{R}^*_{b1} = \int_{\omega^*_{sr}}^{\omega_o} I_b R^*_b\, d\omega \Big/ \int_{-\omega_s}^{\omega_s} I_b\, d\omega \tag{5.75}$$

$$\bar{R}_{b1} = \int_{\omega_{sr}}^{\omega_o} I_b R_b\, d\omega \Big/ \int_{-\omega_s}^{\omega_s} I_b\, d\omega \tag{5.76}$$

$$\bar{R}^*_{b2} = \int_{\omega_o}^{\omega^*_{ss}} I_b R^*_b\, d\omega \Big/ \int_{-\omega_s}^{\omega_s} I_b\, d\omega \tag{5.77}$$

$$\bar{R}_{b2} = \int_{\omega_o}^{\omega_{ss}} I_b R_b\, d\omega \Big/ \int_{-\omega_s}^{\omega_s} I_b\, d\omega \tag{5.78}$$

When $\bar{R}^*_{b1}$, $\bar{R}^*_{b2}$ are defined according to Eqs. (5.75) to (5.78), all-day $\bar{R}^*_b$ and $\bar{R}_b$ are related to the part values by,

$$\bar{R}^*_b = \bar{R}^*_{b1} + \bar{R}^*_{b2} \tag{5.79}$$

$$\bar{R}_b = \bar{R}_{b1} + \bar{R}_{b2} \tag{5.80}$$

$\bar{R}_{b1}$ and $\bar{R}_{b2}$ etc. can be evaluated from Eq. (5.36) using the appropriate limits[2] of integration.

[2]For example, considering $\bar{R}_{b1}$, the limits of integration being ω_{sr} to ω_o in the numerator and $-\omega_s$ to ω_s in the denominator, $\bar{R}_{b1}$ is to be evaluated using Eq. (5.36) modifying Eqs. (5.42) and (5.43) for I_1 and I_2 as,

$I_1 = I_{P1}(\omega_o) - I_{P2}(\omega_{sr})$ if $\omega_{sr} < \omega_o$

$I_2 = I_{P2}(\omega_o) - I_{P2}(\omega_{sr})$ if $\omega_{sr} < \omega_o$

Similar to the relations developed for south facing receivers for $\bar{f}_i$, when $\bar{f}_{i\infty} = 0$, in terms of ω'_s (actually ω'_s can be interpreted as the duration from $\omega = -\omega'_s$ to $\omega = 0$ or $\omega = 0$ to $\omega = \omega'_s$), it is proposed to relate $\bar{f}_{i1}$ when $\bar{f}_{i\infty 1} = 0$, to $(\omega_o - \omega_{sr})$ and $\bar{f}_{i2}$ when $\bar{f}_{i\infty 2} = 0$, to $(\omega_{ss} - \omega_o)$. These durations are commonly designated as ω'_{so}. $\bar{f}_{i1}$ and $\bar{f}_{i2}$, when $\bar{f}_{i\infty 1}$ and $\bar{f}_{i\infty 2}$ are zero, are designated as $\bar{f}^o_{i1}$ and $\bar{f}^o_{i2}$.

Plots of $\bar{f}^o_{i1,2}$ vs ω'_{so} are shown in Figure 5.7 for $e = 0.0$ for $\gamma = \pm 30^o$ and $\pm 60^o$ and for $e = 0.2$ for $\gamma = 30^o$. When $|\gamma| > 60^o$ [actually computed for $|\gamma| = 90^o$] even for $e = 0$, $\bar{f}^o_{i1,2}$ are nearly equal to zero. Also, when $e = 0.2$, $\bar{f}^o_{i1,2}$ values are close to zero for $|\gamma| = 60^o$ and 90^o. the plots shown in Figure 5.7 are for non-zero (significant) values of $\bar{f}^o_{i1,2}$. It may be noted that the values of $\bar{f}^o_{i1,2}$ in Figure 5.7 have been obtained for both negative and positive values of γ since, when $\bar{f}_{i\infty 1} = 0$, $\bar{f}_{i\infty 2} \neq 0$ and vice-versa. It is interesting to note that both $\bar{f}^o_{i1}$ and $\bar{f}^o_{i2}$ are correlated by a single line, which supports the splitting of the duration ω_{sr} to ω_{ss} into two intervals. These correlations are independent of p since $\bar{f}^o_{i1,2}$ are due to radiation entering from the sides. For $\gamma > 0$, $\bar{f}^o_{i1}$ is related to $\omega'_{so}[= (\omega_o - \omega_{sr})]$ by,

$$\bar{f}^o_{i1} = 0.008 + 0.010\omega'_{so} + 0.072{\omega'_{so}}^2 \quad \text{when} \quad e = 0.0, \gamma = 30^o \qquad (5.81)$$

$$= 0.006 + 0.047\omega'_{so} + 0.089{\omega'_{so}}^2 \quad \text{when} \quad e = 0.0, \gamma = 60^o \qquad (5.82)$$

$$= 0.021 - 0.110\omega'_{so} + 0.152{\omega'_{so}}^2 \quad \text{when} \quad e = 0.2, \gamma = 30^o \qquad (5.83)$$

For $\gamma < 0$, Eqs. (5.81) to (5.83) yield $\bar{f}^o_{i2}$ with $\omega'_{so} = [\omega_{ss} - \omega_o]$.

Eqs. (5.81) to (5.83) predict $\bar{f}^o_{i1,2}$ differing by less than 0.008 compared to the values obtained by numerical computations.

The method proposed to evaluate $\bar{f}_i$ for non-south facing receivers in terms of two shading factors $\bar{f}_{i1}$ and $\bar{f}_{i2}$ related to $\bar{f}_{i\infty 1}$ and $\bar{f}_{i\infty 2}$ by the same relations developed for south facing receivers, when $\bar{f}_{i\infty 1}$ and $\bar{f}_{i\infty 2}$ are greater than zero, becomes available when validated. $\bar{f}^o_{i1,2}$ have been related to the extension and a duration of sunshine by Eqs. (5.81) to (5.83). The validation is presented in the section on Results and Discussion, §5.7

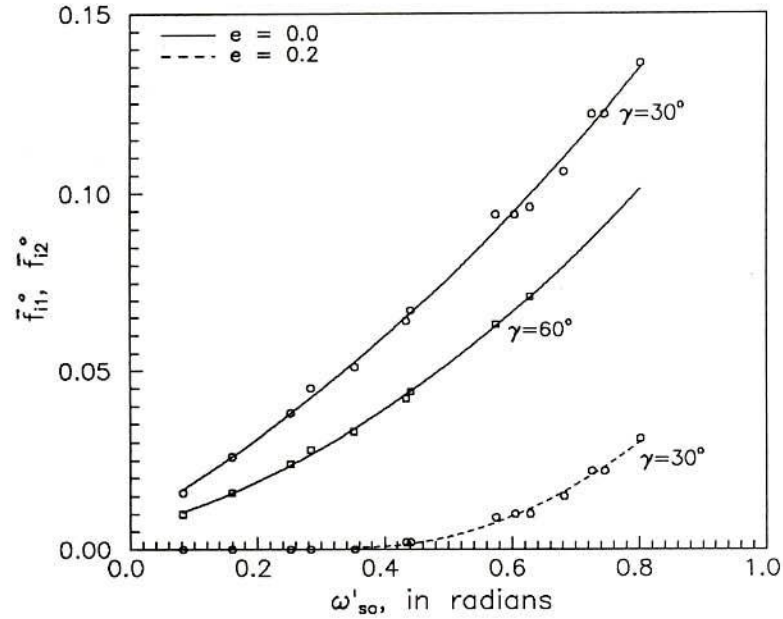

Figure 5.7: Relation between $\bar{f}^{o}_{i1,2}$ and ω'_{so} for different overhang extensions for non-south facing receivers

5.7 Results and Discussion

Numerical values for $\bar{f}_{i\infty}$ obtained using the present algorithm, Eq. (5.34), and $\bar{f}_i$ obtained using the equations[3] developed in the present study have been validated against hour by hour numerical computations according to Eq. (5.8) expressing I_b in terms of r_t [12] and r_d [16] correlations as per Eq. (2.27). In the numerical summation procedure, according to Eq. (5.8), an interval of 5^o for ω has been employed. Values of $\bar{f}_{i\infty}$ obtained by the present algorithm have also been compared against the values obtained using the approach of Utzinger and Klein [125] and the values obtained employing hour by hour summation procedure using solar radiation data.

For the purpose of validation, numerical values have been obtained assuming the gap to be zero and the receiver to be vertical, south facing as well as non-south facing for finite and infinite overhangs. When a gap exists or when the receiver is non-vertical, no new concept is involved and hence no numerical results have been given. Results and discussion are broadly classified into infinite overhangs and finite overhangs. In general,

[3]Eq. (5.55) along with the constants M and N given in Table 5.1 when $\bar{f}_{i\infty} > 0$ and Eq. (5.56) when $\bar{f}_i < \bar{f}_{i\infty}$ as per Eq. (5.55).

Eq. (5.61) along with the constants m and n given in Table 5.2 when $\bar{f}_{i\infty} = 0.0$.

For non-south facing surfaces, Eq. (5.68) has been used along with the aforementioned equations to calculate $\bar{f}_{i1}$ and $\bar{f}_{i2}$.

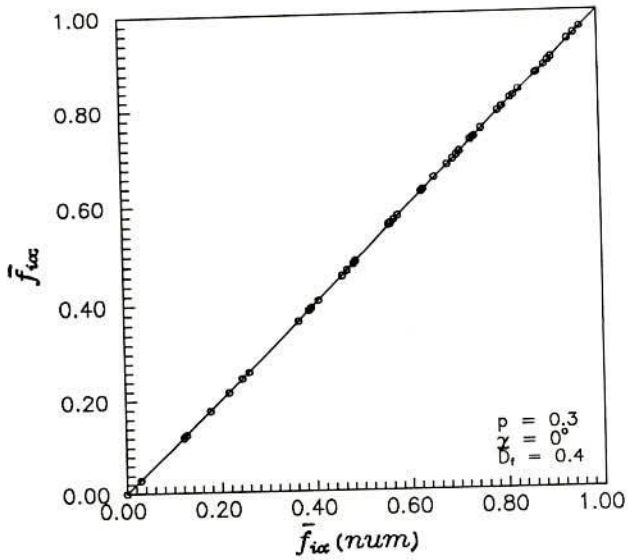

Figure 5.8: Validation of $\bar{f}_{i\infty}$ against $\bar{f}_{i\infty}$(num) for $\gamma = 0^o$, $p = 0.3$ and $\bar{D}_f = 0.4$

the shading factor values obtained by numerical integration are designated by $\bar{f}_{i\infty}$(num) or $\bar{f}_i$(num).

5.7.1 Infinite Overhangs

$\bar{f}_{i\infty}$ values obtained employing Eq. (5.34) have been compared with the values obtained using Eq. (5.8) where Sun's [114] algorithm for the instantaneous shading factor has been used. Utzinger and Klein [125] suggested a value of $e \geq 3$, when $w \geq 1$, for which finite and infinite overhang values differ insignificantly. To obtain $\bar{f}_{i\infty}$(num) values according to Eq. (5.8), $e = 10$ has been employed in the present computations.

Plots of $\bar{f}_{i\infty}$ vs $\bar{f}_{i\infty}$(num) for $\phi = 25^o$, 30^o, 40^o, 50^o and 60^o, $-23.05^o \leq \delta \leq 23.09^o$, $\bar{D}_f = 0.4$, $p = 0.3$ for $\gamma = 0^o$ and 60^o respectively are shown in Figures 5.8 and 5.9. It can be noticed from Figures 5.8 and 5.9 that no difference can be found graphically and the numerical values differed by less than 0.001. This comparison establishes the validity of the algorithm (Eq. (5.34)), particularly, in using and determining the apparent sunrise and sunset hour angles ω^*_{sr} and ω^*_{ss} for the shading plane correctly and replacing ω_{sr} and ω_{ss} of the receiver in Eq. (5.21) with ω^*_{sr} and ω^*_{ss} in Eq. (5.29). In what follows, deviation of $\bar{f}_{i\infty}$ values from $\bar{f}_{io\infty}$ (i.e., the values obtained under extra-terrestrial conditions) values for south facing and non-south facing receivers is discussed.

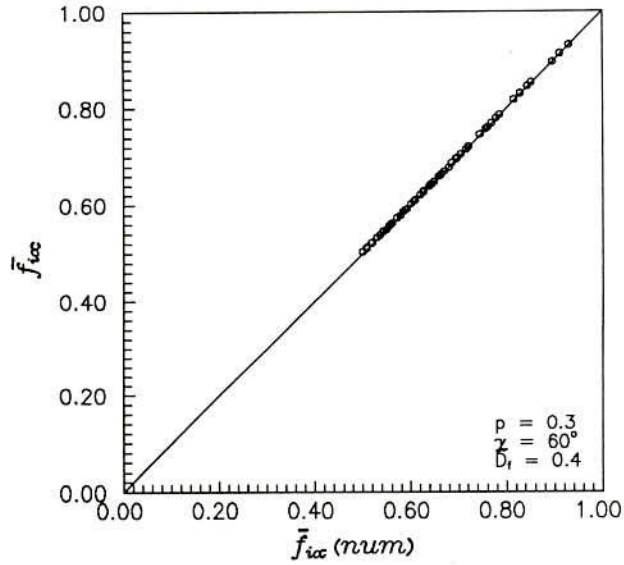

Figure 5.9: Validation of $\bar{f}_{i\infty}$ against $\bar{f}_{i\infty}$(num) for $\gamma = 60^o$, $p = 0.3$ and $\bar{D}_f = 0.4$

South Facing Receivers

Shading factor values for infinite overhangs under extra-terrestrial conditions have been obtained using Eq. (5.35). A plot of $(\bar{f}_{i\infty}/\bar{f}_{io\infty})$ vs declination δ, for monthly average daily diffuse fraction equal to 0.2 and 0.8 is shown in Figure 5.10 for $\phi = 30^o$, $w = 1.0$, $p = 0.3$, $g = 0$ and $\gamma = 0^o$. As can be expected, $(\bar{f}_{i\infty}/\bar{f}_{io\infty})$ differs less from unity when $\bar{D}_f = 0.2$ whereas, $(\bar{f}_{i\infty}/\bar{f}_{io\infty})$ is as high as 1.15 for $\bar{D}_f = 0.8$, when $\delta = 9.4^o$ (April). Thus, for practical values of $\bar{D}_f = 0.4$ to 0.6, differences up to 10 % between $\bar{f}_{i\infty}$ and $\bar{f}_{io\infty}$ can be expected for south facing receivers. It can be noticed also that, $(\bar{f}_{i\infty}/\bar{f}_{io\infty}) > 1.0$ for $\delta > 0$ and $(\bar{f}_{i\infty}/\bar{f}_{io\infty}) < 1.0$, when $\delta < 0$. Also, $(\bar{f}_{i\infty}/\bar{f}_{io\infty}) = 1.0$, when $\delta = 0$. Both these features are in conformity with the behaviour of $\bar{R}_b$, when $\bar{D}_f$ changes. According to present notations, when $\gamma = 0$ and $\delta = 0$, $\bar{R}_{bo} = \bar{R}_b$ for any $\bar{D}_f$ and also, $\bar{R}_b > \bar{R}_{bo}$ when $\delta > 0$ and $\bar{R}_b < \bar{R}_{bo}$ when $\delta < 0$. The same trend is reflected in $\bar{f}_{i\infty}$ also, since it is a function of $(\bar{R}^*_b/\bar{R}_b)$ and both $\bar{R}^*_b$ and $\bar{R}_b$ do not change with $\bar{D}_f$ for $\delta = 0$, when $\gamma = 0$. $(\bar{f}_{i\infty}/\bar{f}_{io\infty})$ for $\delta > 9.4^o$, for $p = 0.3$ and $\phi = 30^o$ takes indeterminate form since $\bar{R}^*_b$ and $\bar{R}^*_{bo}$ are zero. The condition for $\bar{f}_{i\infty}$ or $\bar{f}_{io\infty}$ to be zero for $\gamma = 0^o$, $\delta > 0$ can be easily derived by setting the angle of incidence for the shading plane to be $\pi/2$ at $\omega = 0$. This yields, $\psi \geq (\phi - \delta)$. In terms of the overhang geometry, $\psi \geq (\phi - \delta)$ implies, $p \geq \tan(\phi - \delta)$. For example, for $p = 0.3$, $\phi = 30^o$, $\bar{f}_{i\infty} = \bar{f}_{io\infty} = 0$ for $\delta \geq 13.3^o$.

A plot of $(\bar{f}_{i\infty}/\bar{f}_{io\infty})$ vs $\bar{D}_f$ for $\delta = -23.05^o$ (December) and $\delta = 18.8^o$ (May) for

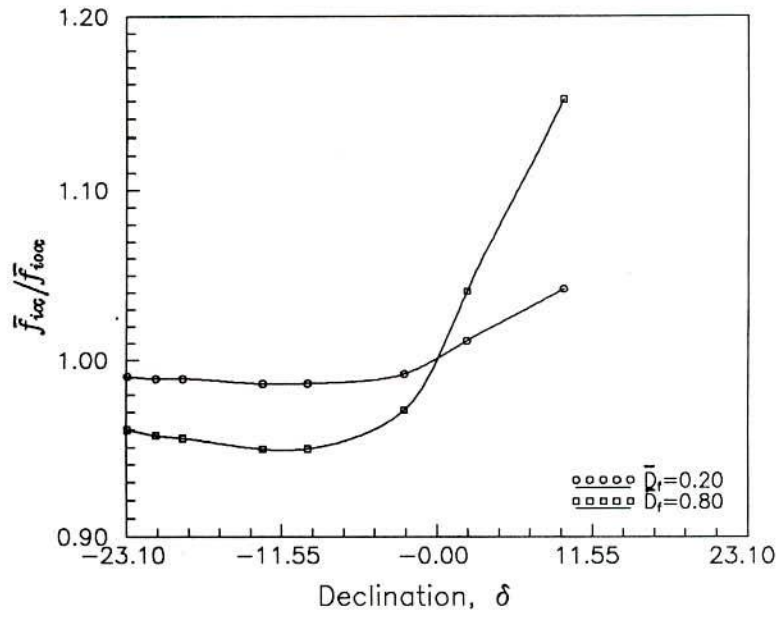

Figure 5.10: Variation of $(\bar{f}_{i\alpha}/\bar{f}_{i o\infty})$ with declination; $\phi = 30^o$, $\gamma = 0^o$, $w = 1.0$, $p = 0.3$, $g = 0.0$ and $\bar{D}_f = 0.2, 0.8$

.

$\phi = 40^o$, $p = 0.3$ and $\gamma = 0^o$ is shown in Figure 5.11. $\delta = 18.8^o$ has been chosen since for higher δ (say, June), the shading factor values are small and the percentage differences could be misleading. $(\bar{f}_{i\alpha}/\bar{f}_{i o\infty})$ varies from 1.02 to 1.10, when $\delta = 18.8^o$ and from 0.995 to 0.975, when $\delta = -23.05^o$ when $\bar{D}_f$ changes from 0 to 0.8. It may be noted, that when $\bar{D}_f = 0$, $\bar{f}_{i\alpha} \neq \bar{f}_{i o\infty}$ since the distribution of I_b obtained from r_t and r_d correlations with $\bar{D}_f = 0$ does not reduce to I_o distribution. Maximum difference between $\bar{f}_{i\alpha}$ and $\bar{f}_{i o\infty}$ is 9.8 %. For typical values of $\bar{D}_f = 0.4$, when $\gamma = 0^o$, 5 % difference between extra-terrestrial and terrestrial value can be expected. However, higher percentage differences occur at lower latitudes.

A plot of $(\bar{f}_{i\alpha}/\bar{f}_{i o\infty})$ vs the projection p is shown in Figure 5.12 for $\delta = -9.6^o$ (October), $\delta = 2.2^o$ (September) and $\delta = 9.4^o$ (April) for $\phi = 30^o$, $\gamma = 0^o$ and $\bar{D}_f = 0.4$. $(\bar{f}_{i\alpha}/\bar{f}_{i o\infty})$ deviates more from unity as p increases. It may be noted that this deviation is higher, in general, when $\delta > 0$, when $\bar{f}_{i\alpha}, \bar{f}_{i o\infty} \neq 0$.

Variation of $(\bar{f}_{i\alpha}/\bar{f}_{i o\infty})$ with latitude for three values $\bar{D}_f = 0.2, 0.4$ and 0.8 are shown in Figures 5.13 and 5.14 for $\delta = -9.6^o$, -18.9^o and $\delta = 9.4^o$, $\delta = 18.8^o$ respectively for $p = 0.3$ and $\gamma = 0^o$. $|1 - (\bar{f}_{i\alpha}/\bar{f}_{i o\infty})|$ decreases as ϕ increases at any given $\bar{D}_f$. In general, diffuse fraction effect is higher at low latitudes and is more significant in summer months.

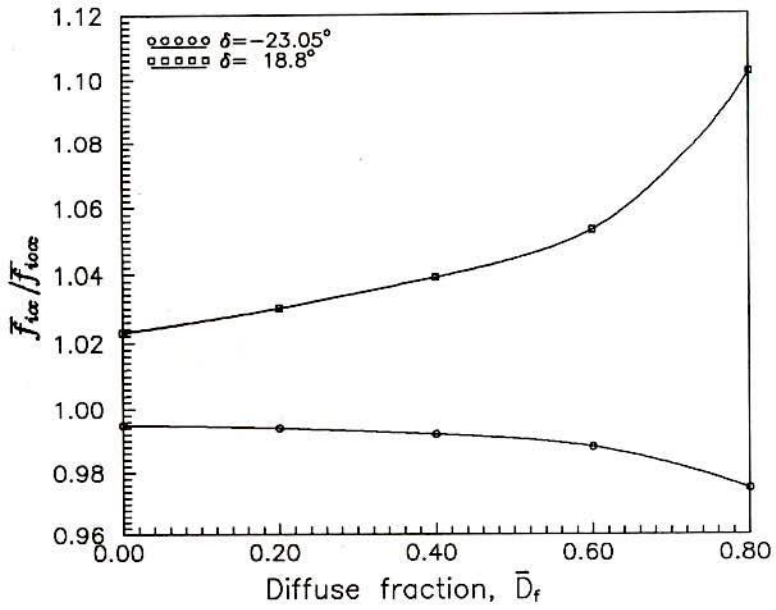

Figure 5.11: Variation of $(\bar{f}_{i\alpha}/\bar{f}_{i\alpha\alpha})$ with diffuse fraction; $\phi = 40^o$, $\gamma = 0^o$, $w = 1.0$, $p = 0.3$, $g = 0.0$ and $\delta = -23.05^o$, $\delta = 18.8^o$

.

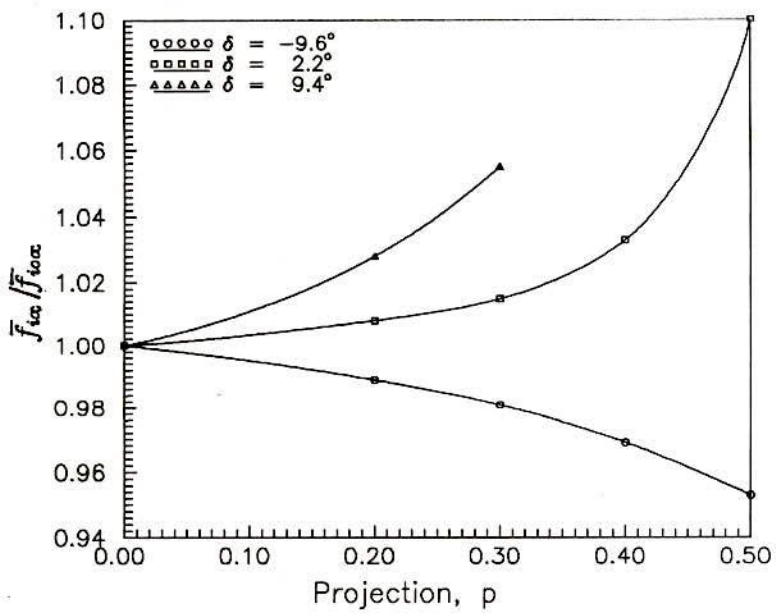

Figure 5.12: Variation of $(\bar{f}_{i\alpha}/\bar{f}_{i\alpha\alpha})$ with overhang projection; $\phi = 30^o$, $\gamma = 0^o$, $w = 1.0$, $g = 0.0$, $\bar{D}_f = 0.4$ and $\delta = -9.6^o$, 2.2^o and 9.4^o

.

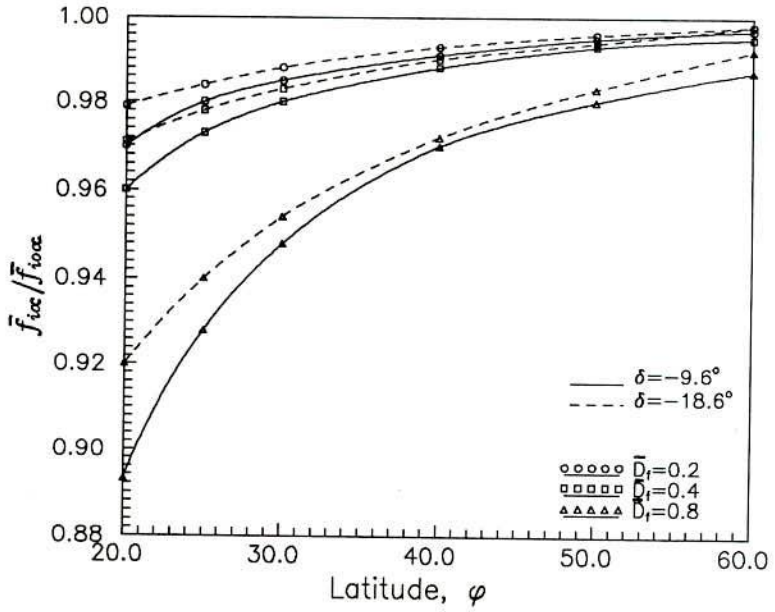

Figure 5.13: Variation of $(\bar{f}_{i\infty}/\bar{f}_{io\infty})$ with latitude; $\gamma = 0^o$, $w = 1.0$, $p = 0.3$, $g = 0.0$ and $\delta = -9.6^o$, $\delta = -18.9^o$

Tabulated Values:

Summary values of $\bar{f}_{io\infty}$ and $\bar{f}_{i\infty}$ for $p = 0.3$ with $w = 1.0$, $g = 0.0$ are given in Table 5.4 for three representative months, March, June and December for $\phi = 20^o$, 25^o, 30^o, 40^o, 50^o and 60^o for $\gamma = 0^o$. Under the column $\bar{D}_f$, 'Ext.' indicates the extra-terrestrial shading factor values $\bar{f}_{io\infty}$, whereas, the other values correspond to $\bar{D}_f = 0.2$ to 0.8. Values of the ratio $\bar{f}_{i\infty}/\bar{f}_{io\infty}$ which indicate the percentage changes are given in Table 5.5.

Non-south Facing receivers

Values of $\bar{f}_{io\infty}$ and $\bar{f}_{i\infty}$ for 30^o, 60^o and 90^o also are given in Table 5.4 and the ratio values in Table 5.5 for the aforementioned values of the other parameters. From the summarized values given in Table 5.4, the following points emerges:

1. As γ increases, both $\bar{f}_{i\infty}$ and $\bar{f}_{io\infty}$ values increase for a given ϕ and diffuse fraction for March and June, whereas, the values decrease in December. It may be noted, in general, that the shading factor values are higher in December.

2. $|\bar{f}_{i\infty} - \bar{f}_{io\infty}|$ increases as γ increases for a given ϕ, month and diffuse fraction. Of course, $|\bar{f}_{i\infty} - \bar{f}_{io\infty}|$ increases as $\bar{D}_f$ increases.

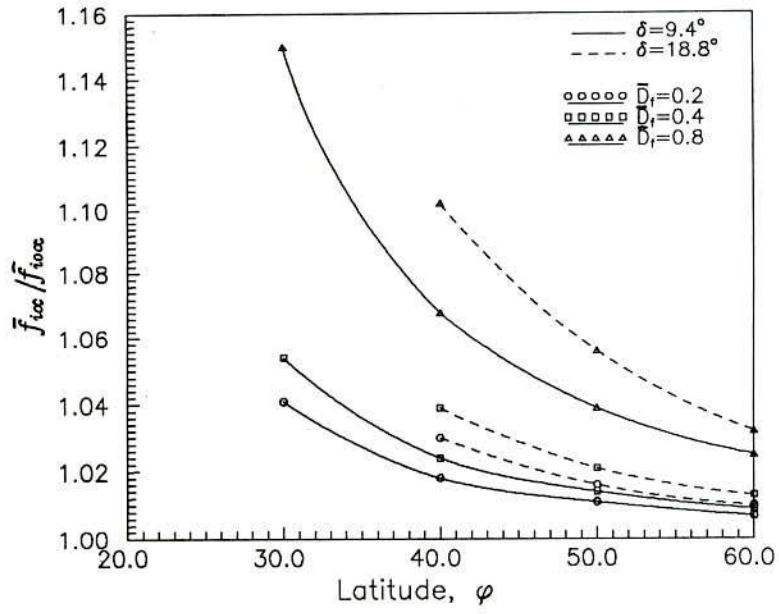

Figure 5.14: Variation of $(\bar{f}_{i\alpha}/\bar{f}_{io\alpha})$ with latitude; $\gamma = 0^o$, $w = 1.0$, $p = 0.3$, $g = 0.0$ and $\delta = 9.4^o$, $\delta = 18.8^o$

3. For a given γ, $|\bar{f}_{i\alpha} - \bar{f}_{io\alpha}|$ decreases as ϕ increases, indicating that at lower latitudes influence of diffuse fraction on the shading factor is significant.

It appears that the influence of diffuse fraction on the shading factor for non-south facing receivers is more significant than that for the south facing receivers. For example, in March, $\phi = 20^o$, $\gamma = 30^o$, $\bar{f}_{io\alpha} = 0.604$ and $\bar{f}_{i\alpha} = 0.546$ at $\bar{D}_f = 0.4$ and $\bar{f}_{i\alpha} = 0.424$ at $\bar{D}_f = 0.8$, percentage chnages of 9.6 % and 29.8 %. For $\gamma = 0^o$, $\bar{f}_{io\alpha} = 0.318$ and $\bar{f}_{i\alpha} = 0.306$ at $\bar{D}_f = 0.4$ and $\bar{f}_{i\alpha} = 0.286$ at $\bar{D}_f = 0.8$, percentage changes of 4 % and 10 %.

Plots of $(\bar{f}_{i\alpha}/\bar{f}_{io\alpha})$ vs γ for $\phi = 20^o$, 40^o and 60^o at $\bar{D}_f = 0.4$ and 0.6 are shown in Figures 5.15 to 5.17. The deviation of $(\bar{f}_{i\alpha}/\bar{f}_{io\alpha})$ from unity indicates the difference between the extra-terrestrial value and the terrestrial value. For example, at $\bar{D}_f = 0.4$, $\bar{f}_{i\alpha} \approx 0.9\, \bar{f}_{io\alpha}$ for $\phi = 20^o$ in the month of March.

5.7.2 Finite Overhangs

South Facing Receivers:

Performance of the equations developed in the present study, to obtain the shading factor

Table 5.4: Tabulated values of $\bar{f}_{i o \infty}$ and $\bar{f}_{i \infty}$ for different azimuthal angles; $p = 0.3$, $g = 0.0$

ϕ	$\bar{D}_f$	Values of $\bar{f}_{i o \infty}$ and $\bar{f}_{i \infty}$											
		March				June				December			
		$\gamma = 0^o$	30^o	60^o	90^o	$\gamma = 0^o$	30^o	60^o	90^o	$\gamma = 0^o$	30^o	60^o	90^o
20	Ext.	0.318	0.604	0.729	0.759	0.000	0.250	0.658	0.738	0.760	0.736	0.774	0.777
	0.2	0.309	0.562	0.689	0.721	0.000	0.209	0.612	0.699	0.747	0.717	0.743	0.741
	0.4	0.306	0.546	0.674	0.704	0.000	0.192	0.593	0.682	0.742	0.712	0.731	0.726
	0.6	0.299	0.510	0.636	0.653	0.000	0.154	0.548	0.641	0.731	0.696	0.703	0.689
	0.8	0.286	0.424	0.530	0.538	0.000	0.055	0.406	0.512	0.708	0.663	0.627	0.569
25	Ext.	0.453	0.630	0.738	0.767	0.000	0.265	0.660	0.741	0.796	0.770	0.790	0.789
	0.2	0.447	0.594	0.701	0.729	0.000	0.227	0.616	0.703	0.785	0.756	0.762	0.756
	0.4	0.444	0.581	0.686	0.714	0.000	0.213	0.598	0.686	0.781	0.750	0.751	0.742
	0.6	0.440	0.551	0.651	0.674	0.000	0.181	0.556	0.647	0.772	0.739	0.726	0.707
	0.8	0.431	0.481	0.555	0.551	0.000	0.096	0.426	0.520	0.754	0.716	0.659	0.593
30	Ext.	0.551	0.661	0.750	0.776	0.000	0.297	0.664	0.746	0.828	0.803	0.807	0.803
	0.2	0.546	0.631	0.715	0.740	0.000	0.264	0.623	0.708	0.819	0.792	0.783	0.772
	0.4	0.544	0.619	0.702	0.725	0.000	0.252	0.606	0.693	0.816	0.788	0.773	0.760
	0.6	0.541	0.596	0.670	0.687	0.000	0.226	0.568	0.655	0.809	0.780	0.752	0.728
	0.8	0.534	0.540	0.582	0.568	0.000	0.155	0.450	0.533	0.794	0.762	0.695	0.621
40	Ext.	0.686	0.727	0.781	0.800	0.002	0.389	0.681	0.760	0.883	0.865	0.848	0.837
	0.2	0.683	0.707	0.751	0.767	0.002	0.369	0.646	0.726	0.878	0.859	0.831	0.813
	0.4	0.682	0.700	0.740	0.753	0.002	0.362	0.632	0.713	0.876	0.857	0.825	0.803
	0.6	0.680	0.684	0.731	0.719	0.002	0.347	0.602	0.680	0.872	0.852	0.811	0.779
	0.8	0.676	0.651	0.643	0.610	0.002	0.305	0.509	0.569	0.861	0.840	0.772	0.691
50	Ext.	0.779	0.792	0.818	0.830	0.297	0.495	0.707	0.781	0.932	0.921	0.895	0.878
	0.2	0.777	0.779	0.795	0.802	0.303	0.485	0.680	0.753	0.929	0.918	0.886	0.862
	0.4	0.777	0.774	0.786	0.790	0.304	0.482	0.670	0.742	0.928	0.916	0.883	0.856
	0.6	0.775	0.765	0.765	0.760	0.307	0.476	0.648	0.716	0.925	0.914	0.876	0.842
	0.8	0.772	0.745	0.711	0.666	0.315	0.457	0.579	0.622	0.919	0.907	0.855	0.783
60	Ext.	0.851	0.852	0.861	0.867	0.506	0.593	0.735	0.808	0.974	0.970	0.951	0.929
	0.2	0.850	0.844	0.844	0.844	0.511	0.589	0.717	0.786	0.973	0.969	0.949	0.924
	0.4	0.849	0.842	0.837	0.835	0.512	0.588	0.711	0.778	0.973	0.969	0.948	0.922
	0.6	0.848	0.836	0.823	0.811	0.515	0.586	0.698	0.760	0.972	0.968	0.947	0.917
	0.8	0.846	0.824	0.784	0.734	0.522	0.581	0.655	0.689	0.971	0.966	0.943	0.902

Table 5.5: Tabulated values of the ratio $\bar{f}_{i\infty}/\bar{f}_{io\infty}$ for different azimuthal angles; $p = 0.3$, $g = 0.0$

ϕ	$\bar{D}_f$	Values of the ratio $\bar{f}_{i\infty}/\bar{f}_{io\infty}$											
		March				June				December			
		$\gamma = 0^o$	30^o	60^o	90^o	$\gamma = 0^o$	30^o	60^o	90^o	$\gamma = 0^o$	30^o	60^o	90^o
20	0.2	0.970	0.929	0.946	0.950	—	0.834	0.931	0.946	0.982	0.974	0.960	0.954
	0.4	0.960	0.903	0.924	0.928	—	0.769	0.902	0.924	0.975	0.965	0.944	0.935
	0.6	0.939	0.844	0.873	0.875	—	0.617	0.832	0.869	0.961	0.945	0.908	0.887
	0.8	0.899	0.701	0.728	0.709	—	0.218	0.617	0.693	0.931	0.901	0.810	0.733
25	0.2	0.986	0.942	0.949	0.951	—	0.856	0.934	0.948	0.986	0.982	0.965	0.958
	0.4	0.981	0.921	0.929	0.931	—	0.802	0.907	0.926	0.981	0.975	0.951	0.940
	0.6	0.970	0.874	0.882	0.880	—	0.683	0.842	0.873	0.971	0.961	0.920	0.896
	0.8	0.951	0.763	0.751	0.719	—	0.363	0.646	0.702	0.947	0.930	0.835	0.751
30	0.2	0.991	0.954	0.953	0.954	—	0.888	0.938	0.950	0.989	0.987	0.970	0.962
	0.4	0.988	0.937	0.935	0.934	—	0.847	0.913	0.929	0.986	0.982	0.958	0.946
	0.6	0.982	0.901	0.892	0.885	—	0.760	0.855	0.879	0.977	0.972	0.932	0.906
	0.8	0.970	0.817	0.775	0.732	—	0.521	0.677	0.714	0.959	0.949	0.861	0.773
40	0.2	0.996	0.973	0.962	0.959	1.034	0.947	0.948	0.956	0.994	0.993	0.980	0.971
	0.4	0.994	0.963	0.947	0.942	1.044	0.929	0.928	0.938	0.992	0.990	0.973	0.959
	0.6	0.991	0.942	0.914	0.899	1.063	0.892	0.884	0.895	0.987	0.984	0.957	0.930
	0.8	0.985	0.895	0.823	0.763	1.111	0.784	0.746	0.748	0.975	0.971	0.910	0.826
50	0.2	0.997	0.984	0.971	0.966	1.018	0.980	0.961	0.964	0.997	0.996	0.990	0.982
	0.4	0.996	0.978	0.960	0.952	1.023	0.973	0.947	0.950	0.996	0.995	0.987	0.975
	0.6	0.994	0.967	0.935	0.916	1.033	0.961	0.916	0.917	0.993	0.992	0.979	0.959
	0.8	0.991	0.941	0.869	0.802	1.059	0.923	0.819	0.796	0.987	0.984	0.955	0.892
60	0.2	0.998	0.991	0.980	0.974	1.010	0.994	0.975	0.973	0.999	0.999	0.998	0.994
	0.4	0.997	0.988	0.972	0.963	1.013	0.993	0.966	0.963	0.999	0.999	0.997	0.992
	0.6	0.996	0.981	0.955	0.935	1.019	0.989	0.948	0.940	0.998	0.998	0.996	0.987
	0.8	0.993	0.967	0.910	0.847	1.033	0.980	0.891	0.852	0.997	0.996	0.992	0.970

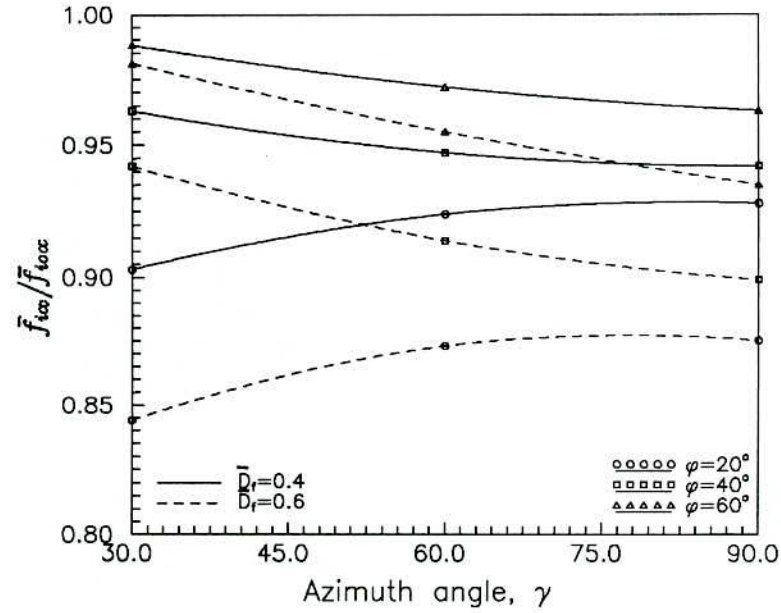

Figure 5.15: Variation of $(\bar{f}_{i\alpha}/\bar{f}_{i\alpha\infty})$ with γ for the month of March; $w = 1.0$, $p = 0.3$, $g = 0.0$ and $\bar{D}_f = 0.4$ and 0.6

.

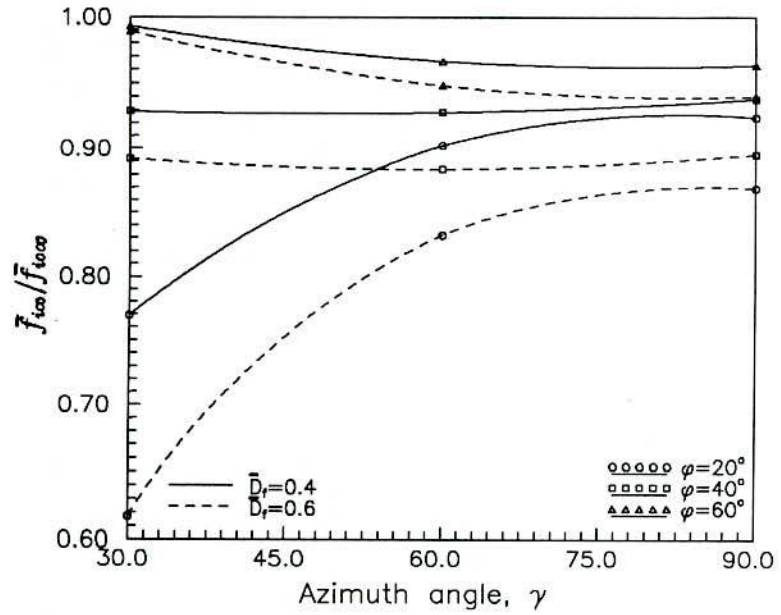

Figure 5.16: Variation of $(\bar{f}_{i\alpha}/\bar{f}_{i\alpha\infty})$ with γ for the month of June; $w = 1.0$, $p = 0.3$, $g = 0.0$ and $\bar{D}_f = 0.4$ and 0.6

.

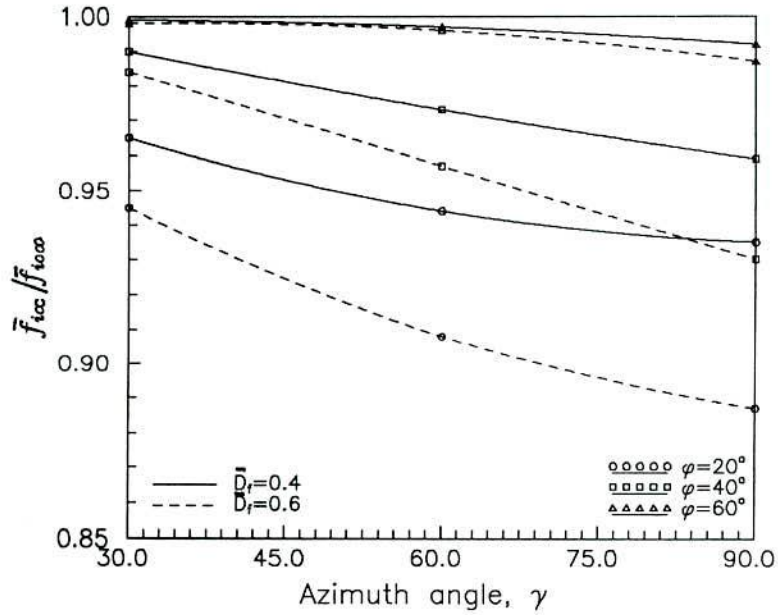

Figure 5.17: Variation of $(\bar{f}_{i\alpha}/\bar{f}_{i\alpha\infty})$ with γ for the month of December; $w = 1.0$, $p = 0.3$, $g = 0.0$ and $\bar{D}_f = 0.4$ and 0.6

.

for finite overhangs from the values for the infinite overhangs, is examined in this section. $\bar{f}_i$ has been calculated numerically by hour by hour summation, using Eq. (5.8), designated as $\bar{f}_i$(num), for $\phi = 25°$, $30°$, $40°$, $50°$ and $60°$ for all the 12 months, $w = 1.0$, $g = 0.0$, $p = 0.2$, 0.3, 0.4 and 0.5, and $e = 0.0$, 0.2, 0.4, 0.6 and 0.8, and $\bar{D}_f = 0.2$, 0.4 and 0.6. $\bar{f}_{i\infty}$ values have been obtained using Eq. (5.34) for the same parameters. $\bar{f}_i$ has been predicted using Eqs. (5.55) and (5.56) along with the constants given in Table 5.1. When $\bar{f}_{i\infty} = 0.0$, $\bar{f}_i$ designated as $\bar{f}_i^o$ has been predicted using Eq. (5.61).

Plots of $\bar{f}_i$ predicted using the aforementioned equations developed in the present study vs $\bar{f}_i$(num) are shown in Figures 5.18, 5.19 and 5.20 for $\bar{D}_f = 0.2$, 0.4 and 0.6 for $\gamma = 0°$. The rms differences are respectively 1.72 %, 1.62 % and 1.63 %, which are comparable and low. Thus, even though Eq. (5.55) and other equations have been developed for $\bar{D}_f = 0.4$, the equations are equally valid for other diffuse fraction values as well, since $\bar{f}_{i\infty}$, the predictor in Eq. (5.55), is a function of diffuse fraction. Thus, the shading factor values for south facing receivers can be calculated under terrestrial conditions for finite overhangs from the easily calculable infinite overhang shading factor values.

The performance of the single equation [Eq. (5.57)] developed for all projections is depicted in Figure 5.21 for the aforementioned parameters for $\bar{D}_f = 0.6$. The rms difference is 2.0 %, which is not significantly higher compared to 1.63 % when different equations for

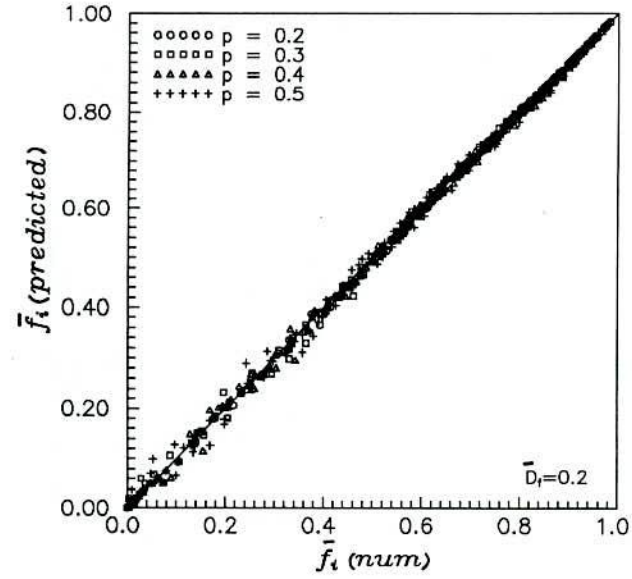

Figure 5.18: Validation of $\bar{f}_i$(predicted) against $\bar{f}_i$(num) for $\bar{D}_f = 0.2$; $w = 1.0$, $g = 0.0$, $\gamma = 0^o$

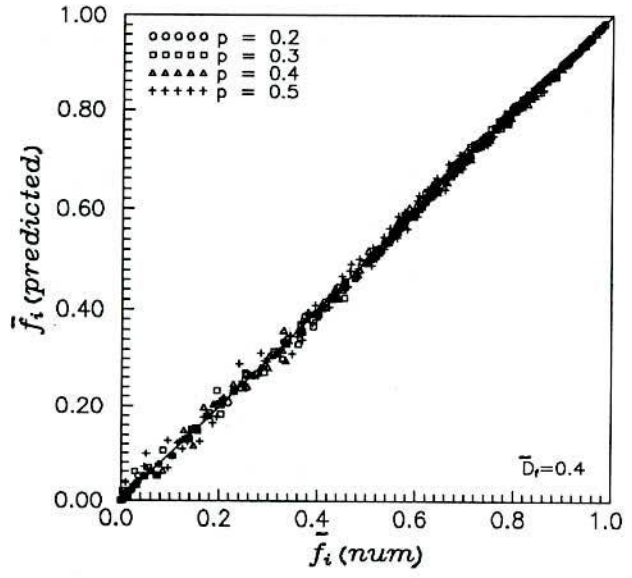

Figure 5.19: Validation of $\bar{f}_i$ (predicted) against $\bar{f}_i$(num) for $\bar{D}_f = 0.4$; $w = 1.0$, $g = 0.0$, $\gamma = 0^o$

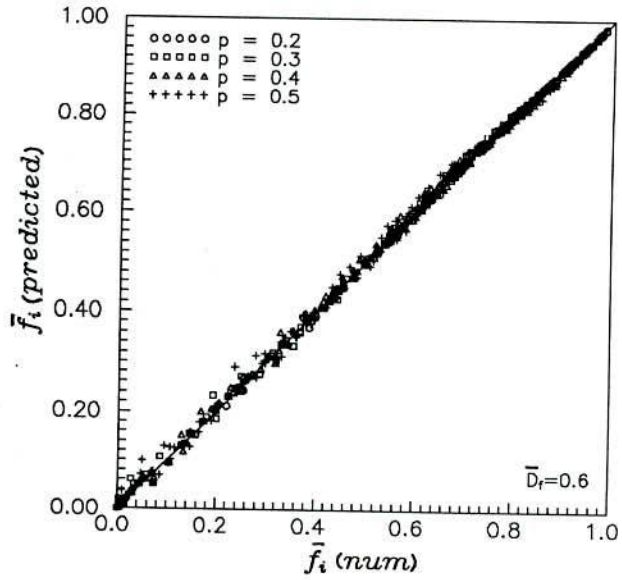

Figure 5.20: Validation of $\bar{f}_i$(predicted) against $\bar{f}_i$(num) for $\bar{D}_f = 0.6$; $w = 1.0$, $g = 0.0$, $\gamma = 0^o$

different projections and extensions have been used. Thus, at a panality of only 0.4 % (rms), shading factor values for south facing overhangs can be predicted using Eq. (5.57), valid for $p = 0.2$ to 0.5, $e = 0.0$ to 0.8. Of course, when $e \geq 1.0$, $\bar{f}_{i\infty}$ values can be used for $\bar{f}_i$ with insignificant difference.

Non-south Facing Receivers:

The procedure suggested in the present study in §5.6 to obtain the shading factor values for non-south facing receivers shaded by finite overhangs is tested by first obtaining $\bar{f}_i$(num) values according to Eq. (5.8) for $\gamma = 30^o$ 60^o and 90^o and then comparing with the values as obtained from Eq. (5.68), designated as $\bar{f}_i$(predicted). It may be noted that $\bar{f}_{i1}$ and $\bar{f}_{i2}$ values needed in Eq. (5.68) are obtained as mentioned in §5.6, from Eq. (5.71) using the same values for M and N (Table 5.1) developed for south facing receivers. $\bar{f}_{i\infty 1,2}$ needed in Eq. (5.71) are obtained using Eqs. (5.73) and (5.74).

Plots of $\bar{f}_i$(predicted) vs $\bar{f}_i$(num) for $\gamma = 30^o$, 60^o and 90^o are shown in Figures 5.22, 5.23 and 5.24. Values of the other parameters are: $\phi = 25^o$, 30^o, 40^o, 50^o and 60^o, $p = 0.2$, 0.3, 0.4 and 0.5 for all 12 months. Compared to $\bar{f}_i$(num), $\bar{f}_i$ is predicted within a rms difference of 2.42 %, 3.65 % and 4.78 % for $\gamma = 30^o$, 60^o and 90^o respectively. Though, these rms differences are not large, they are larger than those for south facing receivers, predicted with even the single equation [Eq. (5.57)] for all projections and extensions.

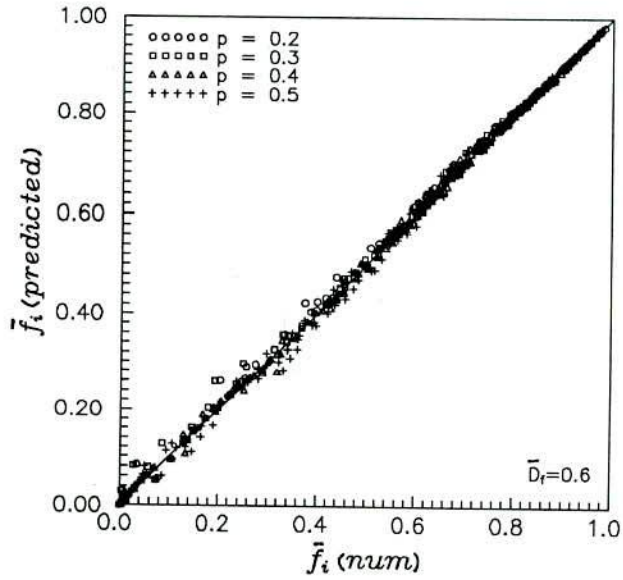

Figure 5.21: Validation of $\bar{f}_i$(predicted) against $\bar{f}_i$(num) for $\bar{D}_f = 0.6$; $w = 1.0$, $g = 0.0$, $\gamma = 0^o$ [from Eq.(5.60)]

Also, the agreement deteriorates as γ increases. A detailed examination on this agreement revealed, that, in general the agreement deteriorates as the projection and azimuthal angle increase. Also, a detailed examination of the agreement between the predicted and the actual part values, i.e., during the two intervals ω_{sr} to ω_o and ω_o to ω_{ss} revealed the same information. The rms differences between $\bar{f}_i$(predicted) and $\bar{f}_i$(num) [the comparisons shown in Figures 5.22 to 5.24 are for $\gamma = 30^o$, 60^o and 90^o respectively] for $p = 0.2$ (only) are respectively 1.53 %, 2.12 % and 2.56 % for $\gamma = 30^o$, 60^o and 90^o. Thus, it is considered that the procedure described in §5.6 to predict $\bar{f}_i$ for non-south facing surfaces from the corresponding values of $\bar{f}_{i\infty}$ is valid for low p, say, upto $p = 0.2$. In what follows a simple procedure to predict $\bar{f}_i$ for higher values of the projection from the values at $p = 0.2$ is described.

Procedure to obtain $\bar{f}_i$ for a desired projection from known values for a particular projection: Consider the finite overhang and the window causing a shadow line $\bar{Y}_1$ from the top edge of the window. The theme is dipicted in Figure 5.25. Let the lit area comprise of $(A_{\infty 1} + A_{f1})$. It is assumed that $A_{\infty 1}$ and $(A_{\infty 1} + A_{f1})$ are the equivalent lit areas corresponding to $\bar{f}_{i\infty p1}$ and $\bar{f}_{ip1}$ at a projection p_1. At another projection, say, p_2, let $\bar{f}_{i\infty p2}$ be the shading factor value when the overhang is infinite. Let $\bar{Y}_2$ be the distance from the top edge of the window to the shadow line caused by an infinite overhang of projection p_2. The objective is to obtain $\bar{f}_{ip2}$ corresponding to p_2 from $\bar{f}_{i\infty p1}$, $\bar{f}_{ip1}$ and

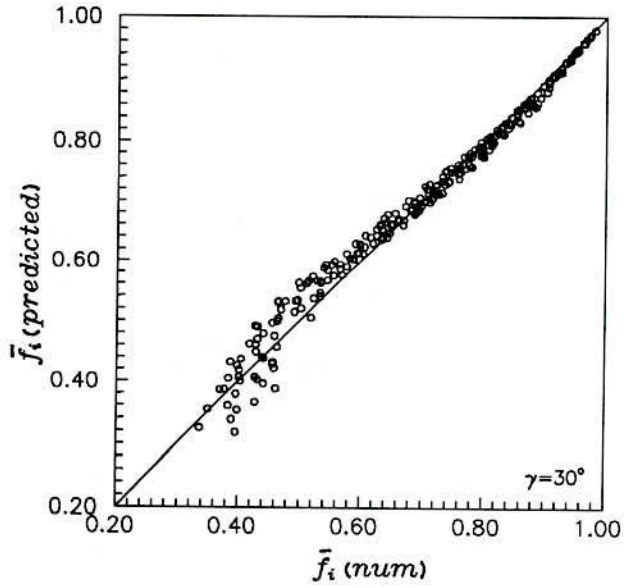

Figure 5.22: Validation of $\bar{f}_i$(predicted) against $\bar{f}_i$(num) for $\bar{D}_f = 0.4$; $w = 1.0$, $0.2 \leq p \leq 0.5$, $g = 0.0$, $\gamma = 30^o$

.

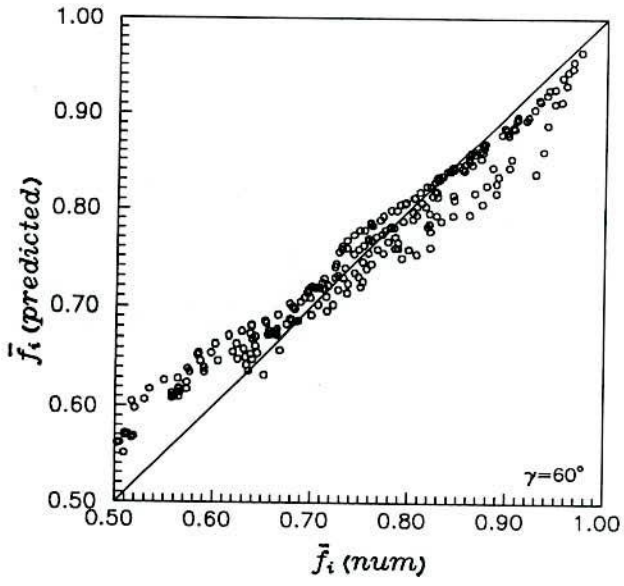

Figure 5.23: Validation of $\bar{f}_i$(predicted) against $\bar{f}_i$(num) for $\bar{D}_f = 0.4$; $w = 1.0$, $0.2 \leq p \leq 0.5$, $g = 0.0$, $\gamma = 60^o$

.

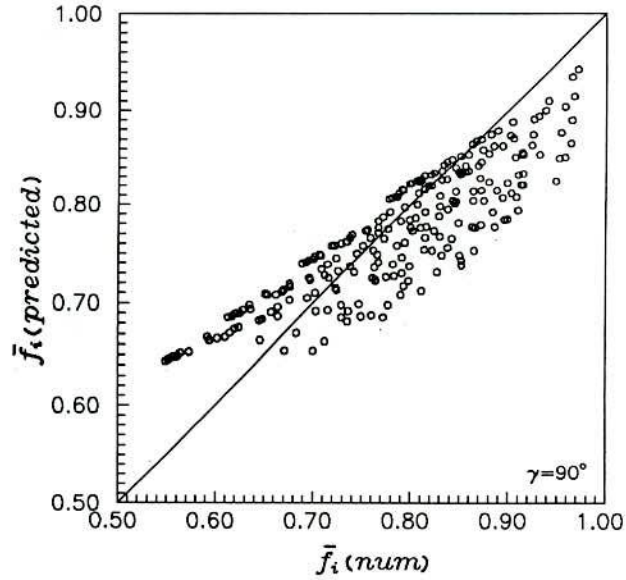

Figure 5.24: Validation of $\bar{f}_i$(predicted) against $\bar{f}_i$(num) for $\bar{D}_f = 0.4$; $w = 1.0$, $0.2 \leq p \leq 0.5$, $g = 0.0$, $\gamma = 90^o$

.

$\bar{f}_{i\infty p2}$. It may be noted that $\bar{f}_{i\infty p1}$ and $\bar{f}_{i\infty p2}$ can be easily calculated from Eq. (5.33) and $\bar{f}_{ip1}$ is predicted by following the procedure of §5.6.

From Figure 5.25, within the frame work of the assumptions made,

$$\bar{f}_{i\infty p1} = \frac{(H_w - Y_1)W}{H_w W} = 1 - \frac{Y_1}{H_w} \tag{5.84}$$

$$\bar{f}_{ip1} = \frac{(H_w - Y_1)W + A_{f1}}{H_w W} = \bar{f}_{i\infty p1} + \frac{A_{f1}}{H_w W} \tag{5.85}$$

Solving for A_{f1},

$$A_{f1} = \bar{f}_{ip1} H_w W - \bar{f}_{i\infty p1} H_w W \tag{5.86}$$

X_1 shown in Figure 5.25 is now given by,

$$X_1 = \frac{2\,W(\bar{f}_{ip1} - \bar{f}_{i\infty p1})}{(1 - \bar{f}_{i\infty p1})} \tag{5.87}$$

Similar to Eq. (5.84), $\bar{f}_{i\infty p2}$ is given by,

$$\bar{f}_{i\infty p2} = 1 - \frac{Y_2}{H_w} \tag{5.88}$$

From Eqs. (5.84) and (5.88),

$$Y_2 - Y_1 = H_w\,(\bar{f}_{i\infty p1} - \bar{f}_{i\infty p2}) \tag{5.89}$$

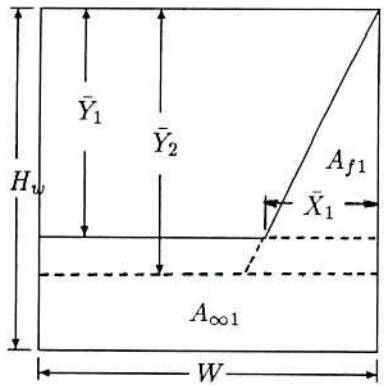

Figure 5.25: Effective shaded areas of window when shaded by finite overhangs of two projections

$\bar{f}_{ip2}$ from geometry is given by,

$$\bar{f}_{ip2} = \frac{(H_w - Y_2)W + A_{f1} + X_1(Y_2 - Y_1)}{H_w W} \tag{5.90}$$

In writing Eq. (5.90) the additional shaded area for the projection p_2 is assumed to be given by $X_1(Y_2 - Y_1)$. Using Eq. (5.86) for A_{f1}, Eq. (5.87) for X_1 and Eq. (5.89) for $(Y_2 - Y_1)$, in Eq. (5.90) $\bar{f}_{ip2}$ can be obtained from,

$$\bar{f}_{ip2} = \bar{f}_{i\infty p2} + (\bar{f}_{ip1} - \bar{f}_{i\infty p1}) \left[\frac{2\,(\bar{f}_{i\infty p1} - \bar{f}_{i\infty p2})}{(1 - \bar{f}_{i\infty p1})}\right] \tag{5.91}$$

Validation of Eq. (5.91):

From the values of $\bar{f}_i$ at $p = 0.2$, values of $\bar{f}_i$ for $p = 0.3$, 0.4 and 0.5 have been obtained using Eq. (5.91). It may be noted that $\bar{f}_i$ at $p = 0.2$ has been calculated using Eq. (5.71) along with the correlations developed for south facing surfaces relating the finite overhang values to the infinite values. $\bar{f}_i$ for $p = 0.3$, 0.4 and 0.5 have been calculated for $\phi = 25^o$, 30^o, 40^o, 50^o and 60^o, for all 12 months, for $\bar{D}_f = 0.4$, $w = 1.0$, $g = 0.0$ and $e = 0.0$. The comparison between $\bar{f}_i$(num) obtained using Eq. (5.8) and $\bar{f}_i$(predicted) using Eq. (5.91) is shown in Figures 5.26, 5.27 and 5.28 for $\gamma = 30^o$, 60^o and 90^o respectively. Now, the agreement is within 0.7 % rms for all the azimuthal angles considered. It is interesting to note that Eq. (5.91) developed based on gross average worked well in predicting the shading factor values for non-south facing receivers shaded by finite overhangs. Of course, Eq. (5.91) calls for the value of $\bar{f}_i$ at some projection. It is recommended that this input

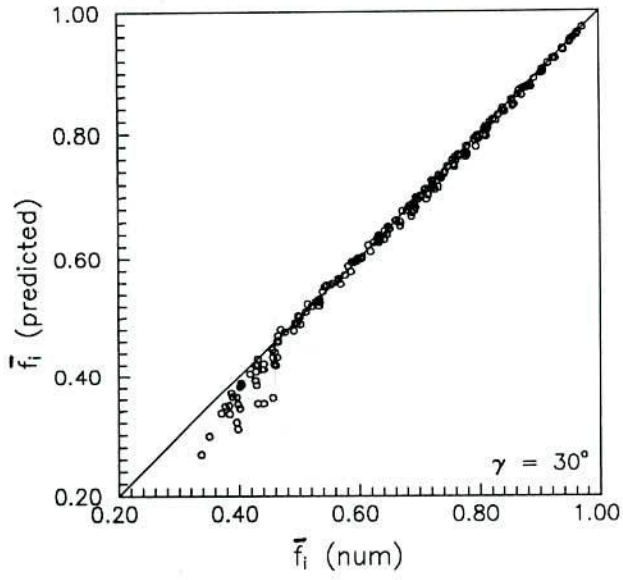

Figure 5.26: Comparison of $\bar{f}_i$(predicted) with $\bar{f}_i$(num) for $\bar{D}_f = 0.4$; $w = 1.0$, $p = 0.3$, 0.4 and 0.5, $g = 0.0$, $\gamma = 30^o$

information is obtained for a low projection say, $p = 0.2$ since the procedure developed in §5.6 for non-south facing receivers yields values within a rms error of 2.5 % for low p.

It may be noted that some deviation can be noticed in Figure 5.26 for low values of $\bar{f}_i$ which have been traced to belong to $\phi < 25^o$ and the extreme declination, $\delta = 23.09^o$. It may be noted that for low latitudes and high positive declinations the sunshine duration itself is low.

5.7.3 Comparison against Other Methods and Values obtained using Solar Radiation Data

Infinite Overhangs

$\bar{f}_{i\infty}$ values have been calculated following Utzinger and Klein's [125] procedure (under extra-terrestrial conditions) as well as using Eq. (5.34) for four locations [3 Indian locations, New Delhi ($\phi = 28.58^o$), Ahmedabad ($\phi = 23.08$) and Trivandrum ($\phi = 8.48^o$) and one US location, Madison, WI ($\phi = 43.10^o$)] for all 12 months. The data have been taken from [132] for Indian locations and the TMY data supplied with TRNSYS, Version 12.1 [133] for Madison, WI. The values obtained using Utzinger and Klein's procedure have been designated as $\bar{f}_{i\infty}$(U&K). $\bar{f}_{i\infty}$ values, designated as $\bar{f}_{i\infty}$(data), have been obtained using Eq. (5.8) by employing hour by hour solar radiation data. Values of the other parameters are: $\gamma = 0^o$, 30^o, 60^o and 90^o, $\rho = 0.3$.

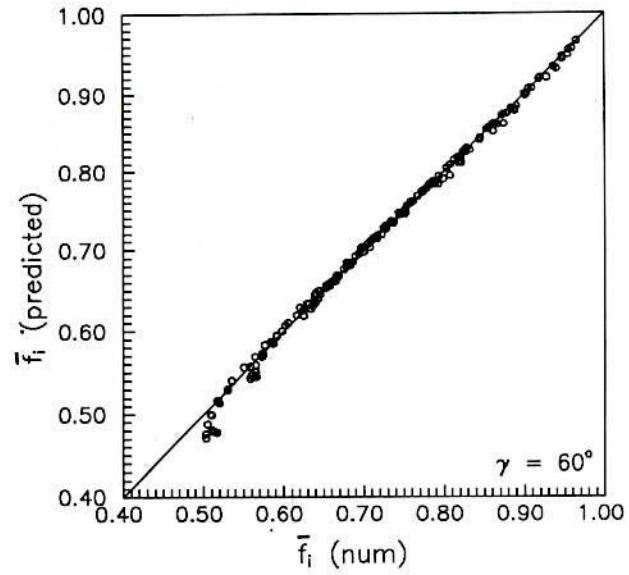

Figure 5.27: Comparison of $\bar{f}_i$(predicted) with $\bar{f}_i$(num) for $\bar{D}_f = 0.4$; $w = 1.0$, $p = 0.3$, 0.4 and 0.5, $g = 0.0$, $\gamma = 60^o$

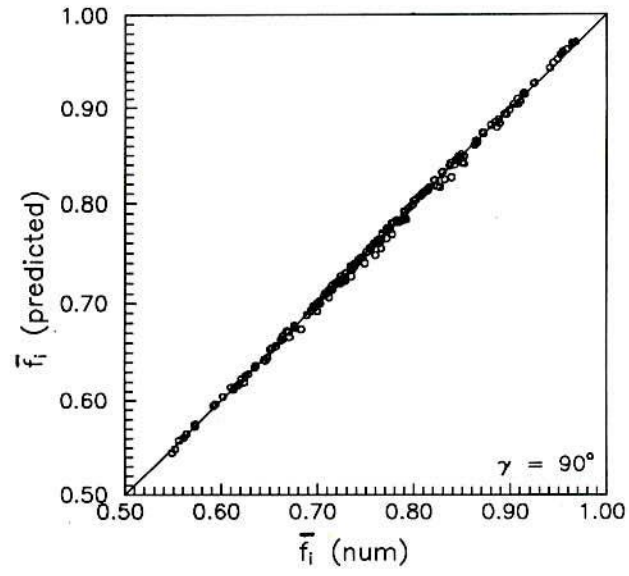

Figure 5.28: Comparison of $\bar{f}_i$(predicted) with $\bar{f}_i$(num) for $\bar{D}_f = 0.4$; $w = 1.0$, $p = 0.3$, 0.4 and 0.5, $g = 0.0$, $\gamma = 90^o$

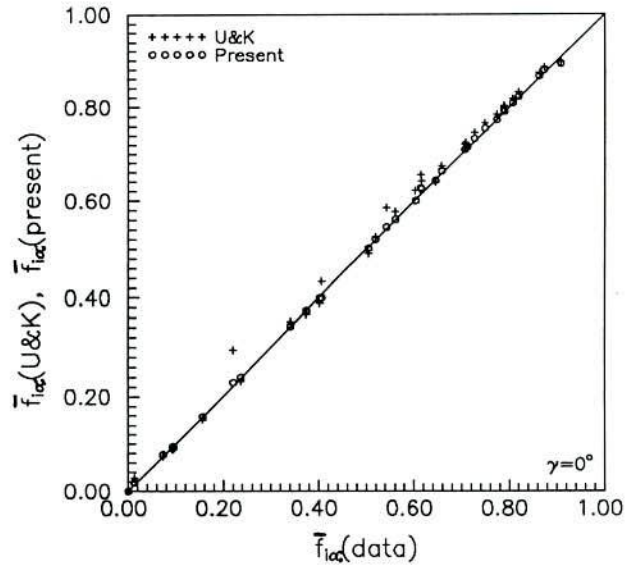

Figure 5.29: Comparison of $\bar{f}_{i\infty}$(U&K) and $\bar{f}_{i\infty}$(present) with $\bar{f}_{i\infty}$(data); $w = 1.0$, $p = 0.3$, $g = 0.0$, $\gamma = 0^o$

Plots of $\bar{f}_{i\infty}$(U&K), $\bar{f}_{i\infty}$(present) vs $\bar{f}_{i\infty}$(data) are shown in Figures 5.29 to 5.32 for $\gamma = 0^o$, 30^o, 60^o and 90^o respectively. $\bar{f}_{i\infty}$(present) values are always closer to $\bar{f}_{i\infty}$(data). The rms differences between $\bar{f}_{i\infty}$(present) and $\bar{f}_{i\infty}$(data) are respectively 1.16 %, 4.31 %, 4.26 % and 4.32 % for $\gamma = 0^o$, 30^o, 60^o and 90^o. The corresponding differences between $\bar{f}_{i\infty}$(U&K) and $\bar{f}_{i\infty}$(data) are 4.68 %, 14.22 %, 11.70 % and 9.92 %. This indicates that diffuse fraction effect needs to be taken in to account for non-south facing receivers.

Finite Overhangs

Similar plots for finite overhangs with $e = 0.0$ and 0.4 are shown in Figures 5.33 to 5.36. It may be noted that $\bar{f}_i$(U&K) is the value for the finite overhangs obtained under extra-terrestrial conditions following Utzinger and Klein [125]. $\bar{f}_i$(present) values are obtained using the equations developed in the present study. $\bar{f}_i$(data) are the shading factor values for the four locations obtained employing hour by hour solar radiation data using Eq. (5.8). The rms differences between $\bar{f}_i$(present) and $\bar{f}_i$(data) are 1.31 %, 4.46 %, 4.62 % and 4.68 % for $\gamma = 0^o$, 30^o, 60^o and 90^o. The corresponding differences between $\bar{f}_i$(U&K) and $\bar{f}_i$(data) are 4.97 %, 10.68 %, 9.64 % and 8.76 %. It may be noted that the rms differences for finite overhangs, when the equations developed in the present study are used, are slightly higher than those for infinite overhangs. This is due to, though not significant, the correlations developed in the present study being used to obtain $\bar{f}_i$ from $\bar{f}_{i\infty}$. For finite overhangs

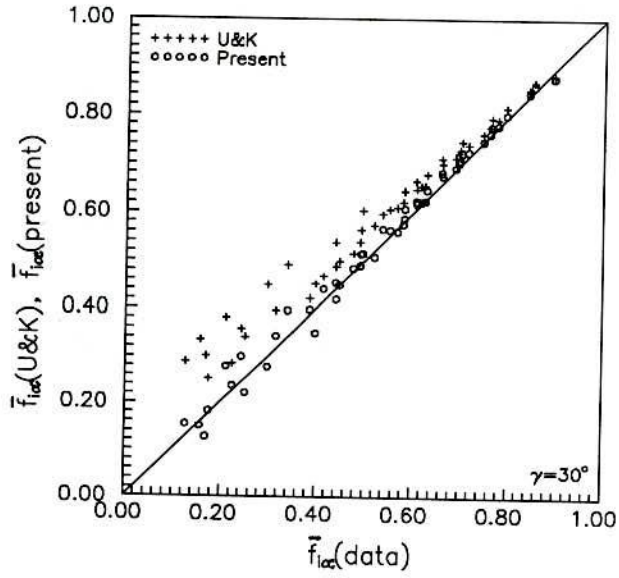

Figure 5.30: Comparison of $\bar{f}_{i\infty}$(U&K) and $\bar{f}_{i\infty}$(present) with $\bar{f}_{i\infty}$(data); $w = 1.0, p = 0.3$, $g = 0.0, \gamma = 30^o$

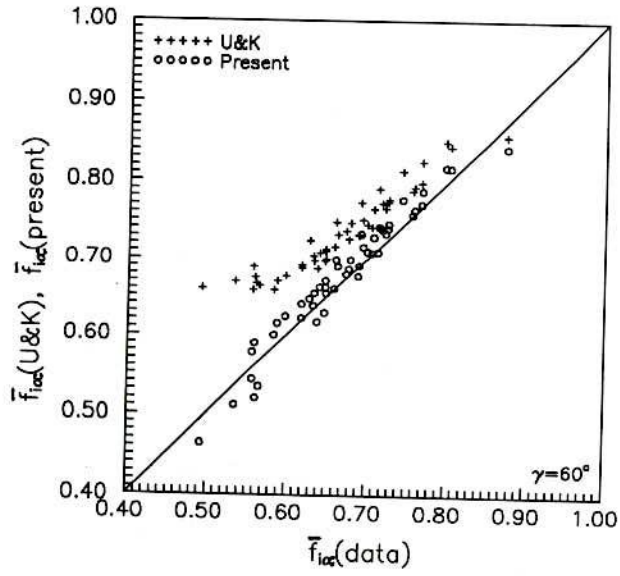

Figure 5.31: Comparison of $\bar{f}_{i\infty}$(U&K) and $\bar{f}_{i\infty}$(present) with $\bar{f}_{i\infty}$(data); $w = 1.0, p = 0.3$, $g = 0.0, \gamma = 60^o$

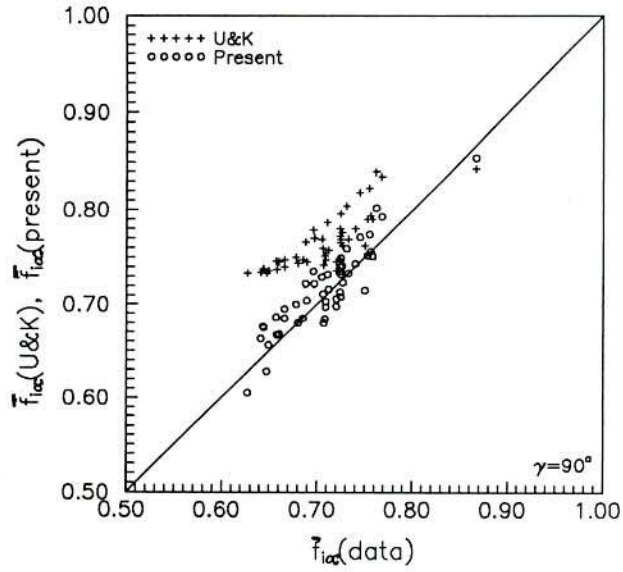

Figure 5.32: Comparison of $\bar{f}_{i\infty}$(U&K) and $\bar{f}_{i\infty}$(present) with $\bar{f}_{i\infty}$(data); $w = 1.0, p = 0.3$, $g = 0.0, \gamma = 90^o$

.

also, calculations under extra-terrestrial conditions according to Utzinger and Klein [125] yield values which differ from the data values. This deviation is higher for higher γ. Thus, monthly average daily diffuse fraction needs to be taken into account in calculating the shading factors for non-south facing receivers.

5.8 Conclusions

Expressing the monthly average shading factor for receivers shaded by infinite overhangs as an integral, on evaluating the integral, it has been shown that the resulting expressions are a statement of the equivalence with the shading plane concept of Jones [126]. This procedure enabled generalization for non-vertical receivers. An examination of the expressions for $\bar{f}_{i\infty}$ show that it depends on the monthly average daily diffuse fraction and the dependence is similar to the dependence of $\bar{R}_b$ on the monthly average daily diffuse fraction.

For south facing surfaces, shading factor values for infinite overhangs under terrestrial and extra-terrestrial conditions coincide when $\delta = 0$. $\bar{f}_{i\infty} > \bar{f}_{io\infty}$ when $\delta > 0$ and $\bar{f}_{i\infty} < \bar{f}_{io\infty}$ when $\delta < 0$ for south facing receivers.

A procedure has been developed to calculate the monthly average shading factor

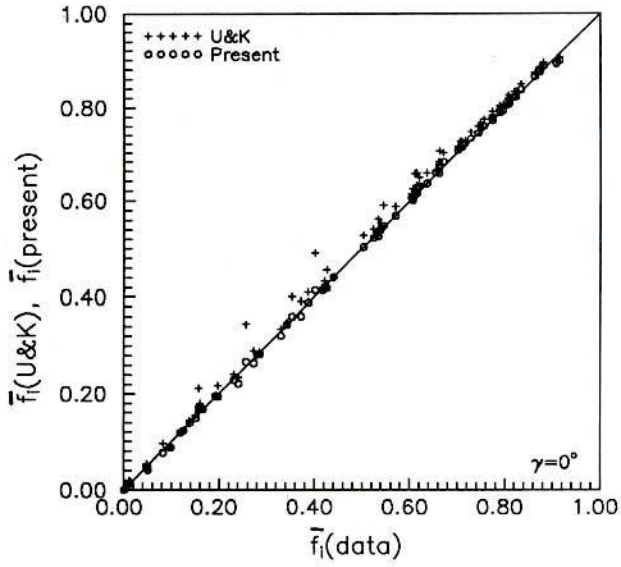

Figure 5.33: Comparison of $\bar{f}_i$(U&K) and $\bar{f}_i$(present) with $\bar{f}_i$(data); $w = 1.0$, $p = 0.3$, $e = 0$ and 0.4, $g = 0.0$, $\gamma = 0^o$

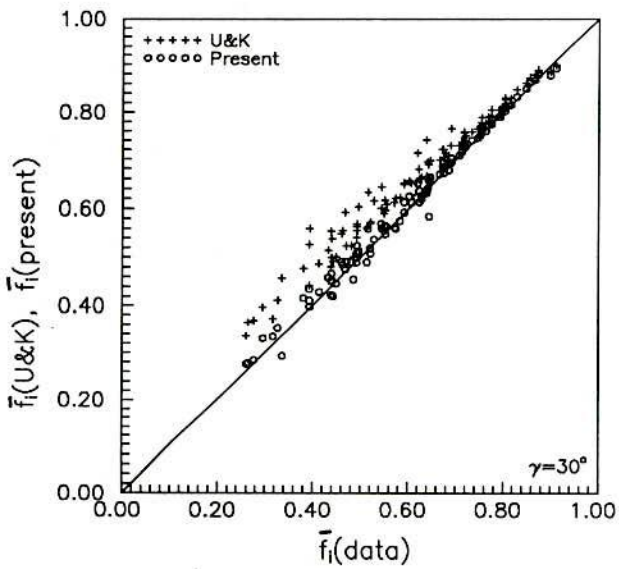

Figure 5.34: Comparison of $\bar{f}_i$(U&K) and $\bar{f}_i$(present) with $\bar{f}_i$(data); $w = 1.0$, $p = 0.3$, $e = 0$ and 0.4, $g = 0.0$, $\gamma = 30^o$

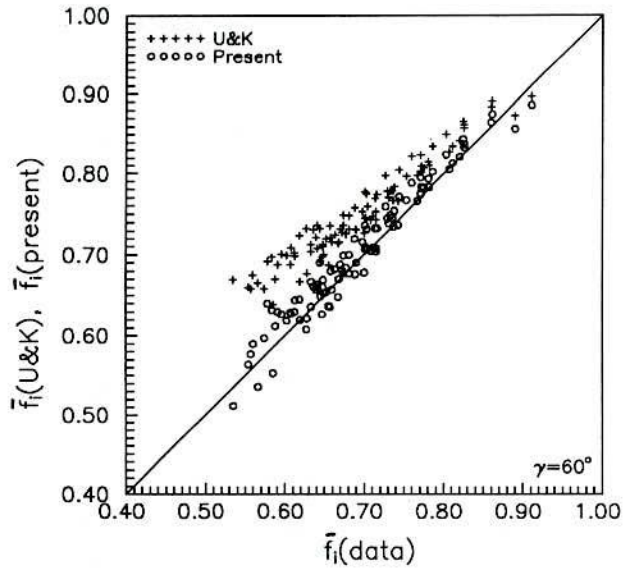

Figure 5.35: Comparison of $\bar{f}_i$(U&K) and $\bar{f}_i$(present) with $\bar{f}_i$(data); $w = 1.0$, $p = 0.3$, $e = 0$ and 0.4, $g = 0.0$, $\gamma = 60^o$

.

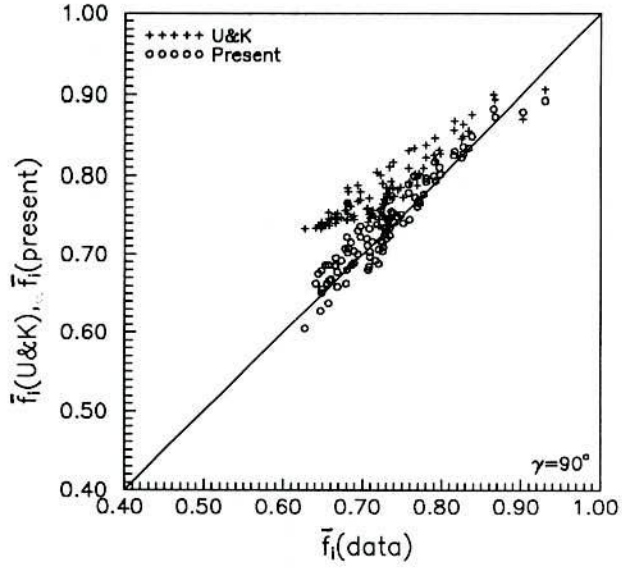

Figure 5.36: Comparison of $\bar{f}_i$(U&K) and $\bar{f}_i$(present) with $\bar{f}_i$(data); $w = 1.0$, $p = 0.3$, $e = 0$ and 0.4, $g = 0.0$, $\gamma = 90^o$

.

for finite overhangs under terrestrial conditions by developing correlations between the finite and infinite shading factor values. This procedure takes advantage of the simplicity in calculating the shading factors for infinite overhangs and the equations developed are linear for a given e and p. Such equations have been applied and validated for non-south facing receivers as well by splitting the duration of sunshine into two time intervals; from apparent sunrise hour angle to ω_o (ω corresponding to $\gamma_d = 0$) and from ω_o to apparent sunset hour angle. The procedure developed to predict the shading factor for finite overhangs for a desired projection from the value for a lower projection (say, $p = 0.2$) is simple and accurate for all γ.

Shading factor values calculated under terrestrial conditions compared to the values obtained under extra-terrestrial conditions typically differ by 5 % for south facing receivers and differences of even 15 % occur when $\bar{D}_f = 0.4$ to 0.6. In general, the percentage differences are higher at lower latitudes. For non-south facing surfaces, as γ increases, the difference between $\bar{f}_{io\infty}$ and $\bar{f}_{i\infty}$ increases. Of course, for finite overhangs also the difference between $\bar{f}_{io}$ and $\bar{f}_i$ increases as γ increases.

Values of the shading factors for infinite as well as finite overhangs obtained following Utzinger and Klein's [125] procedure and the present approach (under terrestrial conditions) have been compared with the values obtained following numerical integration using hour by hour solar radiation data for four locations. Shading factor values obtained by the present approach are always closer to the data values and the rms difference is within 1.5 % to 5 % as γ increases from 0^o to 90^o.

Chapter 6

Evaluation of Monthly Average Shading Factor for Surfaces Shaded by Wingwalls under Terrestrial Conditions

6.1 Introduction

Studies pertaining to evaluation of monthly average shading factor for receivers of general orientation by infinite and finite overhangs, taking into account atmospheric transmittance, have been described in Chapter 5. Windows in general, are provided with vertical projections (commonly referred to as wingwalls) on either sides for reasons of shading, as well as, for architectural aesthetics. Similar to overhangs, wingwalls also cast a shadow on the receiver and the sunlit area depends on the sun's position and the orientation of the receiver. The edge of the shadow, caused by a wingwall, is a vertical line on the receiver, whereas, due to an overhang it is a horizontal line. Studies available in the literature on estimating the solar radiation received by surfaces shaded by wingwalls are far less compared to the studies on overhangs.

Sun's algorithm [114] provides a method to obtain the instantaneous shading factor for surfaces shaded by wingwalls. Studies on monthly average shading factor due to wingwalls in conjunction with the overhang which is commonly referred to as egg-crate structures have been reported by Barozzi and Grossa [129]. Another study by Delsante and Spencer [130] dealt with the estimation of the proportion of sky seen by windows shaded by horizontal or vertical projections which can be used to calculate the diffuse radiation incident on the shaded window. Thus, studies to estimate monthly average shading factor for wingwalls to be associated with the direct radiation and the influence of projection and the receiver orientation are not available in the literature.

In the present study, it is assumed that the wingwalls are infinite in the vertical direction. Even when the wingwalls are finite, this assumption practically yields acceptable results since extensions below the window do not cause or prevent a shadow on the receiver and at the top of the window, generally, an overhang exists which prevents solar radiation entering from the top analogous to side entry of solar radiation when the overhang is finite. Also, in the case of multi-storied tall structures, wingwalls continue throughout the height of the building. The present chapter is devoted to develop a method to estimate the monthly average shading factor for surfaces of general azimuthal angle shaded by infinite wingwalls under terrestrial conditions. Atmospheric transmittance (or clearness index) appears as a parameter through monthly average daily diffuse fraction.

6.2 Basic Geometry and Shading Factor

The basic geometry of a vertical wingwall-shaded receiver (window) of height, H_w and width, W is shown in Figure 6.1. The slope of the vertical receiver, β is equal to 90^o and the azimuthal angle of the receiver is γ. Two vertical wingwalls, perpendicular to the receiver, with projections P_1 and P_2 (usually, $P_1 = P_2$) also are shown in Figure 6.1. The wingwalls are separated from the sides of the window by a gap G. The wingwalls extend in the vertical direction by E from the top of the window. The non-dimensional width w, projections p_1 and p_2, gap g and extensions e are obtained by referring the dimensional quantities to the height of the window. Thus,

$$w = \frac{W}{H_w}, \qquad p_1 = \frac{P_1}{H_w}, \qquad p_2 = \frac{P_2}{H_w}, \qquad g = \frac{G}{H_w} \qquad \text{and} \qquad e = \frac{E}{H_w} \tag{6.1}$$

If A_i is the irradiated area of the window and A_s is the shaded area of the window caused by the wingwalls, the shading factor at any instant, f_i, is given by,

$$f_i = \frac{A_i}{A_w} = 1 - \frac{A_s}{A_w} \tag{6.2}$$

where, A_w $(=H_w W)$ is the window area and $A_w = (A_i + A_s)$.

The solar radiation over a small period of time (say, 1-hr) per unit receiver area, I_s, analogous to Eq. (5.3) is expressed as,

$$\begin{aligned} I_s &= I_{bs} + I_{ds} \\ &= I_b R_b f_i + I_{ds} \end{aligned} \tag{6.3}$$

In Eq. (6.3), I_{bs} is the direct radiation on the receiver surface and I_{ds} is the total diffuse radiation reaching the receiver comprising of sky-diffuse radiation and reflected radiation from the ground and the inner side of the wingwalls. The present study is concerned with estimating the direct radiation I_{bs} given by $I_b R_b f_i$ and its monthly average daily value.

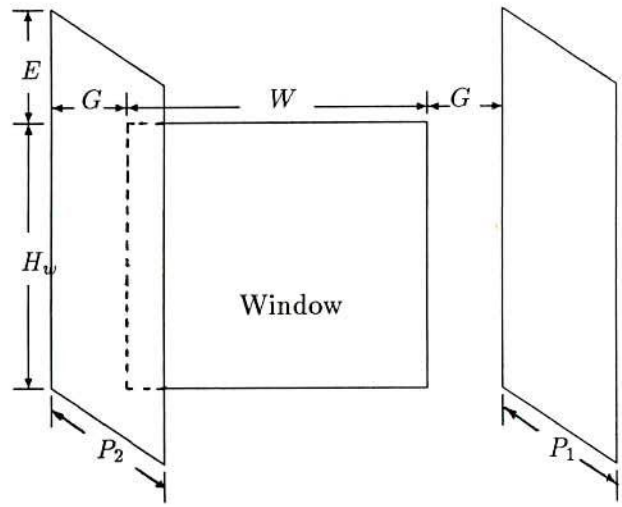

Figure 6.1: Basic geometry of window shaded by wingwalls

Summing Eq. (6.3) over all the hours and days in a month, the monthly average daily solar radiation per unit receiver area, $\bar{H}_s$ can be expressed as,

$$\bar{H}_s = \bar{H}_b \bar{R}_b \bar{f}_i + \bar{H}_{ds} \tag{6.4}$$

where, $\bar{H}_{ds}$ is the monthly average daily diffuse radiation reaching the receiver comprising of sky-diffuse and reflected radiation from the ground and the inner side of the wingwalls. $\bar{R}_b$ is the monthly average daily tilt factor for direct radiation for the vertical receiver.

Analogous to Eq. (5.10), the monthly average shading factor for direct radiation for the receiver shaded by infinite wingwalls 1 and 2 is given by,

$$\bar{f}_{i\infty} = \frac{\int_{\omega_{sr}}^{\omega_o} I_b R_b f_{i1}\, d\omega + \int_{\omega_o}^{\omega_{ss}} I_b R_b f_{i2}\, d\omega}{\int_{\omega_{sr}}^{\omega_{ss}} I_b R_b\, d\omega} \tag{6.5}$$

It may be noted that, in Eq. (6.5), ω_o is the hour angle corresponding to $\gamma_d = |\gamma_s - \gamma| = 0$; where γ is the receiver azimuthal angle and γ_s is the solar azimuthal angle. Since the wingwalls are perpendicular to the receiver, in writing Eq. (6.5), it is realized that, for $\omega > \omega_o$, wingwall-1 does not shade the receiver and for $\omega < \omega_o$, wingwall-2 does not shade the receiver. When there is only one wingwall, say, wingwall-1, $f_{i2} = 1.0$, thereby 2nd integral in the numerator of Eq. (6.5) is nothing but the direct solar radiation received by the window during ω_o to ω_{ss}. Thus, Eq. (6.5) is valid for receivers with an arbitrary azimuthal angle and shaded by either one or two wingwalls.

Following the analysis given in §5.3 of Chapter 5, it is straight forward to show that the monthly average shading factor, evaluated on the mean day of the month, $\bar{f}_i$ is equal to the shading factor under extra-terrestrial conditions $\bar{f}_{io}$, not only when $K_T = 1.0$ but also when k_T is uniform throughout the day, not necessarily equal to unity.

6.3 Monthly Average Shading Factor for Receivers Shaded by Infinite Wingwalls under Terrestrial Conditions

6.3.1 Infinite Wingwall without Gap between the Wingwall and the Window

It is assumed that the wingwall is infinite. There is no gap between the edge of the window and the wingwall. Referring to Figure 6.2, consider wingwall-1 only. Let θ be the angle of incidence at the hour angle ω with respect to the outer normal of the receiver. The projection of the sun's ray on horizontal make an angle γ_d with the projection of the outer normal of the receiver on the horizontal. The width of the shadow in the plane of the receiver is X. Let X' be the length of the projection of the sun's ray on the horizontal between the edge of the wingwall and the shadow edge. If α_s is the altitude angle (complement of the azimuthal angle θ_z), X' is given by,

$$X' = L \cos \alpha_s \tag{6.6}$$

where L is the length of the sun's ray between the edge of the wingwall and the receiver.

Considering the plan (see, Figure 6.2(b)) of the wingwall-receiver geometry along with the sun's ray, it follows,

$$\sin(90^o - \gamma_d) = \frac{P}{X'} = \frac{P}{L \cos \alpha_s} \tag{6.7}$$

from which,

$$L = \frac{P}{\sin(90^o - \gamma_d) \cos \alpha_s} = \frac{P}{\cos \gamma_d \cos \alpha_s} \tag{6.8}$$

Also, from Figure 6.2(b),

$$X = L \cos \alpha_s \cos(90^o - \gamma_d) = L \sin \gamma_d \cos \alpha_s \tag{6.9}$$

Using Eq. (6.8) for L in Eq. (6.9), X is given by,

$$X = \frac{P \sin \gamma_d}{\cos \gamma_d} \tag{6.10}$$

From the definition of the instantaneous shading factor,

$$f_{i1} = \left(1 - \frac{X H_w}{W H_w}\right) = \left(1 - \frac{P \sin \gamma_d}{W \cos \gamma_d}\right) \tag{6.11}$$

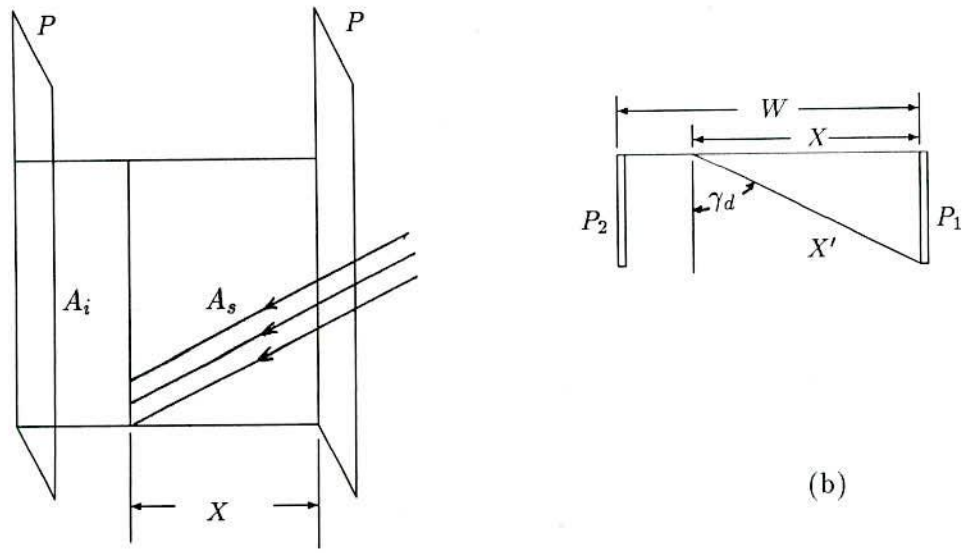

Figure 6.2: (a) Sun's ray on the wingwall-receiver geometry at an hour angle ω; (b) Plan of the sun's rays on horizontal.

Consider the integrand $I_b R_b f_{i1}$ in the first term of the numerator of Eq. (6.5),

$$\begin{aligned} I_b R_b f_{i1} &= I_b R_b \left[1 - \frac{P \sin\gamma_d}{W \cos\gamma_d}\right] \\ &= I_b \left[R_b - R_b \tan\psi_1 \frac{\sin\gamma_d}{\cos\gamma_d}\right] \end{aligned} \tag{6.12}$$

where, ψ_1 is the angle between the receiver and the imaginary plane joining the outer edge of the wingwall-1 to the opposite side of the receiver.

Using $R_b = \cos\theta/\cos\theta_z$ [Eq. (2.3)] and expressing $\cos\theta = \sin\theta_z \cos(\gamma_s - \gamma)$ [Eq. (5.18)], Eq. (6.12) can be re-written as,

$$\begin{aligned} I_b R_b f_{i1} &= I_b \left[\frac{\sin\theta_z \cos\gamma_d}{\cos\theta_z} - \frac{\sin\theta_z \cos\gamma_d \sin\psi_1 \sin\gamma_d}{\cos\theta_z \cos\psi_1 \cos\gamma_d}\right] \\ &= \frac{I_b}{\cos\psi_1}\left[\frac{\sin\theta_z \cos\gamma_d \cos\psi_1 - \sin\theta_z \sin\gamma_d \sin\psi_1}{\cos\theta_z}\right] \\ &= \frac{I_b}{\cos\psi_1}\left[\frac{\sin\theta_z\{\cos\gamma_d \cos\psi_1 - \sin\gamma_d \sin\psi_1\}}{\cos\theta_z}\right] \\ &= \frac{I_b}{\cos\psi_1}\left[\frac{\sin\theta_z \cos(\gamma_d + \psi_1)}{\cos\theta_z}\right] \end{aligned} \tag{6.13}$$

Using $\gamma_d = |\gamma_s - \gamma|$, Eq. (6.13) can be re-written as,

$$I_b R_b f_{i1} = \frac{I_b}{\cos\psi_1}\left[\frac{\sin\theta_z \cos(\gamma_s - \gamma_1^*)}{\cos\theta_z}\right] \tag{6.14}$$

where

$$\gamma_1^* = \gamma + \psi_1 \tag{6.15}$$

Noting the term in the parentheses of Eq. (6.14) is the tilt factor for a vertical surface of azimuthal angle γ_1^*, Eq. (6.14) becomes,

$$I_b R_b f_{i1} = \frac{I_b R_{b1}^*}{\cos\psi_1} \tag{6.16}$$

In Eq. (6.16), $\cos\psi_1$ in terms of the window-wingwall geometry can be expressed as,

$$\cos\psi_1 = \frac{W}{\sqrt{P^2+W^2}} = \frac{WH_w}{H_w\sqrt{P^2+W^2}} = \frac{A_w}{A_{shp1}} \tag{6.17}$$

where A_{shp1} is the area of the imaginary plane-1 pertaining to wingwall-1.

Thus,

$$I_b R_b f_{i1} = \frac{A_{shp1}}{A_w} I_b R_{b1}^* \tag{6.18}$$

Similarly,

$$I_b R_b f_{i2} = \frac{A_{shp2}}{A_w} I_b R_{b2}^* \tag{6.19}$$

In Eqs. (6.18) and (6.19), R_{b1}^* and R_{b2}^* are the instantaneous tilt factor for direct radiation for plane-1 and plane-2 which may be termed as the shading planes for wingwalls 1 and 2 respectively as shown in Figure 6.3. It is interesting to note that the shading plane concept valid for infinite overhangs is valid for infinite wingwalls also, with the following differences.

1. The shading plane is now found by joining the outer edge of the wingwall to the opposite side of the receiver.

2. The shading planes for the wingwalls (1 & 2) differ from the receiver by having different azimuthal angles, γ_1^* and γ_2^*, whereas, the shading plane of the overhang differs from the receiver by having a different slope, β^*.

Using Eqs. (6.18) and (6.19) in Eq. (6.5), monthly average shading factor for infinite wingwalls is given by,

$$\bar{f}_{i\infty} = \frac{\left(\frac{A_{shp1}}{A_w}\right)\int_{\omega_{sr}}^{\omega_o} I_b R_{b1}^*\, d\omega + \left(\frac{A_{shp2}}{A_w}\right)\int_{\omega_o}^{\omega_{ss}} I_b R_{b2}^*\, d\omega}{\int_{\omega_{sr}}^{\omega_{ss}} I_b R_b\, d\omega} \tag{6.20}$$

The lower limit of integration for the first term in the numerator of Eq. (6.20) and the upper limit of integration for the second term in the numerator of Eq. (6.20) can be replaced by ω_{sr1}^* and ω_{ss2}^*, where the superscript '*' refers to the imaginary planes in general and the

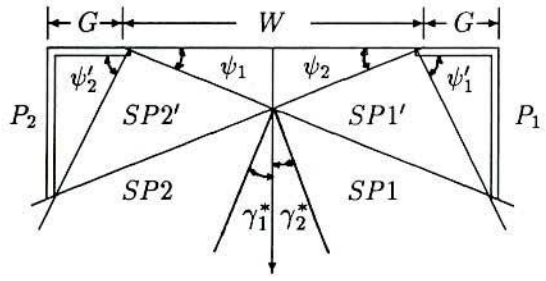

Figure 6.3: Resulting shading planes when a gap is present

subscripts 1 and 2 refer to the imaginary planes 1 and 2. As has been explained in Chapter 5 §5.4.1, this replacement is admissible since $|\omega_{sr1}^*| < |\omega_{sr}|$ and $\omega_{ss2}^* < \omega_{ss}$. Dividing the numerator and the denominator of Eq. (6.20) by $\int_{-\omega_s}^{\omega_s} I_b\, d\omega$ $(=H_b)$, Eq. (6.20) takes the form,

$$\bar{f}_{i\infty} = \frac{\left(\frac{A_{shp1}}{A_w}\right)\bar{R}_{b1}^* + \left(\frac{A_{shp2}}{A_w}\right)\bar{R}_{b2}^*}{\bar{R}_b} \tag{6.21}$$

Similarly, the shading factor under extra-terrestrial conditions can be expressed as,

$$\begin{aligned}\bar{f}_{io\infty} &= \frac{\int_{\omega_{sr}}^{\omega_o} I_o R_b f_{i1}\, d\omega + \int_{\omega_o}^{\omega_{ss}} I_o R_b f_{i2}\, d\omega}{\int_{\omega_{sr}}^{\omega_{ss}} I_o R_b\, d\omega} \\ &= \frac{\left(\frac{A_{shp1}}{A_w}\right)\bar{R}_{bo1}^* + \left(\frac{A_{shp2}}{A_w}\right)\bar{R}_{bo2}^*}{\bar{R}_{bo}}\end{aligned} \tag{6.22}$$

In Eqs. (6.21) and (6.22), $\bar{R}_{b1}^*$, $\bar{R}_{b2}^*$, $\bar{R}_{bo1}^*$ and $\bar{R}_{bo2}^*$ are defined by,

$$\bar{R}_{b1}^* = \frac{\int_{\omega_{sr1}^*}^{\omega_o} I_b R_{b1}^*\, d\omega}{\int_{-\omega_s}^{\omega_s} I_b\, d\omega} \tag{6.23}$$

$$\bar{R}_{b2}^* = \frac{\int_{\omega_o}^{\omega_{ss2}^*} I_b R_{b2}^*\, d\omega}{\int_{-\omega_s}^{\omega_s} I_b\, d\omega} \tag{6.24}$$

$$\bar{R}_{bo1}^* = \frac{\int_{\omega_{sr1}^*}^{\omega_o} I_o R_{b1}^*\, d\omega}{\int_{-\omega_s}^{\omega_s} I_o\, d\omega} \tag{6.25}$$

$$\bar{R}^*_{bo2} = \frac{\int_{\omega_o}^{\omega^*_{ss2}} I_o R^*_{b2}\, d\omega}{\int_{-\omega_s}^{\omega_s} I_o\, d\omega} \tag{6.26}$$

It may be noted that the instantaneous tilt factors R^*_{b1} and R^*_{b2} for the imaginary planes 1 and 2 are to be evaluated with $\gamma = \gamma^*_1$ and $\gamma = \gamma^*_2$ respectively. $\bar{R}^*_{b1}$ and $\bar{R}^*_{b2}$, the part average tilt factors can be evaluated following the procedure exactly similar to that described in Chapter 5 §5.6.

6.3.2 Infinite Wingwall with Gap between the Wingwall and the Window

When a gap exists between the wingwall and the window, the solar radiation reaching the receiver is the sum of the contributions during ω_{sr} to ω_o and ω_o to ωss. Let the shading planes 1′ and 2′, as shown in Figure 6.3, be formed by joining the edges of the wingwalls to the vertical side of the window adjacent to the wingwall under consideration. Referring to Figure 6.3, When a gap exists, solar radiation reaching the receiver during ω_{sr} to ω_o is the difference between the solar radiation falling on the imaginary plane-1 and 1′. Similarly, solar radiation reaching the receiver during ω_o to ω_{ss} is the difference between the solar radiation falling on the imaginary planes 2 and 2′. The imaginary planes 1 and 1′ are characterized by the azimuthal angles $\gamma^*_1 = \gamma + \psi_1$ and $\gamma^*_{1'} = \gamma + \psi_{1'}$. Similarly, for the planes 2 and 2′, $\gamma^*_2 = \gamma - \psi_2$ and $\gamma^*_{2'} = \gamma - \psi_{2'}$. The angles ψ_1, $\psi_{1'}$ and ψ_2, $\psi_{2'}$ are shown in Figure 6.3. Thus, when a gap exists between the wingwall and the sides of the window, the monthly average shading factor can be obtained from,

$$\begin{aligned}\bar{f}_{i\infty} = {} & \left[\left(\frac{A_{shp1}}{A_w}\right)\int_{\omega^*_{sr1}}^{\omega_o} I_b R^*_{b1}\, d\omega - \left(\frac{A_{shp1'}}{A_w}\right)\int_{\omega^*_{sr1'}}^{\omega_o} I_b R^*_{b1'}\, d\omega \right. \\ & \left. + \left(\frac{A_{shp2}}{A_w}\right)\int_{\omega_o}^{\omega^*_{ss2}} I_b R^*_{b2}\, d\omega - \left(\frac{A_{shp2'}}{A_w}\right)\int_{\omega_o}^{\omega^*_{ss2'}} I_b R^*_{b2'}\, d\omega\right] \\ & \div \left[\int_{\omega_{sr}}^{\omega_{ss}} I_b R_b\, d\omega\right]\end{aligned} \tag{6.27}$$

Dividing both the numerator and the denominator of Eq. (6.27) by the horizontal radiation H_b and after rearrangement, Eq. (6.27) can be expressed as,

$$\bar{f}_{i\infty} = \frac{\left[\left(\frac{A_{shp1}}{A_w}\right)\bar{R}^*_{b1} + \left(\frac{A_{shp2}}{A_w}\right)\bar{R}^*_{b2}\right] - \left[\left(\frac{A_{shp1'}}{A_w}\right)\bar{R}^*_{b1'} + \left(\frac{A_{shp2'}}{A_w}\right)\bar{R}^*_{b2'}\right]}{\bar{R}_b} \tag{6.28}$$

Similarly, the shading factor under extra-terrestrial conditions, when a gap exists, can be expressed as,

$$\bar{f}_{io\infty} = \frac{\left[\left(\frac{A_{shp1}}{A_w}\right)\bar{R}^*_{bo1} + \left(\frac{A_{shp2}}{A_w}\right)\bar{R}^*_{bo2}\right] - \left[\left(\frac{A_{shp1'}}{A_w}\right)\bar{R}^*_{bo1'} + \left(\frac{A_{shp2'}}{A_w}\right)\bar{R}^*_{bo2'}\right]}{\bar{R}_{bo}} \tag{6.29}$$

where, $\bar{R}^*_{b1'}$ and $\bar{R}^*_{b2'}$ are defined by,

$$\bar{R}^*_{b1'} = \frac{\int_{\omega^*_{sr1'}}^{\omega_o} I_b R^*_{b1'}\, d\omega}{\int_{-\omega_s}^{\omega_s} I_b\, d\omega} \tag{6.30}$$

$$\bar{R}^*_{b2'} = \frac{\int_{\omega_o}^{\omega^*_{ss2'}} I_b R^*_{b2'}\, d\omega}{\int_{-\omega_s}^{\omega_s} I_b\, d\omega} \tag{6.31}$$

6.4 Results and Discussion

Numerical values for $\bar{f}_{i\infty}$ using Eq. (6.21) when there is no gap between the wingwall and the receiver sides and Eq. (6.28) when the gap exists have been obtained for $\phi = 20^o$, 25^o, 30^o, 40^o, 50^o and 60^o, $-23.05^o \leq \delta \leq 23.09^o$, $\gamma = 0^o$, 30^o, 60^o and 90^o, $p = 0.2$, 0.3, 0.4 and 0.5, $g = 0.0$ and 0.1 for $\bar{D}_f = 0.0$, 0.2, 0.4, 0.6 and 0.8. $\bar{f}_{i\infty}$ values under extra-terrestrial conditions designated as $\bar{f}_{io\infty}$ also have been obtained using Eqs. (6.22) and (6.29) for the same values of other parameters except $\bar{D}_f$; $\bar{f}_{io\infty}$ does not depend on $\bar{D}_f$. In order to validate the algorithms developed in the present study, $\bar{f}_{i\infty}$ values have been obtained by numerical integration also according to,

$$\bar{f}_{i\infty}(\text{num}) = \frac{\sum_{\omega_{sr}}^{\omega_{ss}} I_b R_b f_i}{\sum_{\omega_{sr}}^{\omega_{ss}} I_b R_b} \tag{6.32}$$

where, f_i is the instantaneous shading factor given by Eq. (6.11). I_b expressed in terms of r_t [12] and r_d correlations [16] is given by Eq. (2.27). In evaluating Eq. (6.32) 5^o interval for ω has been employed.

6.4.1 Validation of the Algorithms

A plot of $\bar{f}_{i\infty}$ vs $\bar{f}_{i\infty}$(num) is shown in Figure 6.4 for $25^o \leq \phi \leq 60^o$, $-23.05^o \leq \delta \leq 23.9^o$, $\bar{D}_f = 0.4$, $\gamma = 0^o$ for $p = 0.3$ and $g = 0.0$. There is no difference between $\bar{f}_{i\infty}$ and $\bar{f}_{i\infty}$(num) graphically. Numerical values differed by less than 0.001.

Similar plot is shown in Figure 6.5 for $\gamma = 60^o$ for the same values of the other parameters mentioned above. The agreement is within 0.004.

For $g = 0.1$, $\bar{f}_{i\infty}$ vs $\bar{f}_{i\infty}$(num) for $\gamma = 0^o$ and 60^o are shown in Figures 6.6 and 6.7. The values given by the present algorithm agree with the values obtained by numerical integration when $g \neq 0.0$ also.

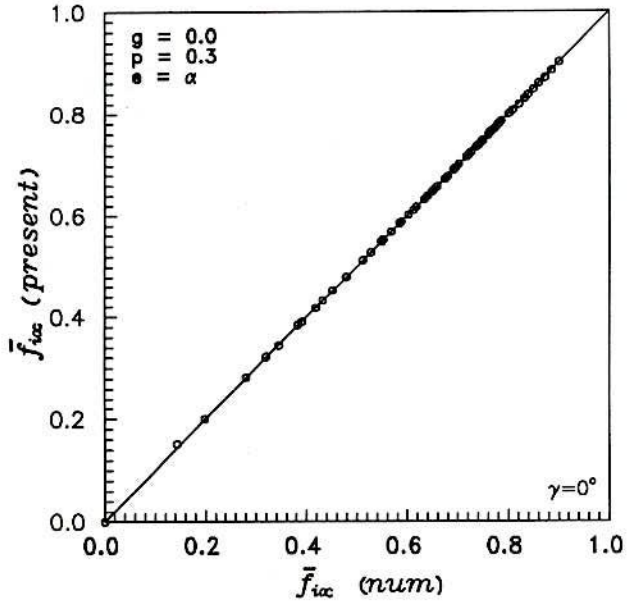

Figure 6.4: Validation of $\bar{f}_{i\infty}$ against $\bar{f}_{i\infty}$(num) for $p = 0.3$, $g = 0.0$, $\bar{D}_f = 0.4$ and $\gamma = 0°$

.

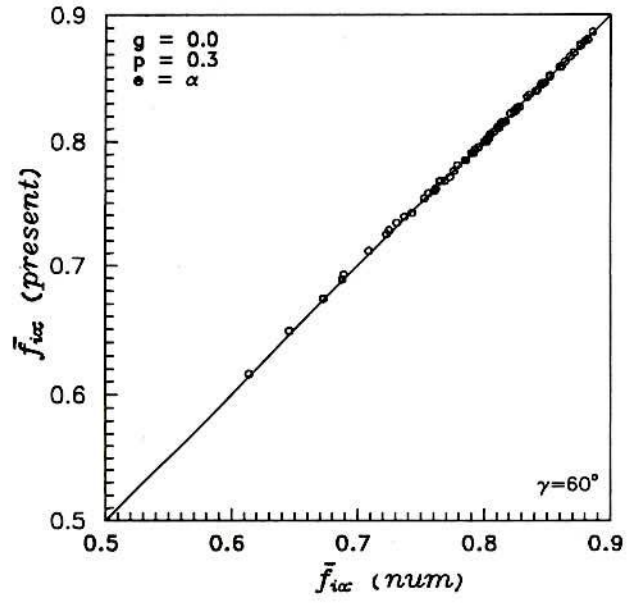

Figure 6.5: Validation of $\bar{f}_{i\infty}$ against $\bar{f}_{i\infty}$(num) for $p = 0.3$, $g = 0.0$, $\bar{D}_f = 0.4$ and $\gamma = 60°$

.

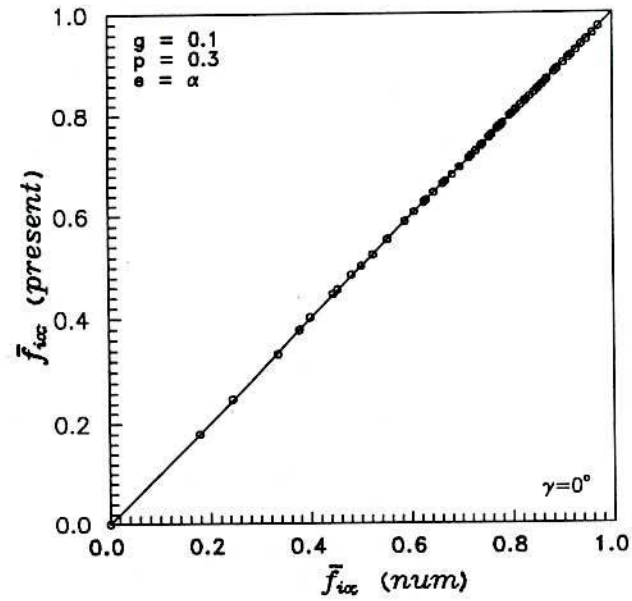

Figure 6.6: Validation of $\bar{f}_{i\infty}$ against $\bar{f}_{i\infty}$(num) for $p = 0.3$, $g = 0.1$, $\bar{D}_f = 0.4$ and $\gamma = 0^o$

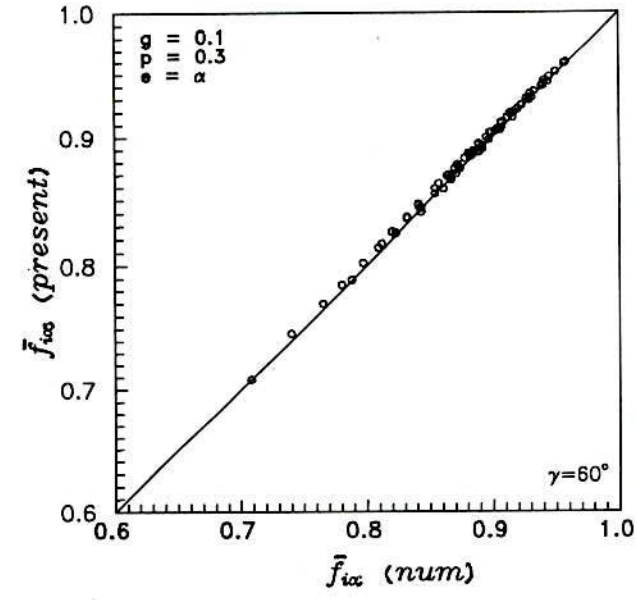

Figure 6.7: Validation of $\bar{f}_{i\infty}$ against $\bar{f}_{i\infty}$(num) for $p = 0.3$, $g = 0.1$, $\bar{D}_f = 0.4$ and $\gamma = 60^o$

These validations essentially establish the validity of converting calculation of solar radiation falling on a shaded receiver (shaded by wingwalls) to calculating solar radiation falling on two appropriately defined shading planes.

6.4.2 Comparison of $\bar{f}_{i\infty}$ and $\bar{f}_{io\infty}$

Shading factor values for the overhangs, taking diffuse fraction in to account (i.e., under terrestrial conditions) differed from the corresponding extra-terrestrial values not to an insignificant extent particularly at lower latitudes and when $\gamma \neq 0^o$. Wingwalls constitute, by virtue of their orientation, shading planes which in general are characterized by $\gamma \neq 0^o$. Thus, it can be expected that $\bar{f}_{i\infty}$ values differ more from $\bar{f}_{io\infty}$ for wingwalls. The values of $\bar{f}_{io\infty}$ and $\bar{f}_{i\infty}$ for three months, March, June and December, for receiver azimuthal angles, $\gamma = 0^o$, 30^o, 60^o and 90^o, for different latitudes, $\phi = 20^o$, 25^o, 30^o, 40^o, 50^o and 60^o, for $p = 0.3$ and $g = 0.0$ are given in Table 6.1. Under the column $\bar{D}_f$, 'Ext.' indicates the extra-terrestrial shading factor values $\bar{f}_{io\infty}$, whereas, the other values correspond to $\bar{D}_f = 0.2$ to 0.8. The values of $(\bar{f}_{i\infty}/\bar{f}_{io\infty})$ which indicate the percentage changes are also given in Table 6.2 for the aforementioned parameters.

A plot of $\bar{f}_{i\infty}$ and $\bar{f}_{io\infty}$ vs $\bar{D}_f$ when the receiver azimuthal angle is zero, for three months, March, June and December, for $p = 0.3$, $g = 0.0$ are shown in Figures 6.8, 6.9 and 6.10 for $\phi = 25^o$, 40^o and 60^o respectively. $\bar{f}_{io\infty}$ does not vary with $\bar{D}_f$. $\bar{f}_{i\infty}$ value at $\bar{D}_f = 0.0$ is not equal to $\bar{f}_{io\infty}$ since r_t and r_d correlations do not yield I_o distribution when $\bar{D}_f = 0.0$. When $\gamma = 0^o$, for typical values of $\bar{D}_f = 0.4$ to 0.6, $\bar{f}_{i\infty}$ differs from $\bar{f}_{io\infty}$ by 10 to 16 % for $\phi = 25^o$ in the month of March. In the month of June, the corresponding difference is small, of the order of 1 %. At a latitude of 40^o, the percentage change is 8 to 12 % in the month of March, whereas, when $\phi = 60^o$, it is 6 to 9 %. When $\gamma \neq 0^o$, the percentage differences are higher in the month of June. For example, when $\gamma = 30^o$, at $\phi = 30^o$ for $\bar{D}_f = 0.6$, $\bar{f}_{i\infty}$ differs from $\bar{f}_{io\infty}$ by 21 %.

It may be noted from the values given in Table 6.2, the ratio $(\bar{f}_{i\infty}/\bar{f}_{io\infty}) > 1$, as well as, $(\bar{f}_{i\infty}/\bar{f}_{io\infty}) < 1$ depending on ϕ, δ, γ combination. $(\bar{f}_{i\infty}/\bar{f}_{io\infty})$ is as low as 0.870 for $\bar{D}_f = 0.6$ for $\phi = 50^o$ in the month of December. This is in contrast to the values given in Table 5.5 for Chapter 5 for overhangs which are in general less than unity. Also, the change in $\bar{f}_{i\infty}$ values for wingwalls is much higher than the corresponding changes for the overhangs. For example, even when the receiver azimuthal angle is zero, at $\phi = 25^o$, for $p = 0.3$, $g = 0.0$, $\bar{D}_f = 0.6$, $\bar{f}_{i\infty} = 0.617$ and $\bar{f}_{io\infty} = 0.532$ for the wingwalls in the month of March. The corresponding values for overhang of the same dimension are $\bar{f}_{i\infty} = 0.440$ and $\bar{f}_{io\infty} = 0.453$. These features may be attributed as due to differing changes due to $\bar{D}_f$ in $\bar{R}_b^*$, the tilt factor for the shading planes of overhangs and wingwalls. The change in $\bar{R}_b^*$

Table 6.1: Tabulated values of $\bar{f}_{io\infty}$ and $\bar{f}_{i\infty}$ for different azimuthal angles; $p = 0.3$, $g = 0.0$

ϕ	$\bar{D}_f$	Values of $\bar{f}_{io\infty}$ and $\bar{f}_{i\infty}$											
		March				June				December			
		$\gamma = 0^o$	30^o	60^o	90^o	$\gamma = 0^o$	30^o	60^o	90^o	$\gamma = 0^o$	30^o	60^o	90^o
20	Ext.	0.472	0.726	0.889	0.882	0.000	0.020	0.679	0.909	0.719	0.794	0.858	0.705
	0.2	0.514	0.740	0.887	0.864	0.000	0.024	0.685	0.912	0.748	0.796	0.834	0.678
	0.4	0.528	0.745	0.886	0.857	0.000	0.025	0.688	0.913	0.759	0.796	0.824	0.666
	0.6	0.558	0.756	0.884	0.838	0.000	0.028	0.695	0.916	0.781	0.797	0.803	0.638
	0.8	0.637	0.782	0.874	0.777	0.000	0.038	0.709	0.923	0.834	0.800	0.739	0.542
25	Ext.	0.532	0.742	0.883	0.860	0.207	0.226	0.725	0.928	0.745	0.795	0.838	0.680
	0.2	0.574	0.754	0.878	0.838	0.209	0.256	0.738	0.935	0.771	0.797	0.812	0.651
	0.4	0.588	0.759	0.876	0.829	0.209	0.267	0.743	0.937	0.781	0.797	0.802	0.638
	0.6	0.617	0.768	0.872	0.807	0.210	0.292	0.755	0.943	0.801	0.798	0.779	0.609
	0.8	0.695	0.789	0.852	0.735	0.211	0.369	0.790	0.961	0.850	0.803	0.713	0.506
30	Ext.	0.579	0.753	0.876	0.840	0.376	0.386	0.754	0.925	0.767	0.796	0.816	0.655
	0.2	0.619	0.764	0.867	0.816	0.382	0.425	0.770	0.929	0.791	0.799	0.789	0.625
	0.4	0.633	0.768	0.864	0.805	0.384	0.439	0.776	0.930	0.800	0.799	0.779	0.612
	0.6	0.662	0.776	0.857	0.781	0.387	0.469	0.791	0.934	0.818	0.801	0.756	0.581
	0.8	0.736	0.793	0.827	0.699	0.396	0.557	0.833	0.942	0.863	0.808	0.690	0.472
40	Ext.	0.646	0.768	0.856	0.802	0.538	0.561	0.779	0.902	0.806	0.797	0.774	0.597
	0.2	0.684	0.777	0.842	0.773	0.550	0.595	0.795	0.900	0.825	0.800	0.747	0.565
	0.4	0.697	0.780	0.836	0.760	0.553	0.606	0.802	0.899	0.831	0.802	0.737	0.552
	0.6	0.724	0.787	0.823	0.731	0.560	0.629	0.816	0.898	0.846	0.804	0.715	0.521
	0.8	0.791	0.799	0.780	0.632	0.577	0.695	0.854	0.884	0.883	0.813	0.650	0.405
50	Ext.	0.689	0.778	0.837	0.770	0.625	0.647	0.772	0.871	0.843	0.800	0.719	0.517
	0.2	0.725	0.785	0.818	0.737	0.637	0.670	0.787	0.866	0.856	0.804	0.697	0.488
	0.4	0.737	0.788	0.811	0.723	0.641	0.677	0.792	0.864	0.861	0.806	0.689	0.477
	0.6	0.762	0.793	0.795	0.689	0.648	0.692	0.804	0.859	0.870	0.809	0.673	0.450
	0.8	0.823	0.803	0.744	0.578	0.666	0.734	0.836	0.836	0.898	0.819	0.619	0.343
60	Ext.	0.718	0.784	0.820	0.745	0.677	0.693	0.740	0.832	0.894	0.820	0.629	0.330
	0.2	0.752	0.791	0.798	0.709	0.688	0.708	0.756	0.829	0.899	0.821	0.618	0.314
	0.4	0.764	0.793	0.790	0.694	0.691	0.712	0.762	0.828	0.901	0.822	0.614	0.309
	0.6	0.787	0.798	0.772	0.656	0.697	0.721	0.774	0.825	0.904	0.822	0.606	0.297
	0.8	0.844	0.806	0.715	0.534	0.713	0.746	0.809	0.809	0.915	0.824	0.582	0.255

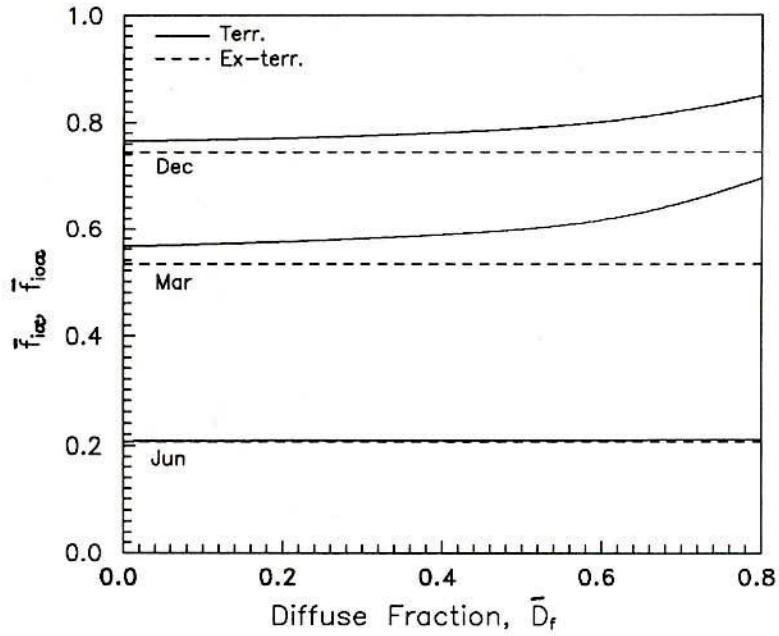

Figure 6.8: Variation of $\bar{f}_{i\infty}$ and $\bar{f}_{i\infty\infty}$ with $\bar{D}_f$ for March, June and December for $\phi = 25°$; $p = 0.3$, $g = 0.0$, $\gamma = 0°$

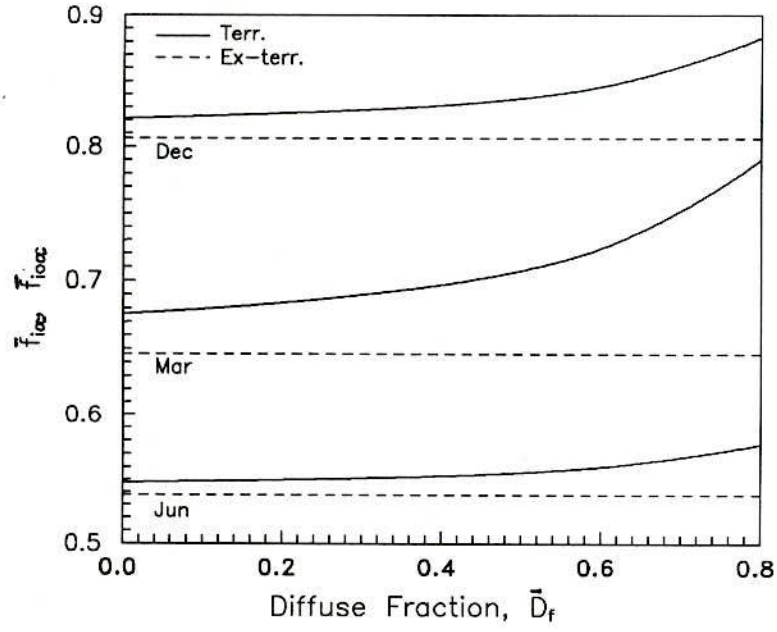

Figure 6.9: Variation of $\bar{f}_{i\infty}$ and $\bar{f}_{i\infty\infty}$ with $\bar{D}_f$ for March, June and December for $\phi = 40°$; $p = 0.3$, $g = 0.0$, $\gamma = 0°$

Table 6.2: Tabulated values of the ratio $\bar{f}_{i\infty}/\bar{f}_{i0\infty}$ for different azimuthal angles; $p = 0.3$, $g = 0.0$

ϕ	$\bar{D}_f$	Values of the ratio $\bar{f}_{i\infty}/\bar{f}_{i0\infty}$											
		March				June				December			
		$\gamma = 0^o$	30^o	60^o	90^o	$\gamma = 0^o$	30^o	60^o	90^o	$\gamma = 0^o$	30^o	60^o	90^o
20	0.2	1.089	1.019	0.998	0.980	—	1.200	1.009	1.003	1.040	1.003	0.972	0.962
	0.4	1.119	1.026	0.997	0.972	—	1.250	1.013	1.004	1.056	1.003	0.960	0.945
	0.6	1.182	1.041	0.994	0.950	—	1.400	1.024	1.008	1.086	1.004	0.936	0.905
	0.8	1.350	1.077	0.983	0.881	—	1.900	1.044	1.015	1.160	1.008	0.861	0.769
25	0.2	1.079	1.016	0.994	0.974	1.010	1.133	1.018	1.008	1.035	1.003	0.969	0.957
	0.4	1.105	1.023	0.992	0.964	1.011	1.181	1.025	1.010	1.048	1.003	0.957	0.938
	0.6	1.160	1.035	0.988	0.938	1.014	1.292	1.041	1.016	1.075	1.004	0.930	0.896
	0.8	1.306	1.063	0.965	0.855	1.019	1.633	1.090	1.036	1.141	1.010	0.851	0.744
30	0.2	1.069	1.015	0.990	0.971	1.016	1.101	1.021	1.004	1.031	1.004	0.967	0.954
	0.4	1.093	1.020	0.986	0.958	1.021	1.137	1.029	1.005	1.043	1.004	0.955	0.934
	0.6	1.143	1.031	0.978	0.930	1.029	1.215	1.049	1.010	1.066	1.006	0.926	0.887
	0.8	1.271	1.053	0.944	0.832	1.053	1.443	1.105	1.018	1.125	1.015	0.846	0.721
40	0.2	1.059	1.012	0.984	0.964	1.022	1.061	1.021	0.998	1.024	1.004	0.965	0.946
	0.4	1.079	1.016	0.977	0.948	1.028	1.080	1.030	0.997	1.031	1.006	0.952	0.925
	0.6	1.121	1.025	0.961	0.911	1.041	1.121	1.047	0.996	1.050	1.009	0.924	0.873
	0.8	1.224	1.040	0.911	0.788	1.072	1.239	1.096	0.980	1.096	1.020	0.840	0.678
50	0.2	1.052	1.009	0.977	0.957	1.019	1.036	1.019	0.994	1.015	1.005	0.969	0.944
	0.4	1.070	1.013	0.969	0.939	1.026	1.046	1.026	0.992	1.021	1.008	0.958	0.923
	0.6	1.106	1.019	0.950	0.895	1.037	1.070	1.041	0.986	1.032	1.011	0.936	0.870
	0.8	1.194	1.032	0.889	0.751	1.066	1.134	1.083	0.960	1.065	1.024	0.861	0.663
60	0.2	1.047	1.009	0.973	0.952	1.016	1.022	1.022	0.996	1.006	1.001	0.983	0.952
	0.4	1.064	1.011	0.963	0.932	1.021	1.027	1.030	0.995	1.008	1.002	0.976	0.936
	0.6	1.096	1.018	0.941	0.881	1.030	1.040	1.046	0.992	1.011	1.003	0.963	0.900
	0.8	1.175	1.028	0.872	0.717	1.053	1.076	1.093	0.972	1.023	1.005	0.925	0.773

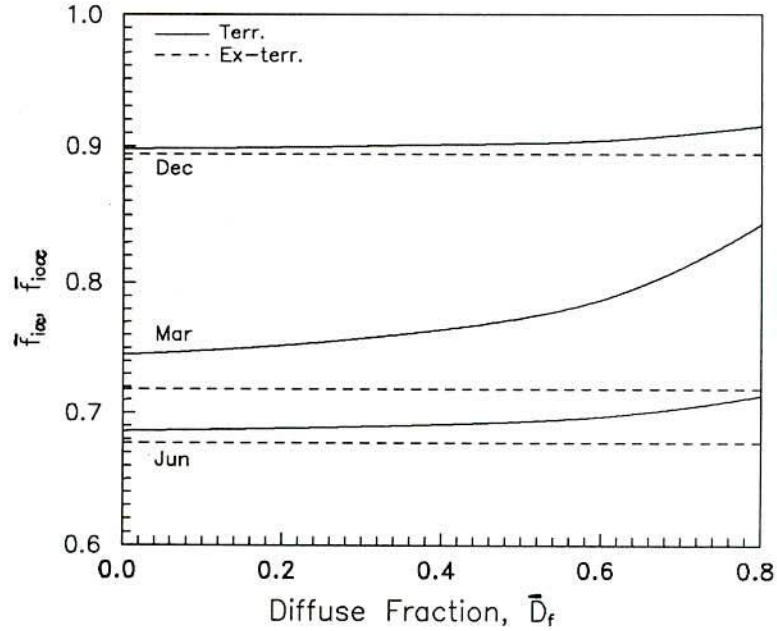

Figure 6.10: Variation of $\bar{f}_{i\infty}$ and $\bar{f}_{i\infty\infty}$ with $\bar{D}_f$ for March, June and December for $\phi = 60^o$; $p = 0.3$, $g = 0.0$, $\gamma = 0^o$

compared to the change in $\bar{R}_b$ (the tilt factor for the receiver) for overhangs is due to $\bar{D}_f$ but at $\beta = 90^o$ and $\beta^* > 90^o$ for a fixed γ. Whereas, for the wingwalls the change is due to $\bar{D}_f$ at γ and γ^* for a fixed β. The influence of $\bar{D}_f$ on $\bar{R}_b$ (or $\bar{R}_b^*$) when $\gamma \neq 0$ is known to be more significant. This can be informed from the results of Klein and Theilacker [66] or detailed studies by Lahiri [67].

6.4.3 Tabulated Values

Values of $\bar{f}_{i\infty}$ for all the 12 months at $\bar{D}_f = 0.2$, 0.4, and 0.6, for $\phi = 20^o$, 40^o and 60^o, $p = 0.2$, 0.3, 0.4 and 0.5, $g = 0.0$ for $\gamma = 0^o$, 30^o, 60^o and 90^o are given in Tables D.1 to D.4 of Appendix D. Values of $\bar{f}_{i\infty}$ for $g = 0.1$ and for the same values of other parameter are given in Tables D.5 to D.8 of Appendix D. With the values given in these tables, shading factor values for infinite wingwalls for a wide range of latitudes, clearness indices (for which the corresponding $\bar{D}_f$ can be calculated if data value is not available) and projections can be readily obtained. Values of $\bar{f}_{i\infty}$ can be graphically interpolated for values of the parameters not given in the range $20^o \leq \phi \leq 60^o$, $0.2 \leq \bar{D}_f \leq 0.8$, $0.2 \leq p \leq 0.5$ with sufficient accuracy.

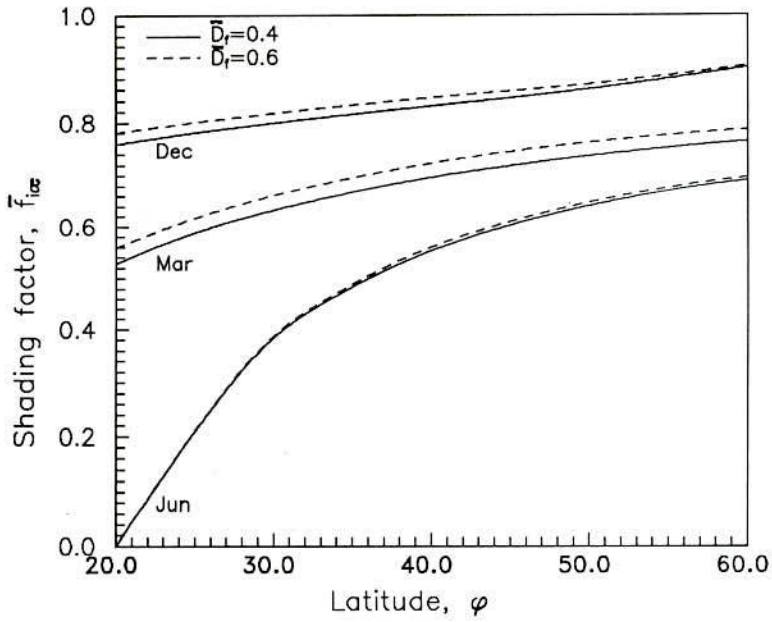

Figure 6.11: Variation of $\bar{f}_{i\infty}$ with latitude, ϕ for the month of March, June and December; $p = 0.3$, $g = 0.0$, and $\gamma = 0^o$

6.4.4 Dependence of $\bar{f}_{i\infty}$ on Latitude

A plot of $\bar{f}_{i\infty}$ vs ϕ at $\bar{D}_f = 0.4$ and 0.6, for the months of March, June and December, for $p = 0.3$, $g = 0.0$ for south facing receivers is shown in Figure 6.11. $\bar{f}_{i\infty}$ monotonically increases with laitude. The increase is steeper in the month of June because at low latitudes the duration of sunshine on the receiver is small.

Values of $\bar{f}_{i\infty}$ for different latitudes and azimuthal angles for all the months can be found in the tables given in Apendix D.

6.4.5 Dependence on Azimuthal Angle

Variation of $\bar{f}_{i\infty}$ with γ at different latitudes is shown in Figure 6.12 for the month of June and in Figure 6.13 for the months of March and December. Values of the other parameters are, $\bar{D}_f = 0.4$, $p = 0.3$, $g = 0.0$. $\bar{f}_{i\infty}$ increases with γ monotonically in the month of June. At lower values of γ, $\bar{f}_{i\infty}$ is higher at higher ϕ, whereas, at higher values of γ, $\bar{f}_{i\infty}$ is lower at higher ϕ. From the variation of $\bar{f}_{i\infty}$ with γ, as shown in Figure 6.13, in the month of December, $\bar{f}_{i\infty}$ decreases as γ increases for higher latitudes and at lower latitudes, say, $\phi = 20^o$, it displays an increasing and decreasing trend with γ. In the month of March, for $\gamma < 35^o$, $\bar{f}_{i\infty}$ is higher at high latitudes, whereas, the opposite is true for $\gamma > 35^o$. It

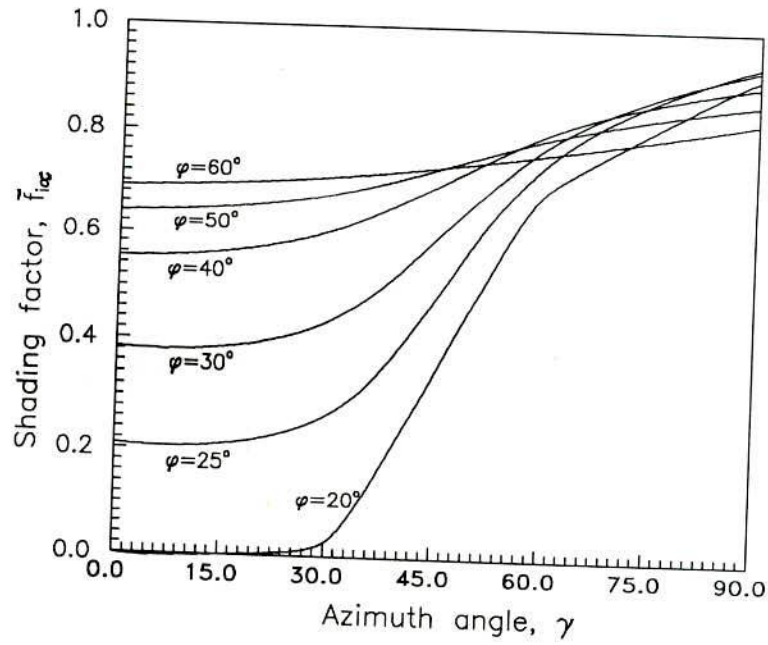

Figure 6.12: Variation of $\bar{f}_{i\infty}$ with azimuth angle, γ for the month of June; $p = 0.3$, $g = 0.0$, $\bar{D}_f = 0.4$

is to be noted that this behaviour for $\bar{f}_{i\infty}$ with γ is a result of $\bar{f}_{i\infty}$ being contributed by shading (or irradiating) of the receiver by one wingwall up to a certain hour angle (ω_o) and the second wingwall takes over beyond that hour angle. Also, the shading planes are characterized by azimuthal angle γ_1^* and γ_2^*. When $\gamma \neq 0^o$, γ_1^* and γ_2^* differ equally from γ but one is higher than γ and the other is lower. This leads to more and more asymmetric contribution to the lit area during the two durations, defined by Eq. (6.5). Thus, it is difficult to explain the behaviour purely on qualitative arguments.

6.4.6 Dependence on Projection

Variation of $\bar{f}_{i\infty}$ with the projection, p, for south facing receivers is shown in Figure 6.14 for the month of June and in Figures 6.15 for the months of March and December for different latitudes. Values of the other parameters are $\bar{D}_f = 0.4$, $g = 0.0$. It is easy to envisage that as projection increases, $\bar{f}_{i\infty}$ decreases. Similar figure for the receiver azimuthal angle $\gamma = 60^o$ is shown in Figure 6.16. For $\gamma \neq 0^o$ also, $\bar{f}_{i\infty}$ decreases as p increases.

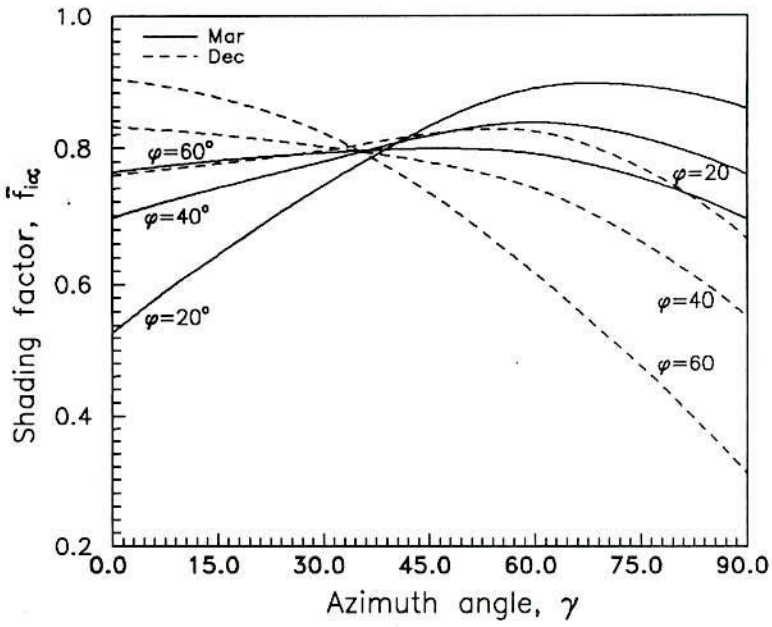

Figure 6.13: Variation of $\bar{f}_{i\infty}$ with azimuth angle, γ for the months of March and December; $p = 0.3$, $g = 0.0$, $\bar{D}_f = 0.4$

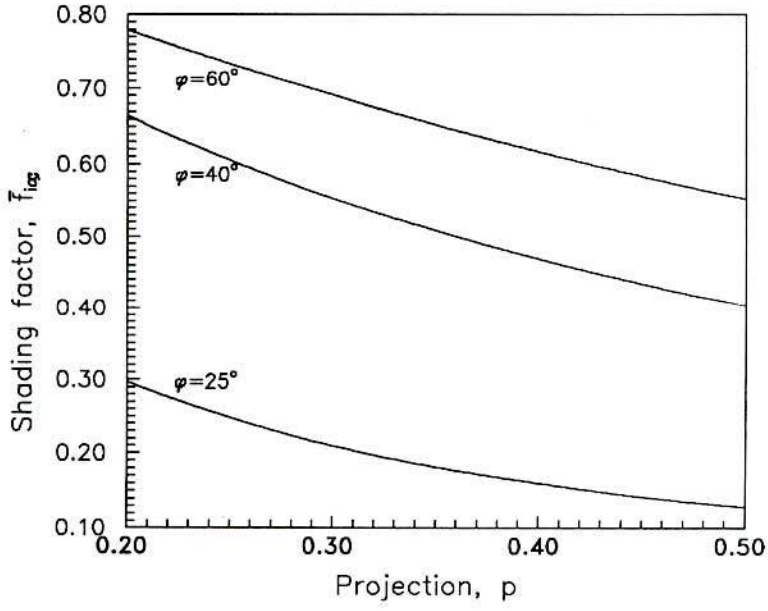

Figure 6.14: Variation of $\bar{f}_{i\infty}$ with wingwalls projection, p for the month of June; $g = 0.0$, $\bar{D}_f = 0.4$ and $\gamma = 0°$

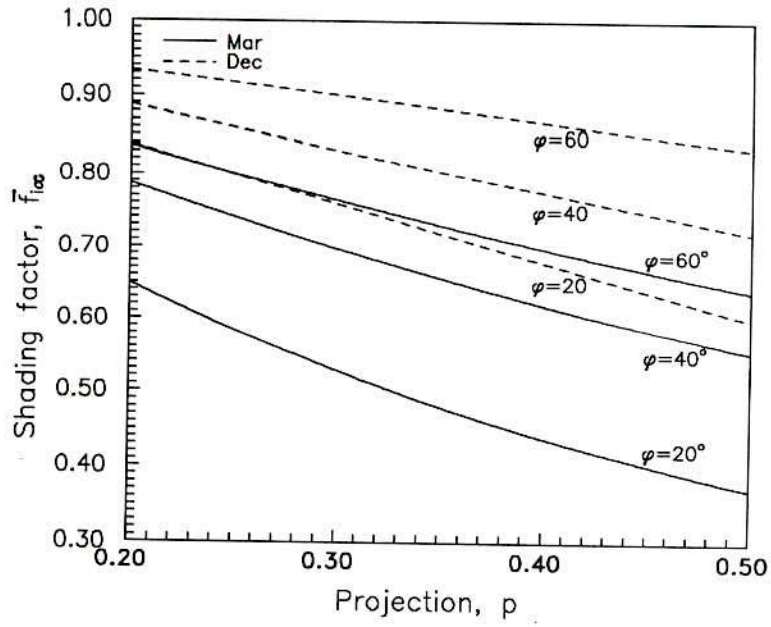

Figure 6.15: Variation of $\bar{f}_{i\infty}$ with wingwalls projection, p for the month of March and December; $g = 0.0$, $\bar{D}_f = 0.4$ and $\gamma = 0^o$

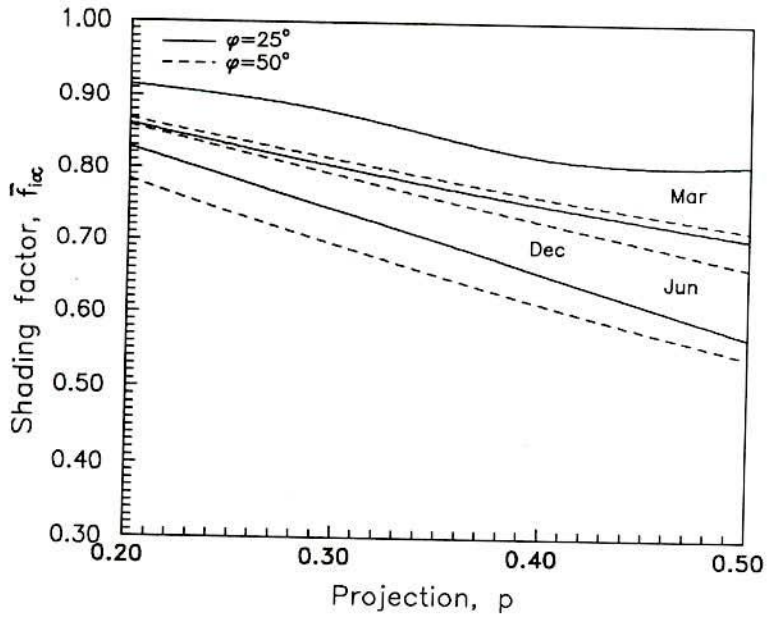

Figure 6.16: Variation of $\bar{f}_{i\infty}$ with wingwalls projection, p for the month of March, June and December; $g = 0.0$, $\bar{D}_f = 0.4$ and $\gamma = 60^o$

6.5 Conclusions

Expressing the instantaneous shading factor in terms of sun-earth-receiver-wingwall geometry, expressions for the monthly average shading factor for receivers shaded by infinite wingwalls on either side of the receiver have been developed. The expressions developed, taking into account atmospheric transmittance characterized by the monthly average daily diffuse fraction, are general enough to accomodate any receiver azimuthal angle and gap between the wingwall and the window. Interestingly, the shading factor is nothing but the ratio of the solar radiation received by a shading plane and the unshaded receiver. However, for wingwalls the shading plane is the plane joining the outer edge of the wingwall to the opposite side of the receiver.

Monthly average shading factors evaluated under terrestrial conditions characterized by the diffuse fraction differ from the extra-terrestrial values considerably. Tabulated values of the shading factor for receivers shaded by wingwalls are given in Appendix D for a wide range of latitudes, azimuthal angles, wingwall projections and gaps for different diffuse fraction, a climatic feature.

Chapter 7

Summary and Conclusions

7.1 Introduction

Based on the literature review, the key processed information required in the design methods for solar energy systems have been identified. They are the monthly average transmittance-absorptance product for flat plate collectors, monthly average optical efficiency for concentrating collectors and monthly average shading factors for receivers of general orientation shaded by overhangs or wingwalls. The definitions available in the literature for transmittance-absorptance product for flat plate collector are either all day average values or the average values over the operating period of the collector both evaluated on the mean day of the month. For concentrating collectors tabulated single day average values for two cut-off periods have been reported by Gaul and Rabl [45] which are independent of latitude and are valid when the daily clearness index is high; $K_T = 0.75$. According to the literature, the monthly average useful energy gain is evaluated as a product of F_R, $\bar{H}_T$, $\bar{\phi}$ and a monthly average transmittance-absorptance product or the optical efficiency. The definition for the transmittance-absorptance product or the optical efficiency should be consistent with the definition of monthly average daily utilizability.

In order to estimate the monthly average daily direct solar radiation received by shaded surfaces, the needed parameter is $\bar{f}_i$. All the methods available in the literature to estimate $\bar{f}_i$ assume the atmospheric transmittance be unity. Also, methods to estimate $\bar{f}_i$ for finite overhangs, shading non-south facing receivers, are not available. When the receivers are shaded by wingwalls, methods reported in the literature deal with the diffuse radiation only.

Aforementioned lacunae in estimating monthly average transmittance-absorptance product, optical efficiency and the shading factors motivated the present studies. In what follows, a summary of the key equations and conclusions drawn from the present studies

are summarized. The equation numbers in the first parenthesis are the original equation numbers as appeared in Chapter 2 to Chapter 6 of the present study. The numbers in the second parenthesis are the numbers in serial order for the present chapter.

7.2 Monthly Useful Energy Gain and a Definition of Transmittance-Absorptance Product for Flat Plate Collectors

Useful energy gain from a flat plate collector of unit area for a single day can be calculated from,

$$Q_{u,day} = F_R(\tau\alpha)^*_{day} H_T \phi_{day} \qquad (2.36) \qquad (7.1)$$

In Eq. (7.1), to be consistent with the definition of ϕ_{day} given by Eq. (2.35), $(\tau\alpha)^*_{day}/(\tau\alpha)_n$ is to be defined as,

$$(\tau\alpha)^*_{day} = \sum [I_T - I_c]^+ (\tau\alpha) \Big/ \sum [I_T - I_c]^+ \qquad (2.38) \qquad (7.2)$$

$Q'_{u,day}$, the useful energy gain for a single day for a flat plate collector of unit area when all day average transmittance-absorptance product is employed, is defined by,

$$(\tau\alpha)_{day} = \sum_{-\omega_s}^{\omega_s} I_T(\tau\alpha) \Big/ \sum_{-\omega_s}^{\omega_s} I_T \qquad (2.40) \qquad (7.3)$$

Normalized difference between $Q_{u,day}$ and $Q'_{u,day}$ is also the normalized difference between the two values of the daily transmittance-absorptance product as obtained from Eqs. (7.2) and (7.3). The percentage difference, Δ_d is defined as,

$$\Delta_d = \frac{Q_{u,day} - Q'_{u,day}}{Q'_{u,day}} \times 100 = \frac{(\tau\alpha)^*_{day} - (\tau\alpha)_{day}}{(\tau\alpha)_{day}} \times 100 \qquad (2.52) \qquad (7.4)$$

Δ_d is not insignificant and in general is large when K_T is high, $\beta = 90^o$ and the latitude is high for non-south facing collectors. For example, when $\gamma = 60^o$, $K_T = 0.7$, $\Delta_d = 5.88\,\%$ for $\phi = 20^o$ and $\Delta_d = 10.22\,\%$ for $\phi = 60^o$ in the month of December.

$\bar{Q}_{u,m}$ and $\bar{Q}'_{u,m}$, the monthly average daily useful energy gain analogous to $Q_{u,day}$ and $Q'_{u,day}$ are given by,

$$\bar{Q}_{u,m} = F_R(\tau\alpha)_n \bar{H}_T \bar{\phi}(\overline{\tau\alpha})^*/(\tau\alpha)_n \qquad (2.47) \qquad (7.5)$$

$$\bar{Q}'_{u,m} = F_R(\tau\alpha)_n \bar{H}_T \bar{\phi}(\overline{\tau\alpha})/(\tau\alpha)_n \qquad (2.50) \qquad (7.6)$$

$(\overline{\tau\alpha})^*/(\tau\alpha)_n$ and $(\overline{\tau\alpha})/(\tau\alpha)_n$ appearing in Eqs. (7.5) and (7.6) are defined by,

$$\frac{(\overline{\tau\alpha})^*}{(\tau\alpha)_n} = \sum_{day}\sum_{hour} (I_T - I_c)^+ (\tau\alpha)/(\tau\alpha)_n \Big/ \sum_{day}\sum_{hour} (I_T - I_c)^+ \qquad (2.49) \qquad (7.7)$$

$$\frac{(\overline{\tau\alpha})}{(\tau\alpha)_n} = \sum_{day}\sum_{hour} I_T(\tau\alpha)/(\tau\alpha)_n \Big/ \sum_{day}\sum_{hour} I_T \qquad (2.51) \qquad (7.8)$$

$\bar{\Delta}_d$, the percentage difference in the monthly average transmittance-absorptance product values [given by Eqs. (7.7) and (7.8)], is defined by,

$$\bar{\Delta}_d = \frac{\bar{Q}_{u,m} - \bar{Q}'_{u,m}}{\bar{Q}'_{u,m}} \times 100 = \frac{(\overline{\tau\alpha})^* - (\overline{\tau\alpha})}{(\overline{\tau\alpha})} \times 100 \qquad (2.60) \qquad (7.9)$$

In general, $\bar{\Delta}_d > \Delta_d$, for $K_T = \bar{K}_T$ and $X_c = \bar{X}_c$. These results warrant developing methods to estimate $(\overline{\tau\alpha})^*/(\tau\alpha)_n$ as defined by Eq. (7.7) in the present studies. Also, Eq. (7.7) is consistent with the definition of monthly average daily utilizability when $\bar{Q}_{u,m}$ is expressed by Eq. (7.5).

7.3 Evaluation of Monthly Average Transmittance-Absorptance Product during the Operational Time Period for Flat Plate Collectors

When Eq. (7.2) is expressed as an integral, $(\tau\alpha)^*_{day}/(\tau\alpha)_n$ is given by,

$$\frac{(\tau\alpha)^*_{day}}{(\tau\alpha)_n} = \int_{\omega_{c1}}^{\omega_{c2}} [I_T - I_c] \frac{(\tau\alpha)}{(\tau\alpha)_n} d\omega \Big/ \int_{\omega_{c1}}^{\omega_{c2}} [I_T - I_c]\, d\omega \qquad (3.2) \qquad (7.10)$$

Expressing I_T in Eq. (7.10) in terms of r_t [12] and r_d [16] correlations, upon integration Eq. (7.10) yields,

$$\begin{aligned}
\frac{(\tau\alpha)^*_{day}}{(\tau\alpha)_n} = {} & \Bigg[2(1+b_o)\Big\{a_1 I_{P3}(\omega_1,\omega'_{c1}) + bI_{P4}(\omega_1,\omega'_{c1})\Big\} + a_1(1-b_o)I_{P1}(\omega_2,\omega_1) \\
& + a_1 b_o(\omega_2-\omega_1) + b(1-b_o)I_{P2}(\omega_2,\omega_1) + bb_o I_{P5}(\omega_2,\omega_1) + \\
& 2(1+b_o)\Big\{a_1 I_{P3}(\omega'_{c2},\omega_2) + bI_{P4}(\omega'_{c2},\omega_2)\Big\} + \\
& K_2 D_f B' \frac{(\tau\alpha)_d}{(\tau\alpha)_n}\Big[I_{P5}(\omega_{c2},\omega_{c1}) - \cos\omega_s(\omega_{c2}-\omega_{c1})\Big] + \\
& K_3 B' \frac{(\tau\alpha)_g}{(\tau\alpha)_n}\Big[K_5 I_{P5}(\omega_{c2},\omega_{c1}) - a\cos\omega_s(\omega_{c2}-\omega c1) + bI_{P6}(\omega_{c2},\omega_{c1})\Big] \\
& - \frac{I_c}{K_4}\frac{(\overline{\overline{\tau\alpha}})}{(\tau\alpha)_n}\Bigg] \div \Bigg[a_1 I_{P1}(\omega'_{c2},\omega'_{c1}) + bI_{P2}(\omega'_{c2},\omega'_{c1}) + \\
& K_2 D_f B'\Big[I_{P5}(\omega_{c2},\omega_{c1}) - \cos\omega_s(\omega_{c2}-\omega_{c1})\Big] + K_3 B'\Big[K_5 I_{P5}(\omega_{c2},\omega_{c1}) - \\
& a\cos\omega_s(\omega_{c2}-\omega_{c1}) + bI_{P6}(\omega_{c2},\omega_{c1})\Big] - \frac{I_c}{K_4}(\omega_{c2}-\omega_{c1})\Bigg] \qquad (3.50) \quad (7.11)
\end{aligned}$$

It has been suggested that $(\overline{\overline{\tau\alpha}})/(\tau\alpha)_n$ appearing in Eq. (7.11) be evaluated at the hour angle $\bar{\bar{\omega}}$ corresponding to a effective angle of incidence $\bar{\bar{\theta}} = (\theta_1+\theta_m+\theta_2)/3$. θ_1, θ_m and θ_2 are the angles of incidence at $\omega = \omega_{c1}$, ω_m and ω_{c2} respectively. $(\overline{\overline{\tau\alpha}})/(\tau\alpha)_n$ evaluated

by this procedure according to Eq. (3.81) agrees within a rms difference of 1 %, compared to the values obtained by numerical integration. $(\tau\alpha)^*_{day}/(\tau\alpha)_n$ calculated according to Eq. (7.11) has been validated by comparing with the values obtained using hourly solar radiation data for three locations. The agreement is within 1.7 % for south facing as well as non-south facing collectors. The agreement is somewhat poor when $K_T < 0.4$.

A procedure based on equivalent mean day (EMD) calculation enabled calculating $(\overline{\tau\alpha})^*/(\tau\alpha)_n$ using Eq. (7.11) developed for a single day. Equivalent mean day is characterized by $\delta = \delta_m$ and $K_T = \bar{K}^*_T$, where $\bar{K}^*_T$ is the average clearness index of the days which contribute to useful energy. Values of $(\overline{\tau\alpha})^*/(\tau\alpha)_n$ obtained by EMD procedure have been validated against the values obtained by numerical integration of the defining equation [Eq. (7.7)] for $\phi = 20^o$, 40^o and 60^o, $\beta = \phi - 15^o$, 0^o, $\phi + 15^o$ and 90^o, $-23.05^o \leq \delta \leq 23.09^o$, $0.2 \leq X_c \leq 2.0$ and $\gamma = 0^o$, 30^o, 60^o and 90^o. $(\overline{\tau\alpha})^*_{emd}/(\tau\alpha)_n$ agrees with $(\overline{\tau\alpha})^*/(\tau\alpha)_n$(num) within 1 % when $\beta = \phi$ for all azimuthal angles and within 1.26 % when $\beta = 90^o$ and $\gamma = 90^o$. Thus, the monthly average transmittance-absorptance product defined in the present studies consistent with the definition of utilizability can be evaluated with the expressions developed for a single day using the EMD procedure.

7.4 Evaluation of Monthly Average Optical Efficiency during the Operational Time Period for Parabolic Trough Concentrators

Analogous to Eq. (7.10), optical efficiency for a single day for concentrating collectors (parabolic trough concentrators) has been expressed as,

$$\left(\frac{\eta^*_{o,day}}{\eta_{o,n}}\right) = \int_0^{\omega_c} [I_T - I_c] \left(\frac{\eta_o}{\eta_{o,n}}\right) d\omega \Big/ \int_0^{\omega_c} [I_T - I_c]\, d\omega \qquad (4.11) \qquad (7.12)$$

A feature of Eq. (7.12) for $(\eta^*_{o,day}/\eta_{o,n})$ is that the cut-off time of Gaul and Rabl [45] is expressed by the hour angle ω_c which is related to the critical radiation level I_c. Explicit equations to determine ω_c for the five tracking modes, by equating $I_T = I_c$, have been developed and are recorded in Chapter 4, §4.3.3.

Essential differences between Eq. (7.10) for flat plate collectors and Eq. (7.12) for concentrating collectors are that $(\eta_o/\eta_{o,n})$ variation with θ is different and estimation of I_T on the aperture of the concentrators depends on the tracking modes. In the present studies, based on the $(\eta_o/\eta_{o,n})$ data and polynomial fits given by Gaul and Rabl [45], an accurate and convenient form for $(\eta_o/\eta_{o,n})$ has been proposed as,

$$\left(\frac{\eta_o}{\eta_{o,n}}\right) = P_i + \frac{Q_i}{\cos\theta} + R_i \cos\theta \qquad \text{if} \qquad 0^o \leq \theta \leq 60^o \qquad (4.6) \qquad (7.13)$$

$$= S_i \cos\theta \qquad \text{if} \quad 60^o \le \theta \le 90^o \qquad (4.7) \qquad (7.14)$$

The form given by Eqs. (7.13) and (7.14) is suitable for adapting to other types of concentrators.

Expressing I_T in terms of r_t [12] and r_d [16]) correlations for the five tracking modes, RHS of Eq. (7.12) has been evaluated to yield expressions for $(\eta^*_{o.day}/\eta_{o,n})$. General expression for $(\eta^*_{o.day}/\eta_{o,n})$ is given by,

$$\left(\frac{\eta^*_{o,day}}{\eta_{o,n}}\right) = \Bigg[a_1 P_i I_{P1}(\omega',0) + a_1 Q_i(\omega'-0) + a_1 R_i I_{P3}(\omega',0) + b P_i I_{P2}(\omega',0) + bQ_i I_{P5}(\omega',0) + bR_i I_{P4}(\omega',0) + S_i\Big\{a_1 I_{P3}(\omega'_c,\omega') + bI_{P4}(\omega'_c,\omega')\Big\} + \left(\frac{B'D_f}{C_r}\right)\left(\frac{\eta_{o,d}}{\eta_{o,n}}\right)\Big\{I_{P5}(\omega_c,0) - \cos\omega_s(\omega_c-0)\Big\} - I_c\left(\frac{\bar{\bar{\eta}}_o}{\eta_{o,n}}\right)\Bigg] \div \Bigg[a_1 I_{P1}(\omega'_c,0) + bI_{P2}(\omega'_c,0) + \left(\frac{B'D_f}{C_r}\right)\Big\{I_{P5}(\omega_c,0) - \cos\omega_s(\omega_c-0)\Big\} - I_c(\omega_c-0)\Bigg] \qquad (4.47) \qquad (7.15)$$

The primitives $I_{P1}(\omega)$ to $I_{P5}(\omega)$ for the five tracking modes are given in Table 4.3. $(\bar{\bar{\eta}}_o/\eta_{o,n})$ appearing in Eq. (7.15) can be evaluated accurately by,

$$\left(\frac{\bar{\bar{\eta}}_o}{\eta_{o,n}}\right) = \frac{I_b(\bar{\bar{\omega}})R_b(\bar{\bar{\omega}})(\eta_{o,b}/\eta_{o,n}) + \frac{1}{C_r}I_d(\bar{\bar{\omega}})(\eta_{o,d}/\eta_{o,n})}{I_b(\bar{\bar{\omega}})R_b(\bar{\bar{\omega}}) + \frac{1}{C_r}I_d(\bar{\bar{\omega}})}(\omega_c - 0) \quad (4.50) \qquad (7.16)$$

where, $\bar{\bar{\omega}}$ is the hour angle corresponding to an effective angle of incidence $\bar{\bar{\theta}}$ defined by,

$$\bar{\bar{\theta}} = \frac{2\,\theta_1 + \theta_n}{3} \qquad (4.48) \qquad (7.17)$$

where, θ_1 and θ_n are the angles of incidence at $\omega = \omega_c$ and $\omega = 0$.

Numerical values for $(\eta^*_{o,day}/\eta_{o,n})$ have been obtained using Eq. (7.15) for the five tracking modes for $\phi = 20^o$, 40^o and 60^o, $-23.05^o \le \delta \le 23.09^o$, $K_T = 0.3$, 0.5 and 0.7, for $0.2 \le X_c \le 0.8$. This range for the non-dimensional critical level includes small to large cut-off time. Significant conclusions obtained from the numerical values of $(\eta^*_{o,day}/\eta_{o,n})$ are as follows:

1. $(\eta^*_{o,day}/\eta_{o,n})$ does depend on the latitude.

2. Dependence of $(\eta^*_{o,day}/\eta_{o,n})$ on the clearness index is as significant as the dependence on declination.

3. Even though $K_T = 0.3$ is a low value when concentrating collectors are not efficient, low values of K_T do occur in a month even when $\bar{K}_T$ is high. Also, assuming

$K_T = 0.75$ by Gaul and Rabl [45] is restrictive since very few locations have a monthly average daily clearness index greater than 0.6.

4. The difference between the values of $(\eta^*_{o,day}/\eta_{o,n})$ and $(\eta^*_{o,day}/\eta_{o,n})_{GR}$ is large, particularly, for tracking mode **c** which experiences a bimodal distribution of solar radiation. When the solar radiation distribution is bimodal, specifying cut-off time only actually includes non-operating time period for the concentrator. Thus, relating I_c to ω_c and considering the weighting function to be $(I_T - I_c)^+$ is not only consistent with the definition of utilizability but also takes into account the correct operational time.

$(\eta^*_{o,day}/\eta_{o,n})$ values compared with the $(\eta^*_{o,day}/\eta_{o,n})$(data) values show good agreement for two locations (Ahmedabad $\phi = 23.07^o$ and New Delhi $\phi = 28.58^o$, India) within a rms difference of 0.5 %. The agreement for Madison, WI, USA is not as good (rms difference of 2.2 %) mainly because of $K_T < 0.4$ for the months of November, December and January.

Monthly average optical efficiency $(\bar{\eta}^*_o/\eta_{o,n})$ has been defined by,

$$\left(\frac{\bar{\eta}^*_o}{\eta_{o,n}}\right) = \sum \sum_{-\omega_s}^{\omega_s} [I_T - I_c]^+ \left(\frac{\eta_o}{\eta_{o,n}}\right) \Big/ \sum \sum_{-\omega_s}^{\omega_s} [I_T - I_c]^+ \qquad (4.90) \qquad (7.18)$$

EMD approach as described for flat plate collectors has been found to be equally successful in predicting $(\bar{\eta}^*_o/\eta_{o,n})$ for concentrating collectors tracked in the five principal modes. The comparisons made have been extensive for $\phi = 20^o$, 40^o and 60^o, $-23.05^o \leq \delta \leq 23.09^o$, $K_T = 0.3$, 0.5 and 0.7, $0.2 \leq X_c \leq 2.0$. The agreement between $(\bar{\eta}^*_{o,emd}/\eta_{o,n})$ and $(\bar{\eta}^*_{o,emd}/\eta_{o,n})$(num) for the tracking modes **a** and **b** is within 0.3 % and for mode **c** is within 0.6 % when $K_T = 0.7$. For tracking modes **d** and **e**, the agreement is within a rms difference of 0.1 % for $K_T = 0.7$.

Thus, a method to estimate monthly average optical efficiency for concentrating collectors tracked in the five principal modes, making use of the expressions developed for a single day, is developed and validated.

7.5 Evaluation of Monthly Average Shading Factor for Surfaces Shaded by Overhangs under Terrestrial Conditions

Monthly average shading factor evaluated on the mean day of the month, expressed in integral form, is given by,

$$\bar{f}_i = \sum_{\overline{day}} I_b\, R_b f_i \Big/ \sum_{\overline{day}} I_b\, R_b = \int_{\overline{day}} I_b R_b f_i\, dt \Big/ \int_{\overline{day}} I_b R_b\, dt \qquad (5.8) \qquad (7.19)$$

When I_b takes into account the atmospheric transmittance, when expressed, say, employing r_t [12] and r_d [16] correlations, $\bar{f}_i$ is a function of the monthly average daily diffuse fraction.

Eq. (7.19) becomes integrable when the overhangs are infinite. The corresponding shading factor is designated by $\bar{f}_{i\infty}$. $\bar{f}_{i\infty}$ has been shown to be,

$$\bar{f}_{i\infty} = \left(\frac{A_{shp}}{A_w}\right) \frac{\bar{R}_b^*}{\bar{R}_b} \qquad (5.34) \qquad (7.20)$$

When a gap exists between the overhang and the window $\bar{f}_{i\infty}$ is given by,

$$\bar{f}_{i\infty} = \left(\frac{1}{\cos\psi_1}\right) \frac{\bar{R}_{b1}^*}{\bar{R}_b} - \left(\frac{1}{\cos\psi_2}\right) \frac{\bar{R}_{b2}^*}{\bar{R}_b} \qquad (5.46) \qquad (7.21)$$

Eqs. (7.20) and (7.21) are analogous to Yanda and Jones' [128] shading plane approach. The difference being that Eqs. (7.20) and (7.21) have been obtained from the defining equation [Eq. (7.19)]. Yanda and Jones [128], however, employed $\bar{R}_{bo}$ and $\bar{R}_{bo}^*$, the tilt factors evaluated under extra-terrestrial conditions. The corresponding shading factor has been desiganted as $\bar{f}_{io\infty}$ in the present studies. $\bar{R}_b$ and $\bar{R}_b^*$ appearing in the present equations [Eqs. (7.20) and (7.21)] depend on the monthly average daily diffuse fraction. In addition, the present approach enabled generalization of the algorithms to include non-vertical receivers. $\bar{f}_{i\infty}$ values obtained using Eq. (7.20), have been validated against the values obtained using hour by hour solar radiation data for 3 locations. The agreement is within 5 % rms difference. Calculations assuming atmospheric transmittance to be unity (i.e., under extra-terrestrial conditions), as has been done by Utzinger and Klein [125] differ from $\bar{f}_{i\infty}$(data) by more than 12 % rms. Influence of diffuse fraction has been evaluated as $\bar{f}_{i\infty}/\bar{f}_{io\infty}$ for a wide range of climates and parameters; $\phi = 20^o$, 25^o, 30^o, 40^o, 50^o and 60^o, $-23.05^o \leq \delta \leq 23.09^o$, $\bar{D}_f = 0.2$, 0.4, 0.6 and 0.8, $p = 0.2$, 0.3, 0.4 and 0.5 and $\gamma = 0^o$, 30^o, 60^o and 90^o. In summary, it is concluded that $\bar{f}_{i\infty}$ differs considerably from $\bar{f}_{io\infty}$ at low latitudes and $\gamma \neq 0$ and in summer months. Though, these results are presented for infinite overhangs, influence of diffuse fraction is similar for finite overhangs.

In order to evaluate the monthly average shading factor, $\bar{f}_i$, when the overhang is finite, $\bar{f}_i$ has been related to $\bar{f}_{i\infty}$ which can be calculated easily. Based on the detailed studies on the relations developed for different projections and extensions, the following equations to evaluate $\bar{f}_i$ are recommended.

When $\bar{f}_{i\infty} > 0$,

$$\bar{f}_i = 0.258\, exp^{-2.90\,e} + [0.703 + 0.627\,e - 0.377\,e^2]\,\bar{f}_{i\infty} \qquad (5.60) \qquad (7.22)$$

$$\bar{f}_i = \bar{f}_{i\infty} \quad \text{if} \quad \bar{f}_i < \bar{f}_{i\infty}, \quad \text{according to Eq. (7.22)} \qquad (5.56) \qquad (7.23)$$

When $\bar{f}_{i\infty} = 0$,

$$\bar{f}_i^o = m\,[\omega_s' - (e + 0.2)]^n \qquad (5.61) \qquad (7.24)$$

Eqs. (7.22), (7.23) and (7.24) predict $\bar{f}_i$ within a rms difference of 2 % tested in the range $\phi = 20^o$, 25^o, 30^o, 40^o, 50^o and 60^o, $-23.05^o \leq \delta \leq 23.09^o$, $\bar{D}_f = 0.2$, 0.4, 0.6 and 0.8, $p = 0.2$, 0.3, 0.4 and 0.5, $\gamma = 0^o$ and $e = 0.0$, 0.2, 0.4, 0.6 and 0.8.

The equations relating $\bar{f}_i$ to $\bar{f}_{i\infty}$ for south facing receivers have been found to be applicable for non-south facing receivers as well. The equations have become applicable when $\bar{f}_i$ for non-south facing receivers has been split into two parts as $\bar{f}_{i1}$ and $\bar{f}_{i2}$. $\bar{f}_{i1}$ and $\bar{f}_{i2}$ are the part shading factor values defined by,

$$\bar{f}_{i1} = \frac{\sum_{\omega_{sr}}^{\omega_o} I_b R_b f_i}{\sum_{\omega_{sr}}^{\omega_o} I_b R_b} = \frac{\int_{\omega_{sr}}^{\omega_o} I_b R_b f_i \, d\omega}{\int_{\omega_{sr}}^{\omega_o} I_b R_b \, d\omega} \qquad (5.69) \qquad (7.25)$$

and

$$\bar{f}_{i2} = \frac{\sum_{\omega_o}^{\omega_{ss}} I_b R_b f_i}{\sum_{\omega_o}^{\omega_{ss}} I_b R_b} = \frac{\int_{\omega_o}^{\omega_{ss}} I_b R_b f_i \, d\omega}{\int_{\omega_o}^{\omega_{ss}} I_b R_b \, d\omega} \qquad (5.70) \qquad (7.26)$$

When $\bar{f}_{i1}$ and $\bar{f}_{i2}$ are given by Eqs. (7.25) and (7.26), $\bar{f}_i$ is obtained from,

$$\bar{f}_i = \frac{H_{bT1}\,\bar{f}_{i1} + H_{bT2}\,\bar{f}_{i2}}{H_{bT}} \qquad (5.68) \qquad (7.27)$$

$\bar{f}_{i1}$ and $\bar{f}_{i2}$ are related to $\bar{f}_{i\infty 1}$ and $\bar{f}_{i\infty 2}$ by the same relations developed for south facing receivers. This procedure yielded $\bar{f}_i$ values within a rms difference of 2.1 % when the projection is small, say, 0.2. A simple procedure to obtain $\bar{f}_i$ at any projection from the value at $p = 0.2$ has been developed. $\bar{f}i$ at a projection p_2 is related to $\bar{f}_i$ at a known small projection p_1 by,

$$\bar{f}_{ip2} = \bar{f}_{i\infty p2} + (\bar{f}_{ip1} - \bar{f}_{i\infty p1}) \left[\frac{2\,(\bar{f}_{i\infty p1} - \bar{f}_{i\infty p2})}{(1 - \bar{f}_{i\infty p1})}\right] \qquad (5.91) \qquad (7.28)$$

From the values of $\bar{f}_i$ at $p = 0.2$ predicted using Eq. (7.27), $\bar{f}_i$ for $p = 0.3$ to 0.5 have been obtained using Eq. (7.28) for $\gamma = 30^o$, 60^o and 90^o for $\phi = 25^o$, 30^o, 40^o, 50^o and 60^o, $\bar{D}_f = 0.4$. The agreements are within 3 %, 1 % and 0.5 % rms for $\gamma = 30^o$, 60^o and 90^o respectively. It is interesting to note that this procedure is accurate for higher azimuthal angles. The reason perhaps is due to, one of the $\bar{f}_{i1}$ or $\bar{f}_{i2}$ values practically becoming zero as γ increases.

7.6 Evaluation of Monthly Average Shading Factor for Surfaces Shaded by Wingwalls under Terrestrial Conditions

When a receiver is shaded by wingwalls on either sides, the monthly average shading factor evaluated on the mean day of the month is expressed by,

$$\bar{f}_{i\infty} = \frac{\int_{\omega_{sr}}^{\omega_o} I_b R_b f_{i1}\, d\omega + \int_{\omega_o}^{\omega_{ss}} I_b R_b f_{i2}\, d\omega}{\int_{\omega_{sr}}^{\omega_{ss}} I_b R_b\, d\omega} \qquad (6.5) \qquad (7.29)$$

It may be noted that ω_o in Eq. (7.29) is the hour angle corresponding to $(\gamma_s - \gamma) = 0$. Assuming the wingwalls to be infinite and expressing f_{i1} and f_{i2} in terms of sun-earth-receiver geometry $\bar{f}_{i\infty}$ has been obtained as,

$$\bar{f}_{i\infty} = \frac{\left(\frac{A_{shp1}}{A_w}\right)\bar{R}^*_{b1} + \left(\frac{A_{shp2}}{A_w}\right)\bar{R}^*_{b2}}{\bar{R}_b} \qquad (6.21) \qquad (7.30)$$

The corresponding monthly average shading factor for wingwalls evaluated under extra-terrestrial conditions, $\bar{f}_{io\infty}$ is obtained by replacing $\bar{R}^*_{b1}$, $\bar{R}^*_{b2}$ and $\bar{R}_b$ with the corresponding extra-terrrestrial tilt factors. Eq. (7.30) is exactly similar to Eq. (7.20) for infinite overhangs. The differences are:

1. $\bar{f}_{i\infty}$ is evaluated in two parts since the first wingwall shades during ω_{sr} to ω_o and the second wingwall shades from ω_o to ω_{ss}.

2. $\bar{R}^*_{b1}$, $\bar{R}^*_{b2}$ are the tilt factors for the planes joining the outer edge of the wingwall to the opposite side of the window. Thus, the azimuthal angle for the shading planes for wingwalls is different from the azimuthal angle of the receiver. Whereas, for the shading plane of the overhangs it is the slope that is different.

$\bar{f}_{i\infty}$ and $\bar{f}_{io\infty}$ have been evaluated and numerical values are presented in tables given in Appendix D. The parameter values are: $\phi = 20^o$, 40^o and 60^o, $\delta = -23.05^o$, -2.2^o and 23.09^o, $\gamma = 0^o$, 30^o, 60^o and 90^o, $g = 0.0$ and 0.1, $p = 0.2$, 0.3, 0.4 and 0.5. $\bar{f}_{i\infty}$ values are geven for $\bar{D}_f = 0.2$, 0.4 and 0.6 which is an additional parameter.

$\bar{f}_{i\infty}$ values obtained from Eq. (7.30) have been validated against $\bar{f}_{i\infty}$ values calculated by hour by hour numerical computations. The agreement is near perfect validating the the splitting of the all day monthly average shading factor values into two parts. Also, it validates that an appropriate shading plane can be defined for the wingwalls. As can be expected, since the shading planes for wingwalls, in general, are charecterized by $\gamma \neq 0$,

$\bar{f}_{i\infty}$ for wingwalls differs from $\bar{f}_{io\infty}$ more than the difference for overhang values. For example, even when the receiver azimuthal angle is zero, at $\phi = 25°$, for $p = 0.3$, $g = 0.0$, $\bar{D}_f = 0.6$, $\bar{f}_{i\infty} = 0.617$ and $\bar{f}_{io\infty} = 0.532$ for the wingwalls in the month of March. The corresponding values for the overhang are $\bar{f}_{i\infty} = 0.440$ and $\bar{f}_{io\infty} = 0.453$. Thus, a simple method to calculate the monthly average shading factor for infinite wingwalls, taking atmospheric transmittance into account, is developed.

7.7 Scope for further work

The following topics are suggested for further investigations.

1. Studies on sensitivity of the design methods for both active and passive solar energy syatems with new $(\overline{\tau\alpha})^*/(\tau\alpha)_n$ and $(\bar{\eta}_o^*/\eta_{o,n})$ be taken up.

2. f-chart [54, 55, 56] an $\bar{\phi}$, f-chart [61, 62] are correlations developed based on the simulation results. Better estimates for $(\overline{\tau\alpha})^*/(\tau\alpha)_n$, $(\bar{\eta}_o^*/\eta_{o,n})$ and in general $\bar{H}_T$ and $\bar{\phi}$ are developed after the correlations have been proposed. In view of this, studies to examine whether the correlations need modification are warranted.

3. Possibilities to develop some superposition techniques to yield long term system performance from the long term component performance be examined. This is advantageous to eventually evolve design methods for non-standard systems.

4. Methods to calculate monthly average shading factor for finite wingwalls can be developed along the lines for overhangs given in the present studies.

5. It appears that combining $\bar{R}_b\bar{f}_i$ into a single factor, $\bar{R}_{bs}$, i.e., the tilt factor for shaded surfaces is desirable since the present definition of f_i does not distinguish between a surface fully shaded and a surface that does not receive any radiation. The combined factor $\bar{R}_{bs}$ will be zero either when the surface is fully shaded or when it does not receive radiation.

6. Studies to estimate $\bar{f}_i$ for eggcrate structures, in terms of $\bar{f}_i$ for overhangs and wingwalls now separetely available, be taken up.

Appendix A

Tabulated Values of Daily and Monthly Average Useful Energy Gain and Transmittance-Absorptance Product for Flat Plate Collectors

A.1 Daily Values

Numerical values for $Q_{u,day}$, $Q'_{u,day}$, $(\tau\alpha)^*_{day}/(\tau\alpha)_n$[1], $(\tau\alpha)_{day}/(\tau\alpha)_n$[2] and the percentage difference, Δ_d as obtained employing Eqs. (2.34), (2.39), (2.40), (2.38) and (2.52) respectively are given in Tables A.1 to A.9.

The parameter values and their ranges are as follows:

$\phi = 20^o$, 40^o and 60^oN

$\beta = \phi + 15^o$, ϕ, $\phi - 15^o$ and 90^o

$\gamma = 0^o$, 30^o, 60^o and 90^o

$-23.45^o \leq \delta \leq 23.45^o$

$b_o = -0.1$ (applicable for flat plate collectors with a single glass cover)

$0.0 \leq Xc \leq 0.8$

$0.3 \leq K_T \leq 0.7$

A.2 Monthly Values

The monthly average daily values are the same as the tabulated values for the single day when read for $X_c = \bar{X}^*_c$ and $K_T = \bar{K}^*_T$.

---

[1] $(\tau\alpha)^*_{day}/(\tau\alpha)_n$ is indicated by Z^* in the tables

[2] $(\tau\alpha)_{day}/(\tau\alpha)_n$ is indicated by Z in the tables

Table A.1: Tabulated values of $Q_{u,day}$, $Q'_{u,day}$, $(\tau\alpha)_{day}/(\tau\alpha)_n$ and $(\tau\alpha)^*_{day}/(\tau\alpha)_n$ for $\phi = 20^o$N, $\delta = \delta_m$, $\gamma = 0^o$

β deg	X_c	Qty.	$K_T = 0.3$			$K_T = 0.5$			$K_T = 0.7$		
			Mar	Jun	Dec	Mar	Jun	Dec	Mar	Jun	Dec
5	0.2	$Q'_{u,day}$	5.354	6.064	3.988	9.108	10.151	6.827	12.982	14.202	9.795
		$Q_{u,day}$	5.361	6.072	3.992	9.196	10.249	6.905	13.314	14.556	10.093
		Z	0.915	0.915	0.912	0.924	0.925	0.911	0.929	0.932	0.902
		Z^*	0.916	0.916	0.913	0.933	0.934	0.921	0.953	0.955	0.929
		Δ_d	0.13	0.14	0.10	0.97	0.96	1.14	2.56	2.49	3.05
	0.4	$Q'_{u,day}$	3.375	3.813	2.518	5.743	6.383	4.314	8.187	8.937	6.185
		$Q_{u,day}$	3.384	3.824	2.524	5.830	6.481	4.395	8.485	9.256	6.476
		Z	0.915	0.915	0.912	0.924	0.925	0.911	0.929	0.932	0.902
		Z^*	0.917	0.918	0.914	0.938	0.939	0.928	0.963	0.966	0.944
		Δ_d	0.28	0.29	0.22	1.51	1.53	1.90	3.63	3.57	4.71
	0.6	$Q'_{u,day}$	1.789	2.018	1.338	3.045	3.381	2.291	4.340	4.736	3.283
		$Q_{u,day}$	1.798	2.028	1.343	3.101	3.444	2.344	4.520	4.929	3.460
		Z	0.915	0.915	0.912	0.924	0.925	0.911	0.929	0.932	0.902
		Z^*	0.919	0.919	0.915	0.941	0.942	0.932	0.968	0.970	0.950
		Δ_d	0.45	0.47	0.36	1.83	1.86	2.28	4.14	4.07	5.40
	0.8	$Q'_{u,day}$	0.618	0.697	0.463	1.051	1.167	0.794	1.499	1.634	1.138
		$Q_{u,day}$	0.622	0.701	0.466	1.073	1.192	0.814	1.566	1.707	1.205
		Z	0.915	0.915	0.912	0.924	0.925	0.911	0.929	0.932	0.902
		Z^*	0.921	0.921	0.917	0.944	0.945	0.934	0.971	0.974	0.954
		Δ_d	0.62	0.64	0.51	2.10	2.13	2.56	4.52	4.45	5.85
20	0.2	$Q'_{u,day}$	5.303	5.904	4.023	9.239	9.546	7.490	13.540	12.804	11.812
		$Q_{u,day}$	5.311	5.910	4.029	9.327	9.633	7.562	13.875	13.125	12.090
		Z	0.920	0.917	0.920	0.930	0.920	0.930	0.935	0.920	0.932
		Z^*	0.921	0.918	0.922	0.939	0.928	0.939	0.958	0.943	0.953
		Δ_d	0.14	0.11	0.14	0.95	0.91	0.97	2.47	2.50	2.35
	0.4	$Q'_{u,day}$	3.339	3.710	2.535	5.823	6.000	4.732	8.536	8.071	7.443
		$Q_{u,day}$	3.348	3.719	2.543	5.908	6.099	4.798	8.830	8.385	7.692
		Z	0.920	0.917	0.920	0.930	0.920	0.930	0.935	0.920	0.932
		Z^*	0.923	0.919	0.923	0.943	0.935	0.943	0.967	0.956	0.963
		Δ_d	0.29	0.23	0.29	1.45	1.65	1.41	3.43	3.90	3.33
	0.6	$Q'_{u,day}$	1.771	1.961	1.349	3.088	3.178	2.513	4.523	4.279	3.951
		$Q_{u,day}$	1.779	1.969	1.355	3.142	3.242	2.555	4.701	4.471	4.102
		Z	0.920	0.917	0.920	0.930	0.920	0.930	0.935	0.920	0.932
		Z^*	0.924	0.921	0.925	0.946	0.939	0.946	0.971	0.961	0.967
		Δ_d	0.46	0.39	0.45	1.76	2.03	1.70	3.92	4.49	3.80
	0.8	$Q'_{u,day}$	0.612	0.676	0.467	1.066	1.095	0.871	1.562	1.479	1.367
		$Q_{u,day}$	0.616	0.680	0.470	1.088	1.120	0.888	1.628	1.552	1.423
		Z	0.920	0.917	0.920	0.930	0.920	0.930	0.935	0.920	0.932
		Z^*	0.926	0.922	0.926	0.949	0.941	0.948	0.975	0.965	0.970
		Δ_d	0.62	0.55	0.61	2.01	2.32	1.94	4.27	4.91	4.16

Table A.1: *Continued*

β deg	X_c	Qty.	$K_T = 0.3$			$K_T = 0.5$			$K_T = 0.7$		
			Mar	Jun	Dec	Mar	Jun	Dec	Mar	Jun	Dec
35	0.2	$Q'_{u,day}$	5.062	5.532	3.911	8.915	8.500	7.763	13.226	10.664	13.089
		$Q_{u,day}$	5.068	5.535	3.918	9.002	8.564	7.820	13.561	10.927	13.307
		Z	0.920	0.913	0.923	0.928	0.906	0.939	0.930	0.893	0.947
		Z^*	0.921	0.914	0.924	0.937	0.913	0.946	0.953	0.915	0.963
		Δ_d	0.13	0.06	0.17	0.98	0.75	0.74	2.53	2.46	1.67
	0.4	$Q'_{u,day}$	3.184	3.476	2.463	5.618	5.340	4.904	8.336	6.736	8.238
		$Q_{u,day}$	3.193	3.482	2.472	5.701	5.432	4.957	8.630	7.036	8.432
		Z	0.920	0.913	0.923	0.928	0.906	0.939	0.930	0.893	0.947
		Z^*	0.922	0.915	0.926	0.941	0.921	0.949	0.962	0.932	0.969
		Δ_d	0.28	0.16	0.35	1.48	1.71	1.07	3.53	4.45	2.36
	0.6	$Q'_{u,day}$	1.689	1.835	1.311	2.979	2.828	2.604	4.416	3.576	4.365
		$Q_{u,day}$	1.697	1.841	1.318	3.032	2.893	2.639	4.593	3.770	4.486
		Z	0.920	0.913	0.923	0.928	0.906	0.939	0.930	0.893	0.947
		Z^*	0.924	0.916	0.928	0.944	0.927	0.951	0.967	0.941	0.973
		Δ_d	0.44	0.31	0.52	1.79	2.30	1.32	4.01	5.41	2.76
	0.8	$Q'_{u,day}$	0.584	0.632	0.454	1.029	0.975	0.903	1.524	1.237	1.507
		$Q_{u,day}$	0.587	0.635	0.457	1.050	1.001	0.917	1.591	1.310	1.553
		Z	0.920	0.913	0.923	0.928	0.906	0.939	0.930	0.893	0.947
		Z^*	0.925	0.918	0.929	0.946	0.930	0.953	0.970	0.946	0.976
		Δ_d	0.60	0.46	0.67	2.04	2.62	1.53	4.37	5.92	3.07
90	0.2	$Q'_{u,day}$	3.051	3.312	2.580	4.521	4.102	5.643	5.294	3.246	10.648
		$Q_{u,day}$	3.043	3.312	2.583	4.545	4.102	5.664	5.441	3.246	10.706
		Z	0.881	0.904	0.911	0.809	0.903	0.920	0.705	0.903	0.924
		Z^*	0.879	0.904	0.912	0.813	0.903	0.924	0.724	0.903	0.929
		Δ_d	-0.26	0.00	0.11	0.53	0.00	0.38	2.77	0.00	0.54
	0.4	$Q'_{u,day}$	1.931	2.124	1.630	2.855	2.610	3.578	3.334	2.058	6.694
		$Q_{u,day}$	1.921	2.124	1.634	2.886	2.610	3.599	3.498	2.058	6.772
		Z	0.881	0.904	0.911	0.809	0.903	0.920	0.705	0.903	0.924
		Z^*	0.877	0.904	0.913	0.818	0.903	0.926	0.739	0.903	0.935
		Δ_d	-0.51	0.00	0.21	1.09	0.00	0.57	4.92	0.00	1.17
	0.6	$Q'_{u,day}$	1.026	1.138	0.873	1.516	1.394	1.907	1.768	1.096	3.539
		$Q_{u,day}$	1.019	1.138	0.875	1.542	1.394	1.921	1.888	1.096	3.592
		Z	0.881	0.904	0.911	0.809	0.903	0.920	0.705	0.903	0.924
		Z^*	0.876	0.904	0.914	0.823	0.903	0.927	0.752	0.903	0.937
		Δ_d	-0.66	0.00	0.31	1.68	0.00	0.73	6.78	0.00	1.48
	0.8	$Q'_{u,day}$	0.355	0.396	0.304	0.524	0.484	0.661	0.611	0.380	1.221
		$Q_{u,day}$	0.353	0.396	0.305	0.536	0.484	0.667	0.663	0.380	1.242
		Z	0.881	0.904	0.911	0.809	0.903	0.920	0.705	0.903	0.924
		Z^*	0.875	0.904	0.915	0.828	0.903	0.928	0.764	0.903	0.940
		Δ_d	-0.68	0.00	0.40	2.30	0.00	0.87	8.47	0.00	1.73

Note: $Z = (\tau\alpha)_{day}/(\tau\alpha)_n$; $Z^* = (\tau\alpha)^*_{day}/(\tau\alpha)_n$; $Q_{u,day}$ and $Q'_{u,day}$ in MJ/m^2-day.

Table A.2: Tabulated values of $Q_{u,day}$, $Q'_{u,day}$, $(\tau\alpha)_{day}/(\tau\alpha)_n$ and $(\tau\alpha)^*_{day}/(\tau\alpha)_n$ for $\phi = 40^o$N, $\gamma = 0^o$

β deg	X_c	Qty.	$K_T = 0.3$			$K_T = 0.5$			$K_T = 0.7$		
			Mar	Jun	Dec	Mar	Jun	Dec	Mar	Jun	Dec
25	0.2	$Q'_{u,day}$	4.232	6.250	2.259	7.829	10.407	4.792	12.228	14.552	8.528
		$Q_{u,day}$	4.238	6.259	2.262	7.916	10.512	4.850	12.558	14.915	8.717
		Z	0.921	0.919	0.920	0.929	0.924	0.922	0.929	0.928	0.916
		Z^*	0.923	0.921	0.922	0.939	0.933	0.933	0.955	0.951	0.936
		Δ_d	0.15	0.14	0.14	1.11	1.01	1.21	2.70	2.49	2.22
	0.4	$Q'_{u,day}$	2.657	3.903	1.429	4.930	6.522	3.033	7.698	9.158	5.380
		$Q_{u,day}$	2.665	3.915	1.433	5.013	6.640	3.087	7.992	9.509	5.575
		Z	0.921	0.919	0.920	0.929	0.924	0.922	0.929	0.928	0.916
		Z^*	0.924	0.922	0.923	0.945	0.941	0.938	0.965	0.963	0.949
		Δ_d	0.32	0.31	0.28	1.68	1.81	1.78	3.81	3.83	3.63
	0.6	$Q'_{u,day}$	1.405	2.057	0.763	2.609	3.443	1.614	4.082	4.852	2.859
		$Q_{u,day}$	1.413	2.067	0.766	2.662	3.519	1.647	4.258	5.066	2.979
		Z	0.921	0.919	0.920	0.929	0.924	0.922	0.929	0.928	0.916
		Z^*	0.926	0.924	0.924	0.948	0.944	0.941	0.970	0.968	0.954
		Δ_d	0.51	0.49	0.43	2.02	2.21	2.09	4.32	4.40	4.19
	0.8	$Q'_{u,day}$	0.485	0.706	0.265	0.901	1.187	0.560	1.412	1.678	0.988
		$Q_{u,day}$	0.488	0.711	0.267	0.921	1.216	0.573	1.478	1.759	1.034
		Z	0.921	0.919	0.920	0.929	0.924	0.922	0.929	0.928	0.916
		Z^*	0.927	0.926	0.926	0.950	0.947	0.943	0.973	0.972	0.958
		Δ_d	0.68	0.68	0.58	2.28	2.51	2.34	4.69	4.82	4.60
40	0.2	$Q'_{u,day}$	4.052	5.850	2.242	7.831	9.523	5.344	12.757	13.014	10.439
		$Q_{u,day}$	4.059	5.857	2.247	7.918	9.611	5.381	13.088	13.337	10.556
		Z	0.922	0.916	0.926	0.933	0.916	0.943	0.935	0.914	0.950
		Z^*	0.924	0.918	0.928	0.943	0.924	0.950	0.959	0.937	0.961
		Δ_d	0.18	0.12	0.21	1.12	0.92	0.70	2.59	2.48	1.12
	0.4	$Q'_{u,day}$	2.540	3.646	1.418	4.930	5.965	3.383	8.027	8.209	6.579
		$Q_{u,day}$	2.549	3.657	1.423	5.010	6.079	3.418	8.313	8.549	6.702
		Z	0.922	0.916	0.926	0.933	0.916	0.943	0.935	0.914	0.950
		Z^*	0.926	0.919	0.930	0.948	0.933	0.953	0.968	0.952	0.968
		Δ_d	0.37	0.29	0.41	1.63	1.91	1.03	3.56	4.14	1.86
	0.6	$Q'_{u,day}$	1.345	1.918	0.758	2.608	3.151	1.799	4.256	4.358	3.488
		$Q_{u,day}$	1.353	1.927	0.762	2.659	3.227	1.822	4.428	4.568	3.568
		Z	0.922	0.916	0.926	0.933	0.916	0.943	0.935	0.914	0.950
		Z^*	0.927	0.921	0.932	0.951	0.938	0.955	0.973	0.958	0.972
		Δ_d	0.57	0.49	0.59	1.96	2.41	1.28	4.04	4.84	2.27
	0.8	$Q'_{u,day}$	0.463	0.657	0.263	0.899	1.087	0.623	1.471	1.506	1.206
		$Q_{u,day}$	0.467	0.662	0.265	0.919	1.117	0.632	1.536	1.586	1.237
		Z	0.922	0.916	0.926	0.933	0.916	0.943	0.935	0.914	0.950
		Z^*	0.929	0.923	0.933	0.953	0.941	0.957	0.976	0.962	0.975
		Δ_d	0.75	0.67	0.75	2.22	2.74	1.49	4.39	5.31	2.59

Table A.2: *Continued*

β deg	X_c	Qty.	$K_T = 0.3$			$K_T = 0.5$			$K_T = 0.7$		
			Mar	Jun	Dec	Mar	Jun	Dec	Mar	Jun	Dec
55	0.2	$Q'_{u,day}$	3.747	5.279	2.146	7.454	8.251	5.588	12.458	10.785	11.619
		$Q_{u,day}$	3.754	5.284	2.152	7.541	8.311	5.611	12.789	11.041	11.682
		Z	0.921	0.911	0.930	0.931	0.902	0.954	0.932	0.889	0.966
		Z^*	0.923	0.911	0.932	0.942	0.908	0.958	0.956	0.910	0.972
		Δ_d	0.19	0.09	0.27	1.17	0.73	0.42	2.66	2.37	0.55
	0.4	$Q'_{u,day}$	2.346	3.286	1.357	4.691	5.170	3.538	7.836	6.813	7.314
		$Q_{u,day}$	2.355	3.294	1.364	4.771	5.267	3.563	8.122	7.126	7.393
		Z	0.921	0.911	0.930	0.931	0.902	0.954	0.932	0.889	0.966
		Z^*	0.925	0.913	0.935	0.946	0.919	0.961	0.966	0.930	0.977
		Δ_d	0.39	0.24	0.50	1.70	1.89	0.69	3.66	4.60	1.07
	0.6	$Q'_{u,day}$	1.244	1.724	0.727	2.481	2.732	1.883	4.155	3.620	3,873
		$Q_{u,day}$	1.251	1.733	0.732	2.531	2.805	1.900	4.327	3.827	3.928
		Z	0.921	0.911	0.930	0.931	0.902	0.954	0.932	0.889	0.966
		Z^*	0.926	0.915	0.936	0.950	0.926	0.963	0.970	0.940	0.980
		Δ_d	0.59	0.49	0.69	2.03	2.70	0.91	4.14	5.74	1.42
	0.8	$Q'_{u,day}$	0.428	0.590	0.252	0.855	0.943	0.651	1.436	1.253	1.341
		$Q_{u,day}$	0.431	0.594	0.254	0.875	0.972	0.658	1.501	1.332	1.364
		Z	0.921	0.911	0.930	0.931	0.902	0.954	0.932	0.889	0.966
		Z^*	0.928	0.917	0.938	0.952	0.929	0.965	0.973	0.945	0.983
		Δ_d	0.78	0.68	0.86	2.30	3.09	1.10	4.50	6.30	1.69
90	0.2	$Q'_{u,day}$	2.688	3.520	1.669	5.276	4.502	4.946	8.698	4.057	11.141
		$Q_{u,day}$	2.690	3.507	1.674	5.361	4.440	4.959	9.014	3.901	11.169
		Z	0.909	0.879	0.928	0.894	0.825	0.953	0.871	0.721	0.964
		Z^*	0.910	0.876	0.931	0.908	0.813	0.955	0.903	0.693	0.966
		Δ_d	0.10	-0.36	0.31	1.60	-1.38	0.26	3.63	-3.84	0.25
	0.4	$Q'_{u,day}$	1.682	2.194	1.060	3.321	2.741	3.134	5.468	2.541	7.057
		$Q_{u,day}$	1.687	2.177	1.066	3.411	2.666	3.149	5.791	2.419	7.101
		Z	0.909	0.879	0.928	0.894	0.825	0.953	0.871	0.721	0.964
		Z^*	0.911	0.872	0.933	0.918	0.802	0.958	0.923	0.686	0.970
		Δ_d	0.25	-0.79	0.53	2.71	-2.73	0.48	5.91	-4.80	0.62
	0.6	$Q'_{u,day}$	0.893	1.143	0.568	1.756	1.446	1.671	2.901	1.358	3.731
		$Q_{u,day}$	0.897	1.129	0.572	1.814	1.399	1.682	3.104	1.300	3.766
		Z	0.909	0.879	0.928	0.894	0.825	0.953	0.871	0.721	0.964
		Z^*	0.913	0.868	0.935	0.923	0.798	0.959	0.932	0.690	0.973
		Δ_d	0.41	-1.26	0.70	3.31	-3.22	0.66	7.02	-4.23	0.93
	0.8	$Q'_{u,day}$	0.307	0.390	0.198	0.605	0.498	0.579	1.003	0.472	1.287
		$Q_{u,day}$	0.309	0.384	0.199	0.627	0.483	0.583	1.078	0.457	1.302
		Z	0.909	0.879	0.928	0.894	0.825	0.953	0.871	0.721	0.964
		Z^*	0.914	0.866	0.936	0.926	0.799	0.961	0.937	0.698	0.975
		δ_d	0.57	-1.52	0.85	3.62	-3.10	0.81	7.53	-3.18	1.16

Note: $Z = (\tau\alpha)_{day}/(\tau\alpha)_n$; $Z^* = (\tau\alpha)^*_{day}/(\tau\alpha)_n$; $Q_{u,day}$ and $Q'_{u,day}$ in MJ/m^2-day.

Table A.3: Tabulated values of $Q_{u,day}$, $Q'_{u,day}$, $(\tau\alpha)_{day}/(\tau\alpha)_n$ and $(\tau\alpha)^*_{day}/(\tau\alpha)_n$ for $\phi = 60^o$N, $\gamma = 0^o$

β deg	X_c	Qty.	$K_T = 0.3$			$K_T = 0.5$			$K_T = 0.7$		
			Mar	Jun	Dec	Mar	Jun	Dec	Mar	Jun	Dec
45	0.2	$Q'_{u,day}$	2.628	5.758	0.660	6.001	9.861	2.666	11.150	14.550	6.497
		$Q_{u,day}$	2.635	5.771	0.661	6.087	9.971	2.669	11.473	14.934	6.502
		Z	0.926	0.917	0.940	0.935	0.919	0.953	0.933	0.922	0.957
		Z^*	0.929	0.919	0.942	0.948	0.930	0.954	0.960	0.946	0.958
		Δ_d	0.26	0.23	0.17	1.44	1.12	0.12	2.90	2.64	0.09
	0.4	$Q'_{u,day}$	1.641	3.541	0.423	3.773	6.160	1.713	7.014	9.175	4.398
		$Q_{u,day}$	1.649	3.561	0.424	3.849	6.306	1.720	7.293	9.575	4.409
		Z	0.926	0.917	0.940	0.935	0.919	0.953	0.933	0.922	0.957
		Z^*	0.931	0.923	0.943	0.954	0.941	0.957	0.970	0.962	0.960
		Δ_d	0.51	0.56	0.31	2.02	2.36	0.36	3.97	4.36	0.26
	0.6	$Q'_{u,day}$	0.870	1.848	0.229	1.996	3.252	0.917	3.722	4.870	2.369
		$Q_{u,day}$	0.877	1.865	0.230	2.044	3.348	0.922	3.889	5.117	2.383
		Z	0.926	0.917	0.940	0.935	0.919	0.953	0.933	0.922	0.957
		Z^*	0.933	0.926	0.944	0.957	0.947	0.959	0.974	0.968	0.963
		Δ_d	0.74	0.89	0.42	2.38	2.96	0.58	4.48	5.06	0.62
	0.8	$Q'_{u,day}$	0.300	0.630	0.081	0.691	1.119	0.320	1.287	1.688	0.812
		$Q_{u,day}$	0.303	0.638	0.081	0.709	1.157	0.322	1.349	1.782	0.820
		Z	0.926	0.917	0.940	0.935	0.919	0.953	0.933	0.922	0.957
		Z^*	0.935	0.928	0.945	0.960	0.950	0.961	0.978	0.973	0.966
		Δ_d	0.96	1.14	0.52	2.67	3.36	0.77	4.86	5.55	0.96
60	0.2	$Q'_{u,day}$	2.471	5.192	0.709	6.028	8.779	3.137	11.700	12.937	7.833
		$Q_{u,day}$	2.479	5.203	0.711	6.114	8.867	3.139	12.022	13.263	7.838
		Z	0.929	0.913	0.956	0.941	0.912	0.974	0.940	0.911	0.979
		Z^*	0.932	0.915	0.958	0.954	0.922	0.974	0.966	0.934	0.979
		Δ_d	0.33	0.21	0.19	1.42	1.00	0.07	2.75	2.52	0.06
	0.4	$Q'_{u,day}$	1.543	3.179	0.456	3.789	5.499	2.026	7.357	8.185	5.344
		$Q_{u,day}$	1.552	3.198	0.457	3.864	5.630	2.031	7.630	8.555	5.353
		Z	0.929	0.913	0.956	0.941	0.912	0.974	0.940	0.911	0.979
		Z^*	0.934	0.919	0.959	0.959	0.934	0.976	0.975	0.952	0.980
		Δ_d	0.61	0.58	0.31	1.96	2.38	0.23	3.70	4.51	0.16
	0.6	$Q'_{u,day}$	0.819	1.656	0.247	2.004	2.899	1.087	3.904	4.355	2.901
		$Q_{u,day}$	0.826	1.672	0.248	2.051	2.991	1.091	4.067	4.590	2.913
		Z	0.929	0.913	0.956	0.941	0.912	0.974	0.940	0.911	0.979
		Z^*	0.937	0.922	0.960	0.963	0.941	0.977	0.980	0.960	0.983
		Δ_d	0.86	0.98	0.41	2.32	3.17	0.39	4.18	5.39	0.41
	0.8	$Q'_{u,day}$	0.282	0.565	0.087	0.693	1.001	0.379	1.349	1.504	1.002
		$Q_{u,day}$	0.285	0.572	0.087	0.711	1.037	0.381	1.410	1.593	1.008
		Z	0.929	0.913	0.956	0.941	0.912	0.974	0.940	0.911	0.979
		Z^*	0.939	0.925	0.961	0.965	0.945	0.979	0.983	0.965	0.985
		Δ_d	1.08	1.26	0.50	2.59	3.61	0.53	4.54	5.95	0.67

Table A.3: *Continued*

β deg	X_c	Qty.	$K_T = 0.3$			$K_T = 0.5$			$K_T = 0.7$		
			Mar	Jun	Dec	Mar	Jun	Dec	Mar	Jun	Dec
75	0.2	$Q'_{u,day}$	2.240	4.501	0.721	5.727	7.380	3.388	11.437	10.623	8.589
		$Q_{u,day}$	2.248	4.508	0.723	5.813	7.438	3.390	11.757	10.874	8.592
		Z	0.929	0.907	0.965	0.940	0.899	0.983	0.938	0.889	0.988
		Z^*	0.932	0.908	0.967	0.954	0.906	0.984	0.965	0.910	0.989
		Δ_d	0.34	0.15	0.18	1.50	0.79	0.05	2.80	2.36	0.04
	0.4	$Q'_{u,day}$	1.399	2.746	0.463	3.599	4.619	2.205	7.189	6.734	5.893
		$Q_{u,day}$	1.409	2.759	0.465	3.673	4.725	2.208	7.461	7.062	5.900
		Z	0.929	0.907	0.965	0.940	0.899	0.983	0.938	0.889	0.988
		Z^*	0.935	0.911	0.968	0.960	0.919	0.985	0.974	0.932	0.989
		Δ_d	0.65	0.48	0.30	2.05	2.29	0.17	3.79	4.86	0.12
	0.6	$Q'_{u,day}$	0.742	1.429	0.251	1.904	2.443	1.180	3.814	3.579	3.217
		$Q_{u,day}$	0.749	1.443	0.252	1.950	2.528	1.184	3.977	3.805	3.227
		Z	0.929	0.907	0.965	0.940	0.899	0.983	0.938	0.889	0.988
		Z^*	0.937	0.916	0.969	0.963	0.930	0.986	0.979	0.945	0.991
		Δ_d	0.91	1.01	0.39	2.41	3.48	0.30	4.28	6.30	0.32
	0.8	$Q'_{u,day}$	0.256	0.487	0.088	0.658	0.842	0.412	1.318	1.242	1.117
		$Q_{u,day}$	0.258	0.494	0.089	0.676	0.876	0.413	1.379	1.329	1.122
		Z	0.929	0.907	0.965	0.940	0.899	0.983	0.938	0.889	0.988
		Z^*	0.939	0.919	0.969	0.966	0.935	0.987	0.982	0.950	0.993
		Δ_d	1.14	1.35	0.48	2.69	4.02	0.42	4.65	6.93	0.53
90	0.2	$Q'_{u,day}$	1.945	3.723	0.694	5.111	5.765	3.401	10.361	7.762	8.709
		$Q_{u,day}$	1.951	3.722	0.695	5.198	5.773	3.402	10.681	7.874	8.712
		Z	0.925	0.895	0.968	0.931	0.872	0.985	0.925	0.843	0.990
		Z^*	0.928	0.894	0.969	0.947	0.873	0.986	0.953	0.855	0.990
		Δ_d	0.34	-0.02	0.18	1.71	0.15	0.04	3.09	1.44	0.03
	0.4	$Q'_{u,day}$	1.216	2.259	0.446	3.211	3.585	2.227	6.512	4.926	6.005
		$Q_{u,day}$	1.223	2.262	0.447	3.287	3.636	2.230	6.794	5.146	6.011
		Z	0.925	0.895	0.968	0.931	0.872	0.985	0.925	0.843	0.990
		Z^*	0.931	0.896	0.970	0.953	0.884	0.987	0.965	0.881	0.991
		Δ_d	0.63	0.12	0.28	2.36	1.40	0.13	4.33	4.47	0.10
	0.6	$Q'_{u,day}$	0.644	1.174	0.241	1.698	1.898	1.191	3.453	2.636	3.302
		$Q_{u,day}$	0.650	1.182	0.242	1.745	1.960	1.194	3.621	2.826	3.310
		Z	0.925	0.895	0.968	0.931	0.872	0.985	0.925	0.843	0.990
		Z^*	0.933	0.901	0.971	0.956	0.900	0.988	0.970	0.904	0.992
		Δ_d	0.89	0.69	0.37	2.75	3.24	0.25	4.87	7.21	0.26
	0.8	$Q'_{u,day}$	0.222	0.400	0.085	0.587	0.652	0.415	1.193	0.917	1.148
		$Q_{u,day}$	0.225	0.406	0.085	0.605	0.682	0.417	1.256	0.999	1.153
		Z	0.925	0.895	0.968	0.931	0.872	0.985	0.925	0.843	0.990
		Z^*	0.935	0.907	0.972	0.959	0.913	0.989	0.973	0.919	0.994
		Δ_d	1.12	1.41	0.44	3.04	4.71	0.36	5.27	9.01	0.46

Note: $Z = (\tau\alpha)_{day}/(\tau\alpha)_n$; $Z^* = (\tau\alpha)^*_{day}/(\tau\alpha)_n$; $Q_{u,day}$ and $Q'_{u,day}$ in MJ/m^2-day.

Table A.4: Tabulated values of $Q_{u,day}$, $Q'_{u,day}$, $(\tau\alpha)_{day}/(\tau\alpha)_n$ and $(\tau\alpha)^*_{day}/(\tau\alpha)_n$ for $\phi = 20^oN$, $(\phi - \beta) = 0^o$

γ deg	X_c	Qty.	$K_T = 0.3$			$K_T = 0.5$			$K_T = 0.7$		
			Mar	Jun	Dec	Mar	Jun	Dec	Mar	Jun	Dec
30	0.4	$Q'_{u,day}$	3.33	3.71	2.52	5.77	6.03	4.63	8.48	8.18	7.22
		$Q_{u,day}$	3.34	3.72	2.53	5.85	6.12	4.70	8.74	8.49	7.46
		Z	0.920	0.917	0.919	0.930	0.921	0.927	0.937	0.923	0.930
		Z^*	0.922	0.919	0.922	0.943	0.936	0.940	0.966	0.957	0.960
		Δ_d	0.28	0.25	0.28	1.38	1.54	1.44	3.11	3.75	3.19
	0.8	$Q'_{u,day}$	0.61	0.68	0.46	1.06	1.10	0.85	1.55	1.50	1.33
		$Q_{u,day}$	0.61	0.68	0.47	1.08	1.13	0.87	1.61	1.57	1.38
		Z	0.920	0.917	0.919	0.930	0.921	0.927	0.937	0.923	0.930
		Z^*	0.925	0.922	0.925	0.948	0.942	0.946	0.974	0.967	0.968
		Δ_d	0.62	0.57	0.59	1.96	2.24	2.00	3.97	4.75	4.07
60	0.4	$Q'_{u,day}$	3.31	3.72	2.48	5.65	6.12	4.37	8.23	8.51	6.58
		$Q_{u,day}$	3.32	3.73	2.49	5.72	6.20	4.43	8.46	8.78	6.79
		Z	0.918	0.917	0.916	0.928	0.925	0.920	0.937	0.931	0.921
		Z^*	0.921	0.920	0.918	0.939	0.937	0.932	0.964	0.961	0.950
		Δ_d	0.27	0.26	0.23	1.24	1.32	1.38	2.80	3.19	3.17
	0.8	$Q'_{u,day}$	0.61	0.68	0.46	1.04	1.12	0.80	1.51	1.56	1.21
		$Q_{u,day}$	0.61	0.68	0.46	1.06	1.14	0.82	1.56	1.62	1.26
		Z	0.918	0.917	0.916	0.928	0.925	0.920	0.937	0.931	0.921
		Z^*	0.924	0.923	0.921	0.946	0.944	0.939	0.972	0.970	0.960
		Δ_d	0.61	0.61	0.57	1.91	2.04	2.16	3.70	4.16	4.27
90	0.4	$Q'_{u,day}$	3.28	3.73	2.43	5.47	6.23	4.00	7.78	8.85	5.61
		$Q_{u,day}$	3.29	3.74	2.43	5.53	6.30	4.04	8.00	9.10	5.81
		Z	0.916	0.918	0.912	0.924	0.927	0.907	0.931	0.937	0.898
		Z^*	0.918	0.920	0.913	0.934	0.938	0.918	0.957	0.964	0.930
		Δ_d	0.23	0.27	0.14	1.15	1.20	1.23	2.81	2.80	3.55
	0.8	$Q'_{u,day}$	0.60	0.68	0.44	1.00	1.14	0.74	1.43	1.62	1.03
		$Q_{u,day}$	0.60	0.68	0.45	1.02	1.16	0.75	1.48	1.68	1.09
		Z	0.916	0.918	0.912	0.924	0.927	0.907	0.931	0.937	0.898
		Z^*	0.922	0.923	0.917	0.941	0.945	0.929	0.967	0.972	0.945
		Δ_d	0.59	0.62	0.55	1.93	1.90	2.42	3.80	3.72	5.22

Note: $Z = (\tau\alpha)_{day}/(\tau\alpha)_n$; $Z^* = (\tau\alpha)^*_{day}/(\tau\alpha)_n$; $Q_{u,day}$ and $Q'_{u,day}$ in MJ/m^2-day.

Table A.5: Tabulated values of $Q_{u,day}$, $Q'_{u,day}$, $(\tau\alpha)_{day}/(\tau\alpha)_n$ and $(\tau\alpha)^*_{day}/(\tau\alpha)_n$ for $\phi = 20°$N, $\beta = 90°$

γ deg	X_c	Qty.	$K_T = 0.3$			$K_T = 0.5$			$K_T = 0.7$		
			Mar	Jun	Dec	Mar	Jun	Dec	Mar	Jun	Dec
30	0.4	$Q'_{u,day}$	1.93	2.17	1.57	2.99	2.76	3.23	4.24	2.14	5.99
		$Q_{u,day}$	1.92	2.17	1.57	2.96	2.77	3.27	4.26	2.11	6.21
		Z	0.892	0.896	0.902	0.875	0.856	0.901	0.856	0.758	0.902
		Z^*	0.888	0.895	0.904	0.867	0.858	0.913	0.861	0.744	0.935
		Δ_d	-0.44	-0.14	0.15	-0.96	0.26	1.36	0.60	-1.80	3.64
	0.8	$Q'_{u,day}$	0.35	0.44	0.29	0.54	0.53	0.59	0.78	0.30	1.10
		$Q_{u,day}$	0.34	0.44	0.29	0.54	0.53	0.61	0.81	0.27	1.16
		Z	0.892	0.896	0.902	0.875	0.856	0.901	0.856	0.758	0.902
		Z^*	0.881	0.895	0.910	0.868	0.857	0.928	0.889	0.673	0.951
		Δ_d	-1.21	-0.09	0.85	-0.82	0.11	3.08	3.78	-11.22	5.47
60	0.4	$Q'_{u,day}$	1.93	2.20	1.46	2.99	3.07	2.61	4.53	3.31	4.80
		$Q_{u,day}$	1.92	2.19	1.46	2.97	3.04	2.60	4.60	3.27	4.94
		Z	0.897	0.896	0.896	0.897	0.882	0.900	0.903	0.864	0.909
		Z^*	0.894	0.893	0.893	0.891	0.873	0.898	0.917	0.854	0.935
		Δ_d	-0.30	-0.26	-0.32	-0.72	-1.06	-0.22	1.57	-1.25	2.77
	0.8	$Q'_{u,day}$	0.34	0.43	0.26	0.50	0.44	0.48	0.86	0.60	0.92
		$Q_{u,day}$	0.33	0.43	0.26	0.50	0.42	0.48	0.90	0.61	0.97
		Z	0.897	0.896	0.896	0.897	0.882	0.900	0.903	0.864	0.909
		Z^*	0.885	0.888	0.888	0.892	0.841	0.916	0.944	0.870	0.959
		Δ_d	-1.28	-0.83	-0.83	-0.52	-4.75	1.77	4.60	0.59	5.42
90	0.4	$Q'_{u,day}$	1.95	2.21	1.45	2.90	3.25	2.15	3.98	4.27	3.10
		$Q_{u,day}$	1.94	2.20	1.44	2.87	3.23	2.13	4.04	4.33	3.14
		Z	0.898	0.898	0.894	0.898	0.898	0.887	0.906	0.904	0.885
		Z^*	0.895	0.896	0.891	0.891	0.891	0.877	0.921	0.916	0.899
		Δ_d	-0.24	-0.23	-0.34	-0.78	-0.79	-1.16	1.71	1.33	1.56
	0.8	$Q'_{u,day}$	0.37	0.42	0.27	0.44	0.49	0.33	0.78	0.82	0.62
		$Q_{u,day}$	0.37	0.42	0.27	0.43	0.48	0.32	0.82	0.85	0.66
		Z	0.898	0.898	0.894	0.898	0.898	0.887	0.906	0.904	0.885
		Z^*	0.889	0.889	0.882	0.884	0.881	0.864	0.951	0.944	0.936
		Δ_d	-1.01	-0.94	-1.33	-1.60	-1.92	-2.62	5.03	4.45	5.71

Note: $Z = (\tau\alpha)_{day}/(\tau\alpha)_n$; $Z^* = (\tau\alpha)^*_{day}/(\tau\alpha)_n$; $Q_{u,day}$ and $Q'_{u,day}$ in MJ/m^2-day.

Table A.6: Tabulated values of $Q_{u,day}$, $Q'_{u,day}$, $(\tau\alpha)_{day}/(\tau\alpha)_n$ and $(\tau\alpha)^*_{day}/(\tau\alpha)_n$ for $\phi = 40°$N, $(\phi - \beta) = 0°$

γ deg	X_c	Qty.	$K_T = 0.3$			$K_T = 0.5$			$K_T = 0.7$		
			Mar	Jun	Dec	Mar	Jun	Dec	Mar	Jun	Dec
30	0.4	$Q'_{u,day}$	2.51	3.63	1.38	4.78	5.96	3.16	7.82	8.32	6.04
		$Q_{u,day}$	2.52	3.64	1.39	4.85	6.06	3.21	8.04	8.65	6.22
		Z	0.920	0.915	0.923	0.931	0.918	0.931	0.940	0.917	0.935
		Z^*	0.923	0.918	0.926	0.945	0.932	0.947	0.966	0.953	0.962
		Δ_d	0.36	0.28	0.38	1.44	1.62	1.63	2.81	3.95	2.89
	0.8	$Q'_{u,day}$	0.46	0.66	0.26	0.88	1.08	0.58	1.43	1.52	1.11
		$Q_{u,day}$	0.46	0.66	0.26	0.90	1.11	0.60	1.49	1.60	1.15
		Z	0.920	0.915	0.923	0.931	0.918	0.931	0.940	0.917	0.935
		Z^*	0.927	0.922	0.930	0.951	0.941	0.952	0.975	0.965	0.970
		Δ_d	0.76	0.74	0.74	2.13	2.60	2.22	3.69	5.15	3.74
60	0.4	$Q'_{u,day}$	2.43	3.60	1.29	4.37	5.93	2.60	7.04	8.56	4.71
		$Q_{u,day}$	2.44	3.61	1.29	4.41	5.99	2.64	7.22	8.81	4.88
		Z	0.914	0.914	0.909	0.923	0.921	0.907	0.933	0.929	0.906
		Z^*	0.916	0.916	0.910	0.933	0.931	0.919	0.958	0.957	0.938
		Δ_d	0.24	0.21	0.19	1.06	1.03	1.41	2.64	2.95	3.44
90	0.8	$Q'_{u,day}$	0.44	0.65	0.24	0.80	1.08	0.48	1.29	1.56	0.87
		$Q_{u,day}$	0.44	0.65	0.24	0.82	1.10	0.50	1.34	1.63	0.92
		Z	0.914	0.914	0.909	0.923	0.921	0.907	0.933	0.929	0.906
		Z^*	0.922	0.921	0.917	0.943	0.941	0.934	0.969	0.968	0.953
		Δ_d	0.82	0.74	0.94	2.20	2.17	3.02	3.80	4.15	5.10
	0.4	$Q'_{u,day}$	2.34	3.58	1.18	3.79	5.82	1.88	5.74	8.53	2.91
		$Q_{u,day}$	2.34	3.58	1.17	3.80	5.86	1.86	5.89	8.75	2.98
		Z	0.907	0.912	0.893	0.908	0.920	0.868	0.911	0.931	0.841
		Z^*	0.907	0.913	0.888	0.911	0.926	0.860	0.934	0.955	0.862
		Δ_d	-0.05	0.12	-0.56	0.30	0.65	-0.84	2.53	2.53	2.52
	0.8	$Q'_{u,day}$	0.42	0.65	0.21	0.70	1.06	0.35	1.06	1.56	0.55
		$Q_{u,day}$	0.42	0.65	0.21	0.71	1.08	0.35	1.11	1.62	0.59
		Z	0.907	0.912	0.893	0.908	0.920	0.868	0.911	0.931	0.841
		Z^*	0.910	0.918	0.881	0.926	0.938	0.872	0.952	0.967	0.897
		Δ_d	0.30	0.61	-1.31	2.01	1.94	0.48	4.45	3.82	6.67

Note: $Z = (\tau\alpha)_{day}/(\tau\alpha)_n$; $Z^* = (\tau\alpha)^*_{day}/(\tau\alpha)_n$; $Q_{u,day}$ and $Q'_{u,day}$ in MJ/m^2-day.

Table A.7: Tabulated values of $Q_{u,day}$, $Q'_{u,day}$, $(\tau\alpha)_{day}/(\tau\alpha)_n$ and $(\tau\alpha)^*_{day}/(\tau\alpha)_n$ for $\phi = 40°$N, $\beta = 90°$

γ deg	X_c	Qty.	$K_T = 0.3$			$K_T = 0.5$			$K_T = 0.7$		
			Mar	Jun	Dec	Mar	Jun	Dec	Mar	Jun	Dec
30	0.4	$Q'_{u,day}$	1.62	2.24	1.00	3.15	3.00	2.76	5.53	3.11	6.12
		$Q_{u,day}$	1.62	2.23	1.00	3.18	2.98	2.82	5.68	3.09	6.33
		Z	0.901	0.888	0.919	0.902	0.843	0.929	0.904	0.766	0.934
		Z^*	0.902	0.883	0.925	0.910	0.837	0.949	0.928	0.761	0.967
		Δ_d	0.08	-0.53	0.59	0.88	-0.71	2.13	2.71	-0.64	3.51
	0.8	$Q'_{u,day}$	0.29	0.39	0.19	0.58	0.51	0.51	1.02	0.58	1.13
		$Q_{u,day}$	0.30	0.38	0.19	0.59	0.50	0.53	1.07	0.59	1.18
		Z	0.901	0.888	0.919	0.902	0.843	0.929	0.904	0.766	0.934
		Z^*	0.909	0.873	0.929	0.927	0.827	0.956	0.947	0.784	0.975
		Δ_d	0.84	-1.64	1.09	2.84	-1.93	2.86	4.79	2.29	4.39
60	0.4	$Q'_{u,day}$	1.54	2.30	0.85	2.70	3.38	1.98	5.03	4.48	4.21
		$Q_{u,day}$	1.54	2.29	0.84	2.70	3.36	2.00	5.15	4.50	4.37
		Z	0.898	0.897	0.894	0.904	0.892	0.902	0.916	0.886	0.912
		Z^*	0.895	0.894	0.892	0.904	0.885	0.912	0.938	0.892	0.947
		Δ_d	-0.27	-0.30	-0.20	-0.10	-0.75	1.10	2.47	0.63	3.86
	0.8	$Q'_{u,day}$	0.27	0.40	0.15	0.49	0.55	0.37	0.94	0.82	0.84
		$Q_{u,day}$	0.26	0.39	0.15	0.50	0.54	0.38	0.98	0.86	0.89
		Z	0.898	0.897	0.894	0.904	0.892	0.902	0.916	0.886	0.912
		Z^*	0.891	0.885	0.900	0.921	0.880	0.936	0.960	0.920	0.968
		Δ_d	-0.74	-1.30	0.59	1.83	-1.24	3.78	4.79	3.84	6.18
90	0.4	$Q'_{u,day}$	1.54	2.34	0.78	2.34	3.51	1.23	3.74	5.00	2.09
		$Q_{u,day}$	1.53	2.33	0.78	2.32	3.48	1.21	3.82	5.08	2.14
		Z	0.896	0.899	0.887	0.897	0.903	0.871	0.906	0.912	0.862
		Z^*	0.893	0.897	0.882	0.890	0.897	0.857	0.927	0.928	0.884
		Δ_d	-0.31	-0.23	-0.60	-0.80	-0.65	-1.68	2.34	1.77	2.47
	0.8	$Q'_{u,day}$	0.28	0.43	0.14	0.37	0.54	0.21	0.73	0.94	0.46
		$Q_{u,day}$	0.28	0.43	0.13	0.36	0.53	0.20	0.78	0.98	0.50
		Z	0.896	0.899	0.887	0.897	0.903	0.871	0.906	0.912	0.862
		Z^*	0.884	0.890	0.865	0.891	0.894	0.853	0.956	0.953	0.936
		Δ_d	-1.31	-1.01	-2.46	-0.69	-0.90	-2.07	5.60	4.54	8.54

Note: $Z = (\tau\alpha)_{day}/(\tau\alpha)_n$; $Z^* = (\tau\alpha)^*_{day}/(\tau\alpha)_n$; $Q_{u,day}$ and $Q'_{u,day}$ in MJ/m^2-day.

Table A.8: Tabulated values of $Q_{u,day}$, $Q'_{u,day}$, $(\tau\alpha)_{day}/(\tau\alpha)_n$ and $(\tau\alpha)^*_{day}/(\tau\alpha)_n$ for $\phi = 60^oN$, $(\phi - \beta) = 0^o$

γ deg	X_c	Qty.	$K_T = 0.3$			$K_T = 0.5$			$K_T = 0.7$		
			Mar	Jun	Dec	Mar	Jun	Dec	Mar	Jun	Dec
30	0.4	$Q'_{u,day}$	1.49	3.15	0.41	3.54	5.43	1.76	7.01	8.23	4.39
		$Q_{u,day}$	1.50	3.16	0.42	3.61	5.54	1.78	7.20	8.59	4.47
		Z	0.923	0.913	0.943	0.937	0.914	0.952	0.946	0.914	0.954
		Z^*	0.929	0.916	0.948	0.954	0.933	0.965	0.972	0.954	0.971
		Δ_d	0.64	0.36	0.49	1.84	2.07	1.45	2.81	4.39	1.80
	0.8	$Q'_{u,day}$	0.27	0.56	0.08	0.65	0.99	0.33	1.28	1.51	0.88
		$Q_{u,day}$	0.27	0.56	0.08	0.66	1.02	0.33	1.33	1.60	0.90
		Z	0.923	0.913	0.943	0.937	0.914	0.952	0.946	0.914	0.954
		Z^*	0.934	0.923	0.950	0.961	0.945	0.970	0.981	0.967	0.979
		Δ_d	1.25	1.13	0.80	2.66	3.46	1.94	3.73	5.86	2.58
60	0.4	$Q'_{u,day}$	1.34	3.09	0.29	2.88	5.21	1.06	5.78	8.24	2.44
		$Q_{u,day}$	1.35	3.09	0.29	2.92	5.28	1.10	5.96	8.57	2.59
		Z	0.908	0.911	0.879	0.920	0.916	0.872	0.932	0.920	0.869
		Z^*	0.910	0.912	0.888	0.932	0.929	0.910	0.961	0.957	0.925
		Δ_d	0.17	0.11	1.07	1.31	1.39	4.42	3.13	3.97	6.39
	0.8	$Q'_{u,day}$	0.24	0.54	0.05	0.53	0.95	0.20	1.06	1.51	0.54
		$Q_{u,day}$	0.24	0.54	0.06	0.54	0.98	0.22	1.11	1.59	0.60
		Z	0.908	0.911	0.879	0.920	0.916	0.872	0.932	0.920	0.869
		Z^*	0.919	0.917	0.909	0.948	0.944	0.937	0.973	0.971	0.955
		Δ_d	1.23	0.71	3.39	3.04	3.00	7.50	4.44	5.51	9.88
90	0.4	$Q'_{u,day}$	1.24	3.04	0.18	2.05	4.91	0.37	3.88	7.98	0.69
		$Q_{u,day}$	1.23	3.04	0.18	2.05	4.92	0.36	4.01	8.20	0.73
		Z	0.896	0.907	0.836	0.894	0.917	0.748	0.897	0.929	0.692
		Z^*	0.892	0.906	0.816	0.890	0.920	0.720	0.927	0.955	0.735
		Δ_d	-0.48	-0.12	-2.42	-0.41	0.35	-3.68	3.32	2.77	6.21
	0.8	$Q'_{u,day}$	0.21	0.51	0.03	0.37	0.87	0.07	0.74	1.46	0.15
		$Q_{u,day}$	0.20	0.51	0.03	0.38	0.89	0.07	0.78	1.52	0.17
		Z	0.896	0.907	0.836	0.894	0.917	0.748	0.897	0.929	0.692
		Z^*	0.882	0.904	0.768	0.909	0.936	0.733	0.954	0.971	0.821
		Δ_d	-1.66	-0.30	-8.14	1.70	2.04	-1.97	6.31	4.51	18.58

Note: $Z = (\tau\alpha)_{day}/(\tau\alpha)_n$; $Z^* = (\tau\alpha)^*_{day}/(\tau\alpha)_n$; $Q_{u,day}$ and $Q'_{u,day}$ in MJ/m^2-day.

Table A.9: Tabulated values of $Q_{u,day}$, $Q'_{u,day}$, $(\tau\alpha)_{day}/(\tau\alpha)_n$ and $(\tau\alpha)^*_{day}/(\tau\alpha)_n$ for $\phi = 60^o$N, $\beta = 90^o$

γ deg	X_c	Qty.	$K_T = 0.3$			$K_T = 0.5$			$K_T = 0.7$		
			Mar	Jun	Dec	Mar	Jun	Dec	Mar	Jun	Dec
30	0.4	$Q'_{u,day}$	1.14	2.26	0.40	2.95	3.59	1.89	6.22	5.22	4.86
		$Q_{u,day}$	1.15	2.26	0.40	3.01	3.64	1.91	6.41	5.45	4.92
		Z	0.915	0.899	0.954	0.927	0.882	0.966	0.935	0.861	0.969
		Z^*	0.922	0.898	0.958	0.946	0.894	0.977	0.964	0.899	0.982
		Δ_d	0.74	-0.06	0.47	2.04	1.37	1.16	3.05	4.47	1.39
	0.8	$Q'_{u,day}$	0.21	0.39	0.07	0.54	0.65	0.35	1.14	0.97	0.99
		$Q_{u,day}$	0.21	0.39	0.07	0.56	0.68	0.36	1.19	1.05	1.02
		Z	0.915	0.899	0.954	0.927	0.882	0.966	0.935	0.861	0.969
		Z^*	0.930	0.902	0.961	0.956	0.915	0.981	0.974	0.930	0.990
		Δ_d	1.62	0.41	0.77	3.15	3.82	1.60	4.18	7.97	2.15
60	0.4	$Q'_{u,day}$	0.99	2.27	0.26	2.27	3.64	1.08	5.08	5.78	2.55
		$Q_{u,day}$	0.99	2.27	0.26	2.30	3.67	1.13	5.25	5.99	2.72
		Z	0.899	0.901	0.879	0.913	0.899	0.884	0.927	0.894	0.886
		Z^*	0.898	0.899	0.894	0.923	0.905	0.928	0.958	0.926	0.946
		Δ_d	-0.12	-0.21	1.67	1.11	0.72	4.98	3.26	3.61	6.75
	0.8	$Q'_{u,day}$	0.17	0.36	0.05	0.42	0.64	0.21	0.95	1.07	0.57
		$Q_{u,day}$	0.17	0.36	0.05	0.43	0.66	0.23	1.00	1.13	0.62
		Z	0.899	0.901	0.879	0.913	0.899	0.884	0.927	0.894	0.886
		Z^*	0.906	0.894	0.918	0.945	0.922	0.954	0.973	0.950	0.972
		Δ_d	0.76	-0.72	4.41	3.46	2.57	7.93	4.93	6.29	9.73
90	0.4	$Q'_{u,day}$	0.93	2.31	0.14	1.54	3.64	0.34	3.25	6.13	0.68
		$Q_{u,day}$	0.93	2.30	0.13	1.53	3.63	0.33	3.36	6.27	0.73
		Z	0.891	0.900	0.833	0.893	0.910	0.772	0.902	0.923	0.741
		Z^*	0.887	0.898	0.807	0.887	0.909	0.761	0.933	0.944	0.799
		Δ_d	-0.53	-0.25	-3.07	-0.69	-0.16	-1.33	3.41	2.29	7.86
	0.8	$Q'_{u,day}$	0.15	0.39	0.02	0.27	0.59	0.07	0.66	1.13	0.13
		$Q_{u,day}$	0.14	0.39	0.02	0.27	0.59	0.08	0.71	1.18	0.15
		Z	0.891	0.900	0.833	0.893	0.910	0.772	0.902	0.923	0.741
		Z^*	0.869	0.890	0.745	0.905	0.921	0.816	0.964	0.965	0.895
		Δ_d	-2.47	-1.17	-10.54	1.37	1.18	5.76	6.79	4.60	20.77

Note: $Z = (\tau\alpha)_{day}/(\tau\alpha)_n$; $Z^* = (\tau\alpha)^*_{day}/(\tau\alpha)_n$; $Q_{u,day}$ and $Q'_{u,day}$ in MJ/m^2-day.

Appendix B

Evaluation of Different Hour Angles

B.1 Evaluation of apparent sunrise and sunset hour angles

Apparent sunrise and sunset hour angles, though, can be estimated from the algorithms given in Klein and Theilacker [66], these expressions fail for certain cases. For example, $\phi = 18^o$, $\beta = 90^o$, $\gamma = 30^o$ and $\delta = 12^o$ (from Lahiri [67]). Lahiri developed algorithm to estimate ω_{sr} and ω_{ss} uniquely. The philosophy being ω_{sr} and ω_{ss} can be expressed as inverse cosine functions or inverse sine functions, when θ is set equal to $\pi/2$ in Eq. (2.4) for $\cos\theta$. Considering the uncertainity in the sign to be assigned for ω_{sr} and ω_{ss} when solved as a cosine inverse and the ambiguity in assigning the magnitute when solved as an inverse sine function. Lahiri suggested, correct apperent sunrise and sunset hour angles be the common values, obtained as inverse cosine and inverse sign roots. Thus, the apparent sunrise and sunset hour angles ω_{sr} and ω_{ss} can be determined unambiguously following Lahiri [67] from,

$$\omega_{sr} = \text{SIGN}\left[\min\left(\omega_s, \omega_1''\right), \omega_1'\right] \tag{B.1}$$

$$\omega_{ss} = \text{SIGN}\left[\min\left(\omega_s, \omega_2''\right), \omega_2'\right] \tag{B.2}$$

where,

$$\alpha_1 = B^2 + C^2 - A^2 \tag{B.3}$$

$$\omega_1'' = \cos^{-1}\left[(-AB + C\sqrt{\alpha_1})/(B^2 + C^2)\right] \tag{B.4}$$

$$\omega_2'' = \cos^{-1}\left[(-AB - C\sqrt{\alpha_1})/(B^2 + C^2)\right] \tag{B.5}$$

$$\omega_1' = \arcsin\left[(-AC - B\sqrt{\alpha_1})/(B^2 + C^2)\right] \tag{B.6}$$

$$\omega_2' = \arcsin\left[(-AC + B\sqrt{\alpha_1})/(B^2 + C^2)\right] \tag{B.7}$$

In Eq. (B.1) and (B.2), "SIGN" means the magnitude of the first quantity associated with the sign of the second quantity within the parentheses. Eqs. (B.1) and (B.2) yield ω_{sr} and ω_{ss} when $\alpha_1 > 0$. When $\alpha_1 < 0$, ω_{sr} and ω_{ss} are estimated from,

$$\omega_{sr} = -\text{SIGN}\,[\omega_s, (A+B)] \tag{B.8}$$

$$\omega_{ss} = \text{SIGN}\,[\omega_s, (A+B)] \tag{B.9}$$

This procedure is to be valid for determining ω_{sr} and ω_{ss} correctly even for surfaces with double sunshine period.

For south facing flat plate collectors the apparent sunrise or sunset hour angle, ω_s', as given in Duffie and Beckman [6] is,

$$\omega_s' = \min\left[\cos^{-1}(-\tan\phi\tan\delta), \cos^{-1}(-\tan(\phi-\beta)\tan\delta)\right] \tag{B.10}$$

B.2 Evaluation of the hour angles ω_1 and ω_2

Hour angles ω_1 and ω_2, corresponding to the angle of incidence $\theta = 60^o$, can be obtained by setting $\cos\theta = 0.5$ in Eq. (2.4). It follows,

$$A + B\cos\omega + C\sin\omega = 0.5 \tag{B.11}$$

Upon solving Eq. (B.11) in terms of $\cos\omega$,

$$\omega_{11} = \cos^{-1}\left[\{-B(A-0.5) + C\sqrt{\alpha'}\}/(B^2+C^2)\right] \tag{B.12}$$

$$\omega_{21} = \cos^{-1}\left[\{-B(A-0.5) - C\sqrt{\alpha'}\}/(B^2+C^2)\right] \tag{B.13}$$

where,

$$\alpha' = B^2 + C^2 - (A-0.5)^2 \tag{B.14}$$

Eq. (B.11) can also be solved in terms of $\sin\omega$ to yield the roots ω_{12} and ω_{22} as,

$$\omega_{12} = \arcsin\left[\{-C(A-0.5) - B\sqrt{\alpha'}\}/(B^2+C^2)\right] \tag{B.15}$$

$$\omega_{22} = \arcsin\left[\{-C(A-0.5) + B\sqrt{\alpha'}\}/(B^2+C^2)\right] \tag{B.16}$$

Then ω_1 and ω_2 are obtained from,

$$\omega_1 = \text{SIGN}\,[\omega_{11}, \omega_{12}] \tag{B.17}$$

$$\omega_2 = \text{SIGN}\,[\omega_{21}, \omega_{22}] \tag{B.18}$$

This procedure determines ω_1 and ω_2 correctly in magnitude as well as sign.

B.3 Evaluation of the critical hour angles

The critical hour angles, ω_{c1} and ω_{c2}, required to evaluate the optical efficiency under operating time periods, is obtained by setting $I_T = I_c$. Using Eqs. (2.25) to (2.27) of Chapter 2, expressing the hourly global, diffuse and beam components of solar radiation, I_T in Eq. (2.2) can be written as,

$$\begin{aligned} I_T &= K_4 \left[(a_1 + b\cos\omega)\cos\theta + K_2 D_f B'(\cos\omega - \cos\omega_s) + \right. \\ &\quad \left. K_3 B'(a + b\cos\omega)(\cos\omega - \cos\omega_s)\right] \end{aligned} \tag{B.19}$$

Specific expressions for $\cos\theta$ applicable for different types of collectors can be deduced from the general form, [$\cos\theta = A + B\cos\omega + C\cos\omega$, given by Eq. (2.4) of Chapter 2] using the expressions for A, B, C for the corresponding collectors. Using the expression for $\cos\theta$, Eq. (B.19) can be re-written as,

$$I_T = K_4 \left[d_1 \cos^2\omega + d_2 \cos\omega + d_3 \cos\omega \sin\omega + d_4 \sin\omega + d_5\right] \tag{B.20}$$

where,

$$d_1 = b(B + b\,K_3 B') \tag{B.21}$$

$$d_2 = b\,A + a_1 B + B'(K_2 D_f + K_3 K_5) \tag{B.22}$$

$$d_3 = b\,C \tag{B.23}$$

$$d_4 = a_1 C \tag{B.24}$$

$$d_5 = a_1 A - B' \cos\omega_s (K_2 D_f + K_3 a) \tag{B.25}$$

In Eqs. (B.21) to (B.25), the constants A, B and C are given by Eqs. (2.5) to (2.7) of Chapter 2 respectively for flat plate collectors.

By definition of the critical hour angle, $I_T = I_c$ when $\omega = \omega_c$. At $\omega = \omega_c$, the expression given by Eq. (B.20) for I_T, after rearrangement reduces to,

$$d_1 \cos^2\omega_c + d_2 \cos\omega_c + d_3 \cos\omega_c \sin\omega_c + d_4 \sin\omega_c + d_5 - I_c/K_4 = 0 \tag{B.26}$$

It may be noted that, the constants d_1, d_2, etc. appearing in Eq. (B.26) do not depend on the hour angles for flat plate collectors and concentrating collectors tracked in modes **a**, **d** and **e**. Eq. (B.26) is the basis to evaluate the critical hour angles. When the sine terms in Eq. (B.26) are eliminated, Eq. (B.26) leads to a quartic equation in $\cos\omega_c$ as follows:

$$\cos^4\omega_c + p_3 \cos^3\omega_c + p_2 \cos^2\omega_c + p_1 \cos\omega_c + p_o = 0 \tag{B.27}$$

where,

$$p_3 = 2\,[d_1 d_2 + d_3 d_4\,]/p_4 \tag{B.28}$$

$$p_2 = [d_2^2 - d_3^2 + d_4^2 + 2d_1 d_6]/p_4 \quad \text{(B.29)}$$

$$p_1 = 2[d_2 d_6 - d_3 d_4]/p_4 \quad \text{(B.30)}$$

$$p_o = [d_6^2 - d_4^2]/p_4 \quad \text{(B.31)}$$

with

$$p_4 = d_1^2 + d_3^2 \quad \text{(B.32)}$$

$$d_6 = d_5 - I_c/K_4 \quad \text{(B.33)}$$

Also, Eq. (B.26) is general enough and yield the critical hour angles for fixed, as well as, tracking collectors when the appropriate expressions for A, B and C are employed. For south facing flat plate collectors and concentrating collectors tracked in modes **a, d** and **e**, valid for symmetric solar radiation distribution, simplifies to a quadratic equation in $\cos\omega_c$, whose solution is straightforward.

Eq. (B.27) yield four roots of which only two roots are relevant. Generally two of the roots are either zeros i. e. $\cos\omega_c$ is beyond the sunset hour angle, ω_s, which are to be rejected. Out of the two remaining roots ω_{c1} is the root closer to ω_{sr} and ω_{c2} is the value closer to ω_{ss}. However, for certain cases, no root may be available in $-\omega_s < \omega_c < \omega_s$. For example, when I_c=0 or a small value, since $I_b R_b$ term in I_T tends to be a finite value at $\omega = \omega_s$ due to the form of the correlations for I, I_b and I_d. Also, certain other special situations such as, $-\omega_s < \omega_{c1} < \omega_{sr}$ and $\omega_{ss} < \omega_{c2} < \omega_s$, which can occur for low critical radiation levels will be discussed later on.

South Facing Flat Plate Collectors

When the solar radiation distribution is symmetric, specific equation governing the critical hour angles, is obtained from Eq. (B.27) after simplification (for south facing flat plate collectors, $C = 0$, leading to $d_3 = d_4 = 0$) as,

$$d_1 \cos^2\omega_c + d_2 \cos\omega_c + d_5 - I_c/K_4 = 0 \quad \text{(B.34)}$$

Eq. (B.34) is quadratic in $\cos\omega_c$. Solving Eq. (B.34) yields,

$$\omega_c = \cos^{-1}\left[\frac{-d_2 \pm \sqrt{d_2^2 - 4d_1(d_5 - I_c/K_4)}}{2d_1}\right] \quad \text{(B.35)}$$

Out of the four roots given by Eq.(B.35), the root obtained considering the positive sign of the radical which lies between $0 < \omega_c < \omega_s'$ is the relevant root. For south facing flat plate collectors,

$$\omega_{c1} = -\omega_c \quad \text{and} \quad \omega_{c2} = \omega_c \quad \text{(B.36)}$$

B.4 Evaluation of ω_m

In order to evaluate the average transmittance-absorptnce product for non-south facing collectors or to evaluate $K_{T,min}$ explicitly, evaluation of the hour angle, ω_m, at which solar radiation on the collector aperture reaches a maximum during a day is needed. In general, for a symmetrically oriented flat plate collector or concentrating collectors tracked according to the five principal modes, this maximum is attained at the solar noon, i.e. for these collector types, $\omega_m = 0$. However, for a non-south facing flat plate collectors ω_m differs from solar noon, for example, for $\gamma > 0$, $\omega_m > 0$ and for $\gamma < 0$, $\omega_m < 0$. Differentiating the expression for $I_{T,m}$, as given by Eq. (2.33), with respect to ω_m and equating to zero yields,

$$-2d_1 \cos\omega_m \sin\omega_m - d_2 \sin\omega_m + d_3 \cos^2\omega_m - d_3 \sin^2\omega_m + d_4 \cos\omega_m = 0 \qquad \text{(B.37)}$$

Eliminating $\sin\omega_m$ terms from Eq. (B.37) and upon re-arranging, Eq. (B.37) takes the form,

$$\cos^4\omega_m + q_3'' \cos^3\omega_m + q_2'' \cos\omega_m + q_1'' \cos\omega_m + q_o'' = 0 \qquad \text{(B.38)}$$

where,

$$q_4'' = 4[d_1^2 + d_3^2] \qquad \text{(B.39)}$$

$$q_3'' = 4[d_1 d_2 + d_3 d_4]/q_4'' \qquad \text{(B.40)}$$

$$q_2'' = [d_2^2 + d_4^2 - q_4'']/q_4'' \qquad \text{(B.41)}$$

$$q_1'' = -2[2d_1 d_2 + d_3 d_4]/q_4'' \qquad \text{(B.42)}$$

$$q_o'' = [d_3^2 - d_2^2]/q_4'' \qquad \text{(B.43)}$$

Eq. (B.38) is a quartic equation in $\cos\omega_m$ and the method to the quartic eqaution is decussed in the following section. Out of the four possible roots, two will always be zeros (i.e. $\cos\omega_m \geq 1$) or more than ω_s and are to be rejected. Only one of the two remaining roots will be $\leq \omega_s$. The sign of ω_m is the same a the sign of γ employed.

B.5 Solution Procedure for Quartic Equations

Determining ω_{c1} and ω_{c2} from Eq. (B.26) after eliminating the sine terms, in general, calls for the solution of a quartic equation (in $\cos\omega_c$). The algorithm to solve quartic equations is available in [135, 134]. The method of solving quartic equations described in [135] is reproduced below for ready application in obtaining ω_{c1}, ω_{c2} and ω_m for non-south facing flat plate collectors and ω_c for the concentrating collectors tracked in the modes **b** and **c**.

A quartic equation of the form,

$$x^4 + p_3 x^3 + p_2 x^2 + p_1 x + p_0 = 0 \qquad \text{(B.44)}$$

can be rewritten as,

$$[x^2 + (p_3/2)x]^2 = [p_3^2/4 - p_2]x^2 - p_1 x - p_0 \tag{B.45}$$

Adding $2(x^2 + p_3x/2)y/2 + (y/2)^2$ on both sides of Eq.(B.31) one obtains

$$[x^2 + p_3x/2 + y/2]^2 = [p_3^2/4 - p_2 + y]x^2 + [p_3y/2 - p_1]x + [y^2/4 - p_0] \tag{B.46}$$

Setting the discriminant of the right hand side of Eq.(B.46) to zero yields

$$y^3 + a'y^2 + b'y + c' = 0 \tag{B.47}$$

where

$$a' = -p_2 \tag{B.48}$$

$$b' = p_1p_2 - 4p_0 \tag{B.49}$$

$$c' = 4p_0p_2 - p_0p_3^2 - p_1^2 \tag{B.50}$$

Putting $y = y' - a'/3$ in Eq.(B.47), Eq.(B.47) takes the form

$$y'^3 + py' + q = 0 \tag{B.51}$$

where

$$p = -a'^2/3 + b' \tag{B.52}$$

$$q = 2(a'/3)^3 - a'b'/3 + c' \tag{B.53}$$

Let y_1' be a root of Eq.(B.51), then y_1' can be obtained as

$$y_1' = A_1 + B_1 \tag{B.54}$$

where

$$A_1 = [-q/2 + \sqrt{Q'}]^{1/3} \tag{B.55}$$

$$B_1 = [-q/2 - \sqrt{Q'}]^{1/3} \tag{B.56}$$

In Eqs.(B.55) and (B.56), Q' is given by

$$Q' = (p/3)^3 + (q/2)^2 \tag{B.57}$$

If $Q' < 0$ then

$$y_1' = 2(-p/3)^{1/2}\cos(\alpha'/3) \qquad (+ \text{ ve root}) \tag{B.58}$$

where

$$\alpha' = \cos^{-1}[-q/\{2(-p/3)^{3/2}\}] \qquad (+ \text{ ve root}) \tag{B.59}$$

With this value of y_1', Eq.(B.45) is rewritten as

$$\begin{aligned} x^2 + p_3 x/2 + y_1'/2 &= \pm[K_2 x^2 + K_1 x + K_0]^{1/2} \\ &= \pm[\pm K_2^{1/2} x \pm K_0^{1/2}] \end{aligned} \tag{B.60}$$

where

$$K_2 = [p_3^2/4] - p_2 + y_1' \tag{B.61}$$

$$K_1 = [p_3 y_1'/2] - p_1 \tag{B.62}$$

$$K_0 = [y_1'^2/4] - p_0 \tag{B.63}$$

Thus the four roots can be obtained from the resulting quadratics,

If $K_1 > 0$

$$x^2 + p'x + q' = 0 \qquad \text{and} \qquad x^2 + p''x + q'' \tag{B.64}$$

If $K_1 < 0$

$$x^2 + p'x + q'' = 0 \qquad \text{and} \qquad x^2 + p''x + q' \tag{B.65}$$

In Eqs.(B.64) and (B.65), p', p'', q' and q'' are given by

$$p' = [p_3/2] - K_2^{1/2} \tag{B.66}$$

$$p'' = [p_3/2] + K_2^{1/2} \tag{B.67}$$

$$q' = [y_1'/2] - K_0^{1/2} \tag{B.68}$$

$$q'' = [y_1'/2] + K_0^{1/2} \tag{B.69}$$

Appendix C

Approximate Analytical Evaluation of Certain Integrals for Concentrating Collectors

C.1 Concentrating Collectors Tracked in Mode b

The expression for $\cos\theta$ for tracking mode **b** is given by,

$$\cos\theta = [1 - \cos^2\delta \sin^{\omega}]^{1/2} \tag{C.1}$$

Eq. (C.1) can be expanded binomially as,

$$\begin{aligned}\cos\theta \approx\ & 1 - \frac{\cos^2\delta}{2}\sin^2\omega - \frac{\cos^4\delta}{8}\sin^4\omega - \frac{\cos^6\delta}{16}\sin^6\omega - \\ & \frac{5\cos^8\delta}{128}\sin^8\omega - \frac{7\cos^{10}\delta}{256}\sin^{10}\omega - \frac{21\cos^{12}\delta}{1024}\sin^{12}\omega - \cdots\end{aligned} \tag{C.2}$$

From Eq. (C.2), the primitives $I_{P1}(\omega)$ and $I_{P2}(\omega)$ can be written as,

$$\begin{aligned}I_{P1}(\omega) &= \int \cos\theta\, d\omega \\ &\approx \omega - \frac{\cos^2\delta}{2}\int \sin^2\omega\, d\omega - \frac{\cos^4\delta}{8}\int \sin^4\omega\, d\omega - \\ &\quad \frac{\cos^6\delta}{16}\int \sin^6\omega\, d\omega - \frac{5\cos^8\delta}{128}\int \sin^8\omega\, d\omega - \\ &\quad \frac{7\cos^{10}\delta}{256}\int \sin^{10}\omega\, d\omega - \frac{21\cos^{12}\delta}{1024}\int \sin^{12}\omega\, d\omega\end{aligned} \tag{C.3}$$

$$I_{P2}(\omega) = \int \cos\theta\cos\omega\, d\omega$$

$$\approx \sin\omega - \frac{\cos^2\delta}{2}\int \sin^2\omega\cos\omega\,d\omega - \frac{\cos^4\delta}{8}\int \sin^4\omega\cos\omega\,d\omega -$$

$$\frac{\cos^6\delta}{16}\int \sin^6\omega\cos\omega\,d\omega - \frac{5\cos^8\delta}{128}\int \sin^8\omega\cos\omega\,d\omega -$$

$$\frac{7\cos^{10}\delta}{256}\int \sin^{10}\omega\cos\omega\,d\omega - \frac{21\cos^{12}\delta}{1024}\int \sin^{12}\omega\cos\omega\,d\omega \qquad \text{(C.4)}$$

The integrals appearing in Eqs. (C.3) and (C.4) can be easily obtained from,

$$\int \sin^2\omega\,d\omega = -\frac{\sin\omega\cos\omega}{2} + \frac{1}{2}\omega \qquad \text{(C.5)}$$

$$\int \sin^4\omega\,d\omega = -\frac{\sin^3\omega\cos\omega}{4} + \frac{3}{4}\int \sin^2\omega\,d\omega \qquad \text{(C.6)}$$

$$\int \sin^6\omega\,d\omega = -\frac{\sin^5\omega\cos\omega}{6} + \frac{5}{6}\int \sin^4\omega\,d\omega \qquad \text{(C.7)}$$

$$\int \sin^8\omega\,d\omega = -\frac{\sin^7\omega\cos\omega}{8} + \frac{7}{8}\int \sin^6\omega\,d\omega \qquad \text{(C.8)}$$

$$\int \sin^{10}\omega\,d\omega = -\frac{\sin^9\omega\cos\omega}{10} + \frac{9}{10}\int \sin^8\omega\,d\omega \qquad \text{(C.9)}$$

$$\int \sin^{12}\omega\,d\omega = -\frac{\sin^{11}\omega\cos\omega}{12} + \frac{11}{12}\int \sin^{10}\omega\,d\omega \qquad \text{(C.10)}$$

$$\int \sin^2\omega\cos\omega\,d\omega = \frac{1}{3}\sin^3\omega \qquad \text{(C.11)}$$

$$\int \sin^4\omega\cos\omega\,d\omega = -\frac{\sin^3\omega\cos^2\omega}{5} + \frac{3}{5}\int \sin^2\omega\cos\omega\,d\omega \qquad \text{(C.12)}$$

$$\int \sin^6\omega\cos\omega\,d\omega = \frac{\sin^5\omega\cos^2\omega}{7} + \frac{5}{7}\int \sin^4\omega\cos\omega\,d\omega \qquad \text{(C.13)}$$

$$\int \sin^8\omega\cos\omega\,d\omega = -\frac{\sin^7\omega\cos^2\omega}{9} + \frac{7}{9}\int \sin^6\omega\cos\omega\,d\omega \qquad \text{(C.14)}$$

$$\int \sin^{10}\omega\cos\omega\,d\omega = -\frac{\sin^9\omega\cos^2\omega}{11} + \frac{9}{11}\int \sin^8\omega\cos\omega\,d\omega \qquad \text{(C.15)}$$

$$\int \sin^{12}\omega\cos\omega\,d\omega = -\frac{\sin^{11}\omega\cos^2\omega}{13} + \frac{11}{13}\int \sin^{10}\omega\cos\omega\,d\omega \qquad \text{(C.16)}$$

C.2 Concentrating Collector tracked in Mode c

The expression for $\cos\theta$ for tracking mode **c** given by,

$$\cos\theta = [(A' + B'\cos\omega)^2 + \cos^2\delta\sin^2\omega]^{1/2} \tag{C.17}$$

where A' and B' are as given by Eq. (3.10).

Eq. (C.17) can be written as,

$$\cos\theta = [A_c + B_c\cos\omega + C_c\cos^2\omega]^{1/2} \tag{C.18}$$

where the constants A_c, B_c and C_c given by,

$$A_c = 1 - \cos^2\phi\sin^2\delta \tag{C.19}$$

$$B_c = 2\cos\phi\cos\delta\sin\phi\sin\delta \tag{C.20}$$

$$C_c = -\cos^2\delta\sin^2\phi \tag{C.21}$$

Expanding Eq. (C.18) binomially one obtains,

$$\begin{aligned}\cos\theta \approx\ & a_0 + a_1\cos\omega + a_2\cos^2\omega + a_3\cos^3\omega + a_4\cos^4\omega + \\ & a_5\cos^5\omega + a_6\cos^6\omega + a_7\cos^7\omega + a_8\cos^8\omega\end{aligned} \tag{C.22}$$

where the coefficients $a_0, a_1, a_2, a_3, a_4, a_5, a_6, a_7$ and a_8 are given by,

$$a_0 = A_c^{1/2} \tag{C.23}$$

$$a_1 = \frac{1}{2}A_c^{-1/2}B_c \tag{C.24}$$

$$a_2 = \frac{1}{2}A_c^{-1/2}C_c - \frac{1}{8}A_c^{-3/2}B_c^2 \tag{C.25}$$

$$a_3 = \frac{1}{16}A_c^{-5/2}B_c^3 - \frac{1}{4}A_c^{-3/2}B_cC_c \tag{C.26}$$

$$a_4 = \frac{3}{16}A_c^{-5/2}B_c^2C_c - \frac{1}{8}A_c^{-3/2}C_c^2 - \frac{5}{128}A_c^{-7/2}B_c^4 \tag{C.27}$$

$$a_5 = \frac{3}{16}A_c^{-5/2}B_cC_c^2 - \frac{5}{32}A_c^{-7/2}B_c^3C_c \tag{C.28}$$

$$a_6 = \frac{1}{16}A_c^{-5/2}C_c^3 - \frac{15}{64}A_c^{-7/2}B_c^2C_c^2 \tag{C.29}$$

$$a_7 = -\frac{5}{32}A_c^{-7/2}B_cC_c^3 \tag{C.30}$$

$$a_8 = -\frac{5}{128}A_c^{-7/2}C_c^4 \tag{C.31}$$

From Eq. (C.22), the primitives $I_{P1}(\omega)$ and $I_{P2}(\omega)$ can be written as,

$$\begin{aligned} I_{P1}(\omega) &= \int \cos\theta \, d\omega \\ &\approx a_0\omega + a_1 \int \cos\omega \, d\omega + a_2 \int \cos^2\omega \, d\omega + a_3 \int \cos^3\omega \, d\omega + \\ &\quad a_4 \int \cos^4\omega \, d\omega + a_5 \int \cos^5\omega \, d\omega + a_6 \int \cos^6\omega \, d\omega + \\ &\quad a_7 \int \cos^7\omega \, d\omega + a_8 \int \cos^8\omega \, d\omega \end{aligned} \tag{C.32}$$

$$\begin{aligned} I_{P2}(\omega) &= \int \cos\theta \cos\omega \, d\omega \\ &\approx a_0 \sin\omega + a_1 \int \cos^2\omega \, d\omega + a_2 \int \cos^3\omega \, d\omega + a_3 \int \cos^4\omega \, d\omega + \\ &\quad a_4 \int \cos^5\omega \, d\omega + a_5 \int \cos^6\omega \, d\omega + a_6 \int \cos^7\omega \, d\omega + \\ &\quad a_7 \int \cos^8\omega \, d\omega + a_8 \int \cos^9\omega \, d\omega \end{aligned} \tag{C.33}$$

The integrals appearing in Eqs. (C.32) and (C.33) can be obtained from standard recursion relations [134] as,

$$\int \cos^2\omega \, d\omega = \frac{\sin\omega\cos\omega}{2} + \frac{1}{2}\omega \tag{C.34}$$

$$\int \cos^3\omega \, d\omega = \frac{\sin\omega\cos^2\omega}{3} + \frac{2}{3}\int \cos\omega \, d\omega \tag{C.35}$$

$$\int \cos^4\omega \, d\omega = \frac{\sin\omega\cos^3\omega}{4} + \frac{3}{4}\int \cos^2\omega \, d\omega \tag{C.36}$$

$$\int \cos^5\omega \, d\omega = \frac{\sin\omega\cos^4\omega}{5} + \frac{4}{5}\int \cos^3\omega \, d\omega \tag{C.37}$$

$$\int \cos^6\omega \, d\omega = \frac{\sin\omega\cos^5\omega}{6} + \frac{5}{6}\int \cos^4\omega \, d\omega \tag{C.38}$$

$$\int \cos^7\omega \, d\omega = \frac{\sin\omega\cos^6\omega}{7} + \frac{6}{7}\int \cos^5\omega \, d\omega \tag{C.39}$$

$$\int \cos^8\omega \, d\omega = \frac{\sin\omega\cos^7\omega}{8} + \frac{7}{8}\int \cos^6\omega \, d\omega \tag{C.40}$$

$$\int \cos^9\omega \, d\omega = \frac{\sin\omega\cos^8\omega}{9} + \frac{8}{9}\int \cos^7\omega \, d\omega \tag{C.41}$$

The primitives $I_{P1}(\omega)$ and $I_{P2}(\omega)$ as exressed by Eqs. (C.3) and Eq. (C.4) for tracking

mode **b** and Eqs.(C.32) and Eq. (C.33) for tracking mode **c**, along with Eqs. (C.5) to (C.16) and Eqs.(C.34) to (C.41) respectively, are evaluated with seven term expansion for mode **b** and five term expansion for mode **c** for $\cos\theta$ differed in the third decimal place only.

Appendix D

Tabulated Values of Monthly Average Shading Factor for Wingwalls under Terrestrial Conditions

Numerical values of $\bar{f}_{i\infty}$ obtained using Eq. (6.21) when $g = 0$ and Eq. (6.28) when $g \neq 0$ are given in Tables D.1 to D.8. The values of the other parameters are:

$\phi = 20^o$, 25^o, 30^o, 40^o, 50^o and 60^o;

$\delta = \delta_m$ for all 12 months;

$\gamma = 0^o$, 30^o, 60^o and 90^o;

$w = 1.0$;

$p = 0.2$, 0.3, 0.4 and 0.5;

$g = 0.0$ and 0.10;

$D_f = 0.2$, 0.4 and 0.6;

$\bar{f}_{i\infty}$ values for $\gamma = 0^o$, 30^o, 60^o and 90^o are given in Tables D.1 to D.4 respectively for $g = 0.0$ and in Tables D.5 to D.8 for $g = 0.10$.

Table D.1: Tabulated values of $\bar{f}_{i\infty}$ for wingwalls; $g = 0.0$, $\gamma = 0^o$

ϕ	Mon	Values of $\bar{f}_{i\infty}$											
		$D_f = 0.2$				$D_f = 0.4$				$D_f = 0.6$			
		$p = 0.2$	0.3	0.4	0.5	$p = 0.2$	0.3	0.4	0.5	$p = 0.2$	0.3	0.4	0.5
20	Jan	0.819	0.729	0.638	0.555	0.827	0.740	0.654	0.573	0.843	0.765	0.686	0.611
	Feb	0.755	0.636	0.539	0.463	0.766	0.652	0.557	0.481	0.790	0.687	0.595	0.518
	Mar	0.635	0.514	0.425	0.360	0.649	0.528	0.439	0.372	0.678	0.558	0.467	0.397
	Apr	0.505	0.386	0.308	0.255	0.510	0.391	0.313	0.259	0.521	0.400	0.321	0.266
	May	0.219	0.151	0.114	0.092	0.219	0.151	0.114	0.092	0.220	0.151	0.115	0.092
	Jun	0.000	0.000	0.000	0.000	0.000	0.000	0.000	0.000	0.000	0.000	0.000	0.000
	Jul	0.000	0.000	0.000	0.000	0.000	0.000	0.000	0.000	0.000	0.000	0.000	0.000
	Aug	0.431	0.319	0.251	0.205	0.434	0.322	0.253	0.207	0.440	0.326	0.257	0.210
	Sep	0.590	0.469	0.384	0.322	0.601	0.480	0.393	0.330	0.623	0.500	0.412	0.347
	Oct	0.716	0.595	0.501	0.428	0.730	0.612	0.518	0.444	0.759	0.647	0.554	0.478
	Nov	0.806	0.708	0.612	0.531	0.814	0.721	0.629	0.549	0.832	0.748	0.664	0.587
	Dec	0.832	0.748	0.664	0.582	0.839	0.759	0.678	0.599	0.854	0.781	0.708	0.636
40	Jan	0.875	0.812	0.749	0.686	0.880	0.819	0.759	0.699	0.890	0.836	0.781	0.726
	Feb	0.837	0.755	0.678	0.611	0.845	0.767	0.693	0.627	0.861	0.791	0.724	0.661
	Mar	0.776	0.684	0.605	0.539	0.787	0.697	0.619	0.553	0.809	0.724	0.648	0.582
	Apr	0.732	0.631	0.549	0.483	0.739	0.639	0.557	0.491	0.752	0.655	0.573	0.506
	May	0.688	0.580	0.496	0.430	0.692	0.585	0.501	0.435	0.701	0.594	0.510	0.443
	Jun	0.661	0.550	0.465	0.400	0.664	0.553	0.469	0.404	0.670	0.560	0.475	0.409
	Jul	0.674	0.564	0.480	0.414	0.678	0.568	0.484	0.418	0.685	0.576	0.491	0.425
	Aug	0.715	0.611	0.528	0.462	0.721	0.618	0.535	0.468	0.732	0.630	0.547	0.480
	Sep	0.759	0.663	0.583	0.517	0.768	0.674	0.595	0.528	0.787	0.696	0.618	0.551
	Oct	0.817	0.729	0.652	0.585	0.826	0.742	0.667	0.601	0.846	0.770	0.699	0.634
	Nov	0.866	0.799	0.732	0.666	0.872	0.808	0.743	0.680	0.884	0.825	0.767	0.709
	Dec	0.883	0.825	0.766	0.708	0.888	0.831	0.775	0.719	0.897	0.846	0.794	0.743
60	Jan	0.922	0.883	0.843	0.804	0.923	0.885	0.847	0.809	0.927	0.890	0.854	0.817
	Feb	0.883	0.825	0.767	0.708	0.888	0.832	0.776	0.720	0.898	0.846	0.795	0.744
	Mar	0.828	0.752	0.684	0.624	0.837	0.764	0.697	0.638	0.855	0.787	0.724	0.667
	Apr	0.803	0.721	0.649	0.587	0.808	0.727	0.657	0.595	0.818	0.740	0.671	0.610
	May	0.785	0.698	0.624	0.561	0.788	0.703	0.629	0.566	0.794	0.710	0.637	0.574
	Jun	0.777	0.688	0.613	0.549	0.779	0.691	0.617	0.553	0.784	0.697	0.623	0.560
	Jul	0.780	0.693	0.618	0.555	0.783	0.696	0.622	0.559	0.789	0.703	0.629	0.566
	Aug	0.795	0.711	0.639	0.576	0.799	0.717	0.645	0.582	0.808	0.727	0.656	0.594
	Sep	0.816	0.738	0.669	0.608	0.824	0.748	0.680	0.619	0.839	0.767	0.701	0.642
	Oct	0.866	0.799	0.733	0.673	0.872	0.808	0.745	0.687	0.885	0.828	0.770	0.716
	Nov	0.912	0.868	0.824	0.780	0.914	0.871	0.829	0.786	0.919	0.879	0.838	0.798
	Dec	0.933	0.899	0.865	0.832	0.934	0.901	0.868	0.834	0.936	0.904	0.872	0.840

Table D.2: Tabulated values of $\bar{f}_{i\infty}$ for wingwalls; $g = 0.0$, $\gamma = 30^o$

ϕ	Mon	Values of $\bar{f}_{i\infty}$											
		$D_f = 0.2$				$D_f = 0.4$				$D_f = 0.6$			
		$p = 0.2$	0.3	0.4	0.5	$p = 0.2$	0.3	0.4	0.5	$p = 0.2$	0.3	0.4	0.5
20	Jan	0.854	0.795	0.741	0.693	0.855	0.795	0.742	0.694	0.856	0.796	0.743	0.696
	Feb	0.849	0.784	0.725	0.669	0.850	0.786	0.727	0.673	0.852	0.790	0.733	0.681
	Mar	0.821	0.740	0.661	0.587	0.825	0.745	0.669	0.597	0.832	0.756	0.685	0.618
	Apr	0.725	0.590	0.460	0.351	0.733	0.602	0.475	0.367	0.750	0.628	0.510	0.404
	May	0.480	0.261	0.116	0.043	0.492	0.273	0.123	0.046	0.519	0.300	0.139	0.054
	Jun	0.242	0.024	0.000	0.000	0.250	0.025	0.000	0.000	0.270	0.028	0.000	0.000
	Jul	0.355	0.124	0.007	0.000	0.366	0.131	0.008	0.000	0.391	0.145	0.009	0.000
	Aug	0.653	0.482	0.335	0.229	0.663	0.497	0.351	0.242	0.684	0.529	0.385	0.272
	Sep	0.796	0.701	0.609	0.518	0.801	0.708	0.619	0.531	0.812	0.725	0.642	0.561
	Oct	0.842	0.774	0.710	0.651	0.844	0.777	0.714	0.656	0.847	0.782	0.722	0.668
	Nov	0.854	0.793	0.739	0.690	0.854	0.794	0.740	0.691	0.855	0.795	0.742	0.694
	Dec	0.855	0.796	0.744	0.697	0.855	0.796	0.744	0.697	0.856	0.797	0.745	0.698
40	Jan	0.861	0.801	0.748	0.700	0.862	0.802	0.749	0.701	0.864	0.804	0.750	0.701
	Feb	0.858	0.797	0.742	0.692	0.859	0.798	0.743	0.693	0.861	0.800	0.745	0.696
	Mar	0.845	0.777	0.714	0.656	0.847	0.780	0.718	0.662	0.851	0.787	0.728	0.674
	Apr	0.809	0.721	0.638	0.568	0.814	0.729	0.649	0.580	0.825	0.746	0.672	0.606
	May	0.744	0.639	0.550	0.476	0.753	0.651	0.563	0.489	0.773	0.675	0.590	0.516
	Jun	0.708	0.595	0.500	0.426	0.717	0.606	0.512	0.438	0.737	0.629	0.536	0.461
	Jul	0.723	0.614	0.523	0.449	0.733	0.626	0.535	0.461	0.753	0.650	0.561	0.486
	Aug	0.785	0.687	0.602	0.530	0.792	0.698	0.615	0.544	0.807	0.720	0.641	0.572
	Sep	0.835	0.761	0.692	0.627	0.838	0.766	0.699	0.636	0.844	0.776	0.713	0.654
	Oct	0.855	0.793	0.736	0.684	0.856	0.794	0.738	0.686	0.858	0.797	0.742	0.692
	Nov	0.860	0.800	0.747	0.699	0.861	0.801	0.748	0.699	0.863	0.803	0.749	0.700
	Dec	0.860	0.800	0.747	0.700	0.862	0.802	0.748	0.700	0.865	0.804	0.750	0.701
60	Jan	0.874	0.812	0.753	0.700	0.875	0.813	0.754	0.701	0.876	0.815	0.756	0.702
	Feb	0.864	0.804	0.750	0.701	0.865	0.805	0.751	0.702	0.867	0.807	0.752	0.702
	Mar	0.855	0.791	0.732	0.677	0.857	0.793	0.734	0.681	0.860	0.798	0.740	0.688
	Apr	0.825	0.747	0.678	0.617	0.829	0.753	0.686	0.626	0.839	0.767	0.702	0.643
	May	0.800	0.718	0.647	0.584	0.805	0.724	0.653	0.590	0.813	0.735	0.665	0.603
	Jun	0.792	0.708	0.634	0.571	0.796	0.712	0.639	0.576	0.803	0.721	0.649	0.587
	Jul	0.796	0.712	0.639	0.577	0.800	0.717	0.645	0.582	0.808	0.727	0.656	0.594
	Aug	0.811	0.731	0.662	0.601	0.816	0.738	0.669	0.609	0.827	0.752	0.685	0.625
	Sep	0.846	0.777	0.714	0.654	0.849	0.781	0.719	0.661	0.854	0.789	0.729	0.674
	Oct	0.862	0.802	0.747	0.697	0.863	0.803	0.748	0.698	0.865	0.805	0.750	0.700
	Nov	0.868	0.806	0.750	0.700	0.870	0.808	0.751	0.701	0.872	0.810	0.754	0.702
	Dec	0.881	0.821	0.762	0.706	0.881	0.822	0.762	0.706	0.881	0.822	0.763	0.706

Table D.3: Tabulated values of $\bar{f}_{i\infty}$ for wingwalls; $g = 0.0$, $\gamma = 60^o$

ϕ	Mon	Values of $\bar{f}_{i\infty}$											
		$D_f = 0.2$				$D_f = 0.4$				$D_f = 0.6$			
		$p = 0.2$	0.3	0.4	0.5	$p = 0.2$	0.3	0.4	0.5	$p = 0.2$	0.3	0.4	0.5
20	Jan	0.892	0.845	0.804	0.767	0.885	0.836	0.792	0.754	0.871	0.816	0.767	0.724
	Feb	0.913	0.876	0.842	0.811	0.909	0.871	0.835	0.803	0.900	0.858	0.819	0.784
	Mar	0.923	0.887	0.854	0.821	0.923	0.886	0.853	0.821	0.921	0.884	0.852	0.820
	Apr	0.898	0.849	0.800	0.751	0.900	0.852	0.805	0.757	0.905	0.861	0.816	0.772
	May	0.838	0.757	0.676	0.595	0.841	0.761	0.681	0.602	0.847	0.770	0.694	0.617
	Jun	0.790	0.685	0.581	0.477	0.792	0.688	0.584	0.481	0.796	0.695	0.593	0.492
	Jul	0.813	0.719	0.626	0.532	0.815	0.723	0.630	0.538	0.820	0.730	0.640	0.550
	Aug	0.878	0.817	0.757	0.698	0.881	0.821	0.763	0.705	0.887	0.831	0.776	0.721
	Sep	0.919	0.880	0.842	0.806	0.920	0.882	0.844	0.809	0.921	0.885	0.848	0.815
	Oct	0.919	0.884	0.850	0.820	0.916	0.880	0.845	0.815	0.909	0.871	0.834	0.802
	Nov	0.898	0.854	0.816	0.780	0.892	0.846	0.806	0.769	0.879	0.827	0.782	0.741
	Dec	0.883	0.834	0.789	0.749	0.876	0.824	0.777	0.735	0.861	0.803	0.750	0.703
40	Jan	0.833	0.763	0.701	0.646	0.826	0.753	0.688	0.631	0.810	0.730	0.660	0.599
	Feb	0.866	0.809	0.759	0.713	0.859	0.800	0.747	0.699	0.844	0.779	0.721	0.668
	Mar	0.890	0.842	0.799	0.759	0.886	0.836	0.792	0.751	0.877	0.823	0.777	0.734
	Apr	0.895	0.847	0.800	0.758	0.895	0.847	0.801	0.759	0.894	0.847	0.802	0.762
	May	0.879	0.820	0.764	0.709	0.882	0.825	0.771	0.717	0.888	0.835	0.785	0.735
	Jun	0.862	0.795	0.728	0.664	0.867	0.802	0.737	0.675	0.876	0.816	0.756	0.700
	Jul	0.870	0.806	0.744	0.684	0.873	0.812	0.752	0.694	0.882	0.825	0.770	0.717
	Aug	0.891	0.840	0.791	0.743	0.892	0.842	0.794	0.747	0.895	0.846	0.801	0.756
	Sep	0.894	0.848	0.805	0.764	0.892	0.845	0.801	0.760	0.886	0.837	0.792	0.750
	Oct	0.875	0.822	0.774	0.732	0.869	0.814	0.764	0.720	0.856	0.795	0.740	0.692
	Nov	0.842	0.775	0.717	0.665	0.835	0.765	0.704	0.650	0.819	0.743	0.676	0.617
	Dec	0.822	0.747	0.681	0.623	0.815	0.737	0.669	0.608	0.799	0.715	0.641	0.577
60	Jan	0.753	0.651	0.561	0.483	0.749	0.646	0.555	0.476	0.742	0.635	0.541	0.460
	Feb	0.818	0.741	0.673	0.614	0.811	0.731	0.661	0.600	0.796	0.711	0.636	0.570
	Mar	0.859	0.798	0.745	0.696	0.853	0.790	0.734	0.684	0.840	0.772	0.712	0.658
	Apr	0.869	0.810	0.756	0.706	0.867	0.808	0.754	0.704	0.864	0.804	0.749	0.700
	May	0.851	0.783	0.718	0.658	0.854	0.786	0.723	0.664	0.858	0.793	0.733	0.677
	Jun	0.831	0.756	0.690	0.630	0.835	0.762	0.697	0.638	0.844	0.774	0.711	0.654
	Jul	0.841	0.768	0.701	0.641	0.845	0.773	0.708	0.649	0.851	0.783	0.720	0.664
	Aug	0.865	0.804	0.747	0.693	0.865	0.804	0.747	0.695	0.865	0.805	0.749	0.698
	Sep	0.867	0.809	0.756	0.709	0.862	0.803	0.749	0.700	0.853	0.790	0.733	0.682
	Oct	0.835	0.766	0.704	0.650	0.828	0.756	0.692	0.636	0.813	0.734	0.665	0.604
	Nov	0.774	0.679	0.597	0.524	0.769	0.673	0.588	0.514	0.759	0.658	0.571	0.494
	Dec	0.729	0.618	0.521	0.437	0.727	0.614	0.516	0.431	0.721	0.606	0.506	0.420

Table D.4: Tabulated values of $\bar{f}_{i\infty}$ for wingwalls; $g = 0.0$, $\gamma = 90^o$

ϕ	Mon	Values of $\bar{f}_{i\infty}$											
		$D_f = 0.2$				$D_f = 0.4$				$D_f = 0.6$			
		$p = 0.2$	0.3	0.4	0.5	$p = 0.2$	0.3	0.4	0.5	$p = 0.2$	0.3	0.4	0.5
20	Jan	0.791	0.698	0.613	0.535	0.783	0.687	0.600	0.520	0.763	0.660	0.568	0.484
	Feb	0.845	0.775	0.708	0.647	0.838	0.765	0.695	0.632	0.821	0.741	0.665	0.597
	Mar	0.908	0.864	0.823	0.784	0.903	0.857	0.813	0.772	0.890	0.838	0.790	0.744
	Apr	0.962	0.944	0.927	0.910	0.960	0.941	0.923	0.906	0.955	0.935	0.915	0.896
	May	0.966	0.949	0.932	0.915	0.967	0.951	0.934	0.918	0.971	0.956	0.941	0.926
	Jun	0.941	0.912	0.882	0.853	0.942	0.913	0.884	0.855	0.944	0.916	0.888	0.860
	Jul	0.953	0.930	0.907	0.884	0.955	0.932	0.909	0.886	0.957	0.936	0.915	0.893
	Aug	0.970	0.954	0.939	0.925	0.969	0.954	0.939	0.925	0.969	0.954	0.939	0.925
	Sep	0.934	0.903	0.872	0.844	0.929	0.896	0.864	0.834	0.918	0.881	0.843	0.809
	Oct	0.865	0.802	0.744	0.689	0.859	0.793	0.732	0.675	0.843	0.771	0.705	0.643
	Nov	0.804	0.718	0.637	0.563	0.796	0.707	0.624	0.548	0.777	0.681	0.593	0.512
	Dec	0.777	0.678	0.588	0.506	0.768	0.666	0.574	0.491	0.748	0.638	0.541	0.454
40	Jan	0.711	0.591	0.486	0.395	0.701	0.578	0.471	0.380	0.677	0.547	0.436	0.343
	Feb	0.774	0.677	0.590	0.512	0.764	0.664	0.574	0.494	0.740	0.631	0.535	0.451
	Mar	0.841	0.773	0.710	0.651	0.833	0.760	0.695	0.634	0.811	0.731	0.658	0.591
	Apr	0.903	0.859	0.818	0.780	0.897	0.851	0.807	0.767	0.883	0.830	0.781	0.736
	May	0.928	0.894	0.862	0.831	0.926	0.891	0.858	0.827	0.920	0.883	0.848	0.815
	Jun	0.932	0.900	0.868	0.838	0.932	0.899	0.867	0.837	0.930	0.898	0.865	0.835
	Jul	0.931	0.899	0.866	0.837	0.930	0.897	0.864	0.834	0.927	0.892	0.859	0.828
	Aug	0.917	0.877	0.842	0.807	0.912	0.871	0.834	0.798	0.901	0.856	0.815	0.775
	Sep	0.869	0.812	0.759	0.710	0.861	0.801	0.744	0.693	0.841	0.773	0.709	0.651
	Oct	0.796	0.708	0.628	0.557	0.787	0.695	0.612	0.540	0.764	0.663	0.574	0.497
	Nov	0.728	0.613	0.513	0.426	0.718	0.600	0.498	0.410	0.693	0.569	0.462	0.371
	Dec	0.692	0.565	0.456	0.362	0.682	0.552	0.441	0.347	0.658	0.521	0.407	0.312
60	Jan	0.557	0.392	0.264	0.166	0.550	0.384	0.257	0.160	0.534	0.367	0.241	0.147
	Feb	0.693	0.569	0.462	0.373	0.683	0.556	0.448	0.358	0.659	0.525	0.414	0.323
	Mar	0.795	0.709	0.633	0.565	0.784	0.694	0.614	0.545	0.757	0.656	0.569	0.494
	Apr	0.865	0.806	0.753	0.706	0.857	0.796	0.740	0.691	0.839	0.770	0.709	0.655
	May	0.884	0.833	0.784	0.739	0.881	0.829	0.780	0.734	0.875	0.819	0.769	0.722
	Jun	0.882	0.829	0.778	0.729	0.881	0.828	0.776	0.727	0.879	0.825	0.773	0.725
	Jul	0.884	0.832	0.783	0.736	0.882	0.830	0.780	0.733	0.878	0.824	0.774	0.726
	Aug	0.877	0.823	0.774	0.729	0.872	0.815	0.765	0.719	0.859	0.797	0.743	0.693
	Sep	0.829	0.756	0.691	0.634	0.818	0.742	0.674	0.613	0.793	0.706	0.630	0.563
	Oct	0.730	0.619	0.522	0.440	0.719	0.604	0.506	0.422	0.693	0.571	0.467	0.381
	Nov	0.601	0.448	0.325	0.226	0.593	0.439	0.315	0.218	0.575	0.417	0.294	0.198
	Dec	0.491	0.314	0.183	0.091	0.486	0.309	0.178	0.088	0.474	0.297	0.169	0.082

Table D.5: Tabulated values of $\bar{f}_{i\infty}$ for wingwalls; $g = 0.1$, $\gamma = 0^o$

ϕ	Mon	Values of $\bar{f}_{i\infty}$											
		$D_f = 0.2$				$D_f = 0.4$				$D_f = 0.6$			
		$p = 0.2$	0.3	0.4	0.5	$p = 0.2$	0.3	0.4	0.5	$p = 0.2$	0.3	0.4	0.5
20	Jan	0.903	0.818	0.730	0.643	0.909	0.828	0.745	0.661	0.924	0.852	0.777	0.701
	Feb	0.841	0.724	0.622	0.539	0.852	0.741	0.641	0.559	0.875	0.775	0.681	0.599
	Mar	0.717	0.591	0.495	0.422	0.732	0.607	0.510	0.436	0.762	0.639	0.541	0.464
	Apr	0.579	0.450	0.363	0.302	0.585	0.456	0.368	0.306	0.597	0.466	0.377	0.315
	May	0.260	0.180	0.137	0.110	0.260	0.180	0.137	0.110	0.261	0.180	0.137	0.111
	Jun	0.000	0.000	0.000	0.000	0.000	0.000	0.000	0.000	0.000	0.000	0.000	0.000
	Jul	0.000	0.000	0.000	0.000	0.000	0.000	0.000	0.000	0.000	0.000	0.000	0.000
	Aug	0.499	0.375	0.297	0.244	0.503	0.378	0.299	0.246	0.509	0.383	0.304	0.250
	Sep	0.670	0.542	0.448	0.379	0.682	0.553	0.459	0.389	0.705	0.577	0.480	0.408
	Oct	0.804	0.679	0.579	0.499	0.817	0.697	0.598	0.518	0.845	0.734	0.637	0.556
	Nov	0.890	0.798	0.703	0.616	0.897	0.810	0.720	0.635	0.914	0.836	0.755	0.676
	Dec	0.915	0.836	0.755	0.673	0.921	0.846	0.769	0.690	0.934	0.867	0.798	0.727
40	Jan	0.950	0.895	0.836	0.776	0.954	0.902	0.846	0.788	0.962	0.916	0.866	0.814
	Feb	0.916	0.841	0.765	0.696	0.922	0.852	0.779	0.712	0.937	0.875	0.810	0.747
	Mar	0.856	0.766	0.686	0.617	0.866	0.779	0.701	0.632	0.888	0.807	0.731	0.663
	Apr	0.813	0.712	0.627	0.556	0.819	0.720	0.636	0.565	0.833	0.736	0.653	0.582
	May	0.769	0.659	0.570	0.499	0.773	0.664	0.576	0.504	0.781	0.674	0.585	0.513
	Jun	0.741	0.627	0.537	0.466	0.745	0.631	0.541	0.469	0.751	0.638	0.548	0.476
	Jul	0.754	0.642	0.553	0.481	0.758	0.646	0.557	0.485	0.765	0.654	0.565	0.493
	Aug	0.796	0.691	0.605	0.533	0.801	0.698	0.612	0.540	0.812	0.711	0.625	0.554
	Sep	0.839	0.745	0.663	0.593	0.848	0.756	0.676	0.606	0.866	0.779	0.700	0.631
	Oct	0.897	0.814	0.736	0.667	0.906	0.827	0.752	0.684	0.923	0.854	0.785	0.720
	Nov	0.942	0.883	0.820	0.755	0.947	0.891	0.831	0.769	0.957	0.907	0.853	0.798
	Dec	0.957	0.907	0.853	0.797	0.960	0.913	0.861	0.808	0.968	0.925	0.879	0.830
60	Jan	0.986	0.958	0.925	0.889	0.987	0.960	0.928	0.893	0.989	0.964	0.934	0.901
	Feb	0.956	0.906	0.852	0.797	0.959	0.912	0.861	0.808	0.966	0.925	0.879	0.831
	Mar	0.903	0.833	0.767	0.706	0.911	0.844	0.780	0.720	0.929	0.868	0.808	0.750
	Apr	0.879	0.802	0.731	0.667	0.884	0.808	0.738	0.675	0.894	0.821	0.753	0.691
	May	0.863	0.779	0.705	0.639	0.866	0.783	0.710	0.644	0.872	0.791	0.718	0.653
	Jun	0.855	0.769	0.693	0.627	0.857	0.772	0.697	0.631	0.862	0.778	0.704	0.638
	Jul	0.858	0.774	0.698	0.632	0.861	0.777	0.702	0.637	0.866	0.784	0.710	0.645
	Aug	0.872	0.792	0.719	0.655	0.876	0.798	0.726	0.662	0.884	0.808	0.737	0.674
	Sep	0.892	0.819	0.751	0.689	0.899	0.829	0.762	0.701	0.914	0.848	0.784	0.725
	Oct	0.940	0.881	0.819	0.758	0.945	0.890	0.830	0.772	0.956	0.907	0.855	0.802
	Nov	0.979	0.945	0.907	0.866	0.980	0.948	0.911	0.871	0.983	0.954	0.919	0.882
	Dec	0.993	0.972	0.944	0.915	0.993	0.973	0.946	0.917	0.994	0.975	0.950	0.922

Table D.6: Tabulated values of $\bar{f}_{i\infty}$ for wingwalls; $g = 0.1$, $\gamma = 30^o$

ϕ	Mon	Values of $\bar{f}_{i\infty}$											
		$D_f = 0.2$				$D_f = 0.4$				$D_f = 0.6$			
		$p = 0.2$	0.3	0.4	0.5	$p = 0.2$	0.3	0.4	0.5	$p = 0.2$	0.3	0.4	0.5
20	Jan	0.926	0.874	0.823	0.776	0.925	0.874	0.823	0.776	0.925	0.873	0.823	0.777
	Feb	0.926	0.867	0.809	0.754	0.926	0.868	0.811	0.757	0.926	0.870	0.816	0.764
	Mar	0.906	0.828	0.752	0.677	0.909	0.833	0.759	0.687	0.914	0.843	0.773	0.707
	Apr	0.820	0.686	0.554	0.434	0.827	0.697	0.570	0.452	0.844	0.723	0.605	0.492
	May	0.578	0.345	0.175	0.075	0.590	0.359	0.185	0.080	0.618	0.391	0.208	0.092
	Jun	0.328	0.073	0.000	0.000	0.338	0.076	0.000	0.000	0.361	0.085	0.000	0.000
	Jul	0.448	0.194	0.039	0.000	0.460	0.203	0.041	0.000	0.488	0.224	0.047	0.000
	Aug	0.750	0.581	0.422	0.299	0.759	0.595	0.440	0.315	0.780	0.627	0.478	0.351
	Sep	0.884	0.792	0.700	0.611	0.888	0.799	0.710	0.623	0.897	0.814	0.732	0.652
	Oct	0.922	0.859	0.798	0.738	0.922	0.861	0.801	0.743	0.924	0.865	0.808	0.753
	Nov	0.927	0.873	0.821	0.773	0.926	0.873	0.822	0.774	0.925	0.873	0.822	0.775
	Dec	0.925	0.873	0.823	0.777	0.925	0.873	0.823	0.777	0.924	0.873	0.823	0.777
40	Jan	0.928	0.876	0.826	0.779	0.929	0.877	0.827	0.780	0.931	0.879	0.828	0.780
	Feb	0.929	0.875	0.823	0.774	0.929	0.876	0.824	0.775	0.929	0.877	0.826	0.777
	Mar	0.921	0.859	0.799	0.741	0.922	0.862	0.802	0.746	0.925	0.867	0.811	0.757
	Apr	0.890	0.806	0.725	0.651	0.894	0.814	0.736	0.664	0.904	0.830	0.758	0.691
	May	0.827	0.724	0.631	0.554	0.837	0.736	0.644	0.568	0.856	0.761	0.673	0.597
	Jun	0.793	0.679	0.581	0.500	0.803	0.691	0.593	0.512	0.823	0.715	0.619	0.538
	Jul	0.808	0.700	0.603	0.524	0.818	0.712	0.616	0.538	0.838	0.737	0.644	0.565
	Aug	0.868	0.773	0.688	0.611	0.875	0.783	0.700	0.625	0.888	0.805	0.727	0.655
	Sep	0.913	0.845	0.778	0.713	0.915	0.849	0.784	0.721	0.920	0.857	0.796	0.738
	Oct	0.927	0.872	0.817	0.766	0.927	0.873	0.819	0.768	0.928	0.875	0.822	0.773
	Nov	0.929	0.877	0.827	0.780	0.929	0.878	0.827	0.780	0.931	0.879	0.828	0.781
	Dec	0.927	0.876	0.825	0.779	0.928	0.877	0.826	0.780	0.931	0.880	0.828	0.781
60	Jan	0.941	0.886	0.831	0.781	0.942	0.888	0.833	0.782	0.944	0.891	0.836	0.784
	Feb	0.932	0.880	0.829	0.781	0.933	0.881	0.830	0.782	0.935	0.883	0.832	0.783
	Mar	0.928	0.871	0.815	0.761	0.929	0.873	0.817	0.764	0.931	0.876	0.823	0.771
	Apr	0.901	0.828	0.760	0.698	0.905	0.835	0.768	0.707	0.913	0.847	0.784	0.725
	May	0.877	0.799	0.727	0.664	0.881	0.804	0.733	0.671	0.889	0.815	0.746	0.684
	Jun	0.870	0.788	0.715	0.650	0.873	0.793	0.720	0.656	0.880	0.802	0.731	0.668
	Jul	0.874	0.793	0.721	0.657	0.877	0.798	0.727	0.663	0.884	0.808	0.738	0.675
	Aug	0.887	0.812	0.743	0.680	0.892	0.819	0.751	0.689	0.902	0.832	0.766	0.706
	Sep	0.920	0.858	0.797	0.739	0.922	0.862	0.802	0.745	0.926	0.869	0.812	0.758
	Oct	0.932	0.880	0.828	0.779	0.933	0.880	0.829	0.780	0.934	0.882	0.830	0.781
	Nov	0.935	0.881	0.829	0.780	0.936	0.882	0.830	0.781	0.939	0.886	0.833	0.783
	Dec	0.948	0.897	0.842	0.787	0.949	0.898	0.843	0.787	0.951	0.899	0.845	0.789

Table D.7: Tabulated values of $\bar{f}_{i\infty}$ for wingwalls; $g = 0.1$, $\gamma = 60^o$

ϕ	Mon	Values of $\bar{f}_{i\infty}$											
		$D_f = 0.2$				$D_f = 0.4$				$D_f = 0.6$			
		$p = 0.2$	0.3	0.4	0.5	$p = 0.2$	0.3	0.4	0.5	$p = 0.2$	0.3	0.4	0.5
20	Jan	0.944	0.905	0.869	0.834	0.940	0.836	0.860	0.823	0.930	0.816	0.838	0.796
	Feb	0.961	0.935	0.908	0.882	0.958	0.871	0.901	0.874	0.951	0.858	0.885	0.856
	Mar	0.980	0.959	0.932	0.904	0.978	0.886	0.930	0.902	0.975	0.884	0.926	0.899
	Apr	0.979	0.938	0.892	0.845	0.980	0.852	0.896	0.851	0.982	0.861	0.906	0.864
	May	0.937	0.857	0.776	0.695	0.940	0.761	0.781	0.702	0.946	0.770	0.793	0.717
	Jun	0.890	0.785	0.681	0.576	0.892	0.688	0.684	0.581	0.896	0.695	0.693	0.592
	Jul	0.913	0.819	0.726	0.632	0.915	0.723	0.730	0.638	0.920	0.730	0.740	0.650
	Aug	0.968	0.912	0.853	0.795	0.970	0.821	0.859	0.802	0.975	0.831	0.871	0.818
	Sep	0.984	0.958	0.926	0.892	0.983	0.882	0.927	0.894	0.981	0.885	0.929	0.898
	Oct	0.968	0.945	0.921	0.895	0.965	0.880	0.915	0.889	0.959	0.871	0.903	0.875
	Nov	0.948	0.913	0.879	0.847	0.944	0.846	0.871	0.836	0.936	0.827	0.851	0.812
	Dec	0.938	0.896	0.855	0.818	0.934	0.824	0.846	0.806	0.924	0.803	0.823	0.778
40	Jan	0.904	0.840	0.780	0.725	0.899	0.753	0.769	0.711	0.888	0.730	0.744	0.681
	Feb	0.927	0.877	0.830	0.788	0.922	0.800	0.819	0.775	0.912	0.779	0.796	0.746
	Mar	0.949	0.913	0.874	0.836	0.945	0.836	0.867	0.828	0.937	0.823	0.852	0.810
	Apr	0.962	0.923	0.883	0.841	0.961	0.847	0.882	0.842	0.958	0.847	0.882	0.843
	May	0.954	0.904	0.851	0.798	0.956	0.825	0.856	0.805	0.960	0.835	0.869	0.822
	Jun	0.942	0.882	0.819	0.755	0.945	0.802	0.827	0.766	0.952	0.816	0.845	0.789
	Jul	0.948	0.892	0.832	0.774	0.950	0.812	0.840	0.784	0.956	0.825	0.856	0.805
	Aug	0.961	0.919	0.875	0.829	0.961	0.842	0.877	0.832	0.961	0.846	0.882	0.840
	Sep	0.956	0.921	0.883	0.846	0.953	0.845	0.878	0.841	0.947	0.837	0.868	0.830
	Oct	0.934	0.889	0.847	0.808	0.930	0.814	0.838	0.796	0.920	0.795	0.816	0.770
	Nov	0.910	0.850	0.793	0.740	0.905	0.765	0.782	0.727	0.894	0.743	0.757	0.697
	Dec	0.897	0.829	0.764	0.706	0.892	0.737	0.753	0.692	0.881	0.715	0.728	0.662
60	Jan	0.847	0.746	0.652	0.569	0.844	0.646	0.645	0.561	0.837	0.635	0.631	0.545
	Feb	0.892	0.821	0.754	0.693	0.887	0.731	0.743	0.680	0.877	0.711	0.720	0.652
	Mar	0.924	0.872	0.822	0.775	0.920	0.790	0.812	0.763	0.909	0.772	0.790	0.737
	Apr	0.938	0.888	0.838	0.789	0.936	0.808	0.835	0.787	0.932	0.804	0.830	0.782
	May	0.925	0.864	0.802	0.741	0.926	0.786	0.806	0.747	0.929	0.793	0.815	0.759
	Jun	0.907	0.838	0.772	0.712	0.910	0.762	0.779	0.720	0.917	0.774	0.793	0.736
	Jul	0.916	0.849	0.784	0.724	0.918	0.773	0.790	0.731	0.923	0.783	0.803	0.746
	Aug	0.936	0.883	0.829	0.777	0.935	0.804	0.830	0.778	0.934	0.805	0.830	0.780
	Sep	0.934	0.884	0.835	0.789	0.930	0.803	0.827	0.781	0.921	0.790	0.811	0.762
	Oct	0.904	0.840	0.781	0.727	0.899	0.756	0.769	0.713	0.888	0.734	0.745	0.683
	Nov	0.863	0.772	0.688	0.612	0.859	0.673	0.679	0.602	0.850	0.658	0.661	0.581
	Dec	0.826	0.711	0.609	0.520	0.823	0.614	0.604	0.514	0.818	0.606	0.594	0.502

Table D.8: Tabulated values of $\bar{f}_{i\infty}$ for wingwalls; $g = 0.1$, $\gamma = 90^o$

ϕ	Mon	Values of $\bar{f}_{i\infty}$											
		$D_f = 0.2$				$D_f = 0.4$				$D_f = 0.6$			
		$p = 0.2$	0.3	0.4	0.5	$p = 0.2$	0.3	0.4	0.5	$p = 0.2$	0.3	0.4	0.5
20	Jan	0.888	0.796	0.708	0.626	0.880	0.784	0.694	0.610	0.860	0.757	0.661	0.572
	Feb	0.932	0.871	0.805	0.742	0.926	0.861	0.792	0.727	0.912	0.837	0.761	0.691
	Mar	0.969	0.938	0.904	0.869	0.966	0.933	0.896	0.859	0.959	0.920	0.876	0.834
	Apr	0.992	0.984	0.975	0.965	0.991	0.982	0.973	0.962	0.989	0.979	0.967	0.954
	May	1.000	1.000	0.995	0.986	1.000	1.000	0.996	0.987	1.000	1.000	0.997	0.991
	Jun	0.999	0.994	0.978	0.953	0.999	0.994	0.979	0.955	0.999	0.995	0.983	0.960
	Jul	1.000	0.998	0.989	0.974	1.000	0.998	0.990	0.976	1.000	0.999	0.993	0.982
	Aug	0.997	0.993	0.989	0.983	0.997	0.993	0.988	0.982	0.996	0.991	0.985	0.979
	Sep	0.980	0.960	0.937	0.912	0.978	0.957	0.931	0.905	0.973	0.948	0.918	0.886
	Oct	0.945	0.893	0.840	0.784	0.941	0.885	0.829	0.770	0.929	0.865	0.801	0.737
	Nov	0.900	0.815	0.732	0.654	0.893	0.805	0.719	0.639	0.874	0.778	0.686	0.601
	Dec	0.874	0.775	0.682	0.597	0.866	0.763	0.668	0.581	0.844	0.734	0.634	0.542
40	Jan	0.808	0.684	0.575	0.478	0.798	0.671	0.559	0.461	0.773	0.638	0.521	0.421
	Feb	0.867	0.771	0.682	0.602	0.858	0.758	0.666	0.583	0.835	0.724	0.625	0.538
	Mar	0.919	0.858	0.797	0.739	0.912	0.847	0.783	0.721	0.895	0.820	0.747	0.679
	Apr	0.958	0.923	0.888	0.853	0.954	0.916	0.879	0.842	0.945	0.900	0.857	0.813
	May	0.979	0.958	0.933	0.907	0.977	0.955	0.929	0.903	0.972	0.947	0.919	0.891
	Jun	0.985	0.966	0.942	0.916	0.984	0.965	0.940	0.914	0.981	0.961	0.937	0.911
	Jul	0.983	0.964	0.939	0.913	0.981	0.961	0.936	0.911	0.977	0.956	0.930	0.903
	Aug	0.968	0.940	0.912	0.882	0.965	0.935	0.905	0.873	0.958	0.922	0.887	0.851
	Sep	0.936	0.887	0.836	0.789	0.931	0.878	0.823	0.774	0.917	0.855	0.792	0.736
	Oct	0.886	0.802	0.723	0.648	0.877	0.789	0.706	0.630	0.856	0.757	0.667	0.585
	Nov	0.825	0.707	0.602	0.509	0.815	0.694	0.586	0.491	0.790	0.661	0.548	0.450
	Dec	0.789	0.658	0.544	0.444	0.779	0.645	0.528	0.428	0.754	0.613	0.491	0.389
60	Jan	0.651	0.479	0.339	0.228	0.644	0.470	0.330	0.221	0.628	0.452	0.312	0.205
	Feb	0.789	0.661	0.550	0.454	0.779	0.648	0.534	0.437	0.754	0.616	0.498	0.399
	Mar	0.878	0.796	0.720	0.651	0.869	0.782	0.701	0.630	0.845	0.746	0.656	0.578
	Apr	0.928	0.878	0.830	0.785	0.923	0.869	0.818	0.770	0.909	0.847	0.789	0.735
	May	0.951	0.908	0.864	0.821	0.948	0.904	0.859	0.815	0.941	0.895	0.848	0.802
	Jun	0.951	0.907	0.859	0.813	0.950	0.905	0.857	0.811	0.947	0.901	0.854	0.808
	Jul	0.952	0.909	0.863	0.819	0.950	0.906	0.860	0.815	0.945	0.900	0.853	0.808
	Aug	0.941	0.897	0.852	0.809	0.936	0.890	0.843	0.798	0.925	0.873	0.822	0.772
	Sep	0.901	0.834	0.770	0.713	0.893	0.821	0.754	0.693	0.873	0.789	0.713	0.645
	Oct	0.825	0.712	0.611	0.523	0.814	0.698	0.594	0.504	0.788	0.662	0.553	0.459
	Nov	0.697	0.538	0.405	0.297	0.688	0.528	0.395	0.287	0.670	0.505	0.371	0.265
	Dec	0.584	0.395	0.248	0.140	0.578	0.389	0.243	0.136	0.566	0.375	0.231	0.127

Bibliography

[1] J. W. Mitchell, W. A. Beckman and M. J. Pawelsky, Comparisons of measured and simulated performance for CSU solar house I, ASME, Paper 79, W/SOL - 35, 1979.

[2] C. B. Winn, G. R. Gordon and T. E. Corder, SIMSHAC– Simulation Program for Solar Heating and Cooling of Buildings. Journal of Simulation, Vol. 23, pp.165, 1975.

[3] C. B. Winn, Solar simulation computer programs. Solar Energy Technology Handbook, Part B – Applications, system design and economics. Edited by W. C. Dickenson and P. N. Cheremisinoff, Marcel and Dekker, Inc., New York and Basel, 1980.

[4] S. A. Klein and W. A. Beckman, TRNSYS – A Transient Simulation Program. ASHRAE Transactions, Vol. 82, pp.623, 1979.

[5] TRNSYS, A Transient Simulation Program, Version 12.1, Users' Manual. Solar Energy Laboratory, University of Wisconsin, Madison, 1983.

[6] J. A. Duffie and W. A. Beckman, Solar Engineering of Thermal Processes, 2nd. Edition. Wiley Interscience, New York, 1991.

[7] SOLMET Manual, US National Climatic Data Center, Asheville, N.C., Vols. 1 and 2, 1978.

[8] TMY2 Manual, National Renewable Energy Laboratory, Boulevard, Colarado, 1995.

[9] Aerological Data of India, Part III, Radiation Data, (1971-78), Published by The Director General of Meteorology, India Meteorological Department, New Delhi.

[10] K. M. Knight, S. A. Klein and J. A. Duffie, A methodology for the synthesis of hourly weather data. Solar Energy, Vol. 46, pp.109-120, 1991.

[11] R. A. Gansler, S. A. Klein and W. A. Beckman, Assessment of the accuracy of generated meteorological data for use in solar energy simulation studies. Solar Energy, Vol. 53, pp.279-287, 1994.

[12] M. Collares-Pereira and A. Rabl, The average distribution of solar radiation – Correlations between diffuse and hemispherical and between daily and hourly insolation values. Solar Energy, Vol. 22, pp.155-164, 1979.

[13] D. G. Erbs, S. A. Klein and J. A. Duffie, Estimation of the diffuse radiation fraction for hourly, daily and monthly average global radiation. Solar Energy, Vol. 28, pp.293-302, 1982.

[14] P. C. Jain, S. Jain and C. F. Ratto, A new model for obtaining horizontal instantaneous global and diffuse radiation from the daily values. Solar Energy, Vol. 41, pp.397-404, 1988.

[15] V. V. Satyamurty and P. K. Lahiri, Estimation of symmetric and asymmetric hourly global and diffuse radiation from the daily values. Solar Energy, Vol. 48, pp.7-17, 1992.

[16] B. Y. H. Liu and R. C. Jordan, The interrelationship and characteristic distribution of direct, diffuse and total solar radiation. Solar Energy, Vol. 4, pp.1-19, 1960.

[17] P. Bendt, M. Collares-Pereira and A. Rabl, The frequency distribution of daily insolation values. Solar Energy, Vol. 27, pp.1, 1981.

[18] J. F. Orgill and K. G. T. Hollands, Correlation equation for hourly diffuse radiation on a horizontal surface. Solar Energy, Vol. 19, pp.357, 1977.

[19] J. M. Spencer, A comparison of methods of estimating hourly diffuse radiation from global solar radiation. Solar Energy, Vol. 29, pp.29, 1982.

[20] K. G. T. Hollands and R. G. Huget, A probability density function for the clearness index, with applications. Solar Energy, Vol. 30, pp.195, 1983.

[21] A. Soler, Estimation of the monthly average hourly direct, diffuse and global radiation. Solar and Wind Technology, Vol. 4, pp.179, 1987.

[22] H. Suehrcke and P. G. McCormick, The distribution of average instantaneous terrestrial solar radiation over the day. Solar Energy, Vol. 42, pp.303, 1989.

[23] D. T. Reindl, W. A. Beckman and J. A. Duffie, Diffuse fraction correlations. Solar Energy, Vol. 45, pp.1-7, 1990.

[24] J. Camps and M. R. Soler, Estimation of diffuse solar irradiance on a horizontal surface to cloudless days – A new approach. Solar Energy, Vol. 49, pp.53, 1992.

[25] G. L. Morrison and Sudjito, Solar radiation data for Indonesia. Solar Energy, Vol. 49, pp.65, 1992.

[26] T. A. Newell, Simple methods for hourly to daily radiation ratio correlations. Solar Energy, Vol. 31, pp.339, 1983.

[27] A. Mani and S. Rangarajan, The techniques for the precise estimation of hourly values of global, diffuse and direct solar radiation. Solar Energy, Vol. 31, pp.577-595, 1983.

[28] A. Soler, Dependence on solar elevation and the daily sunshine fraction of the correlation between monthly average hourly diffuse and global radiation. Solar Energy, Vol. 48, pp.221, 1992.

[29] A. Skartveit and A. Olseth, The probability density and autocorrelation of short-term global and beam irradiance. Solar Energy, Vol. 49, pp.477, 1992.

[30] J. A. Davis and D. C. McKay, Evaluation of selected models for estimating solar radiation on horizontal surfaces. Solar Energy, Vol. 43, pp.153-168, 1989.

[31] M. A. Elhadidy and D. Y. Abdel-Nabi, Diffuse fraction of daily global radiation at Dahran, Soudi Arabia. Solar Energy, Vol. 46, pp.89, 1991.

[32] K. K. Gopinathan, A simple method for predicting global solar radiation on horizontal surface. Solar and Wind Technology, Vol. 5, pp.581, 1988.

[33] N. Al-Hamdani, M. Al-Riahi and K. Tahir, Estimation of the diffuse fraction of daily and monthly average global radiation for Fudhaliyah, Bagdad (IRAQ). Solar Energy, Vol. 42, pp.81, 1989.

[34] A. Soler, Dependence on cloudiness of the relation between the ratio of diffuse to global radiation and the ratio of global to extraterrestrial radiation for average daily values. Solar Energy, Vol. 44, pp.179, 1990.

[35] A. Soler, Dependence on latitude of the relation between the diffuse fraction of solar radiation and the ratio of global to extraterrestrial radiation for monthly average daily values. Solar Energy, Vol. 44, pp.297, 1990.

[36] L. Wenxian, A general correlation for estimating the monthly average daily direct radiation incident on a horizontal surface in Yunnan Province, China. Solar Energy, Vol. 41, pp.1, 1988.

[37] T. Feuilardm J. M. Abillon and R. Bonhomme, Relationship between global solar irradiation and sunshine duration in Guadeloupe. Solar Energy, Vol. 43, pp.359, 1989.

[38] G. Stanhill, The distribution of global solar radiation over the land surfaces of the earth. Solar Energy, Vol. 31, pp.95, 1983.

[39] B. K. Choudhury, Studies on Estimation of Long Term Average Ambient Temperature, Solar Radiation, Asymmetric Transmittance- absorptance Product and Utilizability. Ph. D. Thesis, Department of Mechanical Engineering, I. I. T Kharagpur, 1994.

[40] D. G. Erbs, S. A. Klein and W. A. Beckman, Estimation of degree-days and ambient teperature bin data from monthly average temperatures. ASHRAE Journal, pp.60, June, 1983.

[41] B. Y. H. Liu and R. C. Jordan, A rational procedure for predicting the long-term average performance of flat-plate solar energy collectors. Solar Energy, Vol. 7, pp.53, 1963.

[42] ASHRAE, Standard 93-77, Methods of testing to determine the thermal performance of solar collectors. ASHRAE, New York, 1977.

[43] f-chart Manual, A Design program for solar heating systems, Version 4.0, EES Report 50, Solar Energy Laboratory, University of Wisconsin-Madison, Madison, WI, 1980.

[44] C. Visalakhsi, Prediction of Annual Load Fraction for Active Solar Energy Heating Systems. Ph. D. Thesis, Department of Mathematics, I. I. T. Kharagpur, India, 1985.

[45] H. Gaul and A. Rabl, Incidence-Angle Modifier and Average Optical Efficiency of Parabolic Trough Collectors. Transactions of the ASME, Journal of Solar Energy Engineering, Vol. 102, pp.16-21, 1980.

[46] S. A. Klein, Calculation of Flat-Plate Collector Loss Coefficients. Solar Energy, Vol. 17, pp.79-80, 1975.

[47] H. C. Hottel and B. B. Woertz, Performance of flat plate solar heat collectors. Tanasactions of the ASME, Journal of Solar Energy Engineering, Vol. 64, pp.91, 1942.

[48] S. K. Samdarshi and S. C. Mullick, Generalized Analytical Equation for the Top Heat Loss Factor of a Flat-Plate Solar Collector with N Glass Covers. Transactions of the ASME, Journal of Solar Energy Engineering, Vol. 116, pp.43-46, 1994.

[49] J. D. Balcomb, R. W. Jones, R. D. Mcfarland and W. O. Wray, Passive Solar Heating Analysis - A Design Manual. ASHRAE, Atlanta, 1984.

[50] M. Connely, R. Giellis, G. Jenson and R. McMordie, Solar heating and cooling computer analysis – A simplified sizing method for non-thermal specialists. Proceedings of the International Solar Energy Society Conference, Winnipeg, Vol. 10, pp.220, 1976.

[51] D. Feuermann, J. M. Gordon and Y. Zarmi, A Typical Meteorological Day (TMD) approach for predicting the long-term performance of solar energy systems. Solar Energy, Vol. 35, pp.63, 1985.

[52] T. A. Reddy, The Design and Sizing of Active Solar Energy Thermal Systems, Oxford University Press, New York, 1987.

[53] T. A. Reddy, J. M. Gordon and I. P. D. DeSilva, MIRA : A one-repetitive day method for predicting the long-term performance of solar energy systems. Solar Energy, Vol. 39, pp.123-133, 1987.

[54] S. A. Klein, W. A. Beckman and J. A. Duffie, A design procedure for solar heating systems. Solar Energy, Vol. 18, pp.113, 1976.

[55] S. A. Klein, W. A. Beckman and J. A. Duffie, A design procedure for solar air heating systems. Solar Energy, Vol. 19, pp.509, 1977.

[56] W. A. Beckman, S. A. Klein and J. A. Duffie, Solar Heating Design: The f-chart Method. Wiley Interscience, New York, 1977.

[57] J. A. Duffie and J. W. Mitchell, f-chart: Predictions and measurements. Transactions of the ASME, Journal of Solar Energy Engineering, Vol. 105, No. 3, 1983.

[58] A. H. Fanney and S. A. Klein, Performance of solar demestic hot water systems at the National Bureau of Standards – measurements and predictions. Transactions of the ASME, Journal of Solar Energy Engineering, Vol. 105, No. 3, pp.311, 1983.

[59] W. E. Buckles and S. A. Klein, Analysis of solar domestic hot water systems. Solar Energy, Vol. 25, pp.417, 1980.

[60] P. J. Lunde, Predictions of monthly and annual performance of solar heating systems. Solar Energy, Vol.20, pp.283, 1977.

[61] S. A. Klein and W. A. Beckman, A general design method for closed loop solar energy heating systems. Solar Energy, Vol. 22, pp.269, 1979.

[62] J. E. Braun, S. A. Klein and K. A. Pearson, An improved design method for solar energy heating systems. Solar Energy, Vol. 31, pp.597, 1979.

[63] J. K. Page, The estimation of monthly mean values of daily total shortwave radiation on vertical and inclined surfaces from sunshine records for latitudes 40°N - 40°S. Proceedings U. N. Conference on New Sources of Energy, Paper No. 35/S/98, pp.378, 1964.

[64] B. Y. H. Liu and R. C. Jordan, Daily insolation on surfaces tilted towards the equator. ASHRAE Journal, Vol. 3, pp.53, 1962.

[65] S. A. Klein, Calculation of monthly average insolation on tilted surfaces. Solar Energy, Vol. 19, pp.325-329, 1977.

[66] S. A. Klein and J. C. Theilacker, An algorithm for calculating monthly average radiation on inclined surfaces. Transactions of the ASME, Journal of Solar Energy Engineering, Vol. 103, pp.29-33, 1981.

[67] P. K. Lahiri, Studies on Estimation of Long-term Average Solar Radiation and Utilizability for Principal Types of Collectors. Ph. D. Thesis, Department of Mechanical Engineering, I. I. T. Kharagpur, 1990.

[68] M. Collares-Pereira and A. Rabl, Derivation of method for predicting long-term average energy delivery of solar collectors. Solar Energy, Vol. 23, pp.223-233, 1979.

[69] M. Collares-Pereira and A. Rabl, Simple procedure for predicting long-term average performance of non-concentrating and concentrating solar collectors. Solar Energy, Vol. 23, pp.235-253, 1979.

[70] R. C. Temps and K. L. Coulson, Solar radiation incident upon slopes of different orientations. Solar Energy, Vol. 19, pp.179, 1977.

[71] J. E. Hay, Calculation of the monthly mean solar radiation for horizontal and tilted surfaces. Solar Energy, Vol. 23, pp.301, 1979.

[72] T. M. Klutcher, Evaluation of models to predict insolation on tilted surfaces. Solar Energy, Vol. 23, pp.111-114, 1979.

[73] J. E. Hay and J. A. Davis, Calculation of the solar radiation incident on an inclined surface. (J. E. Hay and T. K. Won, eds), Proceedings of the first Canadian Solar Radiation Data Workshop, Toronto, pp.59-72, 1980.

[74] R. Perez, R. Stewart, C. Arbogast, R. Seals and J. Scott, An anisotropic hourly diffuse radiation model for sloping surfaces: Description, performance validation, site dependency evaluation. Solar Energy, Vol. 36, pp.481, 1986.

[75] C. Gueymard, An isotropic solar irradiance model for tilted surfaces and its comparison with selected engineering algorithms. Solar Energy, Vol. 38, pp.367-386, 1987.

[76] R. Perez, R. Seals, P. Ineichen, R. Stewart, and D. Menicucci, A new simplified version of the Perez diffuse irradiance model for tilted surfaces. Solar Energy, Vol. 39, pp.221-231, 1987.

[77] R. Perez, P. Ineichen, and R. Seals, The importance of correct albedo determination for adequately modelling energy received by tilted surfaces. Solar Energy, Vol. 39, pp.301, 1987.

[78] T. A. Reddy and R. A. Attalage, Differences in computed annual irradiation on inclined surfaces using isotropic and anisotropic sky-diffuse models. Solar Energy, Vol. 40, pp.315-320, 1988.

[79] C. C. Y. Ma and M. Iqbal, Statistical comparison of model for estimating solar radiation on inclined surfaces. Solar Energy, Vol. 31, pp.313, 1983.

[80] M. A. Abdelrahman and M. A. Elhadidy, Comparison of calculated and measured values of total radiation on tilted surfaces in Dahran, Saudi Arabia. Solar Energy, Vol. 37, pp.239, 1986.

[81] M. P. Utrillas and J. A. Martinez-Lozano, Performance evaluation of several versions of the Perez Tilted diffuse irradiance model. Solar Energy, Vol. 53, pp.155-162, 1994.

[82] H. D. kambezidis, B. E. Psiloglou and C. Gueymard, Measurements and models for total solar irradiance on inclined surface in Athens, Greece. Solar Energy, Vol. 53, pp.177-185, 1994.

[83] H. C. Hottel and A. Whillier, Evaluation of flat-plate Solar Collector Performance. In Transactions of the Conference on Use of Solar Energy, University of Arizona Press, Vol. 2, pp.74, 1958.

[84] S. A. Klein, Calculation of flat plate collector utilizability. Solar Energy, Vol. 21, pp.393-402, 1978.

[85] J. C. Theilacker and S. A. Klein, Improvements in the utilizability relationships. Proceedings of the American Section of the International Solar Energy Society Meeting, Phoenix, Arizona, pp.271, 1980.

[86] D. L. Evans, T. T. Rule and B. D. Wood, A new look at long-term collector performance and utilizability. Solar Energy, Vol. 28, pp. 13, 1982.

[87] P. J. Lunde, Solar Thermal Engineering, Wiley Interscience Inc. New York, 1980.

[88] D. R. Clark, S. A. Klein and W. A. Beckman, Algorithm for evaluating the hourly radiation utilizability function. Transactions of the ASME, Vol. 103, pp.281, 1983.

[89] K. G. T. Hollands and R. G. Huget, A probability density function for the clearness index, with applications. Solar Energy, Vol. 30, pp.195, 1983.

[90] S. A. Klein and W. A. Beckman, Review of solar radiation utilizability. Transactions of the ASME, Journal of Solar Energy Engineering, Vol.106, pp.393-402, 1984.

[91] A. Rabl, Yearly Average Performance of Principal Solar Collector Types. Solar Energy, Vol. 18, No. 3, pp.215, 1981.

[92] J. M. Gordon and Y. Zarmi, The utilizability function – I, Theoretical development of a new approach. Solar Energy, Vol. 31, pp.529-536, 1983.

[93] J. M. Gordon and Y. Zarmi, The utilizability function – II, Validation of theory against data-based correlations. Solar Energy, Vol. 31, pp.537-543, 1983.

[94] L. M. Acharya, Studies on Monthly Average Parameters in the Design Methods for Solar Energy Heating Systems. Ph. D. Thesis, Department of Mechanical Engineering, I. I. T. Kharagpur, 1987.

[95] S. A. Klein, Calculation of monthly average transmittance- absorptance product. Solar Energy, Vol. 23, pp.547-551, 1979.

[96] A. A. Sfeir, Monthly average optical efficiency of flat-plate collectors. Solar Energy, Vol. 30, pp.397-399, 1983.

[97] V. V. Satyamurty and L. M. Acharya, Analytical calculation of daily transmittance-absorptance product. Alternative Energy Sources VIII, Proceedings of the 8th Miami International Conference on Alternative Energy Sources, 14-16 December, 1987, Florida, USA, pp.31, 1989.

[98] M. J. Brandemuehl and W. A. Beckman, Transmission of diffuse radiation through CPC and flat-plate collector glazings. Solar Energy, Vol. 24, pp.511, 1980.

[99] C. D. Barley and C. B. Winn, Optimal sizing of solar collectors by the method of relative areas. Solar Energy, Vol. 21, pp.279, 1978.

[100] G. Lameiro and P. Bendt, The GFL method for sizing solar energy space and water heating systems. SERI – 30, Solar Energy Research Institute, Golden, Colorado, May, 1978.

[101] J. C. Ward, Minimum cost sizing of solar heating systems. Sharing the Sun, Proceedings of the International Solar energy Society Conference, Winnipeg, Vol. 4, pp.326, 1976.

[102] V. V. Satyamurty and W. A. Beckman, Influence of collector parameters on load fraction and economic viability, Solar Energy, Vol. 35, pp.497-502, 1985.

[103] V. V. Satyamurty, C. Visalakhsi and K. S. Sastri, Simple correlations for meteorological data with applications to annual performance prediction of solar energy heating systems. Alternative Energy Sources VI, Vol. 1, pp.7, Hemisphere Publishing Corporation, NY, 1983.

[104] V. V. Satyamurty and C. Visalakhsi, Yearly average daily utilizability. Alternative Energy Sources VII, Vol. 1, pp.17, Hemisphere Publishing Corporation, NY, 1985.

[105] V. V. Satyamurty and C. Visalakhsi, Yearly average utilizability method to predict annual solar load fraction for space heating systems. Solar Energy Society of India Journal, Vol. 3, No. 1, 1989.

[106] J. M. Gordon and Y. Zarmi, A simple method for calculating the annual insolation on solar collectors. Solar Energy, Vol. 28, pp.483, 1982.

[107] J. M. Gordon and A. Rabl, Design, analysis and optimization of solar industrial process heat plants without storage. Solar Energy, Vol. 28, pp.519, 1982.

[108] Collares-Pereira, J. M. Gordon, A. Rabl and Y. Zarmi, Design and optimization of solar industrial hot water systems with storage. Solar Energy, Vol. 32, pp.121, 1984.

[109] D. Baer, J. M. Gordon and Y. Zarmi, Design and optimization of solar steam systems for constant load applications. Solar Energy, Vol. 35, pp.137-151, 1985.

[110] J. M. Gordon and Y. Zarmi, An analytic model for the long-term performance of solar thermal systems with well-mixed storage. Solar Energy, Vol. 35, pp.55-61, 1985.

[111] J. I. Ajona and J. M. Gordon, An analytic model for the long term performance of solar air-heating systems, Solar Energy, Vol. 38, pp. 45, 1987.

[112] R. McCluney, The death of the shading coefficient?. ASHRAE Journal, pp.36-45, March 1991.

[113] J. L. Wright, Calculating window solar heat gain. ASHRAE Journal, pp.18-22, July, 1995.

[114] Tseng-Yao Sun, 'SHADOW 1', Procedure for determining heating and cooling loads for computerizing energy calculation, Algorithms for building heat transfer subroutines. ASHRAE, New York, pp.48-56, 1975.

[115] R. D. McFarland, PASOLE: A General Simulation Program for Passive Solar Energy. Los Alamos National Laboratory Report LA-7433-MS, 1978.

[116] J. A. Clarke and D. J. McLean, The ESP User Manual, Available from ABACUS Simulations Limited, 1991.

[117] BLAST 3.0, Users Manual, BLAST Support Office, University of Illinois at Urbana-Champaign, 1986.

[118] E. U. Finlayson, D. K. Arasteh, C. Huizenga, M. D. Rubin and M. S. Reilly, *WINDOW 4.0:* Documentation of Calculation procedures, Energy and Environment Division, Lawrence Berkeley Laboratory, California, 1993.

[119] J. L. Wright and H. F. Sullivan, *VISION3* Glazing System Thermal Analysis: Reference Manual, Advanced Glazing System Laboratory, University of Waterloo, Canada, 1992.

[120] J. D. Balcomb and R. D. McFarland, A simple emperical method for estimating the performance of a passive solar heated building of thermal storage wall type. Proceedings 2nd Annual Passive Solar Energy Conference. Philadelphia, pp.337-389, 16-18 March, 1978.

[121] J. D. Balcomb, R. W. Jones, R. D. McFarland and W. D. Wray, Expanding the SLR method. Passive Solar Journal, Vol. 1, pp.67, 1983.

[122] W. A. Monsen, S. A. Klein and W. A. Beckman, Prediction of Direct Gain Solar Heating System Performance. Solar Energy, vol. 27, p.143, 1981.

[123] W. A. Monsen, S. A. Klein and W. A. Beckman, The Unutilizability Design Method for Collector-Storage Walls. Solar Energy, vol. 29, p.421, 1982.

[124] ASHRAE *Handbook - Fundamentals.* American Society of Heating Refrigeration and Air-Conditioning Engineers, Atlanta, GA, 1989.

[125] D. M. Utzinger and S. A. Klein, A method of estimating monthly average solar radiation on shaded receivers. Solar Energy, Vol. 23. pp.369-373, 1979.

[126] R. E. Jones Jr., Effects of overhang shading of windows having arbitrary azimuth. Solar Energy, Vol. 24, pp.305-312, 1980.

[127] K. Sharp, Calculation of monthly average insolation on a shaded surface of any tilt and azimuth. Solar Energy, Vol. 28, pp.531-538, 1982.

[128] R. F. Yanda and R. E. Jones Jr., Shading effects of finite width overhang on windows facing towards the equator, Solar Energy, vol. 30, p.171-180, 1983.

[129] G. S. Barozzi, Shading effect of eggcrate devices on vertical windows of arbitrary orientation. Solar Energy, Vol. 39, pp.329-342, 1987.

[130] A. E. Delsante and J. W. Spencer, Calculation of the proportion of sky seen by windows with finite horizontal and vertical projections. Solar Energy, Vol. 52, pp.547-551, 1994.

[131] A. Yezioro and E. Shaviv, Shading: A design tool for analyzing mutual shading between buildings. Solar Energy, Vol. 52, pp. 27-37, 1994.

[132] A. Mani, Handbook of Solar Radiation, Data for India, Allied Publishers, New Delhi - 110 064, INDIA, 1980.

[133] TMY Data: Supplied with TRNSYS, a Transient System Simulation Program Version 12.1, University of Wisconsin, Madison, WI, USA, 1983.

[134] M. Abramowitz and I. Stegun (Editors), Handbook of Mathematical Functions. Dover Publications Inc., New York, 1972.

[135] G. A. Korn and T. M. Korn, Mathematical Handbook for Scientists and Engineers. McGraw-Hill Book Company, New York, 1968.

[136] E. Kreyszig, Advanced Engineering Mathematics, pp.764. Wiley Eastern Limited, 1983.

[137] D. D. Houghton (Editor), Handbook of Engineering Meteorology, Wiley-Interscience Publication.